Hamiltonian Discontinuous Galerkin Finite Element Method for Internal Gravity Waves

An Energy and Structure Preserving Discretization

A.M. van Oers

TUDelft

Delft
University of
Technology

Hamiltonian Discontinuous Galerkin Finite Element Method for Internal Gravity Waves

An Energy and Structure Preserving Discretization

MASTER OF SCIENCE THESIS

For the degree of Master of Science in Applied Mathematics at Delft University of Technology

A.M. van Oers

26 March 2015

Faculty of Faculty Electrical Engineering, Mathematics and Computer Science · Delft University of Technology

DELFT UNIVERSITY OF TECHNOLOGY
DEPARTMENT OF
APPLIED MATHEMATICS

The undersigned hereby certify that they have read and recommend to the Faculty of
Faculty Electrical Engineering, Mathematics and Computer Science for acceptance a
thesis entitled

HAMILTONIAN DISCONTINUOUS GALERKIN FINITE ELEMENT METHOD FOR
INTERNAL GRAVITY WAVES

by

A.M. VAN OERS

in partial fulfillment of the requirements for the degree of

MASTER OF SCIENCE APPLIED MATHEMATICS

Dated: 26 March 2015

Supervisors: prof. dr. L.R.M. Maas

                                                          dr.ir. D.R. van der Heul

Readers: prof. dr. ir. C. Vuik

                                                          dr.ir. W.T. van Horssen

Preface

This thesis has been written for the degree of Master of Science in Applied Mathematics at the faculty of Electrical Engineering, Mathematics and Computer Sciences of Delft University of Technology. The graduation is done at the department of Numerical Analysis. The actual research of the graduation project has been carried out at the Physical Oceanography department of the NIOZ Royal Netherlands Institute for Sea Research.

I would like to thank my daily supervisor Leo Maas for his guidance and support. His enthusiasm during our discussions was inspiring and encouraging. A special thanks goes out to Onno Bokhove, who helped me understand Hamiltonian theory and provided invaluable comments during my thesis. I would also like to thank my supervisor at Delft University of Technology, Duncan van der Heul, for his contribution to the project.

Table of Contents

Chapter 1

Introduction

In this thesis internal gravity waves are considered. These are waves that have their maximum displacement in the interior of a fluid. This is different from surface waves, which have their maximum displacement at the surface, or interfacial waves, which have their maximum displacement at the interface between two fluids. These internal gravity waves can only exist when the fluid in which they propagate is stratified in density, i.e. the density decreases continuously in the direction opposite to gravity. Such a stratified fluid is a stable system and occurs in many places in the Earth's oceans. Fluid bodies in nature are often stably stratified in density due to differences in temperature or salt concentration. This provides these fluid bodies with a restoring force in terms of gravity that is absent in homogeneous fully–contained fluids. This restoring force points in a particular direction, which renders the fluid anisotropic. Perturbations of such stably stratified fluids appear as waves that orient themselves to the anisotropic direction; they propagate under a particular fixed direction that is inclined with the anisotropy direction. Waves of given frequency (e.g. tides) preserve this inclination when reflecting from any boundary, in particular also when reflecting from a sloping boundary. The consequence of this constraint is that for almost any shape of basin, these waves are focused onto a particular limit orbit, called wave attractor. The focusing on an attractor is accompanied by an intensification of the wave field, such that intense shearing motion is confined to the immediate vicinity of the wave attractor.

Research in fluid dynamics can be characterized by three branches: theoretical, numerical and experimental. For two–dimensional wave attractors the three branches of research are mature (Maas, 2005). For three–dimensional wave attractors the description is incomplete. Some experimental and some theoretical work has been performed (Manders & Maas, 2004); however, the numerical simulations have lagged behind. The main reason for this is the large computational demand: three–dimensional domains require huge amounts of computer capacity. For wave attractors an additional problem is the focusing of the internal waves onto limit cycles. This focusing leads to small scales and this requires huge amounts of computer capacity to capture all the details. These aspects caused the numerical research branch to lag behind.

An efficient numerical method is needed that requires less computational resources than earlier attempts (Sollie, 2001). This numerical method must also be able to deal with the spatial singularity caused by the focusing effects. Wave attractors appear in asymmetric domains. Many physical systems have very different geometric domains, like laboratory set–ups, bottom profiles of oceans and spherical shells on icy moons. To make the numerical method applicable in a wide range of physical systems it should be possible to choose the geometric domain at will. This geometric flexibility also relates to the multi–scale nature of the problem: Effects of the outer domain boundary, over the width of the wave attractor to the dissipative scale, the numerical method should be able to deal with all of them. Wave attractors in ideal fluids lead to a singularity at the limit cycle: wave energy keeps on focusing there. This requires a numerical method that can deal with large gradients and handles energy conservation correctly. This is even more important on long time–scales. The current work, while linear, aims at developing a numerical method that allows an easy extension to nonlinear flows.

The current work focuses on the development of a numerical method for internal gravity waves that addresses (1) the spatial singularity, where wave energy increases without bound, (2) the geometric flexibility, both for the shape of the domain as well as for the multi–scale effects, and (3) the long time–scales, encountered in many situations in nature.

A discontinuous Galerkin finite element method (DGFEM) has been chosen as numerical method since it allows complex domain geometries, allows hp– as well as r–adaptivity and is ideally suited for conservation laws. By identifying the Hamiltonian structure of the compressible, stratified Euler equations and discretizing this structure phase space conservation and exact conservation of energy are ensured. Applying Dirac's method of constrained Hamiltonian dynamics (Salmon, 1988b; Vanneste & Bokhove, 2002; Bokhove, 2002) to the discretized compressible, stratified Euler equations the incompressibility constraint is enforced and the velocity field stays divergence–free. By applying a symplectic time discretization the discrete Hamiltonian structure is conserved in time. The computational linear algebra demands are handled by using Portable, Extensible Toolkit for Scientific Computation (PETSc) (Balay et al., 2004, 2013) in the DGFEM software environment hpGEM (Pesch et al., 2007).

The developed numerical method can be applied to most problems in ideal fluids. The exact conservation of energy ensures the numerical solution is physically more correct than most general numerical methods. The exact conservation of energy also reduces the computational demands to achieve a certain accuracy since the error made by the numerical method is physically feasible. For incompressible flows the developed numerical method ensures the divergence of the velocity field is zero, even in three dimensional geometries. Methods like pressure stabilization, artificial compressibility are not needed to ensure a zero divergence (solenoidal) velocity field. The developed numerical method is unconditionally stable. The developed numerical method is able to ensure exact conservation of energy and a divergence–free velocity field even with a varying background density and a complex domain.

This thesis is structured as follows. In Chapter 2 the mathematical model is set up. Here the different systems of equations are introduced and their connections are highlighted. Analytical solutions are derived that allow verification of the numerical model. Chapter 3 introduces Hamiltonian theory. The concepts of Hamiltonian dynamics, Poisson and Dirac brackets are explained. In Chapter 4 the Hamiltonian theory is applied to the mathematical model to derive the Hamiltonian structure of the model equations. Dirac's method of constraints

is applied to derive the Hamiltonian structure for incompressible flow. In Chapter 5 this Hamiltonian structure is discretized using DGFEM. The Poisson bracket and Hamiltonian for compressible flow are discretized. Dirac's method of constraints is applied again, now to the discrete Hamiltonian structure, to derive the discrete Hamiltonian structure for incompressible flow. This approach is preferable to discretizing the Hamiltonian structure for incompressible flow directly since the discretization of the compressible Hamiltonian formulation is an intermediate check point and the relatively easy incorporation of boundary conditions which are set automatically by Dirac's theory given the proper boundary conditions for the compressible case. Chapter 6 presents a verification of the numerical model, where DGFEM simulations are compared with analytical solutions. Chapter 7 concludes this report. The future development of the method is outlined.

Chapter 2

Mathematical Model

In this chapter the mathematical model describing the behaviour of internal gravity waves is set up. Several systems of governing equations can be used to describe internal gravity waves. In ideal fluids, the most general equations that allow the propagation of internal gravity waves are the primitive Euler equations. Through approximations these primitive Euler equations are simplified. Figure 2-1 shows the different systems of equations that describe internal gravity waves and shows the connections between these systems. The derivation of the Hamiltonian framework for internal gravity waves in Chapter 4 starts with the primitive Euler equations of fluid dynamics. Approximations are made, both to the differential equations and the Hamiltonian framework. This chapter serves as an overview of the extensive derivations of Chapter 4.

This chapter presents a solution method for the systems of linear equations and presents exact solutions for these systems. These are used in Chapter 6 to verify the numerical model. Several unique properties of internal gravity waves are discussed. As the primitive Euler equations are only used as a starting point for the derivation, no exact solutions are presented for system ⓪. The dispersion relations and solutions can also be found in Gill (1982).
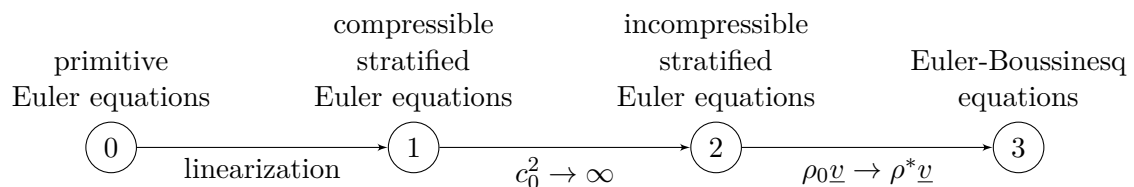
Figure 2-1: The systems of equations discussed in this thesis and their connections. The circled numbers indicate the different systems and the arrows indicate approximations: linearization, incompressibility (letting the speed of sound approach infinity, $c_0^2 \to \infty$) and Boussinesq (replacing the varying background density by a mean value in the inertia terms, $\rho_0 \underline{v} \to \rho^* \underline{v}$). The primitive Euler equations are used as a starting point for the derivations. Systems ① to ③ are solved analytically and numerically.

Section 2-4 discusses wave attractors, the main reason for developing the current numerical method. Wave attractors are complicated solutions to the equations of motion that occur when the geometry is not everywhere parallel or perpendicular to the direction of gravity. Due to the unique reflection properties of internal gravity waves, waves can get focused when reflecting from a wall inclined with the direction of gravity. This focusing leads internal gravity waves to a limit path. Wave attractors pose numerical challenges, due to the large computational demands and the focusing of the wave energy.

Consider motion in a compressible fluid that is stratified in density under the influence of a gravitational field. Assume viscous effects and temperature differences are not important for these motions. Further assume the gravitational field is externally given and is not itself affected by the motion. Let the direction of gravity be aligned with the z–axis of a Cartesian coordinate system. Then the governing equations are the primitive Euler equations, corresponding to system $\textcircled{0}$ in Figure 2-1,

$$
\begin{aligned}
\frac{\partial \underline{v}}{\partial t} &= -(\underline{v}.\nabla)\underline{v} - \frac{1}{\rho}\nabla p - g\hat{\underline{z}}, \\
\frac{\partial \rho}{\partial t} &= -\nabla.(\rho \underline{v}), \\
\frac{\partial s}{\partial t} &= -\underline{v}.\nabla s,
\end{aligned}
\tag{2.1}
$$

where $\underline{v} = (u, v, w)^T$ is the velocity field, p the pressure field, ρ the density field, s the entropy field and g the gravitational acceleration. These equations are derived in Appendix A. Thermodynamic equations relate pressure, density and entropy. The problem to be solved is an initial boundary value problem: given an initial condition and boundary conditions, the temporal evolution of the flow variables is sought. The boundary is considered solid, so the velocity normal to this boundary has to vanish,

$$
\hat{\underline{n}}.\underline{v} = 0,
\tag{2.2}
$$

where $\hat{\underline{n}}$ is the outward normal.

Three approximations can be made to make (2.1) suitable for mathematical analysis. These are

- Linearization: Linearizing around a resting background state and neglecting all products of perturbation quantities removes the phenomenon of wave interactions. This approximation is allowed when the motions are of small amplitude.
- Incompressibility: Letting the Mach number of the fluid approach zero, or letting the speed of sound squared, c_0^2, approach infinity, removes the phenomenon of sound waves. This approximation is allowed when the velocity of the internal waves is much smaller than the speed of sound of the fluid.
- Boussinesq Approximation: Neglecting the density perturbations in the inertia terms simplifies the equations. This approximation is allowed when the density stratification is much smaller than the mean background density.

For internal gravity waves in water usually all three approximations are made.

2-1   Compressible Stratified Euler Equations

Let the background state be $\underline{v} = \underline{v}_0 = \underline{0}$, $p = p_0(z)$, $\rho = \rho_0(z) = \rho^* + \bar{\rho}(z)$ and $s = s_0(z)$. The background density $\rho_0(z)$ consists of a mean background density ρ^* and a varying background density $\bar{\rho}(z)$. In Chapter 4 (2.1) is linearized around the background state. The entropy equation is transformed into a pressure equation using thermodynamic relations, as explained in Section 4-2. The result is the compressible stratified Euler equations, system $\textcircled{1}$ in Figure 2-1,

$$\frac{\partial(\rho_0 \underline{v}')}{\partial t} = -\nabla p' - \rho' g\hat{\underline{z}},$$

$$\frac{\partial \rho'}{\partial t} = -\nabla.(\rho_0 \underline{v}'),$$

$$\frac{\partial p'}{\partial t} = \rho_0 g w' - c_0^2 \rho_0 \nabla.\underline{v}', \qquad (2.3)$$

where the variables are now perturbation quantities, denoted by a prime, and $c_0^2(z) = \left(\frac{\partial p_0}{\partial \rho_0}\right)_{s_0}$ is the speed of sound squared. The buoyancy frequency, or Brunt-Väisälä frequency,

$$N^2(z) = -\frac{g}{\rho_0}\frac{d\rho_0}{dz} - \frac{g^2}{c_0^2} \qquad (2.4)$$

is a measure of how strong the stratification is. In general N^2 is a function of z. For the stratification to be stable $N^2 > 0$, which says that denser liquid must be below liquid of lesser density.

Exact solutions can be found by the method of separation of variables. Let the geometry domain be a rectangular cuboid of size H_x by H_y by H_z, then the domain Ω is $[0, H_x]$ by $[0, H_y]$ by $[0, H_z]$. The boundary in the vertical direction is a solid wall and the boundary in the horizontal directions can either be periodic or a solid wall. When the background density falls off exponentially and the speed of sound is constant, the buoyancy frequency is constant. When the domain is rectangular, the method of separation of variables can be used.

Since the coefficients in (2.3) are only functions of z the ansatz

$$\begin{pmatrix} \rho_0 u \\ \rho_0 v \\ \rho_0 w \\ \rho \\ p \end{pmatrix} = \mathfrak{Re}\left\{ \begin{pmatrix} U(z) \\ V(z) \\ W(z) \\ R(z) \\ P(z) \end{pmatrix} \exp\left[i\left(kx + ly - \sigma t\right)\right] \right\} \qquad (2.5)$$

is substituted into (2.3). Solving for $W(z)$ yields an ordinary differential equation

$$\frac{d^2W}{dz^2} + \left[\frac{N^2}{g} + \frac{g}{c_0^2}\right]\frac{dW}{dz} + \left[\frac{\sigma^2}{c_0^2} - \left(k^2 + l^2\right) + \frac{N^2(k^2 + l^2)}{\sigma^2}\right]W = 0 \qquad (2.6)$$

with solution

$$W = C_{1,2}\exp\left[-\frac{1}{2}\left(\frac{N^2}{g} + \frac{g}{c_0^2}\right)z \pm \frac{1}{2}\sqrt{\left(\frac{N^2}{g} + \frac{g}{c_0^2}\right)^2 - 4\left(\frac{\sigma^2}{c_0^2} - (k^2 + l^2) + \frac{N^2(k^2 + l^2)}{\sigma^2}\right)}z\right],$$

$$(2.7)$$

with constants C_1 and C_2. (2.7) forms a set of solutions to (2.3). More solutions to (2.3) exist, see for example Appendix D. The square root term in (2.7) plays the role of vertical wavenumber m. Let

$$\pm \frac{1}{2} \sqrt{\left(\frac{N^2}{g} + \frac{g}{c_0^2}\right)^2 - 4\left(\frac{\sigma^2}{c_0^2} - (k^2 + l^2) + \frac{N^2(k^2 + l^2)}{\sigma^2}\right)} = im. \tag{2.8}$$

This yields the dispersion relation

$$\frac{\sigma^4}{c_0^2} + \left[-\left(k^2 + l^2 + m^2\right) - \frac{1}{4}\left(\frac{N^2}{g} + \frac{g}{c_0^2}\right)^2\right]\sigma^2 + N^2\left(k^2 + l^2\right) = 0. \tag{2.9}$$

Two frequency regimes appear. Substituting (2.8) for m into (2.9) shows $\sigma = N$ is the root of (2.9). When $\sigma < N$, the solutions are internal gravity waves. The other type of solutions are acoustic waves and are discussed in Appendix D. In this chapter only internal gravity waves are considered.

To satisfy the boundary conditions (2.2) it is required that

$$\begin{aligned} k &= \frac{\pi n_x}{H_x}, \\ l &= \frac{\pi n_y}{H_y}, \\ m &= \frac{\pi n_z}{H_z}, \end{aligned} \tag{2.10}$$

where n_x, n_y and n_z are the modenumbers in $x--$, $y--$ and $z--$direction and $n_x, n_y, n_z \in \mathbb{N}$.

The solution becomes

$$\rho_0 u = e^{-\frac{1}{2}\left(\frac{N^2}{g} + \frac{g}{c_0^2}\right)z} \frac{kc_0^2}{c_0^2\left(k^2 + l^2\right) - \sigma^2} \left[\frac{1}{2}\left(\frac{N^2}{g} - \frac{g}{c_0^2}\right)\sin(mz) + m\cos(mz)\right]\cos\left(kx + ly - \sigma t\right),$$

$$\rho_0 v = e^{-\frac{1}{2}\left(\frac{N^2}{g} + \frac{g}{c_0^2}\right)z} \frac{lc_0^2}{c_0^2\left(k^2 + l^2\right) - \sigma^2} \left[\frac{1}{2}\left(\frac{N^2}{g} - \frac{g}{c_0^2}\right)\sin(mz) + m\cos(mz)\right]\cos\left(kx + ly - \sigma t\right),$$

$$\rho_0 w = e^{-\frac{1}{2}\left(\frac{N^2}{g} + \frac{g}{c_0^2}\right)z} \sin(mz)\sin\left(kx + ly - \sigma t\right),$$

$$p = e^{-\frac{1}{2}\left(\frac{N^2}{g} + \frac{g}{c_0^2}\right)z} \frac{\sigma c_0^2}{c_0^2\left(k^2 + l^2\right) - \sigma^2} \left[\frac{1}{2}\left(\frac{N^2}{g} - \frac{g}{c_0^2}\right)\sin(mz) + m\cos(mz)\right]\cos\left(kx + ly - \sigma t\right),$$

$$\rho = e^{-\frac{1}{2}\left(\frac{N^2}{g} + \frac{g}{c_0^2}\right)z} \frac{\sigma}{c_0^2\left(k^2 + l^2\right) - \sigma^2}$$
$$\left[\frac{2c_0^4\left(k^2 + l^2\right)N^2 - \sigma^2\left(g^2 + N^2 c_0^2\right)}{2\sigma^2 g c_0^2}\sin(mz) + m\cos(mz)\right]\cos\left(kx + ly - \sigma t\right). \tag{2.11}$$

The exponential term on the right hand side is simply $\sqrt{\rho_0}$. Writing the exponential term clarifies the later approximations. This method of solution works for systems $\textcircled{1}$ to $\textcircled{3}$.

Systems $\textcircled{1}$ to $\textcircled{3}$ possess invariants. One of these invariants is the total energy. For the compressible, stratified Euler equations the total energy is found by multiplying (2.3-1) by $\underline{v}$, (2.3-2) by $g^2(\rho - p/c_0^2)/(\rho_0 N^2)$ and (2.3-3) by $p/(\rho_0 c_0^2) + g^2(p/c_0^4 - \rho_0/c_0^2)/(\rho_0 N^2)$, adding the results and integrating over the fixed domain Ω

$$\int_\Omega \frac{\partial}{\partial t}\left[\frac{1}{2}\rho_0|\underline{v}|^2 + \frac{g^2}{2\rho_0 N^2}\left(\rho - \frac{p}{c_0^2}\right)^2 + \frac{p^2}{2\rho_0 c_0^2}\right]\,\mathrm{d}\underline{x} = 0, \qquad (2.12)$$

where the solid wall boundary conditions have been used. The total energy consists of a kinetic, internal and potential part. Since the domain Ω is fixed the integration and differentiation can be interchanged and the total energy $\mathcal{A}_1$ is

$$\mathcal{A}_1 = \int_\Omega \frac{1}{2}\rho_0|\underline{v}|^2 + \frac{g^2}{2\rho_0 N^2}\left(\rho - \frac{p}{c_0^2}\right)^2 + \frac{p^2}{2\rho_0 c_0^2}\,\mathrm{d}\underline{x}. \qquad (2.13)$$

The total energies of systems $\textcircled{2}$ and $\textcircled{3}$ are simplifications of the total energy of system $\textcircled{1}$ and can be found by direct multiplication or by using the approximations directly in (2.13).

The energy conservation implies the uniqueness of the solution to the initial value problem. Suppose two solutions exist for the same initial condition. Then the difference of these two solutions is also a solution of the equations and boundary conditions and has zero energy initially. Since the energy is conserved, the difference solution has zero energy forever. Since the energy is positive definite the difference solution is always zero. So the solution is unique. The existence of a solution is merely assumed here.

2-2   Incompressible Stratified Euler Equations

Letting the speed of sound approach infinity, the pressure and the divergence of the velocity field are zero and (2.3) reduce to the incompressible stratified Euler equations, system $\textcircled{2}$ in Figure 2-1,

$$\begin{aligned}
\frac{\partial(\rho_0\underline{v})}{\partial t} &= -\nabla P - \rho g\hat{\underline{z}}, \\
\frac{\partial\rho}{\partial t} &= -\underline{v}.\nabla\rho_0, \\
\nabla.\underline{v} &= 0.
\end{aligned} \qquad (2.14)$$

The pressure is no longer a thermodynamic variable but an arbitrary function that ensures the velocity field is divergence free; hence the pressure is now denoted by P. The buoyancy frequency reduces to

$$N^2 = -\frac{g}{\rho_0}\frac{d\rho_0}{dz}. \qquad (2.15)$$

When the buoyancy frequency is constant, solutions to the incompressible, stratified Euler equations can be obtained, by using separation of variables or by substituting $c_0^2 \to \infty$ directly into (2.9) and (2.11)

$$\left[\left(k^2 + l^2 + m^2\right) + \frac{1}{4}\left(\frac{N^2}{g}\right)^2\right]\sigma^2 - N^2\left(k^2 + l^2\right) = 0. \qquad (2.16)$$

and

$$\rho_0 u = e^{-\frac{1}{2}\left(\frac{N^2}{g}\right)z} \frac{k}{k^2 + l^2} \left[\frac{N^2}{2g} \sin(mz) + m\cos(mz) \right] \cos\left(kx + ly - \sigma t\right),$$

$$\rho_0 v = e^{-\frac{1}{2}\left(\frac{N^2}{g}\right)z} \frac{l}{k^2 + l^2} \left[\frac{N^2}{2g} \sin(mz) + m\cos(mz) \right] \cos\left(kx + ly - \sigma t\right),$$

$$\rho_0 w = e^{-\frac{1}{2}\left(\frac{N^2}{g}\right)z} \sin(mz) \sin\left(kx + ly - \sigma t\right), \tag{2.17}$$

$$P = e^{-\frac{1}{2}\left(\frac{N^2}{g}\right)z} \frac{\sigma}{k^2 + l^2} \left[\frac{N^2}{2g} \sin(mz) + m\cos(mz) \right] \cos\left(kx + ly - \sigma t\right),$$

$$\rho = e^{-\frac{1}{2}\left(\frac{N^2}{g}\right)z} \frac{N^2}{g\sigma} \sin(mz) \cos\left(kx + ly - \sigma t\right),$$

where the buoyancy frequency is given by (2.15).

The total energy for the incompressible, stratified Euler equations, system $\textcircled{2}$, is

$$\mathcal{A}_2 = \int_\Omega \frac{1}{2}\rho_0 |\underline{v}|^2 + \frac{g^2\rho^2}{2\rho_0 N^2} \, \mathrm{d}\underline{x}. \tag{2.18}$$

2-3   Euler-Boussinesq Equations

The last approximation is the Boussinesq approximation, where the density in the inertia terms is replaced by a constant mean background density, ρ^*, yielding the Euler-Boussinesq equations, system $\textcircled{3}$ in Figure 2-1,

$$\frac{\partial \rho^* \underline{v}}{\partial t} = -\nabla P - \rho g\hat{\underline{z}},$$
$$\frac{\partial \rho}{\partial t} = -\underline{v}.\nabla \rho_0, \tag{2.19}$$
$$\nabla.\underline{v} = 0.$$

The buoyancy frequency reduces to

$$N^2 = -\frac{g}{\rho^*} \frac{d\rho_0}{dz}. \tag{2.20}$$

The Boussinesq approximation is justified when the varying part of the background density, $\bar{\rho}(z)$, is much less than the constant part of the background density, ρ^*. This means the height scale over which the internal gravity wave motion occurs is much less than the height scale over which the background density varies. The scale height of the stratification is g/N^2 and the scale of the internal gravity waves is proportional to $1/|\underline{k}|$, where $\underline{k} = (k, l, m)$ is the wave number vector. Then $N^2 << g|\underline{k}|$. When the buoyancy frequency is constant, solutions to the Euler-Boussinesq equations can be obtained, by using separation of variables or by using $N^2 << g|\underline{k}|$ directly in (2.16) and (2.17)

$$\left(k^2 + l^2 + m^2\right)\sigma^2 - N^2\left(k^2 + l^2\right) = 0. \tag{2.21}$$

and

$$\rho^* u = \frac{mk}{k^2 + l^2} \cos(mz) \cos\left(kx + ly - \sigma t\right),$$

$$\rho^* v = \frac{ml}{k^2 + l^2} \cos(mz) \cos\left(kx + ly - \sigma t\right),$$

$$\rho^* w = \sin(mz) \sin\left(kx + ly - \sigma t\right),$$

$$P = \frac{m\sigma}{k^2 + l^2} \cos(mz) \cos\left(kx + ly - \sigma t\right),$$

$$\rho = \frac{N^2}{g\sigma} \sin(mz) \cos\left(kx + ly - \sigma t\right),$$

(2.22)

where the buoyancy frequency is given by (2.20).

The total energy for the Euler-Boussinesq equations, system $\textcircled{3}$, is

$$\mathcal{A}_3 = \int_\Omega \frac{1}{2} \rho^* |\underline{v}|^2 + \frac{g^2 \rho^2}{2\rho^* N^2} \, \mathrm{d}\underline{x}. \tag{2.23}$$

The direction in which internal gravity waves travel in two dimensions can be found from (2.21). Using a polar description where $\underline{k} = (k, m) = \kappa(\cos(\theta), \sin(\theta))$, yields

$$\frac{\sigma^2}{N^2} = \frac{k^2}{k^2 + m^2} = \cos^2 \theta. \tag{2.24}$$

The frequency σ determines the angle of propagation with the horizontal, θ. The wave frequency is independent of the wave magnitude and only depends on its angle. Upon reflection, the incident and reflected waves will be confined to a fixed angle relative to the vertical (Maas, 2005).

The solutions in Section 2-2 and in this section are internal gravity waves solutions. The compressible stratified Euler equations of Section 2-1 describe a larger class of problems. The solutions (2.9) with (2.11) describe internal gravity waves. The solutions hold for each wavenumber m and represent normal modes of their system. When superposing these modes for the Euler-Boussinesq equations and using a constant frequency a beam of internal gravity waves is found (Gerkema & Zimmerman, 2008).

For a constant buoyancy frequency N and a constant frequency σ, (2.24) shows the angle θ is constant, regardless of the wavenumber m. When superposing these modes one and the same angle pervades all modes. A solution is

$$k_n^2 = \frac{\sigma^2}{N^2 - \sigma^2} m_n^2 = \left(\frac{\pi n_z}{H_z}\right)^2 \frac{\sigma^2}{N^2 - \sigma^2}, \qquad n \in \mathcal{N}, \tag{2.25}$$

and

$$\rho^* u = \sum_n a_n \frac{\pi n_z}{H_z k_n} \cos\left(\frac{\pi n_z z}{H_z}\right) \cos\left(k_n x - \sigma t\right),$$

$$\rho^* w = \sum_n a_n \sin\left(\frac{\pi n_z z}{H_z}\right) \sin\left(k_n x - \sigma t\right),$$

$$P = \sum_n a_n \frac{\pi n_z z \sigma}{H_z k_n^2} \cos\left(\frac{\pi n_z z}{H_z}\right) \cos\left(k_n x - \sigma t\right),$$

$$\rho = \sum_n a_n \frac{N^2}{g\sigma} \sin\left(\frac{\pi n_z z}{H_z}\right) \cos\left(k_n x - \sigma t\right),$$

(2.26)

with coefficients a_n.

Dispersion relation (2.21) reveals that there are two frequency regimes for incompressible fluids: either $0 \leq \sigma \leq N$ or $\sigma > N$. When $0 \leq \sigma \leq N$, m is real, the differential equations are hyperbolic and the motion is oscillatory. When $\sigma > N$, m is imaginary, the differential equations are elliptic and the motion is exponentially decaying. For internal gravity waves to exist, the buoyancy frequency acts as upper bound to the frequency of the internal gravity waves.

For internal gravity waves energy propagates normal to the phase vector. The group velocity is defined as $\underline{c}_g = \nabla_k \sigma$. Using (2.24) yields

$$\underline{c}_g = \nabla_k \sigma = \frac{mN}{\kappa^3}(m, -k). \tag{2.27}$$

The phase speed is defined by $\underline{c} = \sigma / \underline{k}$. Using (2.24) yields

$$\underline{c} = \frac{\sigma}{\kappa^2}(k, m), \tag{2.28}$$

which is perpendicular to $\underline{c}_g$. For more extensive discussions on the properties of internal gravity waves, see (for example) Turner (1979), Gill (1982) and Sutherland (2010).

2-4 Wave Attractors

Internal waves confined to a closed basin can lead to so-called wave attractors. Internal waves reflect from the sides of the basin. When one or more of the sides is tilted with respect to the direction of gravity the reflection at the tilted wall can have a focusing effect. Consider a fluid container in which internal gravity waves propagate. The frequency and direction of the internal gravity waves are governed by (2.24). The internal gravity waves approach a wall, reflect from it and move away from the wall. If the reflection is linear, the frequency σ is preserved by reflection on a fixed wall. By (2.24) the angle θ must be preserved as well. Figure 2-2 shows a focusing reflection from a sloping wall. The incoming beam in Figure 2-2 is focused and the outgoing beam is narrower than the incoming beam.

Since the basin is closed the internal waves keep reflecting. Usually focusing dominates over defocusing and internal waves keep getting focused by the tilted wall. All internal waves are focused onto one limit cycle, the wave attractor. Figure 2-3 shows an example of a wave attractor in a closed basin with a tilted side. The top image shows the predicted path of the wave attractor, based on the basin shape and the forcing frequency, and the center and bottom image show observations of a wave attractor. The measured amplitude and phase show a clear pattern that corresponds with the predicted wave attractor.

In Appendix B a geometric method is discussed that allows the computation of the streamfunction for two dimensional geometries. Figure 2-3(a) is constructed using this geometric method. The geometric method assumes a periodic solution in time.

Figure 2-3(b) shows observations of the focusing and 2-3(a) shows the theoretical, unlimited focusing. The three-dimensional domain and the focusing lead to huge computational costs and causes numerical challenges. An efficient numerical method is needed that requires less computational resources than earlier attempts (Sollie, 2001). In the next chapter, Chapter
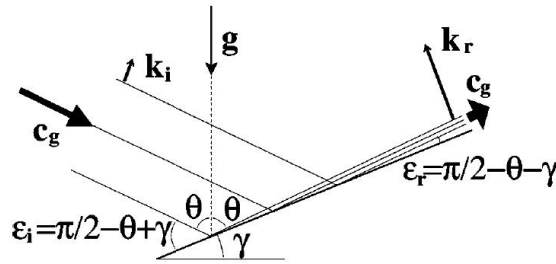
Figure 2-2: The reflection of an internal wave on a wall inclined with respect to the direction of gravity. γ indicates the angle of inclined wall with respect to the horizontal, g indicates the direction of gravity, c_g indicates the group velocity of the internal waves, k_i indicates the wave vector of the incoming beam, k_r indicates the wave vector of the reflecting beam, θ indicates the angle of the internal waves with respect to the direction of gravity, ϵ_i indicates the angle of the incoming internal waves and ϵ_r indicates the angle of the reflected internal waves. Image taken from Staquet & Sommeria (2002).

3, Hamiltonian theory is introduced. This is used to derive the Hamiltonian dynamics of the internal gravity waves in Chapter 4. This Hamiltonian dynamics is used to develop an efficient numerical method in Chapter 5 that can simulate wave attractors in three dimensional geometries and can capture the focusing of the wave energy onto a limit cycle.
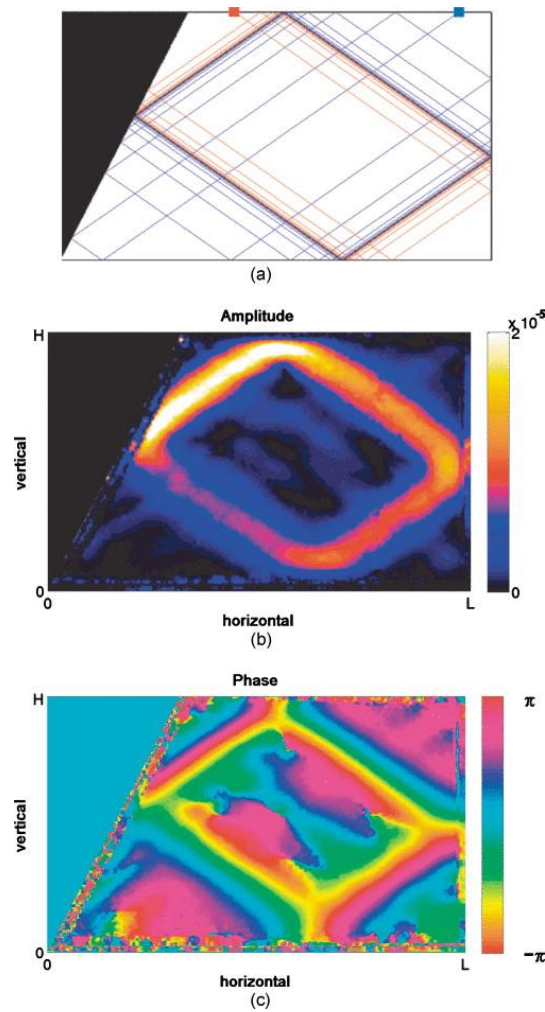
Figure 2-3: Wave Attractor in a closed basin with a tilted side. (a) The predicted limiting path of the wave attractor. (b) The observed amplitude of the wave attractor. (c) The observed phase of the wave attractor. Image taken from Hazewinkel et al. (2010).

Chapter 3

Hamiltonian Dynamics

To derive an energy and structure conserving discretization the geometric structure of the governing equations is used. This chapter introduces this geometric structure, called Hamiltonian dynamics. Hamiltonian dynamics describe the evolution of conservative physical systems. The theory from this chapter is applied in Chapter 4 to derive the Hamiltonian structure of the equations governing internal gravity waves.

Section 3-1 introduces Hamiltonian dynamics and the different representations for finite dimensional systems. Most of this theory carries over to infinite dimensional systems, as discussed in Section 3-2. In Section 3-3 an example from fluid dynamics is discussed to clarify the abstract definitions from the previous two sections. These first three sections are based on Shepherd (1990). Section 3-4 describes the derivation of the energy available to perturbations. Section 3-5 introduces the concept of symplecticity, the basis of numerical methods for Hamiltonian systems. Section 3-6 explains the use of Dirac brackets to enforce constraints.

3-1 Finite Dimensional Dynamical Systems

Canonical Hamiltonian dynamical systems are described by Hamilton's equations

$$
\begin{aligned}
\frac{dq_i}{dt} &= \frac{\partial H}{\partial p_i}, \\
\frac{dp_i}{dt} &= -\frac{\partial H}{\partial q_i}.
\end{aligned}
\tag{3.1}
$$

where $H(q_i, p_i)$ is the Hamiltonian function, usually the energy of the system. The phase space is $\{(q_i, p_i)\}_{i=1,\dots,N}$, where q_i are the generalized coordinates and p_i are the generalized momenta.

For canonical systems, every symmetry in the Hamiltonian function corresponds to an invariant of motion. For example, for conservative (inviscid, unforced) systems the Hamiltonian function does not depend explicitly on time. Then

$$
\frac{dH}{dt} = \frac{\partial H}{\partial q_i}\frac{dq_i}{dt} + \frac{\partial H}{\partial p_i}\frac{dp_i}{dt} = \frac{\partial H}{\partial q_i}\frac{\partial H}{\partial p_i} - \frac{\partial H}{\partial p_i}\frac{\partial H}{\partial q_i} = 0
\tag{3.2}
$$

so that H is an invariant of motion. Similarly, from (3.1) follows that when the system has a symmetry in one of the generalized coordinates (q_i, so that $\frac{\partial H}{\partial q_i} = 0$), the corresponding generalized momentum (p_i) is invariant.

In this case, the reduction of the phase space preserves the canonical Hamiltonian form of (3.1). This preservation does not hold in general for reduction under symmetry. For example, the Eulerian representation of two-dimensional fluid flow is a noncanonical Hamiltonian system obtained by a noninvertible (hence singular) reduction from the canonical, Lagrangian representation. Therefore it is necessary to consider representations of Hamiltonian structure that, unlike (3.1), are not restricted to canonical form.

One such form is Hamilton's principle, which for a canonical system is written as

$$\delta \int_{t_1}^{t_2} (p_i \dot{q}_i - H) \, \mathrm{d}t = 0, \tag{3.3}$$

under variations $\delta p_i(t), \delta q_i(t)$ satisfying $\delta q_i(t_1) = \delta q_i(t_2) = 0$, and where $\dot{q}_i = dq_i/dt$. Writing $f(p, \dot{p}, q, \dot{q}, t) = p_i \dot{q}_i - H$, the Euler-Lagrange equations

$$\begin{aligned}
\frac{d}{dt}\left(\frac{\partial f}{\partial \dot{q}_j}\right) - \frac{\partial f}{\partial q_j} &= 0, \\
\frac{d}{dt}\left(\frac{\partial f}{\partial \dot{p}_j}\right) - \frac{\partial f}{\partial p_j} &= 0,
\end{aligned} \tag{3.4}$$

can be used to derive (3.1).

A dynamical formulation that permits noncanonical representations is the symplectic form

$$\frac{du_i}{dt} = J_{ij}\frac{\partial H(u)}{\partial u_j}, \tag{3.5}$$

where u_i is the dynamical variable and H is the Hamiltonian function. The tensor J_{ij} is skew-symmetric and satisfies the Jacobi condition $\epsilon_{ijk} J_{im}\frac{\partial J_{ik}}{\partial u_m} = 0$. This representation naturally shows the invariance of the Hamiltonian for conservative systems,

$$\frac{dH}{dt} = \frac{\partial H}{\partial u_i}\frac{du_i}{dt} = \frac{\partial H}{\partial u_i} J_{ij} \frac{\partial H}{\partial u_j} = 0, \tag{3.6}$$

by the skew-symmetry of J. The search for Hamiltonian structure should not be framed in terms of the canonical form (3.1) but should rather consist of identifying the fundamental objects $u, H(u)$ and J, and demonstrating that J possesses the requisite abstract-algebraic properties.

The canonical representation (3.1) is obtained from the symplectic form (3.5) for the choice $u = [q_1, \ldots, q_N, p_1, \ldots, p_N]^T, J = \begin{pmatrix} 0 & I \\ -I & 0 \end{pmatrix}$. Whenever J is nonsingular it can locally be brought into the canonical form by an appropriate coordinate transformation. The symplectic form (3.5) can be used for noncanonical dynamical representations with singular J's.

Noncanonical Hamiltonian systems not only posses invariants such as energy and momentum but can also posses so-called Casimir invariants. These invariants are not associated with the Hamiltonian function itself but arise from the degenerate nature of the symplectic tensor J. Casimir invariants C are the solution of

$$J_{ij}\frac{\partial C}{\partial u_j} = 0. \tag{3.7}$$

The solutions of this equation are indeed invariant, since

$$\frac{dC}{dt} = \frac{\partial C}{\partial u_i}\frac{du_i}{dt} = \frac{\partial C}{\partial u_i}J_{ij}\frac{\partial H}{\partial u_j} = -\frac{\partial H}{\partial u_i}J_{ij}\frac{\partial C}{\partial u_j} = 0 \tag{3.8}$$

by the skew-symmetry of J and (3.7).

A canonical system possesses only trivial Casimirs. A canonical system corresponds to an invertible J and from (3.7) follows that the Casimirs C are constants. Noncanonical systems possess nontrivial Casimirs. Noncanonical systems correspond to a singular J and nontrivial solutions of (3.7) may exist.

An alternative notation for the symplectic form of Hamiltonian dynamics is the Poisson bracket. The bracket $[\cdot,\cdot]$ of any two functions of state $F(u)$ and $G(u)$ is defined by

$$[F,G] = \frac{\partial F}{\partial u_i}J_{ij}\frac{\partial G}{\partial u_j} \tag{3.9}$$

and is a bilinear, skew-symmetric map producing another function of state. The bracket corresponding to the canonical system (3.1) is

$$[F,G] = \frac{\partial F}{\partial q_i}\frac{\partial G}{\partial p_i} - \frac{\partial F}{\partial p_i}\frac{\partial G}{\partial q_i}. \tag{3.10}$$

The time evolution of any function of state $F(u)$ is determined by

$$\frac{dF}{dt} = \frac{\partial F}{\partial u_i}\frac{du_i}{dt} = \frac{\partial F}{\partial u_i}J_{ij}\frac{\partial H(u)}{\partial u_j}[F,H], \tag{3.11}$$

where H is the Hamiltonian and (3.5) and (3.9) have been used. Casimirs are those functions of state that annihilate all other functions of state under the bracket. The Casimirs C are the solution of

$$[C,F] = 0 \quad \forall F. \tag{3.12}$$

3-2 Infinite Dimensional Dynamical Systems

The equations of fluid dynamics are continuous in space and thus represent infinite dimensional dynamical systems. Much of the Hamiltonian dynamics for finite dimensional systems carries over to the infinite dimensional case. Instead of the system of ordinary differential equations (3.5), a system of partial differential equations is obtained. Functions of state become functionals of state: the variables of fluid mechanics, e.g. velocity, depend on the position vector and time, and the functionals of state map this function of a vector to the real line. Instead of the partial derivative, $\frac{\partial F}{\partial u_i}$, a functional or variational derivative, $\frac{\delta \mathcal{F}}{\delta u}$, needs to be used, which is defined as

$$\delta\mathcal{F} = \mathcal{F}(u + \delta u) - \mathcal{F}(u) = \left(\frac{\delta\mathcal{F}}{\delta u}, \delta u\right) + \mathcal{O}(\delta u^2), \tag{3.13}$$

where $(\cdot,\cdot)$ is the inner product for the function space $\{u\}$. The Hamiltonian dynamics can then be represented in a form similar to (3.5)

$$u_t = \mathcal{J}\frac{\delta\mathcal{H}}{\delta u}, \tag{3.14}$$

where u_t is the partial derivative of u with respect to t, $\mathcal{H}(u)$ is the Hamiltonian functional and $\mathcal{J}$ is a skew-symmetric transformation from $\{u\}$ to $\{u\}$, satisfying $(u, \mathcal{J}v) = -(\mathcal{J}u, v)$ as well as the Jacobi condition. The Poisson bracket notation provides also in the infinite dimensional case an equivalent expression to the symplectic form (3.14),

$$\frac{d\mathcal{F}}{dt} = \{\mathcal{F}, \mathcal{H}\} = \left(\frac{\delta\mathcal{F}}{\delta u}, \mathcal{J}\frac{\delta\mathcal{H}}{\delta u} \right). \tag{3.15}$$

The Poisson bracket $\{\mathcal{F}, \mathcal{H}\}$ has to satisfy (Salmon, 1988a; Morrison, 1998)

- skew-symmetry: $\{\mathcal{F}, \mathcal{H}\} = -\{\mathcal{H}, \mathcal{F}\}$,

- linearity: $\{\alpha\mathcal{F} + \beta\mathcal{G}, \mathcal{H}\} = \alpha\{\mathcal{F}, \mathcal{H}\} + \beta\{\mathcal{G}, \mathcal{H}\}$,

- Jacobi identity: $\{\mathcal{F}, \{\mathcal{G}, \mathcal{H}\}\} + \{\mathcal{G}, \{\mathcal{H}, \mathcal{F}\}\} + \{\mathcal{H}, \{\mathcal{F}, \mathcal{G}\}\} = 0$,

- Leibniz identity: $\{\mathcal{F}\mathcal{G}, \mathcal{H}\} = \mathcal{F}\{\mathcal{G}, \mathcal{H}\} + \{\mathcal{F}, \mathcal{H}\}\mathcal{G}$,

where α and β are constants.

As in the finite dimensional case, the system (3.14) or (3.15) possesses two sorts of invariants: those associated with the symmetry of the Hamiltonian system itself and the Casimir invariants. The first invariants can be found with Noether's theorem.

Theorem 1. *Noether's Theorem: If $\mathcal{H}$ is invariant under translation in (the coordinate) χ and if the functional $\mathcal{M}$ satisfies $\mathcal{J}\frac{\delta\mathcal{M}}{\delta u} = -u_\chi$, then $\mathcal{M}$ is invariant in time.*

For example, using $\chi = t$ and $\mathcal{M} = -\mathcal{H}$, the Hamiltonian, in Noether's theorem reveals that the Hamiltonian is invariant in time. Noether's theorem can be used to find many more invariants in time, corresponding to continuous symmetries of the Hamiltonian.

The other type of invariants are the Casimir invariants. Similar to (3.7), they are the solution of

$$\mathcal{J}\frac{\delta\mathcal{C}}{\delta u} = 0 \quad \text{or} \quad \{\mathcal{C}, \mathcal{F}\} = 0 \quad \forall F. \tag{3.16}$$

3-3   Two-Dimensional Incompressible Flow

In this section two-dimensional incompressible flow is considered. This serves as an example of the abstract theory of the previous two sections. The example discussed in this section and other examples can be found in Shepherd (1990). In vorticity-streamfunction formulation the governing equation is

$$\frac{\partial q}{\partial t} = \frac{\partial \phi}{\partial y}\frac{\partial q}{\partial x} - \frac{\partial \phi}{\partial x}\frac{\partial q}{\partial y} = -\partial(\phi, q), \tag{3.17}$$

where $q = \nabla^2\phi$ is the vorticity, ϕ is a streamfunction and $\partial(a, b) = a_y b_x - a_x b_y$, where indices denote partial derivatives. Further assume the domain is simply connected and has a solid boundary. Then no flow can pass the boundary. The system is Hamiltonian and can be put into the form of (3.14) with

$$u = q, \qquad \mathcal{J} = -\partial(q, \cdot), \qquad \mathcal{H} = \int_\Omega \frac{1}{2}\left|\nabla\phi\right|^2 \, \mathrm{d}\underline{x}. \tag{3.18}$$

The functional derivative of $\mathcal{H}$ follows from

$$\begin{aligned}
\delta\mathcal{H} &= \delta\int_\Omega \frac{1}{2}|\nabla\phi|^2\,\mathrm{d}\underline{x} \\
&= \int_\Omega \nabla\phi.\delta\nabla\phi\,\mathrm{d}\underline{x} \\
&= -\int_\Omega \phi\delta\nabla^2\phi\,\mathrm{d}\underline{x} \\
&= -\int_\Omega \phi\delta q\,\mathrm{d}\underline{x}
\end{aligned}$$

(3.19)

as

$$\frac{\delta\mathcal{H}}{\delta q} = -\phi. \tag{3.20}$$

Substituting (3.18) and (3.20) into (3.14) yields (3.17). The dynamics can also be expressed using a Poisson bracket, in the form of (3.15)

$$\{\mathcal{F},\mathcal{G}\} = -\int_\Omega \frac{\delta\mathcal{F}}{\delta q}\partial\left(q,\frac{\delta\mathcal{G}}{\delta q}\right)\mathrm{d}\underline{x} = \int_\Omega q\partial\left(\frac{\delta\mathcal{F}}{\delta q},\frac{\delta\mathcal{G}}{\delta q}\right)\mathrm{d}\underline{x}, \tag{3.21}$$

by integration by parts, for solid wall boundary conditions in a simply connected domain. Substituting q for $\mathcal{F}$, $\mathcal{H}$ for $\mathcal{G}$ and using (3.20) yields again (3.17).

The system possesses two types of invariants, those associated with the symmetries of the system and the Casimirs. The form of $\mathcal{J}$ in (3.18) is singular since any function of q in the argument yields zero. The Casimirs of the system are found using (3.16), i.e.

$$\mathcal{J}\frac{\delta\mathcal{C}}{\delta q} = -\partial\left(q,\frac{\delta\mathcal{C}}{\delta q}\right) = 0. \tag{3.22}$$

The solutions are

$$\frac{\delta\mathcal{C}}{\delta q} = C'(q) \Leftrightarrow \mathcal{C} = \int_\Omega C(q)\,\mathrm{d}\underline{x}, \tag{3.23}$$

for some function $C(q)$. Two well-known special cases of Casimirs are the total circulation $\int_\Omega q\,\mathrm{d}\underline{x}$ and the enstrophy $\int_\Omega \frac{1}{2}q^2\,\mathrm{d}\underline{x}$.

The other type of invariants are associated with the symmetries of the Hamiltonian system. These are found using Noether's Theorem. When there is a temporal symmetry a functional $\mathcal{M}$ is sought such that

$$\mathcal{J}\frac{\delta\mathcal{M}}{\delta q} = -q_t \qquad \Leftrightarrow \qquad \partial\left(q,\frac{\delta\mathcal{M}}{\delta q}\right) = q_t. \tag{3.24}$$

From (3.18) and (3.20) follow that $\mathcal{M} = -\mathcal{H}$. So the temporal symmetry corresponds to the conservation of the Hamiltonian, the total energy, in time. When there is a spatial symmetry in x, Noether's Theorem implies

$$\partial\left(q,\frac{\delta\mathcal{M}}{\delta q}\right) = q_x. \tag{3.25}$$

The solution is

$$\frac{\delta\mathcal{M}}{\delta q} = y \qquad \Leftrightarrow \qquad \mathcal{M} = \int_\Omega yq\,\mathrm{d}\underline{x}, \tag{3.26}$$

which is the x-component of Kelvin's impulse. When there is a spatial symmetry in y the y-component of Kelvin's impulse appears. Expressing the vorticity in terms of the velocity, with $\underline{v} = (u, v)$, yields

$$\mathcal{M} = \int_\Omega y \left(\frac{\partial v}{\partial u} - \frac{\partial u}{\partial v} \right) \, \mathrm{d}\underline{x} = - \int_\Omega u \, \mathrm{d}\underline{x} \tag{3.27}$$

by integrating by parts, using the solid wall boundary condition. Kelvin's impulse is related to the ordinary momentum. So the spatial symmetry in the x-direction corresponds to the conservation of momentum in the x-direction. When there is a symmetry in angular coordinate θ yields conservation of angular momentum

$$\mathcal{M} = \int_\Omega r^2 q \, \mathrm{d}\underline{x}. \tag{3.28}$$

All these conserved quantities are well known to fluid dynamicists. The Hamiltonian framework yields a natural way to reveal these conserved quantities through the symmetries of the system or the degenerate nature of the dynamics.

Another form that satisfies (3.14) is

$$u = q, \qquad \mathcal{J} = -\partial(\phi, \cdot), \qquad \mathcal{H} = \int_\Omega \frac{1}{2} q^2 \, \mathrm{d}\underline{x}. \tag{3.29}$$

This also yields (3.17). However the Casimirs are functions of ϕ and not q and are thus wrong. The reason (3.29) does not yield the correct Casimirs is that it is not a Hamiltonian system; the operator $\mathcal{J}$ does not satisfy the Jacobi condition. So (3.14) and (3.15) must not only yield the correct equations of motion but also satisfy the other requirements, i.e., the Jacobi condition.

3-4 Wave-Activity Conservation Laws

The interest of fluid dynamicists often concerns perturbations around a basic state. Expressions for these perturbations are sought by linearizing the full, nonlinear dynamics of the system around this basic state. A wave activity is defined to be a conserved disturbance quantity that is quadratic in the disturbance fields in the limit of small-amplitude disturbances. In this work, the interest is in constructing the available potential energy to the perturbations given a certain background state.

Consider the energy of a fluid dynamics system, given by the kinetic and potential energy (neglecting the internal energy)

$$\mathcal{H} = \int_\Omega \left[\frac{1}{2} \rho |\underline{v}|^2 + g\rho z \right] \, \mathrm{d}\underline{x},$$

where ρ is the density, $\underline{v}$ the velocity, g the gravitational acceleration and $\underline{x} = (x, y, z)^T$ the Cartesian coordinates. Suppose the system is to be linearized around a rest state. Usually, perturbations around a basic state are substituted,

$$\underline{v} = \underline{0} + \epsilon \underline{v}',$$
$$\rho = \rho_0(z) + \epsilon \rho',$$

where ϵ is a small parameter and the subscript 0 denotes the basic state, into the total energy to obtain

$$\mathcal{H} = \int_\Omega \left[\frac{1}{2}(\rho_0(z) + \epsilon\rho')|\epsilon\underline{v}'|^2 + g(\rho_0(z) + \epsilon\rho')z \right] \, \mathrm{d}\underline{x}. \tag{3.30}$$

Immediately a problem becomes clear. The kinetic energy term is $\mathcal{O}(\epsilon^2)$, while the potential energy term is $\mathcal{O}(1)$. Since energy conversions between kinetic and potential energy occur it seems unlikely that the kinetic energy is much smaller than the potential energy and would be neglected in usual linear perturbation theory. One could subtract a term $g\rho_0 z$ from the total energy, but the potential energy would still remain $\mathcal{O}(\epsilon)$, much larger than the kinetic energy.

This example makes it clear that other conservation laws than the conservation of energy are needed to evaluate the energy available for the disturbances given a background state. The reason that additional conservation laws are needed is clear when considering the fluid system in a Hamiltonian formulation. As the Eulerian description of fluid systems is noncanonical, Casimir invariants exist. It is these invariants that require the use of additional conservation laws to derive the available energy for perturbations, or the pseudo-energy (Shepherd, 1993).

Suppose a fluid system has a steady basic state $\underline{u} = \underline{U}$. Then

$$0 = \frac{\partial \underline{u}}{\partial t} = \mathcal{J} \left. \frac{\delta \mathcal{H}}{\delta \underline{u}} \right|_{\underline{u}=\underline{U}}, \tag{3.31}$$

where $|_{\underline{u}=\underline{U}}$ means evaluation at the steady basic state $\underline{U}$. For a canonical system, $\mathcal{J}$ is invertible and $\delta\mathcal{H}/\delta\underline{u} = 0$ at $\underline{u} = \underline{U}$. Then $\mathcal{H}(\underline{u}) - \mathcal{H}(\underline{U})$ is the energy available to the disturbances and is quadratic in the disturbance amplitude. For a noncanonical system, $\mathcal{J}$ is singular, and none of this follows. (3.30) is $\mathcal{H}(\underline{u})$ and the term $g\rho_0 z$ is $\mathcal{H}(\underline{U})$, but the available energy for perturbations is linear in the disturbance amplitude.

From (3.31) and the definition of Casimir invariants (3.16), a Casimir $\mathcal{C}$ can be found such that

$$\left. \frac{\delta \mathcal{H}}{\delta \underline{u}} \right|_{\underline{u}=\underline{U}} = - \left. \frac{\delta \mathcal{C}}{\delta \underline{u}} \right|_{\underline{u}=\underline{U}}. \tag{3.32}$$

Now a new functional can be constructed,

$$\mathcal{A} = \mathcal{H}(\underline{u}) - \mathcal{H}(\underline{U}) + \mathcal{C}(\underline{u}) - \mathcal{C}(\underline{U}), \tag{3.33}$$

that is an exact invariant of the nonlinear dynamics (Shepherd, 1990). It is of quadratic order in disturbance amplitude, because

$$\delta\mathcal{A} = \left(\left. \frac{\delta \mathcal{A}}{\delta \underline{u}} \right|_{\underline{u}=\underline{U}}, \delta\underline{u} \right) + \mathcal{O}\left(\delta\underline{u}^2\right) = \left(\left. \frac{\delta \mathcal{H}}{\delta \underline{u}} \right|_{\underline{u}=\underline{U}} + \left. \frac{\delta \mathcal{C}}{\delta \underline{u}} \right|_{\underline{u}=\underline{U}}, \delta\underline{u} \right) + \mathcal{O}\left(\delta\underline{u}^2\right) = \mathcal{O}\left(\delta\underline{u}^2\right),$$

which follows from (3.13) and (3.32). $\mathcal{A}$ is the pseudo-energy, the energy available to perturbations. In Section 4-3, this is used to derive the available energy after linearizing around a basic state.

3-5 Symplecticity

The reason for considering the Hamiltonian structure as a starting point for the design of numerical methods is symplecticity.

Let J be the skew-symmetric matrix

$$J = \begin{pmatrix} 0 & I_d \\ -I_d & 0 \end{pmatrix},$$

where I_d is the identity matrix of dimension d. A linear map $A : \mathbb{R}^{2d} \to \mathbb{R}^{2d}$ is called symplectic if (Hairer et al., 2006)

$$A^T J A = J.$$

In the case $d = 1$ symplecticity is the same as area preservation. The solution of the canonical Hamiltonian system (3.5) induces a transformation ψ on the phase space $\mathbb{R}^{2d}$ with associated Jacobian matrix, ψ'. Such a map is symplectic if

$$\psi'^T J \psi' = J. \tag{3.34}$$

If ψ and ϕ are symplectic then

$$(\psi'\phi')^T J(\psi'\phi') = \phi'^T \psi'^T J \psi' \phi' = \phi'^T J \phi' = J, \tag{3.35}$$

so the map $\psi \circ \phi$ is also symplectic. The flow (over time) is the mapping which, to any point y_0 in phase space, associates the value of the solution $y(t)$ with initial condition $y(t = 0) = y_0$.

Theorem 2. *Poincaré: The flow induced by a Hamiltonian H of a canonical system is symplectic.*

Hairer et al. (2006) have shown that symplecticity holds if and only if a flow is Hamiltonian.

For noncanonical Hamiltonian systems, where J is not invertible, a small subtlety exists: The Darboux-Lie theorem states that every noncanonical Hamiltonian system can be at least locally written in canonical Hamiltonian form after a suitable change of variables. Hence the flow ψ for noncanonical systems is locally symplectic in the new coordinates.

3-6 Dirac Bracket

Dirac's theory of constraints (Dirac, 1958), (Dirac, 2001) is used to pass from a compressible Hamiltonian formulation to an incompressible Hamiltonian formulation. The case in this thesis is simpler than the general case considered by Dirac since the constraints that are to be placed on the compressible system are known.

Let

$$\phi_l(q, p) = 0 \tag{3.36}$$

be N_l independent constraints with $l = 1, \ldots, N_L$ independent constraints. The exact Lagrangian (3.3) should be stationary with respect to these constraints, i.e.

$$\delta \int_{t_1}^{t_2} (p_i \dot{q}_i - H - \mu_l \phi_l)\, \mathrm{d}t = 0,$$

for variations δu_i and $\delta \mu_l$, where μ_l are the Lagrange multipliers corresponding to the constraints 3.36. This can be seen as transforming the Hamiltonian from H to $H + \mu_l \phi_l$. Using the Euler-Lagrange equations the system (3.1) can be derived for the constrained dynamics

$$
\begin{aligned}
\frac{dq_i}{dt} &= \frac{\partial H}{\partial p_i} + \mu_l \frac{\partial \phi_l}{\partial p_i}, \\
\frac{dp_i}{dt} &= -\frac{\partial H}{\partial q_i} - \mu_l \frac{\partial \phi_l}{\partial q_i}.
\end{aligned}
\tag{3.37}
$$

Using the definition of a canonical Poisson bracket (3.10) the system can be written as

$$
\frac{dF}{dt} = [F, H] + \sum_l \mu_l \left[F, \phi_l \right],
\tag{3.38}
$$

for F any function of the q's and p's (Dirac, 1958).

This incorporation of constraints carries over to the infinite dimensional case. Let $\mathcal{F}$ be a general state function. The change in $\mathcal{F}$ given constraints (3.36) is then (Salmon, 1988b)

$$
\frac{d\mathcal{F}}{dt} \approx \{\mathcal{F}, \mathcal{H}\} + \sum_l \mu_l \{\mathcal{F}, \phi_l\}
\tag{3.39}
$$

and the Lagrange multipliers μ_l must satisfy

$$
\frac{d\phi_l}{dt} \approx 0 \approx \{\phi_l, \mathcal{H}\} + \sum_m \mu_m \{\phi_l, \phi_m\}.
\tag{3.40}
$$

The wavy inequality sign indicates that the constraints must not be applied before working out the Poisson brackets for otherwise these Poisson brackets would no longer be well defined.

Let $\phi_l(p, q)$ be a set of constraints. If $\{\phi_l, \phi_z\}$ is non-singular everywhere then (3.40) allows the Lagrange multipliers to be defined uniquely. Suppose one of the $\{\phi_l, \phi_z\}$ is singular, then the Lagrange multiplier μ_m cannot be determined directly from (3.40), but new constraints

$$
0 \approx \{\phi_l, \mathcal{H}\}
$$

are obtained. The new constraints are enforced as additional constraints on the system and this process repeats until no new constraints appear and the resulting constraints are called consistent. Otherwise, the approach is rendered inconsistent.

Chapter 4

Hamiltonian Description of Internal Gravity Waves

To derive a phase space conserving discretization of the equations governing internal gravity waves the Hamiltonian structure introduced in Chapter 3 is used. However, it must first be shown that these equations from Chapter 2 posses this Hamiltonian structure. The derived geometric structure is used in Chapter 5 to find an exactly energy conserving discretization. The Poisson bracket for the stratified Euler equations is not known yet. This chapter details a complete derivation of this Poisson bracket. It is shown how to apply the different approximations known for partial differential equations to the Poisson bracket.

The Hamiltonian structure of the equations governing internal gravity waves is derived in this chapter. The goal is to show that the equations governing internal waves posses this structure and to find this structure. For this, the derivation starts in Section 4-1 with the primitive Euler equations of fluid motion, for which Morrison (1982) gave the Hamiltonian structure. These primitive Euler equations hold for compressible flows and since the incompressible equations governing internal waves are used the Poisson bracket must be adapted for incompressible flows. Eventually this will be done by the use of Dirac brackets to enforce a zero perturbation pressure. This zero perturbation pressure follows from a Mach number analysis. To enforce this constraint a change of variables in the Poisson bracket is performed; the entropy variable is replaced by the pressure variable. To simplify the Poisson structure the velocity variable is replaced by a momentum variable. These variable transformations are performed in Section 4-2. The next step is the linearization around a resting state with the stratified background density. The equations governing internal waves describe perturbations to this background state and the Hamiltonian formulation needs to be adapted. This is done in Section 4-3.

After linearization the equations are nondimensionalized in Section 4-4, which allows the Mach number analysis and the derivation of the constraint to enforce the incompressibility of the flow. These constraints are then enforced in Section 4-5 to arrive at the incompressible equations of motion for internal gravity waves. In Section 4-6 the Boussinesq approximation is applied to this Poisson bracket.

4-1   Primitive Euler Equations

The primitive Euler equations governing ideal fluids are given by the momentum equations, the continuity equation and conservation of entropy

$$
\begin{aligned}
\frac{\partial \underline{v}}{\partial t} &= -(\underline{v}.\nabla)\underline{v} - \frac{1}{\rho}\nabla p - \nabla(gz), \\
\frac{\partial \rho}{\partial t} &= -\nabla.(\rho\underline{v}), \\
\frac{\partial s}{\partial t} &= -\underline{v}.\nabla s.
\end{aligned}
\tag{4.1}
$$

The system is completed with the thermodynamic relations

$$
\begin{aligned}
\delta U &= T\delta s + \frac{p}{\rho^2}\delta\rho, \\
\delta h &= T\delta s + \frac{1}{\rho}\delta p,
\end{aligned}
\tag{4.2}
$$

where $U(s,\rho)$ is the internal energy and $h(s,p)$ the enthalpy. The Poisson bracket for this system of equations is (Morrison & Greene, 1980; Morrison, 1982)

$$
\{\mathcal{F},\mathcal{G}\} = \int_\Omega \left[-\frac{\delta\mathcal{F}}{\delta\rho}\nabla.\frac{\delta\mathcal{G}}{\delta\underline{v}} + \frac{\delta\mathcal{G}}{\delta\rho}\nabla.\frac{\delta\mathcal{F}}{\delta\underline{v}} + \frac{\nabla\times\underline{v}}{\rho}.\left(\frac{\delta\mathcal{F}}{\delta\underline{v}}\times\frac{\delta\mathcal{G}}{\delta\underline{v}}\right) + \frac{\nabla s}{\rho}.\left(\frac{\delta\mathcal{F}}{\delta\underline{v}}\frac{\delta\mathcal{G}}{\delta s} - \frac{\delta\mathcal{G}}{\delta\underline{v}}\frac{\delta\mathcal{F}}{\delta s}\right) \right] \,\mathrm{d}\underline{x}.
\tag{4.3}
$$

The Hamiltonian for this system corresponds to the total energy of the system, i.e. the sum of the kinetic, internal and potential energies,

$$
\mathcal{H} = \int_\Omega \left[\frac{1}{2}\rho|\underline{v}|^2 + \rho U(\rho,s) + g\rho z \right] \,\mathrm{d}\underline{x}.
\tag{4.4}
$$

This Hamiltonian with this Poisson bracket yield (4.1). To check this take the variation of the Hamiltonian

$$
\delta\mathcal{H} = \int_\Omega \left[\rho\underline{v}.\delta\underline{v} + \rho\left(\frac{\partial U(\rho,s)}{\partial s}\right)_\rho \delta s + \left(\frac{1}{2}|\underline{v}|^2 + gz + \left(\frac{\partial(\rho U(\rho,s))}{\partial\rho}\right)_s\right)\delta\rho \right] \,\mathrm{d}\underline{x},
\tag{4.5}
$$

where the subscript indicates which variable is held constant. Using the definition of the internal energy (4.2) the partial derivatives are evaluated as

$$
\delta\mathcal{H} = \int_\Omega \left[\rho\underline{v}.\delta\underline{v} + \rho T\delta s + \left(\frac{1}{2}|\underline{v}|^2 + gz + U + \frac{p}{\rho}\right)\delta\rho \right] \,\mathrm{d}\underline{x}.
\tag{4.6}
$$

Substituting these variations into the Poisson bracket (4.3) yields

$$
\begin{aligned}
\frac{dF}{dt} = \{\mathcal{F},\mathcal{H}\} = \int_\Omega \Bigg[&-\frac{\delta\mathcal{F}}{\delta\rho}\nabla.(\rho\underline{v}) + \left(\frac{1}{2}|\underline{v}|^2 + gz + U + \frac{p}{\rho}\right)\nabla.\frac{\delta\mathcal{F}}{\delta\underline{v}} \\
&+ \frac{\nabla\times\underline{v}}{\rho}.\left(\frac{\delta\mathcal{F}}{\delta\underline{v}}\times(\rho\underline{v})\right) + \frac{\nabla s}{\rho}.\left(\frac{\delta\mathcal{F}}{\delta\underline{v}}(\rho T) - (\rho\underline{v})\frac{\delta\mathcal{F}}{\delta s}\right) \Bigg] \,\mathrm{d}\underline{x}.
\end{aligned}
$$

To obtain (4.1) the functionals are chosen as

$$\mathcal{F}_{\underline{v}} = \int_{\Omega} \underline{v}(\underline{x}, t).\underline{\phi}_{\underline{v}}(\underline{x}) \, d\underline{x},$$

$$\mathcal{F}_{\rho} = \int_{\Omega} \rho(\underline{x}, t)\phi_{\rho}(\underline{x}) \, d\underline{x}, \tag{4.7}$$

$$\mathcal{F}_{s} = \int_{\Omega} s(\underline{x}, t)\phi_{s}(\underline{x}) \, d\underline{x},$$

with $\phi_{\rho}, \phi_{s} \in \mathcal{Q}$ and $\underline{\phi}_{\underline{v}} \in \mathcal{Y}$ arbitrary test functions, where

$$\mathcal{Q} = \left\{ \phi \in L^{2}(\Omega) \right\},$$

$$\mathcal{Y} = \left\{ \underline{\phi} \in \left(L^{2}(\Omega) \right)^{3} \text{ and } \nabla.\underline{\phi} \in L^{2}(\Omega) : \hat{\underline{n}}.\underline{\phi} = 0 \text{ at } \partial\Omega \right\}, \tag{4.8}$$

where $L^{2}(\Omega)$ is the space of square integrable functions on Ω. The space of restricted test functions, $\mathcal{Y}$, ensures the satisfaction of the solid wall boundary condition. The functional derivatives of (4.7) are

$$\frac{\delta\mathcal{F}_{\underline{v}}}{\delta\underline{v}} = \underline{\phi}_{\underline{v}}(\underline{x}), \quad \frac{\delta\mathcal{F}_{\rho}}{\delta\rho} = \phi_{\rho}(\underline{x}), \quad \frac{\delta\mathcal{F}_{s}}{\delta s} = \phi_{s}(\underline{x}). \tag{4.9}$$

Using these functionals in the bracket formulation yields

$$\frac{\partial\rho}{\partial t} = -\nabla.(\rho\underline{v}),$$

$$\frac{\partial s}{\partial t} = -\underline{v}.\nabla s,$$

$$\frac{\partial\underline{v}}{\partial t} = -\nabla(\frac{1}{2}|\underline{v}|^{2}) + \underline{v} \times (\nabla \times \underline{v}) - \nabla(gz) - \nabla(U + \frac{p}{\rho}) + T\nabla s,$$

where the scalar triple product and $\frac{\delta\mathcal{F}}{\delta\underline{v}}.\left((\nabla \times \underline{v})/\rho \times (\rho\underline{v})\right) = -\frac{\delta\mathcal{F}}{\delta\underline{v}}.\left(\underline{v} \times \nabla \times \underline{v}\right)$, have been used. The first two equations correspond to the conservation of mass and entropy of (4.1). The velocity equation differs from the velocity equation of (4.1) but can be brought into this form by using the vector identity $\nabla(\frac{1}{2}|\underline{v}|^{2}) = \underline{v} \times (\nabla \times \underline{v}) + (\underline{v}.\nabla)\underline{v}$ and the thermodynamic relation $-\nabla(U + p/\rho) + T\nabla s = -\nabla h + T\nabla s = -\frac{1}{\rho}\nabla p$:

$$\frac{\partial\underline{v}}{\partial t} = -(\underline{v}.\nabla)\underline{v} - \nabla(gz) - \frac{1}{\rho}\nabla p.$$

So the Poisson bracket (4.3) and the Hamiltonian (4.4) yield (4.1).

4-2   Transformation to Pressure Variable

Eventually the Hamiltonian structure will be constrained. This constraint will be placed on the pressure variations. To apply this constraint more easily the Hamiltonian structure is cast in one including a pressure variable instead of an entropy variable. To simplify the Poisson bracket the velocity variable is transformed into the momentum per unit volume, $\rho\underline{v}$. The

Poisson bracket (4.3) and the Hamiltonian (4.4) are to be transformed from the variables $(\underline{v}, \rho, s)^T$ to the variables $(\rho \underline{v}, \rho, p)^T$. From the thermodynamic relations (4.2) the pressure is defined as $p = \rho^2 \frac{\partial U(\rho, s)}{\partial \rho}$, so the pressure depends on the density and entropy: $p = p(\rho, s)$ and

$$\delta p = \left(\frac{\partial p}{\partial s} \right)_\rho \delta s + \left(\frac{\partial p}{\partial \rho} \right)_s \delta \rho. \tag{4.10}$$

From this relation the time evolution of the pressure can be found

$$\frac{\partial p}{\partial t} = \left(\frac{\partial p}{\partial s} \right)_\rho \frac{\partial s}{\partial t} + \left(\frac{\partial p}{\partial \rho} \right)_s \frac{\partial \rho}{\partial t} = - \left(\frac{\partial p}{\partial s} \right)_\rho \underline{v}.\nabla s - c_s^2 \nabla.(\rho \underline{v}) = -\underline{v}.\nabla p - c_s^2 \rho \nabla.(\underline{v}), \tag{4.11}$$

where the continuity equation and conservation of entropy equation have been used and $c_s^2 = \left(\frac{\partial p}{\partial \rho} \right)_s$ is the speed of sound squared. The terms $\left(\frac{\partial p}{\partial s} \right)_\rho$ and $c_s^2 = \left(\frac{\partial p}{\partial \rho} \right)_s$ are not assumed constant. The time evolution of the momentum equation is given by

$$\frac{\partial(\rho \underline{v})}{\partial t} = \rho \frac{\partial \underline{v}}{\partial t} + \underline{v} \frac{\partial \rho}{\partial t} = -\rho(\underline{v}.\nabla)\underline{v} - \rho g \hat{\underline{z}} - \nabla p - \underline{v} \nabla.(\rho \underline{v}). \tag{4.12}$$

To transform the derivatives in the Poisson bracket a functional chain rule is needed. Let $\mathcal{F}[\psi]$ be a general functional with functions $\psi(x) = (\psi^1, \psi^2, \ldots, \psi^\nu)$ and $x = (x_1, x_2, \ldots x_n)$. Let ψ be related to $\chi = (\chi^1, \chi^2, \ldots, \chi^\mu)$ in an arbitrary, possibly nonlinear and non-invertible way: $\psi^i = \psi^i[\chi], i = 1, 2, \ldots, \nu$. A variation of ψ induced by χ requires linearization (Morrison, 1998)

$$\delta \psi^i = \frac{\delta \psi^i}{\delta \chi^j} \delta \chi^j, \quad j = 1, 2, \ldots, \mu. \tag{4.13}$$

Substituting (4.13) into a functional $\mathcal{F}$ and using (3.13) to relate the variations yields

$$\left(\frac{\delta \mathcal{F}}{\delta \chi}, \delta \chi \right) = \left(\frac{\delta \mathcal{F}}{\delta \psi}, \delta \psi \right) = \left(\frac{\delta \mathcal{F}}{\delta \psi}, \frac{\delta \psi}{\delta \chi} \delta \chi \right) = \left(\left(\frac{\delta \psi}{\delta \chi} \right)^\dagger \frac{\delta \mathcal{F}}{\delta \psi}, \delta \chi \right), \tag{4.14}$$

where † indicates the adjoint. Taking the adjoint requires a careful analysis of the boundary conditions. Only for suitable boundary conditions this can be done. Then variations of $\mathcal{F}$ are related by

$$\frac{\delta \mathcal{F}}{\delta \chi^j} = \left(\frac{\delta \psi^i}{\delta \chi^j} \right)^\dagger \frac{\delta \mathcal{F}}{\delta \psi^i}. \tag{4.15}$$

Returning to the transformation of the primitive fluid dynamic equations, the transformation for a general state function $\mathcal{F}$ is

$$\begin{aligned}
\frac{\delta \mathcal{F}}{\delta \underline{v}} &= \left(\frac{\delta(\rho \underline{v})}{\delta \underline{v}} \right)^\dagger \frac{\delta \mathcal{F}}{\delta(\rho \underline{v})} + \left(\frac{\delta \rho}{\delta \underline{v}} \right)^\dagger \frac{\delta \mathcal{F}}{\delta \rho} + \left(\frac{\delta p}{\delta \underline{v}} \right)^\dagger \frac{\delta \mathcal{F}}{\delta p}, \\
\frac{\delta \mathcal{F}}{\delta \rho} &= \left(\frac{\delta(\rho \underline{v})}{\delta \rho} \right)^\dagger \frac{\delta \mathcal{F}}{\delta(\rho \underline{v})} + \left(\frac{\delta \rho}{\delta \rho} \right)^\dagger \frac{\delta \mathcal{F}}{\delta \rho} + \left(\frac{\delta p}{\delta \rho} \right)^\dagger \frac{\delta \mathcal{F}}{\delta p}, \\
\frac{\delta \mathcal{F}}{\delta s} &= \left(\frac{\delta(\rho \underline{v})}{\delta s} \right)^\dagger \frac{\delta \mathcal{F}}{\delta(\rho \underline{v})} + \left(\frac{\delta \rho}{\delta s} \right)^\dagger \frac{\delta \mathcal{F}}{\delta \rho} + \left(\frac{\delta p}{\delta s} \right)^\dagger \frac{\delta \mathcal{F}}{\delta p},
\end{aligned} \tag{4.16}$$

where with each the variation on the right-hand side the other variables are held constant. It is clear that the velocity is independent of the pressure and density and that the density variation with entropy at constant density is zero.

The transformation reduces to

$$
\begin{aligned}
\frac{\delta \mathcal{F}}{\delta \underline{v}} &= \rho \frac{\delta \mathcal{F}}{\delta(\rho \underline{v})}, \\
\frac{\delta \mathcal{F}}{\delta \rho} &= \underline{v} \cdot \frac{\delta \mathcal{F}}{\delta(\rho \underline{v})} + \frac{\delta \mathcal{F}}{\delta \rho} + c_s^2 \frac{\delta \mathcal{F}}{\delta p}, \\
\frac{\delta \mathcal{F}}{\delta s} &= \left(\frac{\partial p}{\partial s}\right)_\rho \frac{\delta \mathcal{F}}{\delta p}.
\end{aligned}
\tag{4.17}
$$

Using these expressions in the Poisson bracket (4.3) yields

$$
\begin{aligned}
\{\mathcal{F}, \mathcal{G}\} = \int_\Omega \bigg[&-\left(\underline{v} \cdot \frac{\delta \mathcal{F}}{\delta(\rho \underline{v})} + \frac{\delta \mathcal{F}}{\delta \rho} + c_s^2 \frac{\delta \mathcal{F}}{\delta p}\right) \nabla \cdot \left(\rho \frac{\delta \mathcal{G}}{\delta(\rho \underline{v})}\right) \\
&+ \left(\underline{v} \cdot \frac{\delta \mathcal{G}}{\delta(\rho \underline{v})} + \frac{\delta \mathcal{G}}{\delta \rho} + c_s^2 \frac{\delta \mathcal{G}}{\delta p}\right) \nabla \cdot \left(\rho \frac{\delta \mathcal{F}}{\delta(\rho \underline{v})}\right) \\
&+ \frac{\nabla \times \underline{v}}{\rho} \cdot \left(\left(\rho \frac{\delta \mathcal{F}}{\delta(\rho \underline{v})}\right) \times \left(\rho \frac{\delta \mathcal{G}}{\delta(\rho \underline{v})}\right)\right) \\
&+ \frac{\nabla s}{\rho} \cdot \left(\left(\rho \frac{\delta \mathcal{F}}{\delta(\rho \underline{v})}\right)\left(\left(\frac{\partial p}{\partial s}\right)_\rho \frac{\delta \mathcal{G}}{\delta p}\right) - \left(\rho \frac{\delta \mathcal{G}}{\delta(\rho \underline{v})}\right)\left(\left(\frac{\partial p}{\partial s}\right)_\rho \frac{\delta \mathcal{F}}{\delta p}\right)\right) \bigg] \, \mathrm{d}\underline{x}.
\end{aligned}
\tag{4.18}
$$

Using a similar relation to (4.10) for gradients, this can be rewritten into

$$
\begin{aligned}
\{\mathcal{F}, \mathcal{G}\} = \int_\Omega \bigg[&\frac{\delta \mathcal{G}}{\delta \rho} \nabla \cdot \left(\rho \frac{\delta \mathcal{F}}{\delta(\rho \underline{v})}\right) - \frac{\delta \mathcal{F}}{\delta \rho} \nabla \cdot \left(\rho \frac{\delta \mathcal{G}}{\delta(\rho \underline{v})}\right) \\
&+ \frac{\delta \mathcal{F}}{\delta p}\left(-\nabla p \cdot \frac{\delta \mathcal{G}}{\delta(\rho \underline{v})} - c_s^2 \rho \nabla \cdot \frac{\delta \mathcal{G}}{\delta(\rho \underline{v})}\right) \\
&- \frac{\delta \mathcal{G}}{\delta p}\left(-\nabla p \cdot \frac{\delta \mathcal{F}}{\delta(\rho \underline{v})} - c_s^2 \rho \nabla \cdot \frac{\delta \mathcal{F}}{\delta(\rho \underline{v})}\right) \\
&+ \rho \nabla \times \underline{v} \cdot \left(\frac{\delta \mathcal{F}}{\delta(\rho \underline{v})} \times \frac{\delta \mathcal{G}}{\delta(\rho \underline{v})}\right) \\
&- \underline{v} \cdot \frac{\delta \mathcal{F}}{\delta(\rho \underline{v})} \nabla \cdot \left(\rho \frac{\delta \mathcal{G}}{\delta(\rho \underline{v})}\right) + \underline{v} \cdot \frac{\delta \mathcal{G}}{\delta(\rho \underline{v})} \nabla \cdot \left(\rho \frac{\delta \mathcal{F}}{\delta(\rho \underline{v})}\right) \bigg] \, \mathrm{d}\underline{x}.
\end{aligned}
\tag{4.19}
$$

The Hamiltonian (4.4) is simply rewritten into

$$
\mathcal{H} = \int_\Omega \left[\frac{1}{2}\rho|\underline{v}|^2 + \rho \tilde{U}(\rho, p) + g\rho z\right] \, \mathrm{d}\underline{x},
\tag{4.20}
$$

where $\tilde{U}(\rho, p)$ is the internal energy as a function of density and pressure. This rewritten Hamiltonian and Poisson bracket yield (4.1) when replacing the entropy equation with the pressure equation (4.11). To check this take the variation of the Hamiltonian

$$
\delta \mathcal{H} = \int_\Omega \left[\underline{v} \cdot \delta(\rho \underline{v}) + \rho \left(\frac{\partial \tilde{U}(\rho, p)}{\partial p}\right)_\rho \delta p + \left(-\frac{1}{2}|\underline{v}|^2 + gz + \left(\frac{\partial(\rho \tilde{U}(\rho, p))}{\partial \rho}\right)_p\right) \delta \rho \right] \, \mathrm{d}\underline{x}.
$$

Note that the square of the velocity in the density variation is now negative. In (4.5) the variation of the Hamiltonian with density was performed at constant velocity while here this variation is performed at constant momentum. Using the definition of the internal energy (4.2) the partial derivatives can be evaluated as

$$
\left(\frac{\partial \tilde{U}}{\partial p}\right)_\rho = \left(\frac{\partial U}{\partial s}\frac{\partial s}{\partial p}\right)_\rho = T\left(\frac{\partial s}{\partial p}\right)_\rho,
$$

$$
\left(\frac{\partial \tilde{U}}{\partial \rho}\right)_p = \left(\frac{\partial U}{\partial \rho}\right)_s + \left(\frac{\partial U}{\partial s}\right)_\rho\left(\frac{\partial s}{\partial \rho}\right)_p = \frac{p}{\rho^2} + T\left(\frac{\partial s}{\partial \rho}\right)_p.
$$

Substituting these variations into the Poisson bracket (4.19) yields

$$
\begin{aligned}
\{\mathcal{F}, \mathcal{H}\} = \int_\Omega \Bigg[&\left(-\frac{1}{2}|\underline{v}|^2 + gz + U + \frac{p}{\rho} + \left(\frac{\partial s}{\partial \rho}\right)_p \rho T\right)\nabla.\left(\rho\frac{\delta \mathcal{F}}{\delta(\rho\underline{v})}\right) - \frac{\delta\mathcal{F}}{\delta\rho}\nabla.(\rho\underline{v}) \\
&+ \frac{\delta\mathcal{F}}{\delta p}\left(-\nabla p.\underline{v} - c_s^2\rho\nabla.\underline{v}\right) \\
&- \rho T\left(\frac{\partial s}{\partial p}\right)_\rho\left(-\nabla p.\frac{\delta\mathcal{F}}{\delta(\rho\underline{v})} - c_s^2\rho\nabla.\frac{\delta\mathcal{F}}{\delta(\rho\underline{v})}\right) \\
&+ \rho\nabla\times\underline{v}\left(\frac{\delta\mathcal{F}}{\delta(\rho\underline{v})}\times\underline{v}\right) \\
&- \underline{v}.\frac{\delta\mathcal{F}}{\delta(\rho\underline{v})}\nabla.(\rho\underline{v}) + |\bar{v}|^2\nabla.\left(\rho\frac{\delta\mathcal{F}}{\delta(\rho\underline{v})}\right)\Bigg]\,\mathrm{d}\underline{x}.
\end{aligned}
$$

The density and pressure equations are equal to (4.1) and (4.11). The momentum equation needs further evaluation

$$
\begin{aligned}
\frac{\partial(\rho\underline{v})}{\partial t} = &-\rho\nabla\left(-\frac{1}{2}|\underline{v}|^2 + gz + U + \frac{p}{\rho} + \left(\frac{\partial s}{\partial \rho}\right)_p \rho T\right) + \rho T\left(\frac{\partial s}{\partial p}\right)_\rho\nabla p \\
&- \nabla\left(\left(\frac{\partial s}{\partial p}\right)_\rho c_s^2\rho^2 T\right) \quad - \rho\nabla\times\underline{v}\times\underline{v} - \underline{v}\nabla(\rho\underline{v}) - \rho\nabla(|\underline{v}|^2).
\end{aligned} \tag{4.21}
$$

The triple product rule for the thermodynamic quantities pressure, density and entropy is given by

$$
\left(\frac{\partial p}{\partial \rho}\right)_s\left(\frac{\partial s}{\partial p}\right)_\rho\left(\frac{\partial \rho}{\partial s}\right)_p = -1. \tag{4.22}
$$

Using the relations $\nabla\left(U + \frac{p}{\rho}\right) = \nabla h$, $-\nabla h + T\nabla s = -\frac{1}{\rho}\nabla p$ and $\nabla\left(-\frac{1}{2}|\underline{v}|^2\right) + \underline{v}\times(\nabla\times\underline{v}) = -(\underline{v}.\nabla)\underline{v}$ yields

$$
\frac{\partial(\rho\underline{v})}{\partial t} = -\rho(\underline{v}.\nabla)\underline{v} - \rho g\hat{\underline{z}} - \nabla p - \underline{v}\nabla.(\rho\underline{v}), \tag{4.23}
$$

which is (4.12).

4-3   Linearization around Hydrostatic Rest State

The hydrostatic rest state is given by

$$
\begin{aligned}
\underline{v} &= \underline{0}, \\
\rho &= \rho_0(z), \\
p &= p_0(z), \\
s &= s_0(z),
\end{aligned}
\tag{4.24}
$$

where the hydrostatic pressure and density are related by $\nabla p_0 = -g\rho_0\hat{\underline{z}}$. The entropy basic state follows from the density and pressure basic states. To linearize the equations of motion the perturbations to the basic rest state are denoted by a prime:

$$
\begin{aligned}
\underline{v} &= \underline{0} + \epsilon \underline{v}', \\
\rho &= \rho_0(z) + \epsilon \rho', \\
p &= p_0(z) + \epsilon p', \\
s &= s_0(z) + \epsilon s',
\end{aligned}
$$

where ϵ is a small parameter. First, the equations of motion are linearized:

$$
\begin{aligned}
\frac{\partial((\rho_0(z) + \epsilon\rho')(\underline{0} + \epsilon\underline{v}'))}{\partial t} &= -(\rho_0(z) + \epsilon\rho')((\underline{0} + \epsilon\underline{v}').\nabla)(\underline{0} + \epsilon\underline{v}') - \nabla(p_0(z) + \epsilon p') \\
&\quad - (\rho_0(z) + \epsilon\rho')g\hat{\underline{z}} - (\underline{0} + \epsilon\underline{v}')\nabla.((\rho_0(z) + \epsilon\rho')(\underline{0} + \epsilon\underline{v}')), \\
\frac{\partial(\rho_0(z) + \epsilon\rho')}{\partial t} &= -\nabla.((\rho_0(z) + \epsilon\rho')(\underline{0} + \epsilon\underline{v}')), \\
\frac{\partial(p_0(z) + \epsilon p')}{\partial t} &= -(\underline{0} + \epsilon\underline{v}').\nabla(p_0(z) + \epsilon p') \\
&\quad - \left(\frac{\partial(p_0(z) + \epsilon p')}{\partial(\rho_0(z) + \epsilon\rho')}\right)_{s_0 + \epsilon s'} (\rho_0(z) + \epsilon\rho')\nabla.(\underline{0} + \epsilon\underline{v}')
\end{aligned}
$$

By neglected all second order terms in ϵ and using the hydrostatic balance the linearized equations of motion become

$$
\begin{aligned}
\frac{\partial(\rho_0\underline{v}')}{\partial t} &= -\rho'g\hat{\underline{z}} - \nabla p', \\
\frac{\partial\rho'}{\partial t} &= -\nabla.(\rho_0\underline{v}'), \\
\frac{\partial p'}{\partial t} &= \rho_0 g w' - c_0^2(z)\rho_0\nabla.\underline{v}',
\end{aligned}
\tag{4.25}
$$

where $c_0^2(z) = \left(\frac{\partial p_0}{\partial \rho_0}\right)_{s_0}$ is the speed of sound and w' is the vertical component of the velocity field $\underline{v}'$.

To linearize the Hamiltonian formulation both the Hamiltonian itself and the Poisson bracket need to be linearized. First the Hamiltonian will be linearized around the basic rest state. Following Shepherd (1990) the pseudo energy arises

$$
\mathcal{A}(\underline{u}) = \mathcal{H}(\underline{u}) - \mathcal{H}(\underline{U}) + \mathcal{C}(\underline{u}) - \mathcal{C}(\underline{U}),
\tag{4.26}
$$

where $\underline{u}$ is the state of a system, $\underline{U}$ the steady state, $\mathcal{H}$ the Hamiltonian and $\mathcal{C}$ a Casimir of the system. This pseudo-energy is an exact invariant of the nonlinear dynamics. The dynamics of the nonlinear system can be rewritten as

$$\frac{d\mathcal{F}}{dt} = \{\mathcal{F}, \mathcal{A}\}, \tag{4.27}$$

since the Hamiltonian is arbitrary to within constants and Casimirs. For small-amplitude disturbances, expand $\{\mathcal{F}, \mathcal{G}\}$ and $\mathcal{A}$ in powers of the disturbance amplitude. The leading-order contribution to the right-hand side will be linear in disturbance amplitude and will be obtained from the product of the $\mathcal{O}(1)$ approximation to $\{\mathcal{F}, \mathcal{G}\}$ (namely $\{\mathcal{F}, \mathcal{G}\}$ evaluated for the basic state) and the small-amplitude approximation to the pseudo-energy (Shepherd, 1990).

The $\mathcal{O}(1)$ approximation to the Poisson bracket (4.19) is given by

$$\begin{aligned}
\{\mathcal{F}, \mathcal{G}\} = \int_{\Omega} &\left[\frac{\delta\mathcal{G}}{\delta\rho'}\nabla\cdot\left(\rho_0\frac{\delta\mathcal{F}}{\delta(\rho_0\underline{v}')}\right) - \frac{\delta\mathcal{F}}{\delta\rho'}\nabla\cdot\left(\rho_0\frac{\delta\mathcal{G}}{\delta(\rho_0\underline{v}')}\right) \right.\\
&+ \frac{\delta\mathcal{F}}{\delta p'}\left(\rho_0 g\frac{\delta\mathcal{G}}{\delta(\rho_0 w')} - c_0^2(z)\rho_0\nabla\cdot\frac{\delta\mathcal{G}}{\delta(\rho_0\underline{v}')}\right)\\
&\left. - \frac{\delta\mathcal{G}}{\delta p'}\left(\rho_0 g\frac{\delta\mathcal{F}}{\delta(\rho_0 w')} - c_0^2(z)\rho_0\nabla\cdot\frac{\delta\mathcal{F}}{\delta(\rho_0\underline{v}')}\right) \right]\, \mathrm{d}\underline{x},
\end{aligned} \tag{4.28}$$

where hydrostatic balance has been used.

The next step is the evaluation of the pseudo-energy,

$$\mathcal{A}(\underline{u}) = \mathcal{H}(\underline{u}) - \mathcal{H}(\underline{U}) + \mathcal{C}(\underline{u}) - \mathcal{C}(\underline{U}), \tag{4.29}$$

where $\underline{u}$ is the state of a system, $\underline{U}$ the steady state, $\mathcal{H}$ the Hamiltonian and $\mathcal{C}$ a Casimir of the system. The Casimir $\mathcal{C}$ follows from

$$\left.\frac{\delta\mathcal{H}}{\delta u_j}\right|_{\underline{u}=\underline{U}} = -\left.\frac{\delta\mathcal{C}}{\delta u_j}\right|_{\underline{u}=\underline{U}}. \tag{4.30}$$

A general class of Casimir invariants for this system is (Shepherd, 1993)

$$\mathcal{C} = \int \rho C(s, q)\, \mathrm{d}\underline{x} \quad\text{with}\quad q = \frac{\nabla\times\underline{v}}{\rho}\cdot\nabla s, \tag{4.31}$$

where q is the potential vorticity and C is an arbitrary function with suitable boundary conditions. The functional derivatives are given by

$$\begin{aligned}
\frac{\delta\mathcal{C}}{\delta\underline{v}} &= \nabla\times\left(C_q\nabla s\right),\\
\frac{\delta\mathcal{C}}{\delta s} &= \rho C_s - \nabla\cdot\left(C_q\nabla\times\underline{v}\right),\\
\frac{\delta\mathcal{C}}{\delta\rho} &= C - qC_q,
\end{aligned} \tag{4.32}$$

where subscripts denote partial derivatives. (4.30) now implies

$$\frac{\delta\mathcal{H}}{\delta\underline{v}} = -\frac{\delta\mathcal{C}}{\delta\underline{v}},$$
$$\frac{\delta\mathcal{H}}{\delta s} = -\frac{\delta\mathcal{C}}{\delta s},$$
$$\frac{\delta\mathcal{H}}{\delta\rho} = -\frac{\delta\mathcal{C}}{\delta\rho},$$

at the basic rest state (4.24). Substituting the functional derivatives of the Casimir and of the Hamiltonian (4.6) and substituting the basic state yields $C_q = 0$ from the first condition and

$$C(s_0) = -gz - U(s_0, \rho_0) - \frac{p_0}{\rho_0},$$

from the third condition. This is the defining relation for $C(\cdot)$. Thus, the right hand side has to be expressed in the same argument s_0. This can be done by inverting the functional dependence $s_0(z)$ to obtain $\mathcal{Z}(s_0)$, where $\mathcal{Z}(s_0(z)) = z$. This is possible if $s_0(z)$ is monotonic in z, which is the case for a stably stratified basic state. Since z, ρ_0, p_0 and s_0 depend monotonically on z, functions $\mathcal{Z}$, $\mathcal{R}$ and $\mathcal{P}$ can be defined as

$$z = \mathcal{Z}(s_0),$$
$$\rho_0 = \mathcal{R}(s_0),$$
$$p_0 = \mathcal{P}(s_0).$$

The function C can now be written as

$$C(s) = -g\mathcal{Z}(s) - U(s, \mathcal{R}(s)) - \frac{\mathcal{P}(s)}{\mathcal{R}(s)},$$

which is consistent with the second condition. The exact expression for the available energy, or pseudo-energy, is then given by (Shepherd, 1993)

$$
\begin{aligned}
\mathcal{A} &= \mathcal{H}(\underline{u}) - \mathcal{H}(\underline{U}) + \mathcal{C}(\underline{u}) - \mathcal{C}(\underline{U}) \\
&= \int_\Omega \left[\frac{1}{2}\rho|(\underline{0} + \epsilon\underline{v}')|^2 + \rho U(\rho, s) + g\rho z \right] - \left[\frac{1}{2}\rho|\underline{0}|^2 + \rho_0 U(\rho_0, s_0) + g\rho_0 z \right] \\
&\quad + \rho\left[-g\mathcal{Z}(s) - U(s, \mathcal{R}(s)) - \frac{\mathcal{P}(s)}{\mathcal{R}(s)} \right] - \rho_0\left[-g\mathcal{Z}(s_0) - U(s_0, \mathcal{R}(s_0)) - \frac{\mathcal{P}(s_0)}{\mathcal{R}(s_0)} \right] \mathrm{d}\underline{x} \\
&= \int_\Omega \left[\frac{1}{2}\rho|\epsilon\underline{v}'|^2 + \rho g z - \rho g\mathcal{Z}(s) + \rho U(s, \rho) - \rho U(s, \mathcal{R}(s)) - \rho\frac{\mathcal{P}(s)}{\mathcal{R}(s)} + p_0 \right] \mathrm{d}\underline{x}
\end{aligned}
\tag{4.33}
$$

Andrews (1981) has shown that this expression in the small-amplitude limit reduces to

$$\mathcal{A} = \int_\Omega \left[\frac{1}{2}\rho_0|\underline{v}'|^2 + \frac{1}{2}\frac{g^2}{\rho_0 N^2}\left(\rho' - \frac{p'}{c_0^2(z)} \right)^2 + \frac{1}{2}\frac{p'^2}{\rho_0 c_0^2(z)} \right] \mathrm{d}\underline{x}, \tag{4.34}$$

which is accurate to second order in the perturbation quantities. The available potential energy of this pseudo-energy corresponds to Equation (6.14.8) of Gill (1982). The buoyancy frequency is given by

$$N^2 = -\frac{g}{\rho_0}\frac{d\rho_0}{dz} - \frac{g^2}{c_0^2(z)}. \tag{4.35}$$

The $\mathcal{O}(1)$ approximation to $\{\mathcal{F},\mathcal{G}\}$ and the small-amplitude approximation to the pseudo-energy yield the linearized equations of motion for the perturbations. Substituting the pseudo-energy (4.34) into the Poisson bracket (4.28) yields (4.25). The variation of the pseudo-energy is given by

$$\delta\mathcal{A} = \int_\Omega \left[\underline{v}'.\delta(\rho_0\underline{v}') + \frac{g^2}{\rho_0 N^2}\left(\rho' - \frac{p'}{c_0^2(z)}\right)\delta\rho' + \left(\frac{g^2}{\rho_0 N^2}\left(\frac{p'}{c_0^4(z)} - \frac{\rho'}{c_0^2(z)}\right) + \frac{p'}{\rho_0 c_0^2(z)}\right)\delta p' \right]\,\mathrm{d}\underline{x}$$

(4.36)

Substituting these variations into the Poisson bracket (4.28) yields

$$\{\mathcal{F},\mathcal{A}\} =$$
$$\int_\Omega \left[\frac{g^2}{\rho_0 N^2}\left(\rho' - \frac{p'}{c_0^2(z)}\right)\nabla.\left(\rho_0\frac{\delta\mathcal{F}}{\delta(\rho_0\underline{v}')}\right) - \frac{\delta\mathcal{F}}{\delta\rho'}\nabla.(\rho_0\underline{v}') + \frac{\delta\mathcal{F}}{\delta p'}\left(\rho_0 g w' - c_0^2(z)\rho_0\nabla.\underline{v}'\right) \right.$$
$$\left. - \left(\frac{g^2}{\rho_0 N^2}\left(\frac{p'}{c_0^4(z)} - \frac{\rho'}{c_0^2(z)}\right) + \frac{p'}{\rho_0 c_0^2(z)}\right)\left(\rho_0 g\frac{\delta\mathcal{F}}{\delta(\rho_0 w')} - c_0^2(z)\rho_0\nabla.\frac{\delta\mathcal{F}}{\delta(\rho_0\underline{v}')}\right) \right]\,\mathrm{d}\underline{x}.$$

(4.37)

The density and pressure equations are equal to those of (4.25). To evaluate the momentum equations, split the contributions in the horizontal direction, denoted by the subscript H, and the vertical direction. The momentum equations obtained from the bracket are

$$\frac{\partial(\rho_0\underline{v}'_H)}{\partial t} = -\rho_0\nabla_H\left(\frac{g^2}{\rho_0 N^2}\left(\rho' - \frac{p'}{c_0^2(z)}\right)\right)$$
$$- \nabla_H\left(c_0^2(z)\rho_0\left(\frac{g^2}{\rho_0 N^2}\left(\frac{p'}{c_0^4(z)} - \frac{\rho'}{c_0^2(z)}\right) + \frac{p'}{\rho_0 c_0^2(z)}\right)\right),$$
$$\frac{\partial(\rho_0 w')}{\partial t} = -\rho_0\frac{\partial}{\partial z}\left(\frac{g^2}{\rho_0 N^2}\left(\rho' - \frac{p'}{c_0^2(z)}\right)\right) - \rho_0 g\left(\frac{g^2}{\rho_0 N^2}\left(\frac{p'}{c_0^4(z)} - \frac{\rho'}{c_0^2(z)}\right) + \frac{p'}{\rho_0 c_0^2(z)}\right)$$
$$- \frac{\partial}{\partial z}\left(c_0^2(z)\rho_0\left(\frac{g^2}{\rho_0 N^2}\left(\frac{p'}{c_0^4(z)} - \frac{\rho'}{c_0^2(z)}\right) + \frac{p'}{\rho_0 c_0^2(z)}\right)\right),$$

(4.38)

where ∇_H is the gradient acting in the horizontal directions. Since the background density only varies in the vertical direction, the horizontal gradient does not act on the background density. Using $\frac{\partial\rho_0/\partial z}{\rho_0}\frac{g^2}{N^2} = -g - \frac{g^3}{c_0^2(z)N^2}$ yields

$$\frac{\partial(\rho_0\underline{v}'_H)}{\partial t} = -\nabla_H p',$$
$$\frac{\partial(\rho_0 w')}{\partial t} = -\frac{\partial p'}{\partial z} - g\rho',$$

(4.39)

coinciding precisely with (4.25).

4-4 Non-dimensionalizing

Before using the Dirac procedure to enforce the incompressibility of the system, (4.25), it is scaled. Denoting all dimensionall quantities with primes and all dimensionless quantities without primes the scaling is given by $(x',y') = L(x,y)$, $z' = Dz$, $(u',v') = U(u,v)$, $w' = Ww$, $\rho' = \bar{\rho}\rho$, $\rho_0' = \bar{\rho}\rho_0$, $p' = \bar{\rho}U^2 p$, $(c_0^2(z))' = c^2 c_0^2(z)$ and $t' = L/Ut$. The dimensionless equations

of motion are

$$
\begin{aligned}
\frac{\partial(\rho_0 \underline{v}_H)}{\partial t}\frac{\bar{\rho}U^2}{L} &= -\nabla_H p \frac{\bar{\rho}U^2}{L}, \\
\frac{\partial(\rho_0 w)}{\partial t}\frac{\bar{\rho}UW}{L} &= -\rho g\frac{\bar{\rho}}{1} - \frac{\partial p}{\partial z}\frac{\bar{\rho}U^2}{D}, \\
\frac{\partial \rho}{\partial t}\frac{U\bar{\rho}}{L} &= -\nabla_H.(\rho_0 \underline{v}_H)\frac{\bar{\rho}U}{L} - \frac{\partial}{\partial z}(\rho_0 w)\frac{\bar{\rho}W}{D}, \\
\frac{\partial p}{\partial t}\frac{U^3\bar{\rho}}{L} &= \rho_0 g w\frac{\bar{\rho}W}{1} - c_0^2(z)\rho_0\nabla_H.\underline{v}_H\frac{c^2\bar{\rho}U}{L} - c_0^2(z)\rho_0\frac{\partial}{\partial z}w\frac{c^2\bar{\rho}W}{D}.
\end{aligned}
\tag{4.40}
$$

Taking $D/W = L/U$, the dimensionless equations of motion become

$$
\begin{aligned}
\frac{\partial(\rho_0 \underline{v}_H)}{\partial t} &= -\nabla_H p, \\
\frac{\partial(\rho_0 w)}{\partial t} &= -\rho g\frac{L}{UW} - \frac{\partial p}{\partial z}\frac{UL}{DW}, \\
\frac{\partial \rho}{\partial t} &= -\nabla.(\rho_0 \underline{v}), \\
\frac{\partial p}{\partial t} &= \rho_0 g w\frac{WL}{U^3} - c_0^2(z)\rho_0\nabla.\underline{v}\frac{c^2}{U^2}.
\end{aligned}
\tag{4.41}
$$

Three dimensionless numbers, the Mach number $Ma = U/c$, the Froude number squared $Fr^2 = U^2/(gD)$ and the aspect ratio $\delta = D/L = W/U$, appear in the dimensionless equations of motion

$$
\begin{aligned}
\frac{\partial(\rho_0 \underline{v}_H)}{\partial t} &= -\nabla_H p, \\
\frac{\partial(\rho_0 w)}{\partial t} &= -\frac{1}{Fr^2\delta^2}\rho - \frac{1}{\delta^2}\frac{\partial p}{\partial z}, \\
\frac{\partial \rho}{\partial t} &= -\nabla.(\rho_0 \underline{v}), \\
\frac{\partial p}{\partial t} &= \frac{1}{Fr^2}\rho_0 w - \frac{1}{Ma^2}c_0^2(z)\rho_0\nabla.\underline{v}.
\end{aligned}
\tag{4.42}
$$

Introducing this scaling into the Hamiltonian (4.34) yields, after division by $\bar{\rho}U^2$,

$$
\mathcal{A} = \int_\Omega \frac{1}{2}\frac{1}{\rho_0}\left((\rho_0 u)^2 + (\rho_0 v)^2 + \delta^2(\rho_0 w)^2\right) + \frac{1}{2}\frac{1}{\delta^2 Fr^2}\frac{1}{\rho_0 N^2}\left(\rho - Ma^2\frac{p}{c_0^2}\right)^2 + \frac{1}{2}Ma^2\frac{p^2}{\rho_0 c_0^2}\,d\underline{x},
\tag{4.43}
$$

where the dimensionless buoyancy frequency is

$$
N^2 = -\frac{1}{Fr^2\delta^2}\frac{1}{\rho_0}\frac{d\rho_0}{dz} - \frac{Ma^2}{Fr^4\delta^2}\frac{1}{c_0^2(z)}.
\tag{4.44}
$$

The dimensionless Poisson bracket is given by

$$
\{\mathcal{F},\mathcal{G}\} = \int_\Omega \frac{\delta\mathcal{G}}{\delta\rho}\nabla.\left(\rho_0\begin{pmatrix}1\\1\\\frac{1}{\delta^2}\end{pmatrix}\star\frac{\delta\mathcal{F}}{\delta(\rho_0\underline{v})}\right) - \frac{\delta\mathcal{F}}{\delta\rho}\nabla.\left(\rho_0\begin{pmatrix}1\\1\\\frac{1}{\delta^2}\end{pmatrix}\star\frac{\delta\mathcal{G}}{\delta(\rho_0\underline{v})}\right)
$$
$$
+ \frac{\delta\mathcal{F}}{\delta p}\left(\rho_0\frac{1}{Fr^2\delta^2}\frac{\delta\mathcal{G}}{\delta(\rho_0 w)} - \frac{1}{Ma^2}c_0^2(z)\rho_0\nabla.\left(\begin{pmatrix}1\\1\\\frac{1}{\delta^2}\end{pmatrix}\star\frac{\delta\mathcal{G}}{\delta(\rho_0\underline{v})}\right)\right) \tag{4.45}
$$
$$
- \frac{\delta\mathcal{G}}{\delta p}\left(\rho_0\frac{1}{Fr^2\delta^2}\frac{\delta\mathcal{F}}{\delta(\rho_0 w)} - \frac{1}{Ma^2}c_0^2(z)\rho_0\nabla.\left(\begin{pmatrix}1\\1\\\frac{1}{\delta^2}\end{pmatrix}\star\frac{\delta\mathcal{F}}{\delta(\rho_0\underline{v})}\right)\right)\,\mathrm{d}\underline{x},
$$

where $\star$ indicates component-wise vector multiplication. Substituting (4.43) into (4.45) yields (4.42).

Rescaling (4.42) with $\underline{v} \propto Ma$ and $\rho \propto Ma$ and taking the divergence and curl of the momentum equations yields

$$
\frac{\partial(\nabla\times\underline{v})}{\partial t} = \nabla\times\left(-\frac{\hat{\underline{z}}}{\delta^2 Fr^2\rho_0}\rho\right),
$$
$$
\frac{\partial\rho}{\partial t} = -\nabla.(\rho_0\underline{v}),
$$
$$
\frac{\partial(\nabla.\underline{v})}{\partial t} + \frac{1}{Ma}\nabla.\left(\frac{\nabla_H p}{\rho_0} + \frac{\hat{\underline{z}}}{\delta^2\rho_0}\frac{\partial p}{\partial z}\right) = -\nabla.\left(\frac{\rho\hat{\underline{z}}}{Fr^2\delta^2\rho_0}\right), \tag{4.46}
$$
$$
\frac{\partial p}{\partial t} + \frac{1}{Ma}c_0^2(z)\rho_0\nabla.\underline{v} = \frac{Ma}{Fr^2}\rho_0 w.
$$

For an incompressible flow $c^2 \to \infty$ and consequently $Ma \to 0$. Multiplying (4.46-3) and (4.46-4) with Ma, under the assumption that $Fr = \mathcal{O}(1)$ and $\delta = \mathcal{O}(1)$, yields that the pressure perturbations must be zero (Bokhove, 2002). The stratification in density of the fluid results in a subtlety when taking the incompressible limit. The incompressibility constraint is

$$
\frac{1}{Fr^2}\rho_0 w - \frac{1}{Ma^2}c_0^2(z)\rho_0\nabla.\underline{v} = 0. \tag{4.47}
$$

For a homogeneous fluid, the first term in (4.47) disappears and taking the limit $Ma \to 0$ implies $\nabla.\underline{v} = 0$. From a perturbation perspective the stratified fluid behaves similar. Expanding the velocity $\underline{v}$ as

$$
\underline{v} = \underline{v}^0 + Ma^2\underline{v}^1 + \mathcal{O}\left(Ma^4\right), \tag{4.48}
$$

yields that the zeroth-order term, $\underline{v}^0$, is divergence-free, $\nabla.\underline{v}^0 = 0$. So taking the incompressible limit for a stratified fluid requires an extra perturbation expansion to obtain the incompressible equations of motion.

4-5   Dirac Bracket

Equations (4.25) hold for a compressible, stratified fluid. The linear equations of motion for a incompressible fluid are given by (2.14). Denoting the perturbation quantities with a prime, (2.14) is

$$
\begin{aligned}
\frac{\partial(\rho_0 \underline{v}')}{\partial t} &= -\rho' g\hat{\underline{z}} - \nabla P, \\
\frac{\partial \rho'}{\partial t} &= -\underline{v}'.\nabla(\rho_0), \\
p' &= 0, \quad \nabla.\underline{v}' = 0,
\end{aligned}
\tag{4.49}
$$

where the pressure P is no longer a thermodynamic variable but an arbitrary function that acts as a Lagrange multiplier to enforce a constant volume, i.e., that $\nabla.\underline{v}' = 0$. The thermodynamic pressure $p(\rho, s)$ converges to the pressure P in the following sense: $\nabla p(\rho, s) \to \nabla P$ as $Ma \to 0$.

From these equations the pressure field can be determined from a Poisson equation with Robin boundary conditions. Since the background density is constant in time, taking he divergence of the momentum equation and multiplying by this background density yields that

$$
\rho_0 \nabla.\left(\frac{1}{\rho_0}\nabla P\right) + \rho_0 \nabla.\left(\frac{\rho' g\hat{\underline{z}}}{\rho_0}\right) = 0.
\tag{4.50}
$$

Multiplying the momentum equations with the outward normal vector at the boundaries, $\hat{\underline{n}}$, and assuming a no slip boundary condition, $\hat{\underline{n}}.\underline{v}' = 0$, yields

$$
\frac{1}{\rho_0}\nabla P.\hat{\underline{n}} = -\frac{g\rho'\hat{\underline{z}}}{\rho_0}.\hat{\underline{n}},
\tag{4.51}
$$

at $\partial\Omega$. This equation and boundary condition specify the pressure field.

The pseudo-energy and the Poisson bracket for the incompressible equations of motion are obtained using Dirac brackets from the pseudo-energy (4.34) and the Poisson bracket (4.28) for the compressible equations of motion. By enforcing the constraint $p'(\underline{x}) = 0$, the time evolution of the perturbation pressure p' should be zero

$$
\frac{d\mathcal{F}[p']}{dt} \approx \{\mathcal{F}[p'], \mathcal{A}\} + \int_{\Omega'} \lambda_p(\underline{x}') \{\mathcal{F}[p'(\underline{x})], p'(\underline{x}')\}\, d\underline{x}' \approx 0.
\tag{4.52}
$$

where $\{\cdot, \cdot\}$ denotes the Poisson bracket (4.28) and λ_p is an unknown Lagrange multiplier that is to be determined. The wavy equality indicates the constraints can only applied after working out the Dirac bracket. From (4.28) it follows that $\{\mathcal{F}[p], p'\} = 0$, so λ_p stays undetermined. Hence, a secondary constraints arises,

$$
\{\mathcal{F}[p'], \mathcal{A}\} = 0.
$$

Working out this Poisson bracket yields

$$
0 = \{\mathcal{F}[p'], \mathcal{A}\} = \int_{\Omega} \frac{\delta\mathcal{F}[p']}{\delta p'}\left[\rho_0 g w' - \frac{c_0^2(z)}{Ma^2}\rho_0 \nabla.\underline{v}'\right]\, d\underline{x},
\tag{4.53}
$$

where the Mach number is explicitly shown to clarify the derivation. This implies

$$
g\rho_0 w' - \frac{c_0^2(z)}{Ma^2}\rho_0 \nabla.\underline{v}' = 0.
\tag{4.54}
$$

Here the complication due to the stratification arises: Consistency for the constraint $p' = 0$ does not quite lead to incompressibility, $\nabla.\underline{v}' = 0$, but includes an addition term $\mathcal{O}\left(Ma^2\right)$ smaller in magnitude than $\nabla.\underline{v}' = 0$. After completing the Dirac bracket the leading-order perturbations can be taken to recover incompressibility, $\nabla.\underline{v}' = 0$. However, (4.54) is a consistency condition and has to be enforced as a new constraint to ensure the evolution of the pressure perturbations is zero.

By enforcing both constraints, $p'(\underline{x}) = 0$ and $\Delta(\underline{x}) = g\rho_0 w' - c_0^2(z)/Ma^2\rho_0\nabla.\underline{v}' = 0$, the system becomes "incompressible". The two consistency requirements are stated in weak form by using two (different) arbitrary functionals $\mathcal{F}[p']$ and $\mathcal{F}[\Delta]$, as follows

$$
\begin{aligned}
\frac{d\mathcal{F}[p']}{dt} &= \{\mathcal{F}[p'], \mathcal{A}\} + \int_{\Omega'} \lambda_p(\underline{x}') \left\{\mathcal{F}[p'(\underline{x})], p'(\underline{x}')\right\} \, \mathrm{d}\underline{x}' \\
&\quad + \int_{\Omega'} \lambda_\Delta(\underline{x}') \left\{\mathcal{F}[p'(\underline{x})], \Delta(\underline{x}')\right\} \, \mathrm{d}\underline{x}' \approx 0, \\
\frac{d\mathcal{F}[\Delta]}{dt} &= \{\mathcal{F}[\Delta], \mathcal{A}\} + \int_{\Omega'} \lambda_p(\underline{x}') \left\{\mathcal{F}[\Delta(\underline{x})], p'(\underline{x}')\right\} \, \mathrm{d}\underline{x}' \\
&\quad + \int_{\Omega'} \lambda_\Delta(\underline{x}') \left\{\mathcal{F}[\Delta(\underline{x})], \Delta(\underline{x}')\right\} \, \mathrm{d}\underline{x}' \approx 0,
\end{aligned}
\tag{4.55}
$$

where the explicit time dependence of the Lagrange multipliers in the notation is dropped. These are two equations for the two unknown Lagrange multipliers λ_p and λ_Δ. From (4.28) the following terms are zero:

$$
\{\mathcal{F}[p'], p'\} = 0, \qquad \{\mathcal{F}[\Delta], \Delta\} = 0.
$$

The four remaining terms are evaluated one by one. After these terms have been evaluated they can be combined in (4.55) to determine the unknown Lagrange multipliers.

It will be useful to consider

$$
u(\underline{x}') = \int_\Omega \delta(\underline{x} - \underline{x}')u(\underline{x}) \, \mathrm{d}\underline{x},
$$

where $\delta(\underline{x} - \underline{x}')$ is the Dirac delta function. Applying (3.13) yields (Morrison, 1998)

$$
\int \frac{\delta u(\underline{x}')}{\delta u(\underline{x})} \, \mathrm{d}\underline{x} = \int \delta(\underline{x} - \underline{x}') \, \mathrm{d}\underline{x},
\tag{4.56}
$$

the infinite-dimensional analog of $\frac{\partial x_i}{\partial x_j} = \delta_{ij}$. Another useful identity can be found by considering

$$
\begin{aligned}
\delta\mathcal{F}[\Delta] \equiv \int_\Omega \frac{\delta\mathcal{F}[\Delta]}{\delta\Delta}\delta\Delta \, \mathrm{d}\underline{x} &= \int_\Omega \frac{\delta\mathcal{F}[\Delta]}{\delta\Delta}\delta\left(g\rho_0 w' - \frac{c_0^2(z)}{Ma^2}\rho_0\nabla.\underline{v}'\right) \, \mathrm{d}\underline{x} \\
&= \int_\Omega g\frac{\delta\mathcal{F}[\Delta]}{\delta\Delta}\delta(\rho_0 w') + \frac{1}{\rho_0}\nabla\left(\frac{c_0^2(z)}{Ma^2}\rho_0\frac{\delta\mathcal{F}[\Delta]}{\delta\Delta}\right).\delta(\rho_0\underline{v}') \, \mathrm{d}\underline{x}
\end{aligned}
$$

where $\hat{\underline{n}}.\delta\underline{v}' = 0$ as boundary condition was used. It follows that

$$
\begin{aligned}
\frac{\delta\mathcal{F}[\Delta]}{\delta(\rho_0\underline{w}')} &= g\frac{\delta\mathcal{F}[\Delta]}{\delta\Delta} + \frac{1}{\rho_0}\frac{\partial}{\partial z}\left(\frac{c_0^2(z)}{Ma^2}\rho_0\frac{\delta\mathcal{F}[\Delta]}{\delta\Delta}\right), \\
\frac{\delta\mathcal{F}[\Delta]}{\delta(\rho_0\underline{v}')} &= g\hat{\underline{z}}\frac{\delta\mathcal{F}[\Delta]}{\delta\Delta} + \frac{1}{\rho_0}\nabla\left(\frac{c_0^2(z)}{Ma^2}\rho_0\frac{\delta\mathcal{F}[\Delta]}{\delta\Delta}\right).
\end{aligned}
\tag{4.57}
$$

To evaluate (4.55-1), consider the variation of the perturbation pressure, the first constraint, with arbitrary functional $\mathcal{G}$

$$\{\mathcal{F}[p'],\mathcal{G}\} = \int_\Omega \frac{\delta\mathcal{F}[p']}{\delta p'} \left[\rho_0 g \frac{\delta\mathcal{G}}{\delta(\rho_0 w')} - \frac{c_0^2(z)}{Ma^2}\rho_0\nabla.\left(\frac{\delta\mathcal{G}}{\delta(\rho_0\underline{v}')}\right) \right]\, \mathrm{d}\underline{x}. \tag{4.58}$$

Substituting for $\mathcal{G}$ in (4.58) the Hamiltonian $\mathcal{A}$, (4.34), yields

$$\{\mathcal{F}[p'],\mathcal{A}\} = \int_\Omega \frac{\delta\mathcal{F}[p']}{\delta p'} \left[\rho_0 g w' - \frac{c_0^2(z)}{Ma^2}\rho_0\nabla.\underline{v}' \right]\, \mathrm{d}\underline{x}. \tag{4.59}$$

Substituting for $\mathcal{G}$ in (4.58) the constraint $\Delta(\underline{x}')$, (4.54), yields

$$\{\mathcal{F}[p'(\underline{x})],\Delta(\underline{x}')\} = \int_\Omega \frac{\delta\mathcal{F}[p'(\underline{x})]}{\delta p'} \left[\rho_0 g \frac{\delta\Delta(\underline{x}')}{\delta(\rho_0 w'(\underline{x}))} - \frac{c_0^2(z)}{Ma^2}\rho_0\nabla.\left(\frac{\delta\Delta(\underline{x}')}{\delta(\rho_0\underline{v}'(\underline{x}))}\right) \right]\, \mathrm{d}\underline{x}. \tag{4.60}$$

The second nonzero term of (4.55-1) then becomes

$$\int_{\Omega'}\lambda_\Delta(\underline{x}')\left\{\mathcal{F}[p'(\underline{x})],\Delta(\underline{x}')\right\}\, \mathrm{d}\underline{x}' =$$

$$\int_{\Omega'}\lambda_\Delta(\underline{x}')\int_\Omega \frac{\delta\mathcal{F}[p']}{\delta p'(\underline{x})} \left[\rho_0 g \frac{\delta(g\rho_0 w'(\underline{x}') - \frac{c_0^2(z)}{Ma^2}\rho_0\nabla'.\underline{v}'(\underline{x}'))}{\delta(\rho_0 w'(\underline{x}))} \right.$$

$$\left. -\frac{c_0^2(z)}{Ma^2}\rho_0\nabla.\frac{\delta(g\rho_0 w'(\underline{x}') - \frac{c_0^2(z)}{Ma^2}\rho_0\nabla'.\underline{v}'(\underline{x}'))}{\delta(\rho_0\underline{v}'(\underline{x}))} \right]\, \mathrm{d}\underline{x}\mathrm{d}\underline{x}'. \tag{4.61}$$

Applying integration by parts in $\underline{x}$ yields

$$\int_{\Omega'}\lambda_\Delta(\underline{x}')\left\{\mathcal{F}[p'(\underline{x})],\Delta(\underline{x}')\right\}\, \mathrm{d}\underline{x}' =$$

$$\int_{\Omega'}\lambda_\Delta(\underline{x}')\int_\Omega \frac{\delta\mathcal{F}[p']}{\delta p'(\underline{x})} \left[\rho_0 g^2 \frac{\delta(\rho_0 w'(\underline{x}'))}{\delta(\rho_0 w'(\underline{x}))} - \rho_0^2 g\frac{c_0^2(z)}{Ma^2}\frac{\delta(\nabla'.\underline{v}'(\underline{x}'))}{\delta(\rho_0 w'(\underline{x}))} \right]$$

$$+ \nabla\left(\frac{c_0^2(z)}{Ma^2}\rho_0\frac{\delta\mathcal{F}[p']}{\delta p'(\underline{x})}\right)\cdot\left[g\frac{\delta(\rho_0 w'(\underline{x}'))}{\delta(\rho_0\underline{v}'(\underline{x}))} - \frac{c_0^2(z)}{Ma^2}\rho_0\frac{\delta(\nabla'.\underline{v}'(\underline{x}'))}{\delta(\rho_0\underline{v}'(\underline{x}))} \right]\, \mathrm{d}\underline{x}\mathrm{d}\underline{x}'$$

$$- \int_{\Omega'}\lambda_\Delta(\underline{x}')\int_{\partial\Omega} \frac{c_0^2(z)}{Ma^2}\rho_0\frac{\delta\mathcal{F}[p']}{\delta p'(\underline{x})}\hat{n}.\left[g\frac{\delta(\rho_0 w'(\underline{x}'))}{\delta(\rho_0\underline{v}'(\underline{x}))} - \frac{c_0^2(z)}{Ma^2}\rho_0\frac{\delta(\nabla'.\underline{v}'(\underline{x}'))}{\delta(\rho_0\underline{v}'(\underline{x}))} \right]\, \mathrm{d}\underline{S}\mathrm{d}\underline{x}'. \tag{4.62}$$

The boundary term is zero since (Nurijanyan et al., 2013)

$$n_i\partial_j\left(\frac{\delta v_j'(\underline{x}')}{\delta v_i'(\underline{x})}\right) = \delta_{ij}\partial_i\left(n_i\frac{\delta v_i'(\underline{x})}{\delta v_i'(\underline{x}')}\right), \tag{4.63}$$

by (4.56) and $n_i \delta v_i' = \delta(n_i v_i') = 0$ at $\partial \Omega$. Applying integration by parts in $\underline{x}'$ yields

$$
\int_{\Omega'} \lambda_\Delta(\underline{x}') \left\{ \mathcal{F}[p'(\underline{x})], \Delta(\underline{x}') \right\} \, \mathrm{d}\underline{x}' =
$$

$$
\int_{\Omega'} \lambda_\Delta(\underline{x}') \int_\Omega \frac{\delta \mathcal{F}[p']}{\delta p'(\underline{x})} \rho_0 g^2 \frac{\delta(w'(\underline{x}'))}{\delta(w'(\underline{x}))} + g\nabla \left(\frac{c_0^2(z)}{Ma^2} \rho_0 \frac{\delta \mathcal{F}[p']}{\delta p'(\underline{x})} \right) \cdot \frac{\delta(w'(\underline{x}'))}{\delta(\underline{v}'(\underline{x}))} \, \mathrm{d}\underline{x}\mathrm{d}\underline{x}'
$$

$$
+ \int_{\Omega'} \nabla'\lambda_\Delta(\underline{x}') \cdot \int_\Omega \frac{\delta \mathcal{F}[p']}{\delta p'(\underline{x})} \rho_0 g \frac{c_0^2(z)}{Ma^2} \frac{\delta(\underline{v}'(\underline{x}'))}{\delta(w'(\underline{x}))} + \frac{c_0^2(z)}{Ma^2} \nabla \left(\frac{c_0^2(z)}{Ma^2} \rho_0 \frac{\delta \mathcal{F}[p']}{\delta p'(\underline{x})} \right) \frac{\delta(\underline{v}'(\underline{x}'))}{\delta(\underline{v}'(\underline{x}))} \, \mathrm{d}\underline{x}\mathrm{d}\underline{x}'
$$

$$
- \int_{\partial\Omega'} \lambda_\Delta(\underline{x}') \int_\Omega \frac{\delta \mathcal{F}[p']}{\delta p'(\underline{x})} \rho_0 g \frac{c_0^2(z)}{Ma^2} \hat{n}' \cdot \frac{\delta(\underline{v}'(\underline{x}'))}{\delta(w'(\underline{x}))} + \frac{c_0^2(z)}{Ma^2} \nabla \left(\frac{c_0^2(z)}{Ma^2} \rho_0 \frac{\delta \mathcal{F}[p']}{\delta p'(\underline{x})} \right) \hat{n}' \cdot \frac{\delta(\underline{v}'(\underline{x}'))}{\delta(\underline{v}'(\underline{x}))} \, \mathrm{d}\underline{x}\mathrm{d}\underline{x}'.
$$

$$(4.64)$$

The boundary term is again zero due to (4.63). Applying the infinite-dimensional analog of the delta function, (4.56), yields

$$
\int_{\Omega'} \lambda_\Delta(\underline{x}') \left\{ \mathcal{F}[p'(\underline{x})], \Delta(\underline{x}') \right\} \, \mathrm{d}\underline{x}' =
$$

$$
\int_{\Omega'} \lambda_\Delta \frac{\delta \mathcal{F}[p']}{\delta p'} \rho_0 g^2 + g\lambda_\Delta \frac{\partial}{\partial z} \left(\frac{c_0^2(z)}{Ma^2} \rho_0 \frac{\delta \mathcal{F}[p']}{\delta p'} \right)
$$

$$
+ \frac{\partial \lambda_\Delta}{\partial z} \frac{\delta \mathcal{F}[p']}{\delta p'} \rho_0 g \frac{c_0^2(z)}{Ma^2} + \frac{c_0^2(z)}{Ma^2} \nabla \lambda_\Delta \cdot \nabla \left(\frac{c_0^2(z)}{Ma^2} \rho_0 \frac{\delta \mathcal{F}[p']}{\delta p'} \right) \, \mathrm{d}\underline{x}',
$$

$$(4.65)$$

where the explicit dependence on $\underline{x}'$ has been dropped. Applying integration by parts to free the variations of the functional $\mathcal{F}[p']$ from derivatives yields

$$
\int_{\Omega'} \lambda_\Delta(\underline{x}') \left\{ \mathcal{F}[p'(\underline{x})], \Delta(\underline{x}') \right\} \, \mathrm{d}\underline{x}' =
$$

$$
\int_{\Omega'} \frac{\delta \mathcal{F}[p']}{\delta p'} \left[\rho_0 g^2 \lambda_\Delta - \frac{c_0^2(z)}{Ma^2} \rho_0 \nabla \cdot \left(\frac{c_0^2(z)}{Ma^2} \nabla \lambda_\Delta \right) \right] \, \mathrm{d}\underline{x}'
$$

$$
+ \int_{\delta\Omega'} \frac{\delta \mathcal{F}[p']}{\delta p'} \left[g\rho_0 \frac{c_0^2(z)}{Ma^2} \lambda_\Delta + \frac{c_0^4(z)}{Ma^4} \rho_0 \frac{\partial \lambda_\Delta}{\partial n} \right] \, \mathrm{d}\underline{S}',
$$

$$(4.66)$$

where two terms in the interior canceled and $\partial/\partial n$ is the outward derivative. Using the arbitrariness of the functional $\mathcal{F}[p']$ in the interior and at the boundary,

$$
\rho_0 g^2 \lambda_\Delta - \frac{c_0^2(z)}{Ma^2} \rho_0 \nabla \cdot \left(\frac{c_0^2(z)}{Ma^2} \nabla \lambda_\Delta \right) = 0, \qquad \text{in } \Omega,
$$

$$
g\rho_0 \frac{c_0^2(z)}{Ma^2} \lambda_\Delta + \frac{c_0^4(z)}{Ma^4} \rho_0 \frac{\partial \lambda_\Delta}{\partial n} = 0, \qquad \text{at } \partial\Omega,
$$

$$(4.67)$$

are found. The most simple λ_Δ satisfying (4.67) is $\lambda_\Delta = 0$.

To evaluate (4.55-2), consider the variation of Δ, the second constraint, with arbitrary functional $\mathcal{G}$

$$
\{\mathcal{F}[\Delta], \mathcal{G}\} = \int_\Omega \frac{\delta \mathcal{G}}{\delta \rho'} \nabla \cdot \left(\rho_0 \frac{\delta \mathcal{F}[\Delta]}{\delta(\rho_0 \underline{v}')} \right) - \frac{\delta \mathcal{G}}{\delta p'} \left(\rho_0 g \frac{\delta \mathcal{F}[\Delta]}{\delta(\rho_0 w')} - \frac{c_0^2}{Ma^2} \rho_0 \nabla \cdot \frac{\mathcal{F}[\Delta]}{\delta(\rho_0 \underline{v}')} \right) \, \mathrm{d}\underline{x}. \quad (4.68)
$$

Integrating by parts and rearranging yields

$$
\begin{aligned}
\{\mathcal{F}[\Delta], \mathcal{G}\} = \int_{\Omega} &-\frac{\delta\mathcal{F}[\Delta]}{\delta(\rho_0\underline{v}')}\cdot\rho_0\nabla\left(\frac{\delta\mathcal{G}}{\delta\rho'} + \frac{c_0^2}{Ma^2}\frac{\delta\mathcal{G}}{\delta p'}\right) - \frac{\delta\mathcal{F}[\Delta]}{\delta(\rho_0 w')}\left(\rho_0 g + \frac{c_0^2}{Ma^2}\frac{d\rho_0}{dz}\right)\frac{\delta\mathcal{G}}{\delta p'}\, \mathrm{d}\underline{x}\\
&+ \int_{\partial\Omega}\hat{\underline{n}}\cdot\frac{\delta\mathcal{F}[\Delta]}{\delta(\rho_0\underline{v}')}\rho_0\left(\frac{\delta\mathcal{G}}{\delta\rho'} + \frac{c_0^2}{Ma^2}\frac{\delta\mathcal{G}}{\delta p'}\right)\, \mathrm{d}\underline{S}.
\end{aligned}
\tag{4.69}
$$

Using the definition of the buoyancy frequency, (4.35), yields

$$
\left(\rho_0 g + \frac{c_0^2}{Ma^2}\frac{d\rho_0}{dz}\right) = -\frac{\rho_0 N^2}{g}\frac{c_0^2}{Ma^2},
\tag{4.70}
$$

so (4.69) becomes

$$
\begin{aligned}
\{\mathcal{F}[\Delta], \mathcal{G}\} = \int_{\Omega} &-\frac{\delta\mathcal{F}[\Delta]}{\delta(\rho_0\underline{v}')}\cdot\rho_0\nabla\left(\frac{\delta\mathcal{G}}{\delta\rho'} + \frac{c_0^2}{Ma^2}\frac{\delta\mathcal{G}}{\delta p'}\right) + \frac{\delta\mathcal{F}[\Delta]}{\delta(\rho_0 w')}\frac{\rho_0 N^2}{g}\frac{c_0^2}{Ma^2}\frac{\delta\mathcal{G}}{\delta p'}\, \mathrm{d}\underline{x}\\
&+ \int_{\partial\Omega}\hat{\underline{n}}\cdot\frac{\delta\mathcal{F}[\Delta]}{\delta(\rho_0\underline{v}')}\rho_0\left(\frac{\delta\mathcal{G}}{\delta\rho'} + \frac{c_0^2}{Ma^2}\frac{\delta\mathcal{G}}{\delta p'}\right)\, \mathrm{d}\underline{S}.
\end{aligned}
\tag{4.71}
$$

Substituting for $\mathcal{G}$ in (4.71) the Hamiltonian $\mathcal{A}$, (4.34), yields

$$
\begin{aligned}
\{\mathcal{F}[\Delta], \mathcal{A}\} = \int_{\Omega} &-\frac{\delta\mathcal{F}[\Delta]}{\delta(\rho_0\underline{v}')}\cdot\rho_0\nabla\left(\frac{p'}{\rho_0}\right)\\
&+ \frac{\delta\mathcal{F}[\Delta]}{\delta(\rho_0 w')}\frac{\rho_0 N^2}{g}\frac{c_0^2}{Ma^2}\left(\frac{g^2}{\rho_0 N^2}\left(\frac{Ma^4}{c_0^2}p' - \frac{Ma^2}{c_0^2}\rho'\right) + \frac{Ma^2}{c_0^2}\frac{p'}{\rho_0}\right)\, \mathrm{d}\underline{x}\\
&+ \int_{\partial\Omega}\hat{\underline{n}}\cdot\frac{\delta\mathcal{F}[\Delta]}{\delta(\rho_0\underline{v}')}\rho_0\left(\frac{p'}{\rho_0}\right)\, \mathrm{d}\underline{S}.
\end{aligned}
\tag{4.72}
$$

Applying the constraint $p' = 0$ yields

$$
\{\mathcal{F}[\Delta], \mathcal{A}\} = \int_{\Omega}\frac{\delta\mathcal{F}[\Delta]}{\delta(\rho_0 w')}g\rho'\, \mathrm{d}\underline{x}.
\tag{4.73}
$$

Using (4.57-1) yields

$$
\{\mathcal{F}[\Delta], \mathcal{A}\} = \int_{\Omega}g^2\rho'\frac{\delta\mathcal{F}[\Delta]}{\delta\Delta} + \frac{g\rho'}{\rho_0}\frac{\partial}{\partial z}\left(\frac{c_0^2(z)}{Ma^2}\rho_0\frac{\delta\mathcal{F}[\Delta]}{\delta\Delta}\right)\, \mathrm{d}\underline{x}.
\tag{4.74}
$$

Applying integration by parts on the second term yields

$$
\{\mathcal{F}[\Delta], \mathcal{A}\} = \int_{\Omega}\frac{\delta\mathcal{F}[\Delta]}{\delta\Delta}\left[g^2\rho' - \frac{c_0^2(z)}{Ma^2}\rho_0\frac{\partial}{\partial z}\left(\frac{g\rho'}{\rho_0}\right)\right]\, \mathrm{d}\underline{x} + \int_{\partial\Omega}\frac{\delta\mathcal{F}[\Delta]}{\delta\Delta}\frac{c_0^2(z)}{Ma^2}g\rho'\, \mathrm{d}\underline{S}.
\tag{4.75}
$$

Substituting for $\mathcal{G}$ in (4.68) the constraint $p'(\underline{x}') = 0$, yields

$$
\{\mathcal{F}[\Delta(\underline{x})], p'(\underline{x}')\} = \int_{\Omega}-\frac{\delta p'(\underline{x}')}{\delta p'(\underline{x})}\left(\rho_0 g\frac{\delta\mathcal{F}[\Delta]}{\delta(\rho_0 w')} - \frac{c_0^2}{Ma^2}\rho_0\nabla\cdot\frac{\mathcal{F}[\Delta]}{\delta(\rho_0\underline{v}')}\right)\, \mathrm{d}\underline{x}.
\tag{4.76}
$$

The second nonzero term of (4.55-2) becomes

$$
\int_{\Omega'} \lambda_p(\underline{x}') \left\{ \mathcal{F}[\Delta(\underline{x})], p'(\underline{x}') \right\} \, \mathrm{d}\underline{x}' =
$$
$$
\int_{\Omega'} \lambda_p(\underline{x}') \int_{\Omega} -\frac{\delta p'(\underline{x}')}{\delta p'(\underline{x})} \left(\rho_0 g \frac{\delta \mathcal{F}[\Delta]}{\delta(\rho_0 w')} - \frac{c_0^2}{Ma^2} \rho_0 \nabla . \frac{\mathcal{F}[\Delta]}{\delta(\rho_0 \underline{v}')} \right) \mathrm{d}\underline{x} \mathrm{d}\underline{x}'.
$$
(4.77)

Applying the infinite-dimensional analog of the delta function, (4.56), yields

$$
\int_{\Omega'} \lambda_p(\underline{x}') \left\{ \mathcal{F}[\Delta(\underline{x})], p'(\underline{x}') \right\} \mathrm{d}\underline{x}' = \int_{\Omega'} \lambda_p \left(-\rho_0 g \frac{\delta \mathcal{F}[\Delta]}{\delta(\rho_0 w')} + \frac{c_0^2}{Ma^2} \rho_0 \nabla . \frac{\mathcal{F}[\Delta]}{\delta(\rho_0 \underline{v}')} \right) \mathrm{d}\underline{x}', \quad (4.78)
$$

where the explicit dependence on $\underline{x}'$ has been dropped. Applying integration by parts to free the variations of the functional $\mathcal{F}[\Delta]$ from derivatives yields

$$
\int_{\Omega'} \lambda_p(\underline{x}') \left\{ \mathcal{F}[\Delta(\underline{x})], p'(\underline{x}') \right\} \mathrm{d}\underline{x}' =
$$
$$
\int_{\Omega'} -\rho_0 g \lambda_p \frac{\delta \mathcal{F}[\Delta]}{\delta(\rho_0 w')} - \nabla \left(\frac{c_0^2}{Ma^2} \rho_0 \lambda_p \right) . \frac{\mathcal{F}[\Delta]}{\delta(\rho_0 \underline{v}')} \mathrm{d}\underline{x}' + \int_{\partial \Omega'} \frac{c_0^2}{Ma^2} \rho_0 \lambda_p \hat{n} . \frac{\mathcal{F}[\Delta]}{\delta(\rho_0 \underline{v}')} \mathrm{d}\underline{S}'.
$$
(4.79)

Using (4.57) and rewriting yields

$$
\int_{\Omega'} \lambda_p(\underline{x}') \left\{ \mathcal{F}[\Delta(\underline{x})], p'(\underline{x}') \right\} \mathrm{d}\underline{x}' =
$$
$$
\int_{\Omega'} -\rho_0 g^2 \lambda_p \frac{\delta \mathcal{F}[\Delta]}{\delta \Delta} - g \lambda_p \frac{\partial}{\partial z} \left(\frac{c_0^2}{Ma^2} \rho_0 \frac{\delta \mathcal{F}[\Delta]}{\delta \Delta} \right) - g \frac{\partial}{\partial z} \left(\frac{c_0^2}{Ma^2} \rho_0 \lambda_p \right) \frac{\delta \mathcal{F}[\Delta]}{\delta \Delta}
$$
$$
- \frac{1}{\rho_0} \nabla \left(\frac{c_0^2}{Ma^2} \rho_0 \lambda_p \right) . \nabla \left(\frac{c_0^2}{Ma^2} \rho_0 \frac{\delta \mathcal{F}[\Delta]}{\delta \Delta} \right) \mathrm{d}\underline{x}'
$$
$$
+ \int_{\partial \Omega'} \frac{c_0^2}{Ma^2} g \rho_0 \lambda_p \frac{\delta \mathcal{F}[\Delta]}{\delta \Delta} + \frac{c_0^2}{Ma^2} \lambda_p \frac{\partial}{\partial n} \left(\frac{c_0^2}{Ma^2} \rho_0 \frac{\delta \mathcal{F}[\Delta]}{\delta \Delta} \right) \mathrm{d}\underline{S}',
$$
(4.80)

where $\partial / \partial n$ is the outward derivative. Part of the second and the third terms in the interior cancel and the last boundary term $\partial(\delta \mathcal{F}[\Delta]/\delta \Delta)/\partial n$ is zero because it is imposed as extra gauge or boundary condition. Integrating by parts to to free the variations of the functional $\mathcal{F}[\Delta]$ from derivatives yields

$$
\int_{\Omega'} \lambda_p(\underline{x}') \left\{ \mathcal{F}[\Delta(\underline{x})], p'(\underline{x}') \right\} \mathrm{d}\underline{x}' =
$$
$$
\int_{\Omega'} \frac{\delta \mathcal{F}[\Delta]}{\delta \Delta} \left[-\rho_0 g^2 \lambda_p - g \lambda_p \frac{\partial}{\partial z} \left(\frac{c_0^2}{Ma^2} \rho_0 \right) + \frac{c_0^2}{Ma^2} \rho_0 \nabla . \left(\frac{1}{\rho_0} \nabla \left(\frac{c_0^2}{Ma^2} \rho_0 \lambda_p \right) \right) \right] \mathrm{d}\underline{x}' \quad (4.81)
$$
$$
+ \int_{\partial \Omega'} \frac{\delta \mathcal{F}[\Delta]}{\delta \Delta} \frac{c_0^2}{Ma^2} \frac{\partial}{\partial n} \left(\frac{c_0^2}{Ma^2} \rho_0 \lambda_p \right) \mathrm{d}\underline{S}'.
$$

Substituting (4.75) for the first nonzero term in (4.55) and (4.81) for the second nonzero term in (4.55) allows the Lagrange multiplier λ_p to be determined,

$$
0 = \int_{\Omega'} \frac{\delta \mathcal{F}[\Delta]}{\delta \Delta} \left[g^2 \rho' - \frac{c_0^2(z)}{Ma^2} \rho_0 \frac{\partial}{\partial z} \left(\frac{g\rho'}{\rho_0} \right) - \rho_0 g^2 \lambda_p - g\lambda_p \frac{\partial}{\partial z} \left(\frac{c_0^2}{Ma^2} \rho_0 \right) \right.
$$
$$
\left. + \frac{c_0^2}{Ma^2} \rho_0 \nabla \cdot \left(\frac{1}{\rho_0} \nabla \left(\frac{c_0^2}{Ma^2} \rho_0 \lambda_p \right) \right) \right] \mathrm{d}\underline{x}' \tag{4.82}
$$
$$
+ \int_{\partial\Omega'} \frac{\delta \mathcal{F}[\Delta]}{\delta \Delta} \left[\frac{c_0^2(z)}{Ma^2} g\rho' + \frac{c_0^2}{Ma^2} \frac{\partial}{\partial n} \left(\frac{c_0^2}{Ma^2} \rho_0 \lambda_p \right) \right] \mathrm{d}\underline{S}'.
$$

The same subtlety as in (4.46) arises: the leading order Mach number differs for the density perturbation terms and the Lagrange multiplier terms. The Lagrange multiplier λ_p is scaled with the Mach number squared. Multiplying (4.82) with Ma^2 and letting $Ma \to 0$ yields

$$
0 = \int_{\Omega'} \frac{\delta \mathcal{F}[\Delta]}{\delta \Delta} \left[-c_0^2 \rho_0 \frac{\partial}{\partial z} \left(\frac{g\rho'}{\rho_0} \right) + c_0^2 \rho_0 \nabla \cdot \left(\frac{1}{\rho_0} \nabla \left(c_0^2 \rho_0 \lambda_p \right) \right) \right] \mathrm{d}\underline{x}'
$$
$$
+ \int_{\partial\Omega'} \frac{\delta \mathcal{F}[\Delta]}{\delta \Delta} \left[c_0^2 g\rho' + c_0^2 \frac{\partial}{\partial n} \left(c_0^2 \rho_0 \lambda_p \right) \right] \mathrm{d}\underline{S}'. \tag{4.83}
$$

Using the arbitrariness of the functional $\mathcal{F}[\Delta]$ in (4.82) yields

$$
-\frac{\partial}{\partial z} \left(\frac{g\rho'}{\rho_0} \right) + \nabla \cdot \left(\frac{1}{\rho_0} \nabla \left(c_0^2 \rho_0 \lambda_p \right) \right) = 0, \qquad \text{in } \Omega,
$$
$$
g\rho' + \frac{\partial}{\partial n} \left(c_0^2 \rho_0 \lambda_p \right) = 0, \qquad \text{at } \partial\Omega. \tag{4.84}
$$

The product $-c_0^2 \rho_0 \lambda_p$ plays the role of pressure P.

The bracket formulation for incompressible flow is given by

$$
\frac{d\mathcal{F}}{dt} = \{\mathcal{F}, \mathcal{A}\} + \int_{\Omega}' \lambda_p \{\mathcal{F}, p'\} \, \mathrm{d}\underline{x}' \tag{4.85}
$$

Again, the Mach order scaling is in the way: rescaling the Lagrange multiplier λ_p with the Mach number squared yields a solution to this problem. Applying the constraints $p' = 0$ yields

$$
\frac{d\mathcal{F}}{dt} = \int_{\Omega} \frac{\delta \mathcal{A}}{\delta \rho'} \nabla \cdot \left(\rho_0 \frac{\delta \mathcal{F}}{\delta(\rho_0 \underline{v}')} \right) - \frac{\delta \mathcal{F}}{\delta \rho'} \nabla \cdot \left(\rho_0 \frac{\delta \mathcal{A}}{\delta(\rho_0 \underline{v}')} \right) - c_0^2 \rho_0 \lambda_p \nabla \cdot \frac{\delta \mathcal{F}}{\delta(\rho_0 \underline{v}')} \, \mathrm{d}\underline{x}. \tag{4.86}
$$

Together with (4.84) the dynamics is obtained. Substituting $P = -c_0^2 \rho_0 \lambda_p$ yields the Poisson bracket

$$
\frac{d\mathcal{F}}{dt} = \int_{\Omega} \frac{\delta \mathcal{A}}{\delta \rho'} \nabla \cdot \left(\rho_0 \frac{\delta \mathcal{F}}{\delta(\rho_0 \underline{v}')} \right) - \frac{\delta \mathcal{F}}{\delta \rho'} \nabla \cdot \left(\rho_0 \frac{\delta \mathcal{A}}{\delta(\rho_0 \underline{v}')} \right) + P \nabla \cdot \frac{\delta \mathcal{F}}{\delta(\rho_0 \underline{v}')} \, \mathrm{d}\underline{x}
$$
$$
0 = \int_{\Omega} \frac{\delta \mathcal{F}}{\delta \Delta} \left[\frac{\partial}{\partial z} \left(\frac{g\rho'}{\rho_0} \right) + \nabla \cdot \left(\frac{1}{\rho_0} \nabla P \right) \right] \mathrm{d}\underline{x} + \int_{\partial\Omega} \frac{\delta \mathcal{F}}{\delta \Delta} \left[g\rho' - \frac{\partial}{\partial n} P \right] \mathrm{d}\underline{S}, \tag{4.87}
$$

with constrained Hamiltonian

$$
\mathcal{A} = \int_{\Omega} \frac{1}{2} \rho_0 |\underline{v}'|^2 + \frac{1}{2} \frac{g^2 \rho'^2}{\rho_0 N^2} \, \mathrm{d}\underline{x}, \tag{4.88}
$$

and buoyancy frequency

$$N^2 = \frac{-g}{\rho_0} \frac{d\rho_0}{dz}. \tag{4.89}$$

Now that the Dirac bracket has been obtained, the variables are replaced by perturbation series

$$
\begin{aligned}
\underline{v}' &= v^0 + Ma^2 v^1 + \mathcal{O}\left(Ma^4\right), \\
\rho' &= \rho^0 + Ma^2 \rho^1 + \mathcal{O}\left(Ma^4\right), \\
P &= P^0 + Ma^2 P^1 + \mathcal{O}\left(Ma^4\right),
\end{aligned}
\tag{4.90}
$$

Substituting (4.90) into (4.54) yields to leading order: $\nabla.\underline{v}^0 = 0$. Keeping the leading order terms in (4.87) – (4.89) yields

$$
\begin{aligned}
\frac{d\mathcal{F}}{dt} &= \int_\Omega \frac{\delta\mathcal{A}_0}{\delta\rho^0} \nabla.\left(\rho_0 \frac{\delta\mathcal{F}}{\delta(\rho_0 \underline{v}^0)}\right) - \frac{\delta\mathcal{F}}{\delta\rho^0} \nabla.\left(\rho_0 \frac{\delta\mathcal{A}_0}{\delta(\rho_0 \underline{v}^0)}\right) + P^0 \nabla.\frac{\delta\mathcal{F}}{\delta(\rho_0 \underline{v}^0)} \, \mathrm{d}\underline{x} \\
0 &= \int_\Omega \frac{\delta\mathcal{F}}{\delta\Delta} \left[\frac{\partial}{\partial z}\left(\frac{g\rho^0}{\rho_0}\right) + \nabla.\left(\frac{1}{\rho_0}\nabla P^0\right)\right] \mathrm{d}\underline{x} + \int_{\partial\Omega} \frac{\delta\mathcal{F}}{\delta\Delta}\left[g\rho^0 - \frac{\partial}{\partial n}P^0\right] \mathrm{d}\underline{S},
\end{aligned}
\tag{4.91}
$$

with constrained Hamiltonian

$$\mathcal{A}_0 = \int_\Omega \frac{1}{2}\rho_0 |\underline{v}^0|^2 + \frac{1}{2}\frac{g^2 \left(\rho^0\right)^2}{\rho_0 N^2} \, \mathrm{d}\underline{x}. \tag{4.92}$$

Substituting (4.90) into the constraint (4.54) yields as leading order term the standard incompressibility constraint: $\nabla.\underline{v}^0 = 0$. Since $\delta\mathcal{A}_0/\delta(\rho_0 \underline{v}^0) = \underline{v}^0$, the term $\nabla.\delta\mathcal{A}_0/\delta(\rho_0 \underline{v}^0)$ disappears from the bracket. Since the bracket is anti-symmetric also $\nabla.\delta\mathcal{F}/\delta(\rho_0 \underline{v}^0)$ must disappear. The bracket for incompressible flow becomes

$$
\begin{aligned}
\frac{d\mathcal{F}}{dt} &= \int_\Omega \left(\frac{\delta\mathcal{A}_0}{\delta\rho^0}\frac{\delta\mathcal{F}}{\delta(\rho_0 w^0)} - \frac{\delta\mathcal{F}}{\delta\rho^0}\frac{\delta\mathcal{A}_0}{\delta(\rho_0 w^0)}\right)\frac{d\rho_0}{dz} + P^0 \nabla.\frac{\delta\mathcal{F}}{\delta(\rho_0 \underline{v}^0)} \, \mathrm{d}\underline{x} \\
0 &= \int_\Omega \frac{\delta\mathcal{F}}{\delta\Delta}\left[\frac{\partial}{\partial z}\left(\frac{g\rho^0}{\rho_0}\right) + \nabla.\left(\frac{1}{\rho_0}\nabla P^0\right)\right]\mathrm{d}\underline{x} + \int_{\partial\Omega}\frac{\delta\mathcal{F}}{\delta\Delta}\left[g\rho^0 - \frac{\partial}{\partial n}P^0\right]\mathrm{d}\underline{S}.
\end{aligned}
\tag{4.93}
$$

The incompressible, stratified Euler equations (2.14) can be derived from (4.89), (4.92) and (4.93) by choosing functionals

$$
\begin{aligned}
\mathcal{F}_{\underline{v}} &= \int_\Omega \underline{v}^0(\underline{x}, t).\underline{\phi}_{\underline{v}}(\underline{x}) \, \mathrm{d}\underline{x}, \\
\mathcal{F}_\rho &= \int_\Omega \rho^0(\underline{x}, t)\phi_\rho(\underline{x}) \, \mathrm{d}\underline{x}, \\
\mathcal{F}_\Delta &= \int_\Omega \Delta^0(\underline{x}, t)\phi_\Delta(\underline{x}) \, \mathrm{d}\underline{x},
\end{aligned}
\tag{4.94}
$$

with with $\phi_\rho, \phi_\Delta \in \mathcal{Q}$ and $\underline{\phi}_{\underline{v}} \in \mathcal{Y}$, similar to (4.7), with the additional constraint that $\hat{\underline{n}}.\nabla\phi_\Delta = 0$.

The combination of the conservation of volumes of water parcels, due to the incompressibility constraint, and the variation in density means that mass is no longer conserved. For waves, which are basically oscillations, this problem is not too serious, because mass gains and mass losses follow each other. The discrete results in Chapter 6 show that the compressible test cases conserve the discrete mass exactly while the incompressible test cases do not conserve the discrete mass. The error in the discrete mass for incompressible test cases is very small.

4-6 Boussinesq Approximation

The Boussinesq approximation consists of replacing the background density in the inertia terms by a constant background reference density, ρ^*. The equations of motion are then given by

$$\frac{\partial(\rho^* \underline{v}^0)}{\partial t} = -g\rho^0 \hat{\underline{z}} - \nabla P^0,$$
$$\frac{\partial \rho^0}{\partial t} = -\underline{v}^0 . \nabla(\rho_0), \tag{4.95}$$
$$\nabla . \underline{v}^0 = 0.$$

The buoyancy frequency, (4.89) is redefined to

$$N^2 = \frac{-g}{\rho^*} \frac{d\rho_0}{dz}. \tag{4.96}$$

This approximation can be obtained in the Hamiltonian framework by perturbing the Hamiltonian (4.92) to

$$\mathcal{A}_\prime = \int_\Omega \frac{1}{2}\rho^* |\underline{v}^0|^2 + \frac{1}{2}\frac{g^2 \left(\rho^0\right)^2}{\rho^* N^2} \, \mathrm{d}\underline{x} \tag{4.97}$$

and taking the variations in the Poisson bracket (4.93) with respect to $\rho^* \underline{v}^0$

$$\frac{d\mathcal{F}}{dt} = \int_\Omega \left(\frac{\delta \mathcal{A}_0}{\delta \rho^0} \frac{\delta \mathcal{F}}{\delta(\rho^* w^0)} - \frac{\delta \mathcal{F}}{\delta \rho^0} \frac{\delta \mathcal{A}_0}{\delta(\rho^* w^0)} \right) \frac{d\rho_0}{dz} + P^0 \nabla . \frac{\delta \mathcal{F}}{\delta(\rho^* \underline{v}^0)} \, \mathrm{d}\underline{x}$$
$$0 = \int_\Omega \frac{\delta \mathcal{F}}{\delta \Delta} \left[\frac{\partial}{\partial z} \left(\frac{g\rho^0}{\rho_0} \right) + \nabla . \left(\frac{1}{\rho_0} \nabla P^0 \right) \right] \mathrm{d}\underline{x} + \int_{\partial \Omega} \frac{\delta \mathcal{F}}{\delta \Delta} \left[g\rho^0 - \frac{\partial}{\partial n} P^0 \right] \mathrm{d}\underline{S}. \tag{4.98}$$

All symmetry properties and Casimirs are the same as those of the system of the previous section (Shepherd, 1990).

4-7 Concluding Remarks

This chapter provided a derivation of the Hamiltonian dynamics for the Euler-Boussinesq equations, (4.95). The Hamiltonian dynamics for the primitive Euler equations were given and approximations were directly applied to these dynamics. Each approximation preserved the Hamiltonian structure, resulting in the Hamiltonian dynamics for the Euler-Boussinesq equations. The construction ensured the Poisson bracket satisfied all the required properties, (3.15), and the Hamiltonian was an invariant of the motion.

Section 4-1 showed the Poisson bracket, (4.3), and the Hamiltonian, (4.4), for the primitive Euler equations. Using appropriate functionals, (4.7), the Poisson bracket and Hamiltonian were shown to be equivalent to the formulation of the primitive equations in partial differential equations. The primitive Euler equations describe many phenomena in ideal fluid mechanics. By applying approximations to these primitive equations, simpler systems of equations can be derived that focus on the phenomenon to be studied. The Hamiltonian dynamics for the primitive Euler equations are known. So the primitive Euler equations form an excellent starting point in the derivation.

The first change in the formulation was a transformation of the variables, $(\underline{v}, \rho, s) \rightarrow (\rho\underline{v}, \rho, p)$. Section 4-2 showed the equivalent to this change of variables for functionals. The functionals with respect to the old variables in the Poisson bracket and Hamiltonian were replaced by functionals with respect to the new variables. The transformation from velocity, $\underline{v}$, to momentum, $\rho\underline{v}$, simplified the bracket structure while the transformation from entropy, s, to pressure, p, prepared the Hamiltonian dynamics for incompressibility.

In Section 4-3 an approximation was performed: the variables were linearized around a resting background state. This yielded the compressible stratified Euler equations. The Hamiltonian dynamics for the perturbations around this background state required a careful analysis of the energy available to these perturbations. Casimirs, invariants of motion, had to be included in the Hamiltonian to derive an expression of the available energy for perturbations.

In Section 4-4 both the differential equations and the Poisson bracket and Hamiltonian governing internal gravity waves have been nondimensionalized. This nondimensionalization showed a subtlety for stratified fluids when taking the incompressible limit: a Mach number analysis revealed that the "incompressibility" constraint was (4.47),

$$\frac{1}{Fr^2}\rho_0 w - \frac{1}{Ma^2}c_0^2(z)\rho_0\nabla.\underline{v} = 0. \tag{4.99}$$

This is different from a homogeneous fluid, where the constraint is $\nabla.\underline{v} = 0$. The stratification in z–direction adds a complexity when passing to the incompressible limit. The incompressibility constraint, $\nabla.\underline{v} = 0$, for stratified fluids is regained by a perturbation analysis. The leading order velocity term is divergence-free.

Using Dirac's method of constraints, the "incompressibility" of the flow was enforced. This required a zero perturbations pressure and (4.99) to be enforced. Two Lagrange multipliers ensured these two constraint remained zero. After a lengthy derivation, one of the Lagrange multipliers turned out to be equivalent to the standard role of pressure in the incompressible formulation: ensuring the velocity stays divergence-free. After the Dirac bracket had been derived, a perturbation analysis allowed the derivation of the incompressibility constraint, $\nabla.\underline{v} = 0$, from (4.99).

In Section 4-6 the Boussinesq approximation was made to derive the Hamiltonian dynamics for the Euler-Boussinesq equations.

The bracket and Hamiltonian for the compressible stratified Euler equations are used as starting point for the development of the numerical method. By discretizing the compressible dynamics first, the developed method can be checked. Afterwards the incompressible limit is taken for the discrete system.

Chapter 5

Discontinuous Galerkin Finite Element Method

The exactly energy conserving discretization of the equations governing internal gravity waves is derived in this chapter. The discrete brackets are derived from the compressible Hamiltonian structure (using the bracket (4.45) and Hamiltonian (4.43)) in Chapter 4. The discretized equations are implemented in the hpGEM C++ software framework (Pesch et al., 2007). In Chapter 6 the discretization and implementation is verified.

Discretizing the equations of motion of a system usually destroys the Hamiltonian structure of the equations and as a consequence conservation of energy is then usually also lost. To prevent this loss of structure, the equations of motion are not discretized directly. Instead, the Poisson bracket is discretized such that the skew-symmetry of the bracket is preserved. Consequently, the system conserves the discrete energy. From the discrete Poisson bracket and discrete Hamiltonian the discrete equations of motion are derived. These turn out to be a discretization of the continuous equations. However, it is not clear how to derive the discrete equations such that energy is conserved directly beforehand. By discretizing the Poisson bracket this is taken care of automatically.

The discrete equations for the incompressible equations of motion are again derived by the Dirac's theory. This is preferable to directly discretizing the incompressible equations since: the compressible Hamiltonian formulation forms a check on the introduced discretisation algorithm and the relatively easy incorporation of boundary conditions which is automatic by Dirac's theory. The discrete Poisson bracket for compressible flow is constrained to incompressible flow by introducing Lagrange multipliers. From the discrete Poisson bracket for incompressible flow the discrete equations of motion for incompressible flow are found. Again, these turn out to be discretizations of the continuous equations. However, because of the construction via Poisson brackets the discrete equations turn out to conserve not only energy but also the divergence of the velocity field.

The discretized equations are more compatible to the continuous equations because of the exact energy conservation than a general discretization of the continuous equations. This allows numerical simulations of internal gravity waves that obey the physics of the problem better and are more efficient (achieve the same level of accuracy in less time). The discrete incompressible equations of motion conserve energy and divergence of the velocity field exactly. This has the added benefit that the numerical scheme is unconditionally stable. Stabilization techniques like pressure stabilization techniques, penalty methods, or artificial compressibility methods are not needed to ensure numerical stability.

In Section 5-1 the Discontinuous Galerkin Finite Element Method (DGFEM) is introduced. This numerical method is chosen because of the geometric flexibility of the method and the localized nature of internal gravity waves. This introduction explains the main differences between DGFEM, Finite Element and Finite Volume Methods.

The Hamiltonian dynamics for compressible flow derived in Chapter 4 is discretized in Section 5-2. Here the discrete equations for compressible flow are derived from the discrete Poisson bracket. The resulting scheme is shown to be exactly energy conserving. In Section 5-3 the discrete Poisson bracket for compressible flow is constrained to incompressible flow. The discrete equations for incompressible flow are then derived from the discrete Poisson bracket. The resulting scheme is shown to be exactly energy conserving and exactly velocity-divergence conserving. In Section 5-4 the Boussinesq approximation is made in the discretized system. Section 5-5 discusses the implementation and the properties of the discretization.

5-1   Preliminaries

Finite element methods constitute a well-known approach to discretizing systems of partial differential equations and are often used to solve problems in technical applications. In many applications phenomena occur at different length scales. For example, wave attractors are a localized phenomenon while in other parts of the domain the energy density is (much) smaller. To achieve the same accuracy throughout the entire domain local refinement of the mesh (h-refinement) or local adjustment of the polynomial order of the solution representation (p-refinement) or both (hp-refinement) are needed. However, this is not trivial in a classical finite element formulation.

The Discontinuous Galerkin Finite Element Method (DGFEM) is a finite element method that allows functions to be discontinuous across the boundaries between elements. This discontinuity allows hp-refinement that is much simpler than for the classical finite element method. The DGFEM can be seen as a combination of the classical finite element method and the finite volume method, where the space basis functions and test functions are close to that of the classical finite element method but the equations are satisfied in a sense closer to the finite volume method.

Figure 5-1 shows an example of the basis functions for the classical finite elements on the left and for the DGFEM on the right. For the DGFEM a linear polynomial with mean ϕ_0 and slope ϕ_1 is shown. When the order is reduced and only the mean ϕ_0 is used the finite volume method is obtained. p-refinement consist of adding higher order polynomials, ϕ_2, ϕ_3, ... to the approximation of the solution in the element K. Due to the discontinuous elements the

order of the polynomial representation of the solution in the element to the left and the right of element K, $K-1$ and $K+1$ respectively, can be different. In the classical finite element method special care must to taken to connect elements with different orders of polynomial approximation.

In the DGFEM a space of basis function V_h is defined, without continuity requirement at element boundaries, which would be the case for the classical finite element approach. In Figure 5-1 the difference in basis functions is shown. In Figure 5-2 possible representations of a function in the discrete spaces spanned by these sets of basis functions are presented. The left-hand figure shows the numerical approximation of the function for the classical finite element method with continuous values at the edges of each element. The right-hand figure shows the numerical approximation of the function for the DGFEM with discontinuous values at the edges of each element.
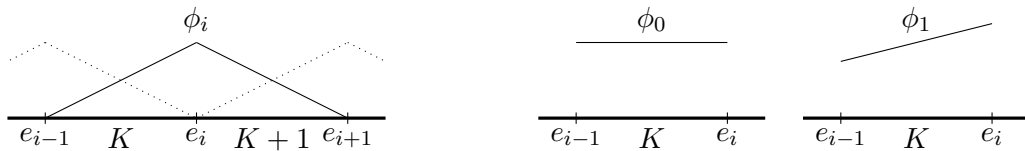
Figure 5-1: Basis functions for the classical finite element method (left) and for the DGFEM (right). The element has number K, the element to the right has $K+1$, e_{i_1} is the left boundary of element K, e_i is the right boundary of element K and the left boundary of element $K+1$ and e_{i+1} is the right boundary of element $K+1$. For the classical finite element method (left) ϕ_i is the basis function. For the DGFEM (right) the polynomial order can be varied. Shown are a constant basis function, ϕ_0, with polynomial order zero and a linear basis function, ϕ_1, with polynomial order one.
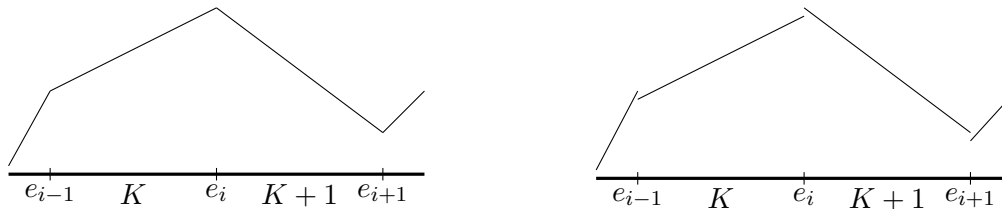
Figure 5-2: Representation of a function for the classical finite element method (left) and for the DGFEM (right). The element has number K, the element to the right has $K+1$, e_{i_1} is the left boundary of element K, e_i is the right boundary of element K and the left boundary of element $K+1$ and e_{i+1} is the right boundary of element $K+1$. For the classical finite element method (left) the values at the element boundaries (e_{i-1}, e_i and e_{i+1}) are connected while for the DGFEM (right) the values are disconnected and two values exist at the boundaries.

Suppose a conservation law of the form

$$\frac{\partial u}{\partial t} + \nabla.f(u) = 0 \quad \text{in} \quad \Omega, \tag{5.1}$$

with initial condition $u(\underline{x}, t) = u_0(\underline{x})$ and boundary conditions $u(\underline{x}, t) = g(\underline{x}, t)$, is to be solved. u is a conserved quantity, f is a flux function and Ω the physical domain. To solve this problem with the DGFEM the physical domain, Ω, is approximated by the computational domain, Ω_h, which consists of K elements, i.e.

$$\Omega \approx \Omega_h = \bigcup_{K \in \Omega_h} K, \tag{5.2}$$

where K is one of the elements. For one-dimensional problems the element K would just be a line segment, as depicted in Figure 5-1. The solution to the partial differential equation, u, is assumed to be approximated by a numerical solution, u_h. This numerical solution u_h is constructed from the numerical solution on each element, u_h^i, as

$$u \approx u_h = \sum_K u_h^K \in V_h. \tag{5.3}$$

Multiplying the conservation law with some test function $v_h \in V_h$, integrating over each element and performing integration by parts once yields

$$\frac{\partial}{\partial t} \int_{E_i} u_h v_h \, \mathrm{d}\underline{x} - \int_{E_i} \nabla v_h . f(u_h) \, \mathrm{d}\underline{x} + \int_{\partial E_i} v_h \underline{\hat{n}} . \hat{f}(u_h^-, u_h^+) \, \mathrm{d}S \quad \forall i, \tag{5.4}$$

where ∂E_i denotes the boundary of element E_i. The flux across a boundary of an element $\hat{f}$ needs special care. Since the solution is allowed to be discontinuous the value of the numerical approximation, u_h, at an element boundary is not single valued. Consider again the one-dimensional situation depicted in Figure 5-2. Element E_i has a right boundary at x_i. At this boundary two values of the solution live, the value of the element to the left, u_h^-, and the value of the element to the right, u_h^+. Different choices exist for combining these two values in the numerical flux across the boundary, $\hat{f}$.

The numerical solution, u_h^i, is expanded on each element as

$$u_h^i(\underline{x}, t) = \sum_{n=1}^{p} \hat{u}_n^i(t) \phi_n(\underline{x}) \quad \forall i, \tag{5.5}$$

where $\hat{u}_n^i(t)$ are the expansion coefficients and $\phi_n(\underline{x})$ the basis functions. Here, p is the number of basis functions in an element and may vary for different elements. The semi-discrete problem consists of a set of ordinary differential equations in each element, which can be solved using a wide variety of time integration methods.

5-2   Discrete Compressible Dynamics

The starting point are the nondimensionalized Hamiltonian (4.43) and Poisson bracket (4.45). Scale such that $\delta = Fr = Ma = 1$. The physical domain Ω is approximated by a computational domain Ω_h, consisting of nonoverlapping elements K. Let $\mathcal{P}^p(K)$ be the space of polynomials of at most degree p on K. The finite element spaces required are

$$\begin{aligned} V_h &= \left\{ \psi \in L^2(\Omega) : \psi|_K \in \mathcal{P}^p(K), \forall K \in \Omega_h \right\}, \\ W_h &= \left\{ \underline{\psi} \in \left(L^2(\Omega) \right)^3 : \psi|_K \in \left(\mathcal{P}^p(K) \right)^3, \forall K \in \Omega_h \right\}, \end{aligned} \tag{5.6}$$

where $L^2(\Omega)$ is the space of square integrable function on Ω. The discrete Hamiltonian is then

$$H = \sum_{K \in \Omega_h} \int_K \frac{1}{2} \frac{1}{\rho_0} (\rho_0 \underline{v})_h^2 + \frac{1}{2} \frac{1}{\rho_0 N^2} \left(\rho_h - \frac{p_h}{c_0^2} \right)^2 + \frac{1}{2} \frac{p_h^2}{\rho_0 c_0^2} \, \mathrm{d}K, \tag{5.7}$$

where $(\rho_0 \underline{v})_h \in W_h$ and $\rho_h, p_h \in V_h$ are the discrete variables and ρ_0, N^2 and c_0^2 are conveniently taken to be continuous functions. The subscript h indicates discrete quantities. No explicit reference to element K is shown, but for each element the variables are different. The variational derivatives are

$$
\begin{aligned}
\frac{\delta H}{\delta(\rho_0 \underline{v})_h} &= \underline{v}_h, \\
\frac{\delta H}{\delta \rho_h} &= \frac{1}{\rho_0 N^2} \left(\rho_h - \frac{p_h}{c_0^2} \right), \\
\frac{\delta H}{\delta p_h} &= \frac{1}{\rho_0 N^2} \left(\frac{p_h}{c_0^4} - \frac{\rho_h}{c_0^2} \right) + \frac{p_h}{\rho_0 c_0^2}.
\end{aligned}
\tag{5.8}
$$

There is some abuse of notation here, because the functions F and H are used for functionals. However, if approximations $(\rho_0 \underline{v})_h, \rho_h$ and p_h are viewed as finite-dimensional expansions, then function derivatives with respect to the expansion coefficients emerge.

The interim discrete Poisson bracket (cf. (4.45)) is

$$
\begin{aligned}
[F, G] = \sum_{K \in \Omega_h} \int_K & \frac{\delta G}{\delta \rho_h} \nabla_h \cdot \left(\rho_0 \frac{\delta F}{\delta(\rho_0 \underline{v})_h} \right) - \frac{\delta F}{\delta \rho_h} \nabla_h \cdot \left(\rho_0 \frac{\delta G}{\delta(\rho_0 \underline{v})_h} \right) \\
& + \frac{\delta F}{\delta p_h} \left(\rho_0 \frac{\delta G}{\delta(\rho_0 w)_h} - c_0^2 \rho_0 \nabla_h \cdot \left(\frac{\delta G}{\delta(\rho_0 \underline{v})_h} \right) \right) \\
& - \frac{\delta G}{\delta p_h} \left(\rho_0 \frac{\delta F}{\delta(\rho_0 w)_h} - c_0^2 \rho_0 \nabla_h \cdot \left(\frac{\delta F}{\delta(\rho_0 \underline{v})_h} \right) \right) \, \mathrm{d}K,
\end{aligned}
\tag{5.9}
$$

with element-wise differential operator ∇_h. Working out the brackets in the density variations yields

$$
\begin{aligned}
[F, G] = \sum_{K \in \Omega_h} \int_K & \frac{\delta G}{\delta \rho_h} \left(\frac{d\rho_0}{dz} \frac{\delta F}{\delta(\rho_0 w)_h} + \rho_0 \nabla_h \cdot \frac{\delta F}{\delta(\rho_0 \underline{v})_h} \right) \\
& - \frac{\delta F}{\delta \rho_h} \left(\frac{d\rho_0}{dz} \frac{\delta G}{\delta(\rho_0 w)_h} + \rho_0 \nabla_h \cdot \frac{\delta G}{\delta(\rho_0 \underline{v})_h} \right) \\
& + \frac{\delta F}{\delta p_h} \left(\rho_0 \frac{\delta G}{\delta(\rho_0 w)_h} - c_0^2 \rho_0 \nabla_h \cdot \frac{\delta G}{\delta(\rho_0 \underline{v})_h} \right) \\
& - \frac{\delta G}{\delta p_h} \left(\rho_0 \frac{\delta F}{\delta(\rho_0 w)_h} - c_0^2 \rho_0 \nabla_h \cdot \frac{\delta F}{\delta(\rho_0 \underline{v})_h} \right) \, \mathrm{d}K.
\end{aligned}
\tag{5.10}
$$

These two interim brackets are incomplete because there is no connection between the elements, an issue that is repaired next. Integrating by parts over each element K yields

$$
\begin{aligned}
[F, G] = \sum_{K \in \Omega_h} \int_K & -\nabla_h \left(\rho_0 \frac{\delta G}{\delta \rho_h} \right) . \frac{\delta F}{\delta(\rho_0 \underline{v})_h} + \nabla_h \left(\rho_0 \frac{\delta F}{\delta \rho_h} \right) . \frac{\delta G}{\delta(\rho_0 \underline{v})_h} \\
& + \sum_{K \in \Omega_h} \int_{\partial K} \rho_0 \frac{\delta G}{\delta \rho_h} \hat{\underline{n}} . \widehat{\frac{\delta F}{\delta(\rho_0 \underline{v})_h}} - \widehat{\frac{\delta G}{\delta(\rho_0 \underline{v})_h}} . \hat{\underline{n}} \rho_0 \frac{\delta F}{\delta \rho_h} \, \mathrm{d}\Gamma \\
& + \sum_{K \in \Omega_h} \int_K \frac{d\rho_0}{dz} \left(\frac{\delta G}{\delta \rho_h} \frac{\delta F}{\delta(\rho_0 w)_h} - \frac{\delta F}{\delta \rho_h} \frac{\delta G}{\delta(\rho_0 w)_h} \right) \mathrm{d}K \\
& - \sum_{K \in \Omega_h} \int_K \rho_0 \left(\frac{\delta G}{\delta p_h} \frac{\delta F}{\delta(\rho_0 w)_h} - \frac{\delta F}{\delta p_h} \frac{\delta G}{\delta(\rho_0 w)_h} \right) \mathrm{d}K \\
& + \sum_{K \in \Omega_h} \int_K -\nabla_h \left(c_0^2 \rho_0 \frac{\delta G}{\delta p_h} \right) . \frac{\delta F}{\delta(\rho_0 \underline{v})_h} + \nabla_h \left(c_0^2 \rho_0 \frac{\delta F}{\delta p_h} \right) . \frac{\delta G}{\delta(\rho_0 \underline{v})_h} \, \mathrm{d}K \\
& + \sum_{K \in \Omega_h} \int_{\partial K} c_0^2 \rho_0 \frac{\delta G}{\delta p_h} \hat{\underline{n}} . \widehat{\frac{\delta F}{\delta(\rho_0 \underline{v})_h}} - \widehat{\frac{\delta G}{\delta(\rho_0 \underline{v})_h}} . \hat{\underline{n}} c_0^2 \rho_{0_h} \frac{\delta F}{\delta p_h} \, \mathrm{d}\Gamma,
\end{aligned}
\tag{5.11}
$$

where wide hats indicate numerical fluxes. When choosing the numerical flux $\widehat{\frac{\delta F}{\delta(\rho_0 \underline{v})_h}}$ the same as for $\widehat{\frac{\delta G}{\delta(\rho_0 \underline{v})_h}}$, the discrete bracket is skew-symmetric. Now choose the following alternating fluxes

$$
\begin{aligned}
\widehat{\frac{\delta F}{\delta(\rho_0 \underline{v})_h}} &= (1 - \theta^e) \frac{\delta F}{\delta(\rho_0 \underline{v})_h^L} + \theta^e \frac{\delta F}{\delta(\rho_0 \underline{v})_h^R}, \\
\widehat{\frac{\delta G}{\delta(\rho_0 \underline{v})_h}} &= (1 - \theta^e) \frac{\delta G}{\delta(\rho_0 \underline{v})_h^L} + \theta^e \frac{\delta G}{\delta(\rho_0 \underline{v})_h^R},
\end{aligned}
\tag{5.12}
$$

where the superscript L indicates the element to the left of the boundary and the superscript R indicates the element to the right of the boundary. The parameter θ^e controls the type of flux function and can be varied across internal boundaries $e \in \Gamma_i$.

The summation over all element boundaries comprises two types of boundaries: exterior boundaries Γ_Ω, those aligned with $\partial \Omega_h$, and interior boundaries Γ_i, those in between the elements. To evaluate the fluxes across the exterior boundary the boundary condition at $\partial \Omega$ is used. A no-slip boundary condition holds,

$$
\hat{\underline{n}} . \underline{v} = 0 \quad \text{at} \quad \partial \Omega.
\tag{5.13}
$$

The same should hold for the numerical flux across the computational domain. From (5.8-1) follows that

$$
\hat{\underline{n}} . \widehat{\frac{\delta H}{\delta(\rho_0 \underline{v})_h}} = 0 \quad \text{at} \quad \partial \Omega_h.
\tag{5.14}
$$

To ensure the skew-symmetry of the bracket a similar boundary condition is required for the arbitrary functions F

$$
\hat{\underline{n}} . \widehat{\frac{\delta F}{\delta(\rho_0 \underline{v})_h}} = 0 \quad \text{at} \quad \partial \Omega_h.
\tag{5.15}
$$

If $\underline{\hat{n}}.\underline{v} = 0$ holds then also $\underline{\hat{n}}.(\rho_0\underline{v}) = 0$ and the boundary conditions for the corresponding numerical fluxes are also zero. So all terms containing fluxes across the external boundary are zero in the Poisson bracket.
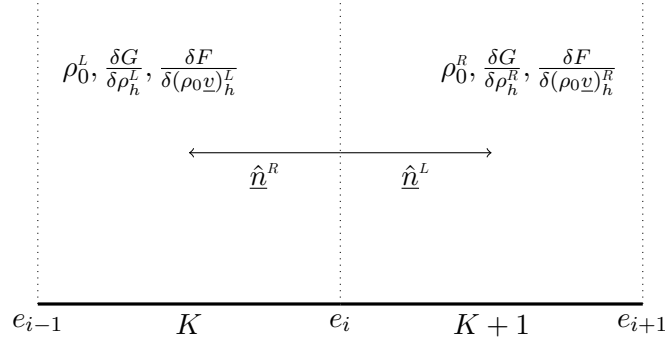

Figure 5-3: The interior boundary e_i is counted twice in the summation: Once for element K and once for element $K+1$. The superscript L indicates quantities living on the left of the boundary e_i and the superscript R indicates quantities living on the right of the boundary e_i. $\underline{\hat{n}}^L$, the outward normal of the element to the left of the boundary e_i, points to the right and $\underline{\hat{n}}^R$, the outward normal of the element to the right of the boundary e_i, points to the left.

All interior boundaries occur twice in the summation, see Figure 5-3. When summing over all elements $K \in \Omega_h$, the flux across boundary e_i is first evaluated for element K and then for element $K+1$. All variables in element K are living to the left of boundary e_i and all elements in element $K+1$ are living to the right of boundary e_i. The outward normal $\underline{\hat{n}}$ points in opposite direction for the two elements. Consider the first term of the first summation over the boundary terms from (5.11). Substituting (5.12), the expression for the integration over boundary e_i from element K is

$$\int_{e_i} \rho_0^L \frac{\delta G}{\delta \rho_h^L} \underline{\hat{n}}^L \cdot \left[(1 - \theta^{e_i}) \frac{\delta F}{\delta(\rho_0\underline{v})_h^L} + \theta^{e_i} \frac{\delta F}{\delta(\rho_0\underline{v})_h^R} \right] \, \mathrm{d}\Gamma, \tag{5.16}$$

and from element $K+1$ is

$$\int_{e_i} \rho_0^R \frac{\delta G}{\delta \rho_h^R} \underline{\hat{n}}^R \cdot \left[(1 - \theta^{e_i}) \frac{\delta F}{\delta(\rho_0\underline{v})_h^L} + \theta^{e_i} \frac{\delta F}{\delta(\rho_0\underline{v})_h^R} \right] \, \mathrm{d}\Gamma. \tag{5.17}$$

Adding these contributions yields the expression for the integration over boundary e_i from both elements,

$$\int_{e_i} \left(\rho_0^L \frac{\delta G}{\delta \rho_h^L} - \rho_0^R \frac{\delta G}{\delta \rho_h^R} \right) \underline{\hat{n}}^L \cdot \left[(1 - \theta^{e_i}) \frac{\delta F}{\delta(\rho_0\underline{v})_h^L} + \theta^{e_i} \frac{\delta F}{\delta(\rho_0\underline{v})_h^R} \right] \, \mathrm{d}\Gamma, \tag{5.18}$$

where $\underline{\hat{n}}^R = -\underline{\hat{n}}^L$ has been used. So the summation over elements $K \in \Omega_h$ of all boundary terms can be replaced by a summation over all interior boundaries.

Substituting the epxpressions (5.12) for the numerical fluxes into (5.11) and rewriting the summation over all elements for the boundary fluxes into a summation over all interior boundaries yields

$$
\begin{aligned}
[F, G] = &\sum_K \int_K -\nabla_h\left(\frac{\delta G}{\delta \rho_h}\rho_0\right) \cdot \frac{\delta F}{\delta(\rho_0 \underline{v})_h} + \nabla_h\left(\frac{\delta F}{\delta \rho_h}\rho_0\right)\cdot\frac{\delta G}{\delta(\rho_0 \underline{v})_h}\, \mathrm{d}K \\
&+ \sum_{e\in\Gamma_i} \int_e \left(\rho_0^L\frac{\delta G}{\delta\rho_h^L} - \rho_{0h}^R\frac{\delta G}{\delta\rho_h^R}\right)\underline{\hat{n}}^L\cdot\left((1-\theta^e)\frac{\delta F}{\delta(\rho_0\underline{v})_h^L} + \theta^e\frac{\delta F}{\delta(\rho_0\underline{v})_h^R}\right) \\
&\quad - \left(\rho_0^L\frac{\delta F}{\delta\rho_h^L} - \rho_0^R\frac{\delta F}{\delta\rho_h^R}\right)\underline{\hat{n}}^L\cdot\left((1-\theta^e)\frac{\delta G}{\delta(\rho_0\underline{v})_h^L} + \theta^e\frac{\delta G}{\delta(\rho_0\underline{v})_h^R}\right)\, \mathrm{d}\Gamma \\
&+ \sum_K \int_K \frac{d\rho_0}{dz}\left(\frac{\delta G}{\delta\rho_h}\frac{\delta F}{\delta(\rho_0 w)_h} - \frac{\delta F}{\delta\rho_h}\frac{\delta G}{\delta(\rho_0 w)_h}\right)\, \mathrm{d}K \\
&- \sum_K \int_K \rho_0\left(\frac{\delta G}{\delta p_h}\frac{\delta F}{\delta(\rho_0 w)_h} - \frac{\delta F}{\delta p_h}\frac{\delta G}{\delta(\rho_0 w)_h}\right)\, \mathrm{d}K \\
&+ \sum_K \int_K -\nabla_h\left(c_0^2\rho_0\frac{\delta G}{\delta p_h}\right)\cdot\frac{\delta F}{\delta(\rho_0\underline{v})_h} + \nabla_h\left(c_0^2\rho_0\frac{\delta F}{\delta p_h}\right)\cdot\frac{\delta G}{\delta(\rho_0\underline{v})_h}\, \mathrm{d}K \\
&+ \sum_{e\in\Gamma_i}\int_e\left(c_0^{2L}\rho_0^L\frac{\delta G}{\delta p_h^L} - c_0^{2R}\rho_0^R\frac{\delta G}{\delta p_h^R}\right)\underline{\hat{n}}^L\cdot\left((1-\theta^e)\frac{\delta F}{\delta(\rho_0\underline{v})_h^L} + \theta^e\frac{\delta F}{\delta(\rho_0\underline{v})_h^R}\right) \\
&\quad - \left(c_0^{2L}\rho_0^L\frac{\delta F}{\delta p_h^L} - c_0^{2R}\rho_0^R\frac{\delta F}{\delta p_h^R}\right)\underline{\hat{n}}^L\cdot\left((1-\theta^e)\frac{\delta G}{\delta(\rho_0\underline{v})_h^L} + \theta^e\frac{\delta G}{\delta(\rho_0\underline{v})_h^R}\right)\, \mathrm{d}\Gamma.
\end{aligned}
\tag{5.19}
$$

Consider the time evolution of the Hamiltonian, $dH/dt = [H, H]$. By the skew-symmetry of the bracket this is zero. So the pseudo-energy is preserved.

The total numerical solution is obtained from the numerical solutions on each element as

$$
\begin{aligned}
(\rho_0\underline{v})_h(\underline{x}, t) &= \sum_K (\rho_0\underline{v})_h^K(\underline{x}, t), \\
\rho_h(\underline{x}, t) &= \sum_K \rho_h^K(\underline{x}, t), \\
p_h(\underline{x}, t) &= \sum_K p_h^K(\underline{x}, t),
\end{aligned}
\tag{5.20}
$$

where the superscript K was not explicitly shown before. On each element the numerical solution is expanded by using local basis functions,

$$
\begin{aligned}
(\rho_0\underline{v})_h^K(\underline{x}, t) &= \sum_{\beta=1}^p (\rho_0\underline{v})_\beta^K(t)\phi_\beta(\underline{x})^K, \\
\rho_h^K(\underline{x}, t) &= \sum_{\beta=1}^p \rho_\beta^K(t)\phi_\beta(\underline{x})^K, \\
p_h^K(\underline{x}, t) &= \sum_{\beta=1}^p p_\beta^K(t)\phi_\beta(\underline{x})^K,
\end{aligned}
\tag{5.21}
$$

where $(\rho_0 \underline{v})_\beta^K (t)$, etc. are the expansion coefficients and should not be confused with the numerical solution on an element. Dropping the superscript K again and using the summation convention simplifies the notation. Variational and function derivatives can now be related by (Xu et al., 2008; Nurijanyan et al., 2013)

$$
\begin{aligned}
\delta \mathcal{F} &= \sum_K \int_K \frac{\delta \mathcal{F}}{\delta (\rho_0 \underline{v})_h} \delta (\rho_0 \underline{v})_h + \frac{\delta \mathcal{F}}{\delta \rho_h} \delta \rho_h + \frac{\delta \mathcal{F}}{\delta p_h} \delta p_h \, \mathrm{d}K \\
&= \sum_K \int_K \frac{\delta \mathcal{F}}{\delta (\rho_0 \underline{v})_h} \delta \phi_\beta(\underline{x})(\rho_0 \underline{v})_\beta(t) + \frac{\delta \mathcal{F}}{\delta \rho_h} \delta \phi_\beta(\underline{x}) \rho_\beta(t) + \frac{\delta \mathcal{F}}{\delta p_h} \delta \phi_\beta(\underline{x}) p_\beta(t) \, \mathrm{d}K \\
&= \sum_K \left(\int_K \frac{\delta \mathcal{F}}{\delta (\rho_0 \underline{v})_h} \phi_\beta(\underline{x}) \, \mathrm{d}K \right) \delta (\rho_0 \underline{v})_\beta(t) + \left(\int_K \frac{\delta \mathcal{F}}{\delta \rho_h} \phi_\beta(\underline{x}) \, \mathrm{d}K \right) \delta \rho_\beta(t) \\
&\qquad + \left(\int_K \frac{\delta \mathcal{F}}{\delta p_h} \phi_\beta(\underline{x}) \, \mathrm{d}K \right) \delta p_\beta(t) \\
&= \sum_K \frac{\partial F}{\partial (\rho_0 \underline{v})_\beta} \delta (\rho_0 \underline{v})_\beta(t) + \frac{\partial F}{\partial \rho_\beta} \delta \rho_\beta(t) + \frac{\partial F}{\partial p_\beta} \delta p_\beta(t).
\end{aligned}
\tag{5.22}
$$

Define the local mass matrix $M_{\alpha\beta}^K = M_{\alpha\beta}$ as

$$
M_{\alpha\beta} = \int_K \phi_\alpha \phi_\beta \, \mathrm{d}K,
\tag{5.23}
$$

then the following holds

$$
M_{\alpha\beta} (\rho_0 \underline{v})_\beta = \int_K \phi_\alpha \phi_\beta \, \mathrm{d}K \, (\rho_0 \underline{v})_\beta (t) = \int_K \phi_\alpha \phi_\beta (\rho_0 \underline{v})_\beta (t) \, \mathrm{d}K = \int_K \phi_\alpha (\rho_0 \underline{v})_h \, \mathrm{d}K.
\tag{5.24}
$$

From (5.22), then it follows that

$$
\begin{aligned}
\frac{\delta \mathcal{F}}{\delta (\rho_0 \underline{v})_h} &= M_{\beta\gamma}^{-1} \frac{\partial F}{\partial (\rho_0 \underline{v})_\beta} \phi_\gamma, \\
\frac{\delta \mathcal{F}}{\delta \rho_h} &= M_{\beta\gamma}^{-1} \frac{\partial F}{\partial \rho_\beta} \phi_\gamma, \\
\frac{\delta \mathcal{F}}{\delta p_h} &= M_{\beta\gamma}^{-1} \frac{\partial F}{\partial p_\beta} \phi_\gamma.
\end{aligned}
\tag{5.25}
$$

Substituting these relations into (5.19) yields

$$[F, G] =$$

$$\sum_K \int_K -\nabla_h \left(\rho_0 M_{\alpha\mu}^{-1} \frac{\partial G}{\partial \rho_\alpha} \phi_\mu \right).M_{\beta\gamma}^{-1} \frac{\partial F}{\partial(\rho_0 \underline{v})_\beta} \phi_\gamma + M_{\beta\gamma}^{-1} \frac{\partial G}{\partial(\rho_0 \underline{v})_\beta} \phi_\gamma.\nabla_h \left(\rho_0 M_{\alpha\mu}^{-1} \frac{\partial F}{\partial \rho_\alpha} \phi_\mu \right) \, \mathrm{d}K$$

$$+ \sum_{e \in \Gamma_i} \int_e \left(\rho_0^L M_{\alpha\mu}^{-L} \frac{\partial G}{\partial \rho_\alpha^L} \phi_\mu^L - \rho_0^R M_{\alpha\mu}^{-R} \frac{\partial G}{\partial \rho_\alpha^R} \phi_\mu^R \right) \hat{\underline{n}}^L . \left((1 - \theta^e) M_{\beta\gamma}^{-L} \frac{\partial F}{\partial(\rho_0\underline{v})_\beta^L} \phi_\gamma^L + \theta^e M_{\beta\gamma}^{-R} \frac{\partial F}{\partial(\rho_0\underline{v})_\beta^R} \phi_\gamma^R \right)$$

$$- \left(\rho_0^L M_{\alpha\mu}^{-L} \frac{\partial F}{\partial \rho_\alpha^L} \phi_\mu^L - \rho_0^R M_{\alpha\mu}^{-R} \frac{\partial F}{\partial \rho_\alpha^R} \phi_\mu^R \right) \hat{\underline{n}}^L . \left((1 - \theta^e) M_{\beta\gamma}^{-L} \frac{\partial G}{\partial(\rho_0\underline{v})_\beta^L} \phi_\gamma^L + \theta^e M_{\beta\gamma}^{-R} \frac{\partial G}{\partial(\rho_0\underline{v})_\beta^R} \phi_\gamma^R \right) \, \mathrm{d}\Gamma$$

$$+ \sum_K \int_K \frac{d\rho_0}{dz} \left(M_{\alpha\mu}^{-1} \frac{\partial G}{\partial \rho_\alpha} \phi_\mu M_{\beta\gamma}^{-1} \frac{\partial F}{\partial(\rho_0 w)_\beta} \phi_\gamma - M_{\alpha\mu}^{-1} \frac{\partial F}{\partial \rho_\alpha} \phi_\mu M_{\beta\gamma}^{-1} \frac{\partial G}{\partial(\rho_0 w)_\beta} \phi_\gamma \right) \, \mathrm{d}K$$

$$- \sum_K \int_K \rho_0 \left(M_{\alpha\mu}^{-1} \frac{\partial G}{\partial p_\alpha} \phi_\mu M_{\beta\gamma}^{-1} \frac{\partial F}{\partial(\rho_0 w)_\beta} \phi_\gamma - M_{\alpha\mu}^{-1} \frac{\partial F}{\partial p_\alpha} \phi_\mu M_{\beta\gamma}^{-1} \frac{\partial G}{\partial(\rho_0 w)_\beta} \phi_\gamma \right) \, \mathrm{d}K$$

$$+ \sum_K \int_K -\nabla_h \left(c_0^2 \rho_0 M_{\alpha\mu}^{-1} \frac{\partial G}{\partial p_\alpha} \phi_\mu \right).M_{\beta\gamma}^{-1} \frac{\partial F}{\partial(\rho_0 \underline{v})_\beta} \phi_\gamma + \nabla_h \left(c_0^2 \rho_0 M_{\alpha\mu}^{-1} \frac{\partial F}{\partial p_\alpha} \phi_\mu \right).M_{\beta\gamma}^{-1} \frac{\partial G}{\partial(\rho_0 \underline{v})_\beta} \phi_\gamma \, \mathrm{d}K$$

$$+ \sum_{e \in \Gamma_i} \int_e \left(c_0^{2L} \rho_0^L M_{\alpha\mu}^{-L} \frac{\partial G}{\partial p_\alpha^L} \phi_\mu^L - c_0^{2R} \rho_0^R M_{\alpha\mu}^{-R} \frac{\partial G}{\partial p_\alpha^R} \phi_\mu^R \right) \hat{\underline{n}}^L . \left((1 - \theta^e) M_{\beta\mu}^{-L} \frac{\partial F}{\partial(\rho_0\underline{v})_\beta^L} \phi_\gamma^L + \theta^e M_{\beta\gamma}^{-R} \frac{\partial F}{\partial(\rho_0\underline{v})_\beta^R} \phi_\gamma^R \right)$$

$$- \left(c_0^{2L} \rho_0^L M_{\alpha\mu}^{-L} \frac{\partial F}{\partial p_\alpha^L} \phi_\mu^L - c_0^{2R} \rho_0^R M_{\alpha\mu}^{-R} \frac{\partial F}{\partial p_\alpha^R} \phi_\mu^R \right) \hat{\underline{n}}^L . \left((1 - \theta^e) M_{\beta\gamma}^{-L} \frac{\partial G}{\partial(\rho_0\underline{v})_\beta^L} \phi_\gamma^L + \theta^e M_{\beta\gamma}^{-R} \frac{\partial G}{\partial(\rho_0\underline{v})_\beta^R} \phi_\gamma^R \right) \, \mathrm{d}\Gamma.$$

(5.26)

Rewriting this expression allows the introduction of elemental (vector) matrices

$$[F, G] = \sum_K \left(\frac{\partial G}{\partial(\rho_0\underline{v})_\beta} \frac{\partial F}{\partial \rho_\alpha} - \frac{\partial F}{\partial(\rho_0\underline{v})_\beta} \frac{\partial G}{\partial \rho_\alpha} \right) \cdot \underbrace{\int_K \phi_\gamma \nabla_h (\rho_0 \phi_\mu) \, \mathrm{d}K}_{^1\underline{E}_{\gamma\mu}} M_{\alpha\mu}^{-1} M_{\beta\gamma}^{-1}$$

$$+ \sum_{e \in \Gamma_i} (1 - \theta^e) \left(\frac{\partial G}{\partial \rho_\alpha^L} \frac{\partial F}{\partial(\rho_0\underline{v})_\beta^L} - \frac{\partial F}{\partial \rho_\alpha^L} \frac{\partial G}{\partial(\rho_0\underline{v})_\beta^L} \right) \cdot \underbrace{\int_e \hat{\underline{n}}^L \phi_\mu^L \rho_0^L \phi_\gamma^L \, \mathrm{d}\Gamma}_{^1\underline{G}_{\gamma\mu}^{LL}} M_{\alpha\mu}^{-L} M_{\beta\gamma}^{-L}$$

$$+ \theta^e \left(\frac{\partial G}{\partial \rho_\alpha^L} \frac{\partial F}{\partial (\rho_0 \underline{v})_\beta^R} - \frac{\partial F}{\partial \rho_\alpha^L} \frac{\partial G}{\partial (\rho_0 \underline{v})_\beta^R} \right) \cdot \underbrace{\int_e \underline{\hat{n}}^L \phi_\mu^L \rho_0^L \phi_\gamma^R \, \mathrm{d}\Gamma}_{^1\underline{G}_{\gamma\mu}^{RL}} M_{\alpha\mu}^{-L} M_{\beta\gamma}^{-R}$$

$$- (1 - \theta^e) \left(\frac{\partial G}{\partial \rho_\alpha^R} \frac{\partial F}{\partial (\rho_0 \underline{v})_\beta^L} - \frac{\partial F}{\partial \rho_\alpha^R} \frac{\partial G}{\partial (\rho_0 \underline{v})_\beta^L} \right) \cdot \underbrace{\int_e \underline{\hat{n}}^L \phi_\mu^R \rho_0^R \phi_\gamma^L \, \mathrm{d}\Gamma}_{^1\underline{G}_{\gamma\mu}^{LR}} M_{\alpha\mu}^{-R} M_{\beta\gamma}^{-L}$$

$$- \theta^e \left(\frac{\partial G}{\partial \rho_\alpha^R} \frac{\partial F}{\partial (\rho_0 \underline{v})_\beta^R} - \frac{\partial F}{\partial \rho_\alpha^R} \frac{\partial G}{\partial (\rho_0 \underline{v})_\beta^R} \right) \cdot \underbrace{\int_e \underline{\hat{n}}^L \phi_\mu^R \rho_0^R \phi_\gamma^R \, \mathrm{d}\Gamma}_{^1\underline{G}_{\gamma\mu}^{RR}} M_{\alpha\mu}^{-R} M_{\beta\gamma}^{-R}$$

$$- \sum_K \left(\frac{\partial G}{\partial (\rho_0 w)_\beta} \frac{\partial F}{\partial \rho_\alpha} - \frac{\partial F}{\partial (\rho_0 w)_\beta} \frac{\partial G}{\partial \rho_\alpha} \right) \underbrace{\int_K \phi_\mu \frac{d\rho_0}{dz} \phi_\gamma \, \mathrm{d}K}_{^1N_{\gamma\mu}} M_{\alpha\mu}^{-1} M_{\beta\gamma}^{-1} \tag{5.27}$$

$$+ \sum_K \left(\frac{\partial G}{\partial (\rho_0 w)_\beta} \frac{\partial F}{\partial p_\alpha} - \frac{\partial F}{\partial (\rho_0 w)_\beta} \frac{\partial G}{\partial p_\alpha} \right) \underbrace{\int_K \phi_\mu \rho_0 \phi_\gamma \, \mathrm{d}K}_{N_{\gamma\mu}} M_{\alpha\mu}^{-1} M_{\beta\gamma}^{-1}$$

$$+ \sum_K \left(\frac{\partial G}{\partial (\rho_0 \underline{v})_\beta} \frac{\partial F}{\partial p_\alpha} - \frac{\partial F}{\partial (\rho_0 \underline{v})_\beta} \frac{\partial G}{\partial p_\alpha} \right) \cdot \underbrace{\int_K \phi_\gamma \nabla_h \left(c_0^2 \rho_0 \phi_\mu \right) \, \mathrm{d}K}_{^2\underline{E}_{\gamma\mu}} M_{\alpha\mu}^{-1} M_{\beta\gamma}^{-1}$$

$$+ \sum_{e \in \Gamma_i} (1 - \theta^e) \left(\frac{\partial G}{\partial p_\alpha^L} \frac{\partial F}{\partial (\rho_0 \underline{v})_\beta^L} - \frac{\partial F}{\partial p_\alpha^L} \frac{\partial G}{\partial (\rho_0 \underline{v})_\beta^L} \right) \cdot \underbrace{\int_e \underline{\hat{n}}^L c_0^{2L} \rho_0^L \phi_\gamma^L \phi_\mu^L \, \mathrm{d}\Gamma}_{^2\underline{G}_{\gamma\mu}^{LL}} M_{\alpha\mu}^{-L} M_{\beta\gamma}^{-L}$$

$$+ \theta^e \left(\frac{\partial G}{\partial p_\alpha^L} \frac{\partial F}{\partial (\rho_0 \underline{v})_\beta^R} - \frac{\partial F}{\partial p_\alpha^L} \frac{\partial G}{\partial (\rho_0 \underline{v})_\beta^R} \right) \cdot \underbrace{\int_e \underline{\hat{n}}^L c_0^{2L} \rho_0^L \phi_\gamma^R \phi_\mu^L \, \mathrm{d}\Gamma}_{^2\underline{G}_{\gamma\mu}^{RL}} M_{\alpha\mu}^{-L} M_{\beta\gamma}^{-R}$$

$$- (1 - \theta^e) \left(\frac{\partial G}{\partial p_\alpha^R} \frac{\partial F}{\partial (\rho_0 \underline{v})_\beta^L} - \frac{\partial F}{\partial p_\alpha^R} \frac{\partial G}{\partial (\rho_0 \underline{v})_\beta^L} \right) \cdot \underbrace{\int_e \hat{\underline{n}}^L c_0^{2R} \rho_0^R \phi_\gamma^L \phi_\mu^R \, \mathrm{d}\Gamma}_{{}^2 \underline{G}_{\gamma\mu}^{LR}} M_{\alpha\mu}^{-R} M_{\beta\gamma}^{-L}$$

$$- \theta^e \left(\frac{\partial G}{\partial p_\alpha^R} \frac{\partial F}{\partial (\rho_0 \underline{v})_\beta^R} - \frac{\partial F}{\partial p_\alpha^R} \frac{\partial G}{\partial (\rho_0 \underline{v})_\beta^R} \right) \cdot \underbrace{\int_e \hat{\underline{n}}^L c_0^{2R} \rho_0^R \phi_\gamma^R \phi_\mu^R \, \mathrm{d}\Gamma}_{{}^2 \underline{G}_{\gamma\mu}^{RR}} M_{\alpha\mu}^{-R} M_{\beta\gamma}^{-R}.$$

In terms of the elemental matrices

$$[F, G] =$$

$$\sum_K \left(\frac{\partial G}{\partial (\rho_0 \underline{v})_\beta} \frac{\partial F}{\partial \rho_\alpha} - \frac{\partial F}{\partial (\rho_0 \underline{v})_\beta} \frac{\partial G}{\partial \rho_\alpha} \right) \cdot {}^1 \underline{E}_{\gamma\mu} M_{\alpha\mu}^{-1} M_{\beta\gamma}^{-1} + \left(\frac{\partial G}{\partial (\rho_0 w)_\beta} \frac{\partial F}{\partial p_\alpha} - \frac{\partial F}{\partial (\rho_0 w)_\beta} \frac{\partial G}{\partial p_\alpha} \right) N_{\gamma\mu} M_{\alpha\mu}^{-1} M_{\beta\gamma}^{-1}$$

$$+ \left(\frac{\partial G}{\partial (\rho_0 \underline{v})_\beta} \frac{\partial F}{\partial p_\alpha} - \frac{\partial F}{\partial (\rho_0 \underline{v})_\beta} \frac{\partial G}{\partial p_\alpha} \right) \cdot {}^2 \underline{E}_{\gamma\mu} M_{\alpha\mu}^{-1} M_{\beta\gamma}^{-1} - \left(\frac{\partial G}{\partial (\rho_0 \underline{v})_\beta} \frac{\partial F}{\partial \rho_\alpha} - \frac{\partial F}{\partial (\rho_0 \underline{v})_\beta} \frac{\partial G}{\partial \rho_\alpha} \right) \cdot {}^1 N_{\gamma\mu} M_{\alpha\mu}^{-1} M_{\beta\gamma}^{-1}$$

$$+ \sum_{e \in \Gamma_i} (1 - \theta^e) \left(\frac{\partial G}{\partial \rho_\alpha^L} \frac{\partial F}{\partial (\rho_0 \underline{v})_\beta^L} - \frac{\partial F}{\partial \rho_\alpha^L} \frac{\partial G}{\partial (\rho_0 \underline{v})_\beta^L} \right) \cdot {}^1 \underline{G}_{\gamma\mu}^{LL} M_{\alpha\mu}^{-L} M_{\beta\gamma}^{-L} + \theta^e \left(\frac{\partial G}{\partial \rho_\alpha^L} \frac{\partial F}{\partial (\rho_0 \underline{v})_\beta^R} - \frac{\partial F}{\partial \rho_\alpha^L} \frac{\partial G}{\partial (\rho_0 \underline{v})_\beta^R} \right) \cdot {}^1 \underline{G}_{\gamma\mu}^{RL} M_{\alpha\mu}^{-L} M_{\beta\gamma}^{-R}$$

$$- (1 - \theta^e) \left(\frac{\partial G}{\partial \rho_\alpha^R} \frac{\partial F}{\partial (\rho_0 \underline{v})_\beta^L} - \frac{\partial F}{\partial \rho_\alpha^R} \frac{\partial G}{\partial (\rho_0 \underline{v})_\beta^L} \right) \cdot {}^1 \underline{G}_{\gamma\mu}^{LR} M_{\alpha\mu}^{-R} M_{\beta\gamma}^{-L} - \theta^e \left(\frac{\partial G}{\partial \rho_\alpha^R} \frac{\partial F}{\partial (\rho_0 \underline{v})_\beta^R} - \frac{\partial F}{\partial \rho_\alpha^R} \frac{\partial G}{\partial (\rho_0 \underline{v})_\beta^R} \right) \cdot {}^1 \underline{G}_{\gamma\mu}^{RR} M_{\alpha\mu}^{-R} M_{\beta\gamma}^{-R}$$

$$+ (1 - \theta^e) \left(\frac{\partial G}{\partial p_\alpha^L} \frac{\partial F}{\partial (\rho_0 \underline{v})_\beta^L} - \frac{\partial F}{\partial p_\alpha^L} \frac{\partial G}{\partial (\rho_0 \underline{v})_\beta^L} \right) \cdot {}^2 \underline{G}_{\gamma\mu}^{LL} M_{\alpha\mu}^{-L} M_{\beta\gamma}^{-L} + \theta^e \left(\frac{\partial G}{\partial p_\alpha^L} \frac{\partial F}{\partial (\rho_0 \underline{v})_\beta^R} - \frac{\partial F}{\partial p_\alpha^L} \frac{\partial G}{\partial (\rho_0 \underline{v})_\beta^R} \right) \cdot {}^2 \underline{G}_{\gamma\mu}^{RL} M_{\alpha\mu}^{-L} M_{\beta\gamma}^{-R}$$

$$- (1 - \theta^e) \left(\frac{\partial G}{\partial p_\alpha^R} \frac{\partial F}{\partial (\rho_0 \underline{v})_\beta^L} - \frac{\partial F}{\partial p_\alpha^R} \frac{\partial G}{\partial (\rho_0 \underline{v})_\beta^L} \right) \cdot {}^2 \underline{G}_{\gamma\mu}^{LR} M_{\alpha\mu}^{-R} M_{\beta\gamma}^{-L} - \theta^e \left(\frac{\partial G}{\partial p_\alpha^R} \frac{\partial F}{\partial (\rho_0 \underline{v})_\beta^R} - \frac{\partial F}{\partial p_\alpha^R} \frac{\partial G}{\partial (\rho_0 \underline{v})_\beta^R} \right) \cdot {}^2 \underline{G}_{\gamma\mu}^{RR} M_{\alpha\mu}^{-R} M_{\beta\gamma}^{-R}.$$

$$(5.28)$$

For the discrete Hamiltonian, the same substitution is made. Substituting (5.21) into (5.7) yields

$$
\begin{aligned}
H = &\sum_K \int_K \frac{1}{2} \frac{1}{\rho_{0_h}} \left(\rho_0 \underline{v}\right)_\alpha \phi_\alpha \cdot \left(\rho_0 \underline{v}\right)_\beta \phi_\beta + \frac{1}{2} \frac{1}{\rho_{0_h} N_h^2} \left(\rho_\alpha \phi_\alpha \rho_\beta \phi_\beta - \frac{2 \rho_\alpha \phi_\alpha p_\beta \phi_\beta}{c_0^2} + \frac{p_\alpha \phi_\alpha p_\beta \phi_\beta}{c_0^4} \right) \\
&+ \frac{1}{2} \frac{p_\alpha \phi_\alpha p_\beta \phi_\beta}{\rho_{0_h} c_0^2} \, \mathrm{d}K \\
= &\sum_K \frac{1}{2} \underbrace{\left(\int_K \frac{\phi_\alpha \phi_\beta}{\rho_{0_h}} \, \mathrm{d}K \right)}_{{}^1 M_{\alpha\beta}} \left(\rho_0 \underline{v}\right)_\alpha \cdot \left(\rho_0 \underline{v}\right)_\beta + \frac{1}{2} \underbrace{\left(\int_K \frac{\phi_\alpha \phi_\beta}{\rho_{0_h} N_h^2} \, \mathrm{d}K \right)}_{{}^2 M_{\alpha\beta}} \rho_\alpha \rho_\beta \\
&- \underbrace{\left(\int_K \frac{\phi_\alpha \phi_\beta}{\rho_{0_h} N_h^2 c_0^2} \, \mathrm{d}K \right)}_{{}^3 M_{\alpha\beta}} \rho_\alpha p_\beta + \frac{1}{2} \underbrace{\left(\int_K \frac{\phi_\alpha \phi_\beta}{\rho_{0_h} N_h^2 c_0^4} \, \mathrm{d}K \right)}_{{}^4 M_{\alpha\beta}} p_\alpha p_\beta + \frac{1}{2} \underbrace{\left(\int_K \frac{\phi_\alpha \phi_\beta}{\rho_{0_h} c_0^2} \, \mathrm{d}K \right)}_{{}^5 M_{\alpha\beta}} p_\alpha p_\beta.
\end{aligned}
\tag{5.29}
$$

In terms of the elemental matrices

$$
H = \sum_K \frac{1}{2} {}^1 M_{\alpha\beta} \left(\rho_0 \underline{v}\right)_\alpha \cdot \left(\rho_0 \underline{v}\right)_\beta + \frac{1}{2} {}^2 M_{\alpha\beta} \rho_\alpha \rho_\beta - {}^3 M_{\alpha\beta} \rho_\alpha p_\beta + \frac{1}{2} {}^4 M_{\alpha\beta} p_\alpha p_\beta + \frac{1}{2} {}^5 M_{\alpha\beta} p_\alpha p_\beta.
\tag{5.30}
$$

A global formulation is introduced, using global coefficients $\underline{U}_i = (U, V, W)_i^T$, R_i and P_i. These represent the expansion coefficients from (5.21) and the index i runs over their global ranges. All elemental matrices extend to global matrices. The global formulation becomes

$$
\begin{aligned}
[F, G] = &\left(\frac{\partial G}{\partial \underline{U}_j} \frac{\partial F}{\partial R_i} - \frac{\partial F}{\partial \underline{U}_j} \frac{\partial G}{\partial R_i} \right) . \underline{DIV}^1_{kl} M_{ik}^{-1} M_{jl}^{-1} \\
&+ \left(\frac{\partial G}{\partial \underline{U}_j} \frac{\partial F}{\partial P_i} - \frac{\partial F}{\partial \underline{U}_j} \frac{\partial G}{\partial P_i} \right) . \underline{DIV}^2_{kl} M_{ik}^{-1} M_{jl}^{-1} \\
&+ \left(\frac{\partial G}{\partial W_j} \frac{\partial F}{\partial P_i} - \frac{\partial F}{\partial W_j} \frac{\partial G}{\partial P_i} \right) N_{kl} M_{ik}^{-1} M_{jl}^{-1} \\
&- \left(\frac{\partial G}{\partial \underline{U}_j} \frac{\partial F}{\partial R_i} - \frac{\partial F}{\partial \underline{U}_j} \frac{\partial G}{\partial R_i} \right) . \underline{N}_{kl} M_{ik}^{-1} M_{jl}^{-1},
\end{aligned}
\tag{5.31}
$$

with divergence operators $\underline{DIV}^1_{kl} = {}^1\underline{E}_{kl} - {}^1\underline{G}_{kl}$ and $\underline{DIV}^2_{kl} = {}^2\underline{E}_{kl} - {}^2\underline{G}_{kl}$ and global Hamiltonian

$$
H = \frac{1}{2} {}^1 M_{ij} \underline{U}_i . \underline{U}_j + \frac{1}{2} {}^2 M_{ij} R_i R_j - {}^3 M_{ij} R_i P_j + \frac{1}{2} {}^4 M_{ij} P_i P_j + \frac{1}{2} {}^5 M_{ij} P_i P_j.
\tag{5.32}
$$

Note the correspondence of the formulation of the discrete bracket (5.31) with the continuum bracket (4.28).

The resulting equations of motion are

$$
\begin{aligned}
\underline{\dot{U}}_j &= \left(-{}^2M_{il}\underline{DIV}^1_{kl} + {}^2M_{il}\underline{N}_{kl} + {}^3M_{il}\underline{DIV}^2_{kl} + {}^3M_{il}N_{kl}\hat{\underline{z}}\right)R_l M^{-1}_{ik}M^{-1}_{jl} \\
&\quad + \left({}^3M_{il}\underline{DIV}^1_{kl} - {}^3M_{il}\underline{N}_{kl} - {}^4M_{il}\underline{DIV}^2_{kl} - {}^5M_{il}\underline{DIV}^2_{kl}\right. \\
&\qquad \left. -{}^4M_{il}N_{kl}\hat{\underline{z}} - {}^5M_{il}N_{kl}\hat{\underline{z}}\right)P_l M^{-1}_{ik}M^{-1}_{jl} \\
\dot{R}_l &= \underline{U}_j.\underline{DIV}^1_{jk}{}^1 M_{ij}M^{-1}_{lj}M^{-1}_{ik} - \underline{U}_j.\underline{N}_{jk}{}^1 M_{ij}M^{-1}_{lj}M^{-1}_{ik} \\
\dot{P}_l &= W_j{}^1 M_{ij}N_{jk}M^{-1}_{lj}M^{-1}_{ik} + \underline{U}_j.\underline{DIV}^2_{jk}{}^1 M_{ij}M^{-1}_{lj}M^{-1}_{ik}.
\end{aligned}
\tag{5.33}
$$

Applying the modified midpoint scheme, conform Hairer et al. (2006), yields

$$
\begin{aligned}
\frac{U^{n+1}_j - U^n_j}{\Delta t} &= \left(-{}^2M_{il}\underline{DIV}^1_{kl} + {}^2M_{il}\underline{N}_{kl} + {}^3M_{il}\underline{DIV}^2_{kl} + {}^3M_{il}N_{kl}\hat{\underline{z}}\right)\frac{R^{n+1}_l + R^n_l}{2}M^{-1}_{ik}M^{-1}_{jl} \\
&\quad + \left({}^3M_{il}\underline{DIV}^1_{kl} - {}^3M_{il}\underline{N}_{kl} - {}^4M_{il}\underline{DIV}^2_{kl} - {}^5M_{il}\underline{DIV}^2_{kl}\right. \\
&\qquad \left. -{}^4M_{il}N_{kl}\hat{\underline{z}} - {}^5M_{il}N_{kl}\hat{\underline{z}}\right)\frac{P^{n+1}_l + P^n_l}{2}M^{-1}_{ik}M^{-1}_{jl} \\
\frac{R^{n+1}_l - R^n_l}{\Delta t} &= \frac{U^{n+1}_j + U^n_j}{2}.\underline{DIV}^1_{jk}{}^1 M_{ij}M^{-1}_{lj}M^{-1}_{ik} - \frac{U^{n+1}_j + U^n_j}{2}.\underline{N}_{jk}{}^1 M_{ij}M^{-1}_{lj}M^{-1}_{ik} \\
\frac{P^{n+1}_l - P^n_l}{\Delta t} &= \frac{W^{n+1}_j + W^n_j}{2}{}^1 M_{ij}N_{jk}M^{-1}_{lj}M^{-1}_{ik} + \frac{U^{n+1}_j + U^n_j}{2}.\underline{DIV}^2_{jk}{}^1 M_{ij}M^{-1}_{lj}M^{-1}_{ik}.
\end{aligned}
\tag{5.34}
$$

Multiplying (5.34-1) with

$$
\frac{1}{2}{}^1 M_{ij}\left(\underline{U}^{n+1}_i + \underline{U}^n_i\right),
$$

(5.34-2) with

$$
\frac{1}{2}{}^2 M_{kl}\left(R^{n+1}_k + R^n_k\right) - \frac{1}{2}{}^3 M_{kl}\left(P^{n+1}_k + P^n_k\right)
$$

and (5.34-3) with

$$
-\frac{1}{2}{}^3 M_{kl}\left(R^{n+1}_k + R^n_k\right) + \frac{1}{2}{}^4 M_{kl}\left(P^{n+1}_k + P^n_k\right) + \frac{1}{2}{}^5 M_{kl}\left(P^{n+1}_k + P^n_k\right)
$$

yields

$$
\frac{H^{n+1} - H^n}{\Delta t} = 0.
\tag{5.35}
$$

So the numerical scheme (5.34) is exactly energy conserving.

When the speed of sound, c_0^2, is constant, which is what will be chosen for the derivation of the incompressible case, then (5.29)-(5.34) greatly simplify; the distinction between $\underline{DIV}_{kl}^1$ and $\underline{DIV}_{kl}^2$ disappears, the distinction between $^1M_{ij}$ and $^5M_{ij}$ disappears and the distinction between $^2M_{ij}$, $^3M_{ij}$ and $^4M_{ij}$ disappears. The discrete Poisson bracket (5.31) simplifies to

$$
\begin{aligned}
[F, G] = \frac{\partial F}{\partial R_i} & \left(\frac{\partial G}{\partial \underline{U}_j} . \underline{DIV}_{kl} M_{ik}^{-1} M_{jl}^{-1} - \frac{\partial G}{\partial W_j} {}^1N_{kl} M_{ik}^{-1} M_{jl}^{-1} \right) \\
& - \frac{\partial G}{\partial R_i} \left(\frac{\partial F}{\partial \underline{U}_j} . \underline{DIV}_{kl} M_{ik}^{-1} M_{jl}^{-1} - \frac{\partial F}{\partial W_j} {}^1N_{kl} M_{ik}^{-1} M_{jl}^{-1} \right) \\
& + \frac{\partial F}{\partial P_i} \left(\frac{\partial G}{\partial W_j} N_{kl} M_{ik}^{-1} M_{jl}^{-1} + c_0^2 \frac{\partial G}{\partial \underline{U}_j} . \underline{DIV}_{kl} M_{ik}^{-1} M_{jl}^{-1} \right) \\
& - \frac{\partial G}{\partial P_i} \left(\frac{\partial F}{\partial W_j} N_{kl} M_{ik}^{-1} M_{jl}^{-1} + c_0^2 \frac{\partial F}{\partial \underline{U}_j} . \underline{DIV}_{kl} M_{ik}^{-1} M_{jl}^{-1} \right) .
\end{aligned}
\tag{5.36}
$$

The correspondence of the formulation of the discrete bracket (5.36) with the continuum bracket (4.28) is even clearer with the speed of sound, c_0^2, explicitly shown. The discrete Hamiltonian (5.32) simplifies to

$$
H = \frac{1}{2} {}^1M_{ij} \underline{U}_i . \underline{U}_j + \frac{1}{2} {}^2M_{ij} R_i R_j - \frac{1}{c_0^2} {}^2M_{ij} R_i P_j + \frac{1}{2} \frac{1}{c_0^4} {}^2M_{ij} P_i P_j + \frac{1}{2} \frac{1}{c_0^2} {}^1M_{ij} P_i P_j .
\tag{5.37}
$$

The resulting equations of motion are

$$
\begin{aligned}
\dot{\underline{U}}_j = & \left({}^2M_{il} {}^1N_{kl} + \frac{1}{c_0^2} {}^2M_{il} N_{kl} \right) \underline{\hat{z}} R_l M_{ik}^{-1} M_{jl}^{-1} \\
& + \left(-\frac{1}{c_0^2} {}^2M_{il} {}^1N_{kl} \underline{\hat{z}} - \frac{1}{c_0^4} {}^2M_{il} N_{kl} \underline{\hat{z}} - \frac{1}{c_0^2} {}^1M_{il} N_{kl} \underline{\hat{z}} - {}^1M_{il} \underline{DIV}_{kl} \right) P_l M_{ik}^{-1} M_{jl}^{-1} \\
\dot{R}_l = & \underline{U}_j . \underline{DIV}_{jk} {}^1M_{ij} M_{lj}^{-1} M_{ik}^{-1} - W_j . {}^1N_{jk} {}^1M_{ij} M_{lj}^{-1} M_{ik}^{-1} \\
\dot{P}_l = & W_j {}^1M_{ij} N_{jk} M_{lj}^{-1} M_{ik}^{-1} + c_0^2 \underline{U}_j . \underline{DIV}_{jk} {}^1M_{ij} M_{lj}^{-1} M_{ik}^{-1} .
\end{aligned}
\tag{5.38}
$$

Applying the modified midpoint scheme, conform Hairer et al. (2006), yields

$$
\begin{aligned}
\frac{\underline{U}_j^{n+1} - \underline{U}_j^n}{\Delta t} = & \left({}^2M_{il} {}^1N_{kl} + \frac{1}{c_0^2} {}^2M_{il} N_{kl} \right) \underline{\hat{z}} \frac{R_l^{n+1} + R_l^n}{2} M_{ik}^{-1} M_{jl}^{-1} \\
& + \left(-\frac{1}{c_0^2} {}^2M_{il} {}^1N_{kl} \underline{\hat{z}} - \frac{1}{c_0^4} {}^2M_{il} N_{kl} \underline{\hat{z}} - \frac{1}{c_0^2} {}^1M_{il} N_{kl} \underline{\hat{z}} - {}^1M_{il} \underline{DIV}_{kl} \right) \frac{P_l^{n+1} + P_l^n}{2} M_{ik}^{-1} M_{jl}^{-1} \\
\frac{R_l^{n+1} - R_l^n}{\Delta t} = & \frac{\underline{U}_j^{n+1} + \underline{U}_j^n}{2} . \underline{DIV}_{jk} {}^1M_{ij} M_{lj}^{-1} M_{ik}^{-1} - \frac{W_j^{n+1} + W_j^n}{2} . {}^1N_{jk} {}^1M_{ij} M_{lj}^{-1} M_{ik}^{-1} \\
\frac{P_l^{n+1} - P_l^n}{\Delta t} = & \frac{W_j^{n+1} + W_j^n}{2} {}^1M_{ij} N_{jk} M_{lj}^{-1} M_{ik}^{-1} + c_0^2 \frac{\underline{U}_j^{n+1} + \underline{U}_j^n}{2} . \underline{DIV}_{jk} {}^1M_{ij} M_{lj}^{-1} M_{ik}^{-1} .
\end{aligned}
\tag{5.39}
$$

5-3   Discrete Incompressible Dynamics

The discrete equations of motion for the incompressible case are obtained with two methods. The first method uses Dirac's theory of constraints. In the same manner as the continuous case, the bracket for compressible flow is constrained to incompressible flow. This is again done using Lagrange multipliers to enforce the constraint. The second method is ensuring the time scheme fixes the two constraints in time. The second method is a heuristic method that serves as an illustration of the more rigorous first method.

In the second method the pressure in (5.39-1) is replaced by a Lagrange multiplier Θ_l^{n+1} and for $c_0^2 \to \infty$,

$$
\begin{aligned}
\frac{U_j^{n+1} - U_j^n}{\Delta t} &= \left({}^2M_{il}{}^1N_{kl} + \frac{1}{c_0^2}{}^2M_{il}N_{kl}{}^{\nearrow 0} \right)\hat{\underline{z}}\frac{R_l^{n+1} + R_l^n}{2}M_{ik}^{-1}M_{jl}^{-1} \\
&+ \left(-\frac{1}{c_0^2}{}^2M_{il}{}^1N_{kl}\hat{\underline{z}}^{\nearrow 0} - \frac{1}{c_0^4}{}^2M_{il}N_{kl}\hat{\underline{z}}^{\nearrow 0} - \frac{1}{c_0^2}{}^1M_{il}N_{kl}\hat{\underline{z}}^{\nearrow 0} - {}^1M_{il}\underline{DIV}_{kl} \right)\Theta_l^{n+1}M_{im}^{-1}M_{jl}^{-1} \\
\frac{R_l^{n+1} - R_l^n}{\Delta t} &= \frac{U_j^{n+1} + U_j^n}{2}.\underline{DIV}_{jk}{}^1M_{ij}M_{lj}^{-1}M_{ik}^{-1} - \frac{W_j^{n+1} + W_j^n}{2}.{}^1N_{jk}{}^1M_{ij}M_{lj}^{-1}M_{ik}^{-1} \\
\frac{P_l^{n+1} - P_l^n}{\Delta t} &= \frac{W_j^{n+1} + W_j^n}{2}{}^1M_{ij}N_{jk}M_{lj}^{-1}M_{ik}^{-1} + c_0^2\frac{U_j^{n+1} + U_j^n}{2}.\underline{DIV}_{jk}{}^1M_{ij}M_{lj}^{-1}M_{ik}^{-1}.
\end{aligned}
$$
$$(5.40)$$

Assume the divergence of the velocity field at the current time level is zero,

$$
{}^1M_{jk}\underline{U}_k^n.\underline{DIV}_{kl}^1M_{jk}^{-1} = 0.
$$

Rescaling, as in Section 4-4, $\underline{U}_j^{n+1} \propto Ma$ yields that that the pressure evolution is zero,

$$
(P_l^{n+1} - P_l^n) = 0,
$$

if the divergence at the next time level is zero,

$$
{}^1M_{jk}\underline{U}_k^{n+1}.\underline{DIV}_{kl}^1M_{jk}^{-1} = 0.
$$

Now

$$
{}^1M_{jk}\underline{U}_k^{n+1}.\underline{DIV}_{kl}^1M_{jk}^{-1}
$$

remains zero if

$$
\begin{aligned}
{}^1M_{ij}\underline{DIV}_{jk}^1M_{ij}^{-1}.{}^2M_{il}\underline{N}_{kl}\frac{R_l^{n+1} + R_l^n}{2}M_{ik}^{-1}M_{jl}^{-1} &= \\
= {}^1M_{ij}\underline{DIV}_{jk}^1M_{ij}^{-1}.{}^1M_{il}\underline{DIV}_{ml}^1\Theta_l^{n+1}M_{im}^{-1}M_{jl}^{-1}.
\end{aligned}
$$
$$(5.41)$$

The equations of motion for incompressible flow are

$$
\begin{aligned}
\frac{U_j^{n+1} - U_j^n}{\Delta t} &= {}^2M_{il}{}^1N_{kl}\hat{\underline{z}}\frac{R_l^{n+1} + R_l^n}{2}M_{ik}^{-1}M_{jl}^{-1} - {}^1M_{il}\underline{DIV}_{ml}^1\Theta_l^{n+1}M_{im}^{-1}M_{jl}^{-1} \\
\frac{R_l^{n+1} - R_l^n}{\Delta t} &= -{}^1M_{ij}\frac{U_j^{n+1} + U_j^n}{2}.\underline{N}_{jk}M_{lj}^{-1}M_{ik}^{-1}.
\end{aligned}
$$
$$(5.42)$$

Note that the minus in the first term is hidden in the definition of the buoyancy frequency in $^2M_{il}$ and the z-direction in the first term is hidden in the gradient of the background density in $\underline{N}_{kl}$.

For the first method, the constraint of zero perturbation pressure in the continuous case yields the discrete constraint

$$D_k = M_{kl}P_l = 0. \tag{5.43}$$

The time evolution of this pressure perturbation should be zero, so

$$0 \approx \dot{D}_k = [D_k, H] + \lambda_l [D_k, D_l]. \tag{5.44}$$

From (5.36) follows $[D_k, D_l] = 0$, just as in the continuous case. There should still hold

$$
\begin{aligned}
0 = [D_k, H] &= \frac{\partial D_k}{\partial P_i} \left(\frac{\partial H}{\partial W_j} N_{kl} M_{ik}^{-1} M_{jl}^{-1} + \frac{c_0^2}{Ma^2} \frac{\partial H}{\partial \underline{U}_j} . \underline{DIV}_{kl} M_{ik}^{-1} M_{jl}^{-1} \right) \\
&= {}^1 M_{jk} W_k M_{il} N_{kl} M_{ik}^{-1} M_{jl}^{-1} + \frac{c_0^2}{Ma^2} {}^1 M_{jk} \underline{U}_k M_{il} . \underline{DIV}_{kl} M_{ik}^{-1} M_{jl}^{-1}.
\end{aligned}
\tag{5.45}
$$

A secondary constraint is obtained. This is the discrete version of (4.54). The difference in order of the Mach number between the two terms is clear. Scaling with $\underline{U}_j \propto Ma$, as in Section 4-4, and taking the limit of zero Mach number, $Ma \to 0$, the first term disappears. The second constraint is

$$L_k = {}^1 M_{jk} \underline{U}_k . \underline{DIV}_{kl}^1 M_{jk}^{-1} = 0, \tag{5.46}$$

which is a discrete version of the divergence of the velocity field.

Enforcing both constraints in time requires

$$
\begin{aligned}
0 &\approx \dot{D}_k = [D_k, H] + \mu_l [D_k, L_l], \\
0 &\approx \dot{L}_k = [L_k, H] + \lambda_l [L_k, D_l] + \mu_l [L_k, L_l].
\end{aligned}
\tag{5.47}
$$

From (5.36) the "double" term, $[L_k, L_l]$, is zero and the term $[D_k, H]$ is zero after using the constraints. The Lagrange multiplier μ_l is determined from

$$
\begin{aligned}
0 = \mu_l [D_k, L_l] &= \mu_l \frac{\partial D_k}{\partial P_i} \left(\frac{\partial L_l}{\partial W_j} N_{kl} M_{ik}^{-1} M_{jl}^{-1} + \frac{c_0^2}{Ma^2} \frac{\partial L_l}{\partial \underline{U}_j} . \underline{DIV}_{kl} M_{ik}^{-1} M_{jl}^{-1} \right) \\
0 = \mu_l &\left(\underline{\hat{z}} . {}^1 M_{jm} \underline{DIV}_{ml} M_{jm}^{-1} M_{jm}^{-1} N_{jk} + \frac{c_0^2}{Ma^2} {}^1 M_{jm} \underline{DIV}_{ml} M_{jm}^{-1} M_{jm}^{-1} . \underline{DIV}_{jk} \right)
\end{aligned}
\tag{5.48}
$$

This equation determines the Lagrange multiplier μ_l. The most simple solution is $\mu_l = 0$.

The second Lagrange multiplier can be determined from

$$0 = [L_k, H] + \lambda_l [L_k, D_l]$$

$$
\begin{aligned}
0 = & -\frac{\partial H}{\partial R_i} \left(\frac{\partial L_k}{\partial \underline{U}_j} \cdot \underline{DIV}_{kl} - \frac{\partial L_k}{\partial W_j} {}^1 N_{kl} \right) M_{ik}^{-1} M_{jl}^{-1} \\
& - \frac{\partial H}{\partial P_i} \left(\frac{\partial L_k}{\partial W_j} N_{kl} + \frac{c_0^2}{Ma^2} \frac{\partial L_k}{\partial \underline{U}_j} \cdot \underline{DIV}_{kl} \right) M_{ik}^{-1} M_{jl}^{-1} \\
& - \lambda_l \frac{\partial D_l}{\partial P_i} \left(\frac{\partial L_k}{\partial W_j} N_{kl} + \frac{c_0^2}{Ma^2} \frac{\partial L_k}{\partial \underline{U}_j} \cdot \underline{DIV}_{kl} \right) M_{ik}^{-1} M_{jl}^{-1} \\
= & \; {}^2 M_{il} R_l \underline{\hat{z}} . {}^1 M_{ij} \underline{DIV}_{jk} M_{ij}^{-1} \left({}^1 N_{kl} + \frac{Ma^2}{c_0^2} N_{kl} \right) \\
& + \lambda_l {}^1 M_{ij} \underline{DIV}_{jk} M_{ij}^{-1} . \left(-\underline{\hat{z}} M_{il} N_{ml} - \frac{c_0^2}{Ma^2} M_{il} \underline{DIV}_{ml} \right) M_{ik}^{-1} M_{jl}^{-1},
\end{aligned}
\tag{5.49}
$$

where the constraint $P_l = 0$ was used. This equation determines the Lagrange multiplier λ_l. Again, a difference in the order of the Mach number is present. Scaling the Lagrange multiplier with the Mach number squared and taking the limit of $Ma \to 0$ yields

$$0 = {}^2 M_{il} R_l \underline{\hat{z}} . {}^1 M_{ij} \underline{DIV}_{jk} M_{ij}^{-1}{}^1 N_{kl} - \lambda_l {}^1 M_{ij} \underline{DIV}_{jk} M_{ij}^{-1} . M_{il} \underline{DIV}_{ml} M_{ik}^{-1} M_{jl}^{-1}. \tag{5.50}$$

The Lagrange multiplier plays the role of pressure as: ${}^1 M_{il} \Theta_l M_{il} = c_0^2 \lambda_l$.

The resulting discrete, linear, incompressible Hamiltonian dynamics is given by

$$
\begin{aligned}
\frac{dF}{dt} = & -\left(\frac{\partial H}{\partial W_j} \frac{\partial F}{\partial R_i} - \frac{\partial F}{\partial W_j} \frac{\partial H}{\partial R_i} \right) {}^1 N_{kl} M_{ik}^{-1} M_{jl}^{-1} - {}^1 M_{il} \Theta_l M_{il}^{-1} \frac{\partial F}{\partial \underline{U}_j} . \underline{DIV}_{ml}^1 M_{jm}^{-1} \\
0 = & \; {}^2 M_{il} R_l \underline{\hat{z}} . {}^1 M_{ij} \underline{DIV}_{jk} M_{ij}^{-1}{}^1 N_{kl} - \lambda_l {}^1 M_{ij} \underline{DIV}_{jk} M_{ij}^{-1} . M_{il} \underline{DIV}_{ml} M_{ik}^{-1} M_{jl}^{-1}
\end{aligned}
\tag{5.51}
$$

with constrained Hamiltonian

$$H = \frac{1}{2} {}^1 M_{ij} \underline{U}_i . \underline{U}_j + \frac{1}{2} {}^2 M_{ij} R_i Rj. \tag{5.52}$$

The equations of motion obtained from the bracket are

$$
\begin{aligned}
\dot{\underline{U}}_j &= \underline{\hat{z}} {}^2 M_{il} {}^1 N_{kl} R_l M_{ik}^{-1} M_{jl}^{-1} - {}^1 M_{il} \Theta_l M_{il}^{-1} \underline{DIV}_{ml}^1 M_{jm}^{-1} \\
\dot{R}_l &= -{}^1 M_{ij} {}^1 N_{jk} W_j M_{jl}^{-1} M_{ik}^{-1},
\end{aligned}
\tag{5.53}
$$

combined with (5.50). Applying the modified midpoint scheme yields

$$
\begin{aligned}
\frac{U_j^{n+1} - U_j^n}{\Delta t} &= \underline{\hat{z}} {}^2 M_{il} {}^1 N_{kl} \frac{R_l^{n+1} + R_l^n}{2} M_{ik}^{-1} M_{jl}^{-1} - {}^1 M_{il} \Theta_l^{n+1} M_{il}^{-1} \underline{DIV}_{ml}^1 M_{jm}^{-1} \\
\frac{R_l^{n+1} - R_l^n}{\Delta t} &= -{}^1 M_{ij} {}^1 N_{jk} \frac{W_j^{n+1} + W_j^n}{2} M_{lj}^{-1} M_{ik}^{-1} \\
{}^1 M_{ij} \underline{DIV}_{jk}^1 M_{ij}^{-1} . \underline{\hat{z}} {}^2 M_{il} {}^1 N_{kl} & \frac{R_l^{n+1} + R_l^n}{2} M_{ik}^{-1} M_{jl}^{-1} = \\
&= {}^1 M_{ij} \underline{DIV}_{jk}^1 M_{ij}^{-1}{}^1 M_{il} \Theta_l^{n+1} M_{il}^{-1} M_{jm}^{-1} . \underline{DIV}_{ml}^1.
\end{aligned}
\tag{5.54}
$$

Assume that the velocity at time level n is divergence free, so ${}^1M_{ij}\underline{DIV}^1_{jk}M^{-1}_{ij}.\underline{U}^n_j = 0$. To show the velocity stays divergence free, multiply (5.54-1) by ${}^1M_{ij}\underline{DIV}^1_{jk}M^{-1}_{ij}$ to obtain

$$
\begin{aligned}
{}^1M_{ij}\underline{DIV}^1_{jk}M^{-1}_{ij}.\frac{\underline{U}^{n+1}_j - \underline{U}^n_j}{\Delta t} &= \frac{1}{\Delta t}{}^1M_{ij}\underline{DIV}^1_{jk}M^{-1}_{ij}.\underline{U}^{n+1}_j = \\
&= {}^1M_{ij}\underline{DIV}^1_{jk}M^{-1}_{ij}.\left(\underline{\hat{z}}^2 M_{il}{}^1N_{kl}\frac{R^{n+1}_l + R^n_l}{2}M^{-1}_{ik}M^{-1}_{jl} - {}^1M_{il}\Theta^{n+1}_l M^{-1}_{il}\underline{DIV}^1_{ml}M^{-1}_{jm} \right) \\
&= 0,
\end{aligned}
$$

(5.55)

by (5.54-3). To show the Hamiltonian is preserved, multiply (5.54-1) with $\frac{1}{2}{}^1M_{ij}\left(\underline{U}^{n+1}_i + \underline{U}^n_i\right)$ and (5.54-2) with $\frac{1}{2}{}^2M_{kl}\left(R^{n+1}_k + R^n_k\right)$ and add over all elements to obtain

$$
\frac{H^{n+1} - H^n}{\Delta t} = -\frac{1}{2}{}^1M_{ij}\left(\underline{U}^{n+1}_i + \underline{U}^n_i\right).\underline{DIV}^1_{ml}{}^1M_{il}\Theta^{n+1}_l M^{-1}_{il}M^{-1}_{jm} = 0,
$$

(5.56)

by the zero divergence of the velocity field. So the numerical scheme (5.54) conserves the energy and the divergence of the velocity field exactly.

5-4   Boussinesq Approximation

The Boussinesq approximation in the continuous case consists of replacing the background density in the inertia terms by a constant background reference density, ρ^*. This corresponded to replacing the background density by the constant reference density and redefining the buoyancy frequency to (2.20) in the Hamiltonian and replacing the variations with respect to the product of the background density and the velocity with the variations with respect to the product of the reference density and the velocity in the Poisson bracket. In the discrete case the scaled, constant reference density is ρ^*_h. The discrete momenta, $\underline{U}$, need to be redefined to

$$
\underline{U} = (\rho^*\underline{v})_h,
$$

(5.57)

so the background density is replaced by the constant reference density. From (5.29) follows that the first term of the Hamiltonian no longer is a function of the background density. The discrete Hamiltonian (5.52) is changed to

$$
H = \frac{1}{2}{}^1M_{ij}\underline{U}_i.\underline{U}_j + \frac{1}{2}{}^2M_{ij}R_iR_j
$$

(5.58)

and in the Poisson bracket (5.51) the $\underline{U}_j$ are replaced by their new definition. Scale $\rho^*_h = 1$. Since the first term in the Hamiltonian no longer depends on the background density, the numerical fluxes (5.12) show that the discrete divergence operators $\underline{DIV}_{ml}$ no longer depend on ρ_{0_h}. Also the discrete divergence (5.46) does not depend on ρ_{0_h} anymore. The equations of motion obtained from the bracket are

$$
\begin{aligned}
\dot{\underline{U}}_j &= \underline{\hat{z}}^2 M_{il}{}^1N_{kl}R_l M^{-1}_{ik}M^{-1}_{jl} - \Theta_l\underline{DIV}^1_{ml}M^{-1}_{jm} \\
\dot{R}_l &= -\underline{N}_{jk}.\underline{U}_j M^{-1}_{lk}.
\end{aligned}
$$

(5.59)

Applying the modified midpoint scheme yields

$$\frac{U_j^{n+1} - U_j^n}{\Delta t} = \underline{\hat{z}}^2 M_{il}^{-1} N_{kl} \frac{R_l^{n+1} + R_l^n}{2} M_{ik}^{-1} M_{jl}^{-1} - \Theta_l^{n+1} \underline{DIV}_{ml}^1 M_{jm}^{-1}$$

$$\frac{R_l^{n+1} - R_l^n}{\Delta t} = -^1 N_{jk} \cdot \frac{W_j^{n+1} + W_j^n}{2} M_{lk}^{-1} \tag{5.60}$$

$$\underline{DIV}_{jk}^1 \cdot \underline{\hat{z}}^2 M_{il}^{-1} N_{kl} \frac{R_l^{n+1} + R_l^n}{2} M_{ik}^{-1} M_{jl}^{-1} = \underline{DIV}_{jk}^1 \Theta_l^{n+1} M_{jm}^{-1} \cdot \underline{DIV}_{ml}^1.$$

The scheme is again exactly energy conserving and exactly velocity-divergence conserving.

5-5   Implementation of the Discrete System

From (5.34) a global system is formulated. All terms multiplying the coefficients at the next time step are collected in a matrix P and all terms multiplying the coefficients at the current time step are collected in a matrix Q. The matrices P and Q are time independent. Denoting the vector of coefficients with X the constructed system is

$$PX^{n+1} = QX^n. \tag{5.61}$$

The discretization was implemented in the hpGEM C++ software framework Pesch et al. (2007). The computational linear algebra demands were handled by using PETSc Balay et al. (2013). This tool kit PETSc, a "Portable, Extensible Toolkit for Scientific Computation", consists of a number of sparse matrix storage routines and both iterative and direct sparse linear solvers.

Figure 5-4 shows the P–matrix for three-dimensional compressible flow. The symbols on the left and the bottom correspond to the discrete variables. The discrete gradient operator, DIV, appears in the top left and twice in the bottom right. For compressible flow a GMRES iterative solver was used to reach the desired tolerance of 10^{-14}. For incompressible flow a ILU preconditioner was added to speed up the computations.

Figure 5-5 shows the P–matrix for three-dimensional (incompressible) Euler-Boussinesq flow. The bottom right shows the Poisson like structure. A BiCGStab (Stabilized version of Bi-Conjugate Gradient Squared) iterative solver with an SOR preconditioner was used to reach the desired tolerance of 10^{-14}.

The exact preservation of the Hamiltonian dynamics as well as the constraints make the system unconditionally stable. Explicit pressure stabilization, artificial compressibility or projection are not needed to ensure a zero divergence velocity field. A direct DGFEM discretization of the incompressible Euler equations generally requires the inf-sup condition to be satisfied to attain numerical stability. The developed numerical method is unconditionally stable. This invites a study into whether or how this Hamiltonian DGFEM discretization satisfies the inf-sup condition.

The designed discretization conserves the discrete divergence of the velocity exactly. Even though the continuous initial condition is divergence-free, the discrete initial condition is not: the projection of the initial, divergence-free velocity field on the chosen discontinuous Galerkin finite element space only satisfies discrete zero-divergence up to the order of accuracy. A new
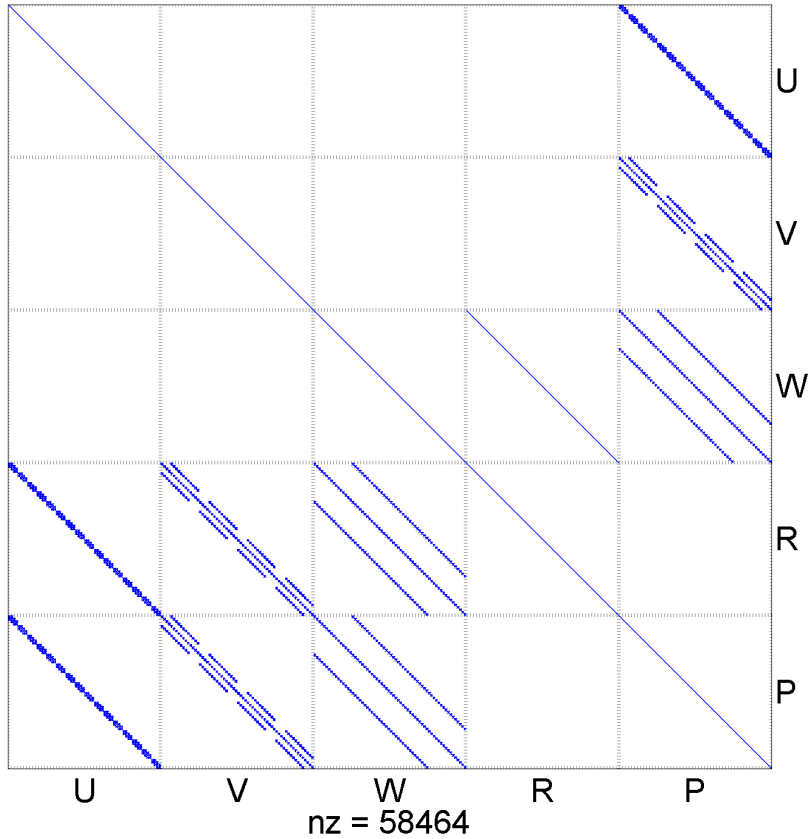
Figure 5-4: The P–matrix for three-dimensional compressible flow. All nonzero elements are shown. The letters indicate the discrete variables. nz denotes the number of nonzero entries. The number of elements in each direction was four and the polynomial order was two.

initial velocity, $\underline{U}^*$, is sought such that the discrete divergence of the velocity, (5.46), is zero, $^1 M_{jk} \underline{U}^*_k . \underline{DIV}^1_{kl} M^{-1}_{jk} = 0$ and the distance between the old initial velocity, $\underline{U}$, and the new initial velocity, $||\underline{U}^* - \underline{U}||$, is minimal. A projection of the vector $\underline{U}$ on the space kernel of the discrete divergence matrix operator is sought. Denote this projection with P_U. Then

$$\underline{U}^* = P_U \underline{U} = \underline{U} + \underline{U}^\perp, \tag{5.62}$$

where $\underline{U}^\perp$ is perpendicular to the kernel. Applying the discrete divergence operator to 5.62 yields (cf.Nurijanyan et al. (2013))

$$0 = {}^1 M_{jk} \underline{U}_k . \underline{DIV}^1_{kl} M^{-1}_{jk} + {}^1 M_{jk} \underline{U}^\perp_k . \underline{DIV}^1_{kl} M^{-1}_{jk}, \tag{5.63}$$

where the discrete divergence of the new initial velocity, $\underline{U}^*$, being zero, was used. (5.63) is solved for $\underline{U}^\perp$ via a least-square approximation. Then the new, divergence-free, initial velocity, $\underline{U}^*$, is computed with (5.62). Now that the initial velocity is divergence-free, the solution stays divergence-free due to the conservation of divergence of the velocity due to the dynamics.
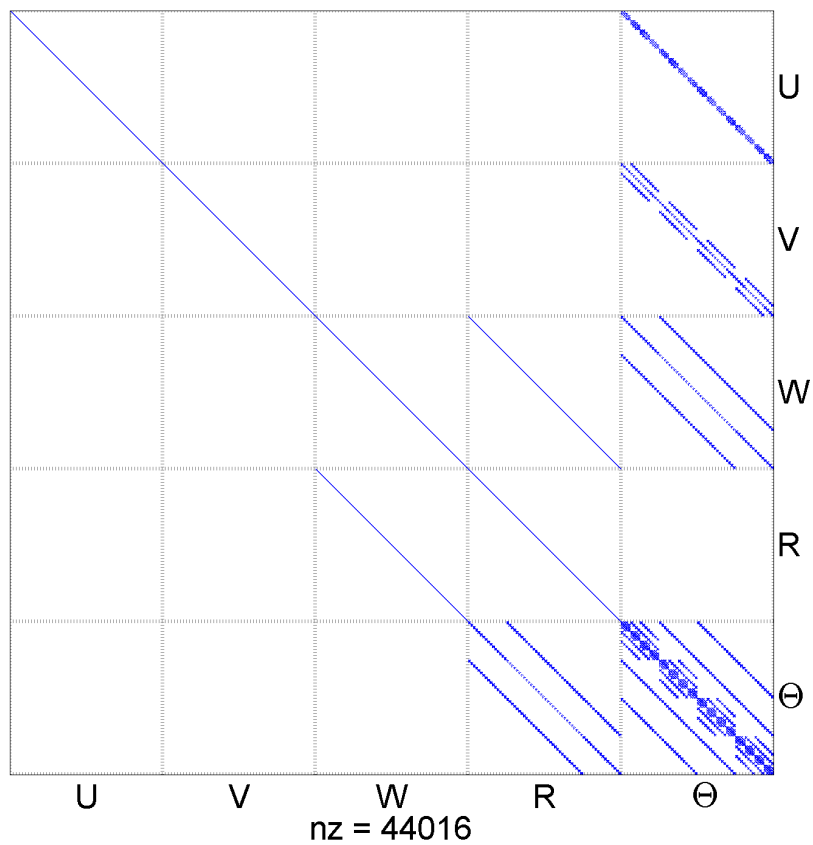
Figure 5-5: The P–matrix for three-dimensional (incompressible) Euler-Boussinesq flow. All nonzero elements are shown. The letters indicate the discrete variables. nz denotes the number of nonzero entries. The number of elements in each direction was four and the polynomial order was two.

Chapter 6

Verification

In this chapter the numerical model is verified. Figure 6-1 shows again the different systems of model equations. For systems ① to ③ Chapter 2 presented analytical solutions. The numerical solutions are compared to these analytical solutions.

primitive Euler equations — compressible stratified Euler equations — incompressible stratified Euler equations — Euler-Boussinesq equations

$$\boxed{0} \xrightarrow{\text{linearization}} \boxed{1} \xrightarrow{c_0^2 \to \infty} \boxed{2} \xrightarrow{\rho_0 \underline{v} \to \rho^* \underline{v}} \boxed{3}$$
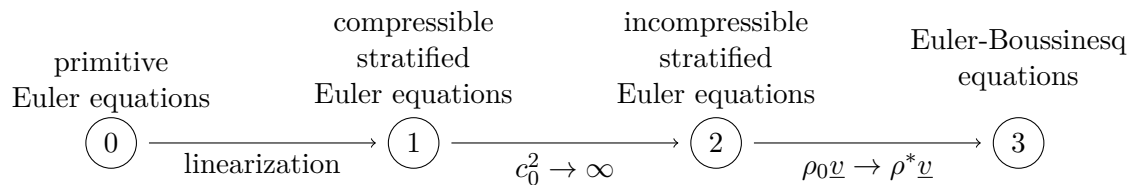
Figure 6-1: The systems of equations discussed in this thesis and their connections. The circled numbers indicate the different systems and the arrows indicate approximations: linearization, incompressibility ($c_0^2 \to \infty$) and Boussinesq ($\rho_0 \underline{v} \to \rho^* \underline{v}$). Systems ① to ③ are analytically and numerically solved.

Unless specified otherwise, $\theta = 1/2$ was used in the numerical flux. For other constant values of $0 \leq \theta \leq 1$ the results are similar to those presented here. Several test cases are presented where the parameter θ is randomly varied along the interior boundaries.

6-1   Compressible Stratified Euler Equations

Consider (2.3) and nondimensionalize as in Section 4-4. Scale such that $Ma = Fr = \delta = 1$. Assume c_0^2 is uniform and scale such that $c_0^2 = 1$. Then the (2.3) reduces to

$$
\begin{aligned}
\frac{\partial(\rho_0 u)}{\partial t} &= -\frac{\partial p}{\partial x}, \\
\frac{\partial(\rho_0 v)}{\partial t} &= -\frac{\partial p}{\partial y}, \\
\frac{\partial(\rho_0 w)}{\partial t} &= -\rho - \frac{\partial p}{\partial z}, \\
\frac{\partial \rho}{\partial t} &= -\left(\frac{\partial(\rho_0 u)}{\partial x} + \frac{\partial(\rho_0 v)}{\partial y} + \frac{\partial(\rho_0 w)}{\partial z}\right), \\
\frac{\partial p}{\partial t} &= \rho_0 w - \rho_0\left(\frac{\partial u}{\partial x} + \frac{\partial v}{\partial y} + \frac{\partial w}{\partial z}\right).
\end{aligned}
\tag{6.1}
$$

6-1-1   One-Dimensional Waves

A one-dimensional solution to (6.1), with constant N^2, is obtained from (2.9) – (2.11). Taking a background density field of $\rho_0 = \exp(-3z)$ yields a buoyancy frequency of $N^2 = 2$. For $H_z = 1$ and $n_z = 2$ in (2.10), a one-dimensional solution is

$$
\begin{aligned}
\rho_0 w &= \exp^{-\frac{1}{2}\left(N^2+1\right)z} \sin(2\pi z)\sin(\sigma t + 0.1), \\
\rho &= \exp^{-\frac{1}{2}\left(N^2+1\right)z}\left(-\frac{N^2+1}{2\sigma}\sin(2\pi z) + \frac{2\pi}{\sigma}\cos(2\pi z)\right)\cos(\sigma t + 0.1), \\
p &= \exp^{-\frac{1}{2}\left(N^2+1\right)z}\left(\frac{N^2-1}{2\sigma}\sin(2\pi z) + \frac{2\pi}{\sigma}\cos(2\pi z)\right)\cos(\sigma t + 0.1)
\end{aligned}
\tag{6.2}
$$

with dispersion relation

$$
4\sigma^2 = \left(N^2 + 1\right)^2 + 16\pi^2.
\tag{6.3}
$$

The boundary condition is no normal flow in the z–direction. The energy of the system is found from (2.13) as

$$
\mathcal{H} = \int_0^1 \frac{1}{2}\frac{1}{\rho_0}(\rho_0 w)^2 + \frac{1}{2}\frac{1}{\rho_0 N^2}\left(\rho - p\right)^2 + \frac{1}{2}\frac{p^2}{\rho_0}\,\mathrm{d}z = \frac{1}{4}.
\tag{6.4}
$$

The numerical discretization is initialized at time $t = 0$ and compared to the exact solution. By introducing a phase shift of 0.1 in (6.2) all variables of the solution were ensured to be nonzero. The background density ρ_0 was used as a continuous function. Table 6-1 presents the L^2–error and the order of convergence of the numerical solution after five periods. The order of convergence approaches polynomial order plus one. Figure 6-2 shows the error in the energy for 100 periods.
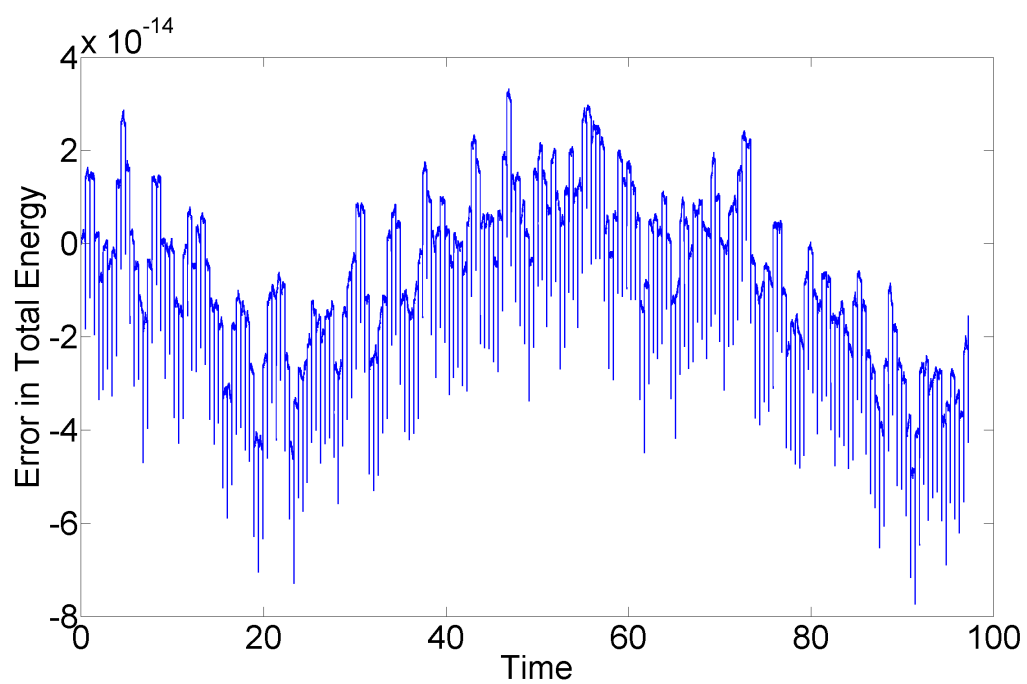
Figure 6-2: The error in the total energy periods for one-dimensional waves in a solid wall domain for a stratified compressible fluid during 100 periods. The spatial step size was $1/32$ and the polynomial order was two.

Table 6-1: L^2–error and order of convergence of the numerical solution after three periods for one-dimensional waves in a solid wall domain for a stratified compressible fluid. The polynomial is varied from zero to three. The number of time steps per period equals ten times the square of the number of elements in a direction.

p=0	$\rho_0 w$		ρ		p	
K	L^2–error	Order	L^2–error	Order	L^2–error	Order
4	4.812E-1	-	4.787E-1	-	3.823E-1	-
8	3.896E-1	0.30	5.098E-1	-0.09	5.184E-1	-0.44
16	1.644E-1	1.24	6.230E-2	3.03	4.902E-2	3.40
32	4.365E-2	1.91	1.488E-2	2.07	9.868E-3	2.31
64	1.107E-2	1.98	4.707E-3	1.66	2.934E-3	1.75
128	2.898E-3	1.93	1.736E-3	1.44	1.098E-3	1.42
p=1	$\rho_0 w$		ρ		p	
K	L^2–error	Order	L^2–error	Order	L^2–error	Order
4	3.271E-1	-	2.036E-1	-	2.232E-1	-
8	9.643E-2	1.76	3.131E-2	2.70	3.545E-2	2.65
16	2.345E-2	2.04	1.044E-2	1.58	7.643E-3	2.21
32	6.264E-3	1.90	3.239E-3	1.69	1.598E-3	2.26
64	1.672E-3	1.91	1.103E-3	1.55	3.786E-4	2.08
128	4.599E-4	1.86	3.814E-4	1.53	9.331E-5	2.02
p=2	$\rho_0 w$		ρ		p	
K	L^2–error	Order	L^2–error	Order	L^2–error	Order
4	1.426E-2	-	1.084E-2	-	9.922E-3	-
8	1.777E-3	3.00	2.325E-3	2.22	2.190E-3	2.18
16	1.757E-4	3.34	2.146E-4	3.44	2.057E-4	3.41
32	1.783E-5	3.30	1.610E-5	3.74	1.576E-5	3.71
64	5.368E-7	5.05	1.401E-6	3.52	1.387E-6	3.51
128	6.874E-8	2.97	1.314E-7	3.41	1.290E-7	3.43
p=3	$\rho_0 w$		ρ		p	
K	L^2–error	Order	L^2–error	Order	L^2–error	Order
4	2.507E-3	-	2.310E-3	-	2.049E-3	-
8	2.525E-4	3.31	1.506E-4	3.94	1.334E-4	3.94
16	1.815E-5	3.80	9.952E-6	3.92	8.421E-6	3.99
32	2.993E-6	2.60	7.235E-7	3.78	5.995E-7	3.81
64	2.318E-7	3.69	4.531E-8	4.00	3.314E-8	4.18

6-1-2 Two-dimensional Waves

A two-dimensional solution to (6.1), with constant N^2, is obtained from (2.9) – (2.11). Taking a background density field of $\rho_0 = \exp(-3z)$ yields a buoyancy frequency of $N^2 = 2$. For $H_x = H_z = 1$ and $n_x = n_z = 2$ in (2.10), a two-dimensional solution is

$$\rho_0 u = \exp^{-\frac{1}{2}(N^2+1)z} \frac{2\pi}{4\pi^2 - \sigma^2} \left(-2\pi \cos(2\pi z) - \frac{N^2 - 1}{2} \sin(2\pi z) \right) \sin(2\pi x) \sin(\sigma t + 0.1),$$

$$\rho_0 w = \exp^{-\frac{1}{2}(N^2+1)z} \sin(2\pi z) \cos(2\pi x) \sin(\sigma t + 0.1),$$

$$\rho = \exp^{-\frac{1}{2}(N^2+1)z} \frac{\sigma}{4\pi^2 - \sigma^2} \left[\left(\frac{N^2 + 1}{2} - \frac{4\pi^2 N^2}{\sigma^2} \right) \sin(2\pi z) \right.$$

$$\left. -2\pi \cos(2\pi z) \right] \cos(2\pi x) \cos(\sigma t + 0.1),$$

$$p = \exp^{-\frac{1}{2}(N^2+1)z} \frac{\sigma}{4\pi^2 - \sigma^2} \left(-\frac{N^2 - 1}{2} \sin(2\pi z) - 2\pi \cos(2\pi z) \right) \cos(2\pi x) \cos(\sigma t + 0.1)$$

$$(6.5)$$

with dispersion relation

$$2\sigma^2 = 8\pi^2 + \frac{1}{4} \left(N^2 + 1 \right)^2 + \sqrt{ \left(8\pi^2 + \frac{1}{4} \left(N^2 + 1 \right)^2 \right)^2 - 16\pi^2 N^2 }. \qquad (6.6)$$

The boundary condition is no normal flow in the z–direction. The boundary condition in the x–direction can either be no normal flow or periodic. The energy of the system is found from (2.13) as

$$\mathcal{H} = \int_0^1 \int_0^1 \frac{1}{2} \frac{1}{\rho_0} \left((\rho_0 u)^2 + (\rho_0 w)^2 \right) + \frac{1}{2} \frac{1}{\rho_0 N^2} (\rho - p)^2 + \frac{1}{2} \frac{p^2}{\rho_0} \, \mathrm{d}x \mathrm{d}z \approx 0.239476. \qquad (6.7)$$

The numerical discretization is initialized at time $t = 0$ and compared to the exact solution. Table 6-2 presents the L^2–error and the order of convergence of the numerical solution after three periods. The total energy is conserved up to machine precision. Figure 6-3 shows the error in the total energy, the mass, the momentum in the x–direction and the momentum in the z–direction for 100 periods for a polynomial order zero. Figure 6-4 shows the same for a polynomial order two. Figure 6-5 shows the vertical velocity of the numerical solution during one period.
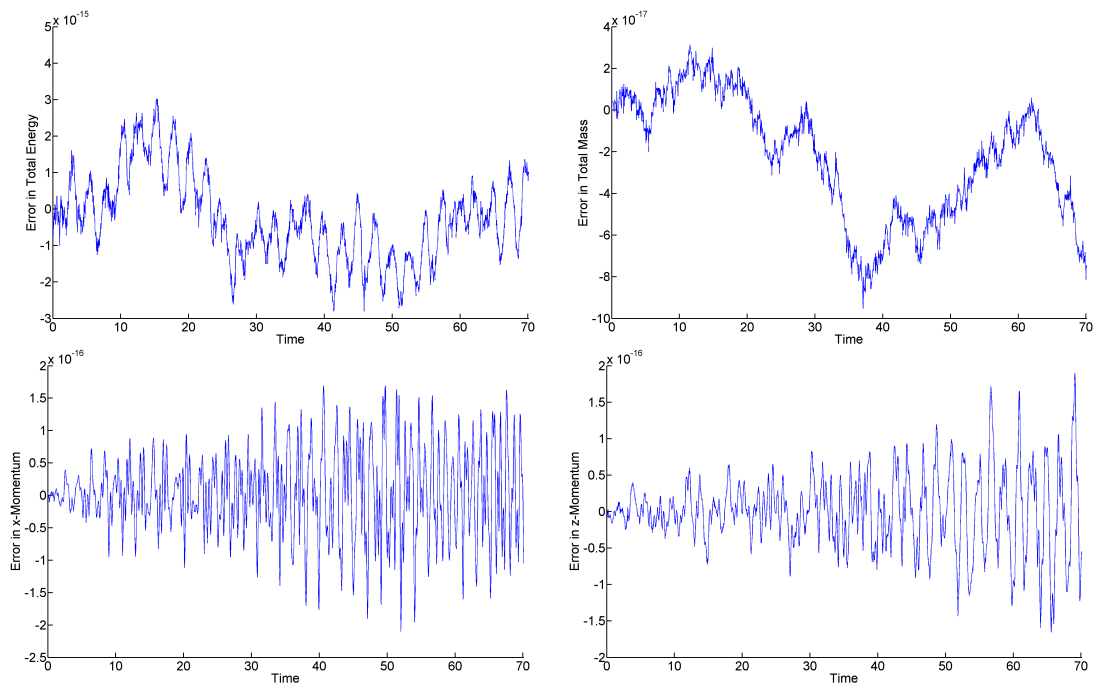
Figure 6-3: The conserved quantities for the numerical solution for two-dimensional waves in a solid wall domain for a stratified compressible fluid during 100 periods. The top left image shows the error in the total energy, the top right image the error in the total mass, the bottom left image the error in the total momentum in the x–direction and the bottom right image the error in the total momentum in the z–direction. The polynomial order was zero, the spatial and temporal step size were $1/16$.

Table 6-2: L^2–error and order of convergence of the numerical solution after three periods for two-dimensional waves in a solid wall domain for a stratified compressible fluid. The polynomial is varied from zero to three. The number of time steps per period equals ten times the square of the number of elements in a direction.

| $p = 0$	$\rho_0 u$		$\rho_0 w$		ρ		p	
K	L^2–error	Order	L^2–error	Order	L^2–error	Order	L^2–error	Order
4	2.044E-1	-	1.679E-1	-	4.171E-1	-	3.437E-1	-
8	2.827E-1	-0.47	2.651E-1	-0.66	6.026E-1	-0.53	6.121E-1	-0.83
16	1.437E-1	0.98	1.385E-1	0.94	7.002E-2	3.11	6.380E-2	3.26
32	3.645E-2	1.98	3.513E-2	1.98	1.406E-2	2.32	1.076E-2	2.57
64	8.987E-3	2.02	8.722E-3	2.01	4.955E-3	1.50	3.719E-3	1.53
128	2.230E-3	2.01	2.297E-3	1.92	1.605E-3	1.63	1.153E-3	1.69
256	5.554E-4	2.01	6.702E-4	1.78	5.103E-4	1.65	3.413E-4	1.76
$p = 1$	$\rho_0 u$		$\rho_0 w$		ρ		p	
K	L^2–error	Order	L^2–error	Order	L^2–error	Order	L^2–error	Order
4	7.001E-2	-	1.058E-1	-	1.267E-1	-	1.445E-1	-
8	5.668E-2	0.30	6.388E-2	0.73	3.114E-2	2.02	3.036E-2	2.25
16	1.761E-2	1.69	2.891E-2	1.14	6.584E-3	2.24	5.692E-3	2.41
32	5.073E-3	1.80	8.970E-3	1.69	1.314E-3	2.32	9.670E-4	2.55
64	1.426E-3	1.83	2.875E-3	1.64	3.526E-4	1.90	2.099E-4	2.20
128	4.165E-4	1.78	9.828E-4	1.55	1.069E-4	1.72	5.027E-5	2.06
$p = 2$	$\rho_0 u$		$\rho_0 w$		ρ		p	
K	L^2–error	Order	L^2–error	Order	L^2–error	Order	L^2–error	Order
4	6.061E-2	-	6.237E-2	-	5.136E-2	-	3.708E-2	-
8	4.476E-3	3.76	3.837E-3	4.02	4.534E-3	3.50	5.250E-3	2.82
16	4.741E-4	3.24	5.144E-4	2.90	4.440E-4	3.35	4.585E-4	3.52
32	3.255E-5	3.86	4.451E-5	3.53	5.360E-5	3.05	3.884E-5	3.56
64	1.886E-6	4.11	2.701E-6	4.04	6.700E-6	3.00	2.961E-6	3.71
$p = 3$	$\rho_0 u$		$\rho_0 w$		ρ		p	
K	L^2–error	Order	L^2–error	Order	L^2–error	Order	L^2–error	Order
4	5.195E-3	-	6.185E-3	-	3.669E-2	-	1.670E-2	-
8	1.182E-4	5.46	1.145E-3	2.43	2.223E-3	4.04	7.295E-4	4.52
16	1.806E-5	2.71	7.786E-5	3.88	1.967E-4	3.50	6.128E-5	3.57
32	9.773E-7	4.21	4.797E-6	4.02	1.701E-5	3.53	3.825E-6	4.00
64	7.967E-8	3.62	3.522E-7	3.77	1.485E-6	3.52	2.732E-7	3.81
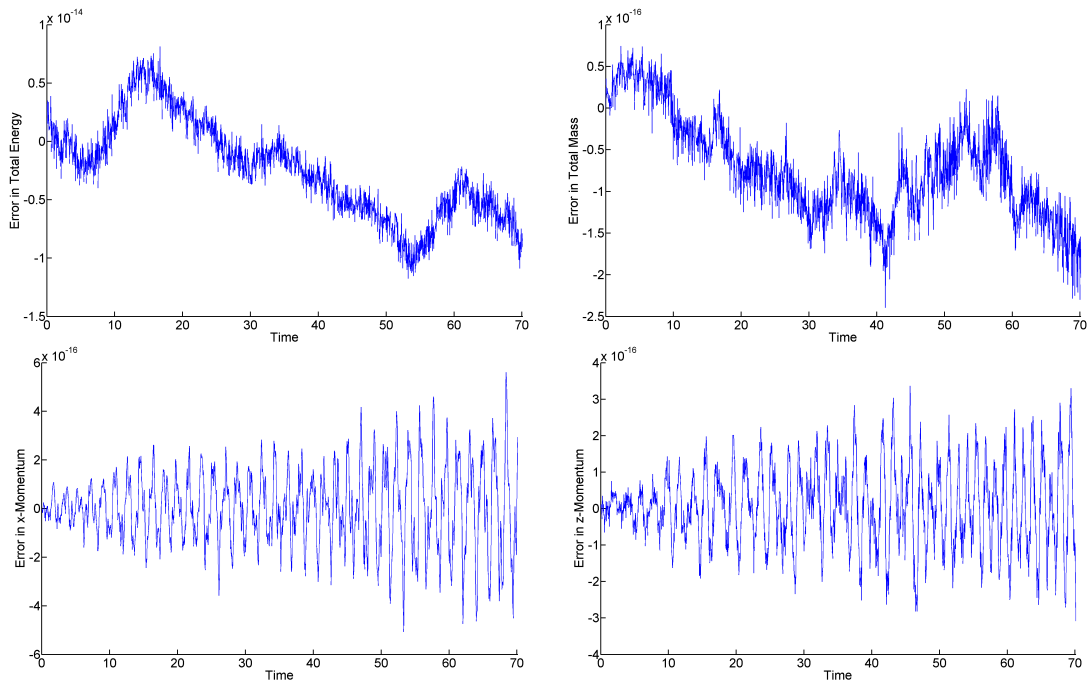
Figure 6-4: The conserved quantities for the numerical solution for two-dimensional waves in a solid wall domain for a stratified compressible fluid during 100 periods. The top left image shows the error in the total energy, the top right image the error in the total mass, the bottom left image the error in the total momentum in the x–direction and the bottom right image the error in the total momentum in the z–direction. The polynomial order was two, the spatial and temporal step size were $1/16$.
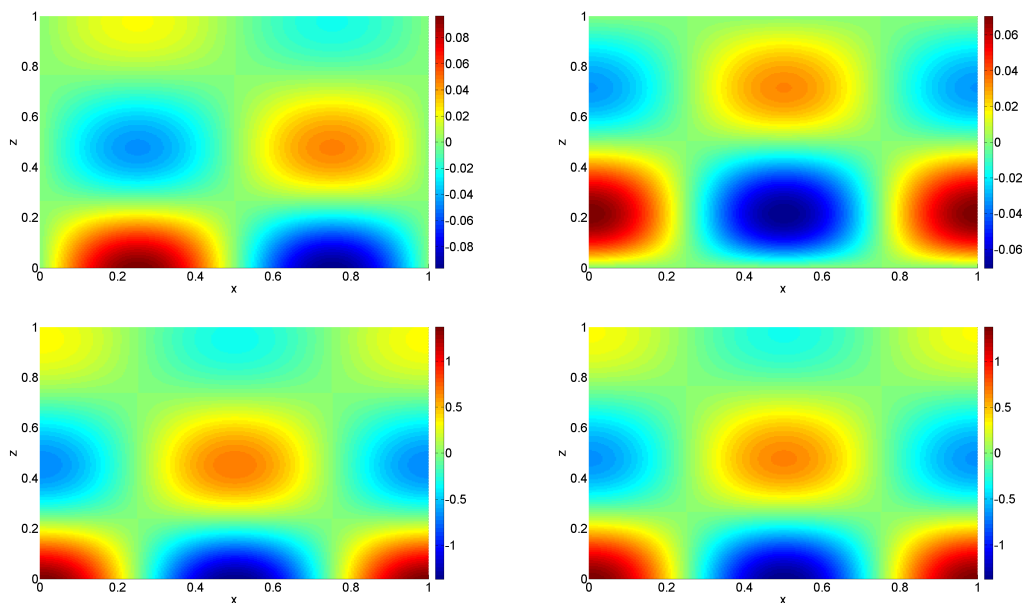
Figure 6-5: The numerical solution for two-dimensional waves in a solid wall domain in a stratified compressible fluid. The top left image shows the horizontal velocity field, the top right image the vertical velocity field, the bottom left image the density field and the bottom right image the pressure field. The spatial step size was $1/32$ and the polynomial order was one.

6-1-3 Three-Dimensional Waves

A three-dimensional solution to (6.1), with constant N^2, is obtained from (2.9) – (2.11). Taking a background density field of $\rho_0 = \exp(-3z)$ yields a buoyancy frequency of $N^2 = 2$. For $H_x = H_y = H_z = 1$ and $n_x = n_y = n_z = 2$ in (2.10), a three-dimensional solution is

$$\rho_0 u = \exp^{-\frac{1}{2}(N^2+1)z} \frac{2\pi}{8\pi^2 - \sigma^2} \left(-2\pi\cos(2\pi z) - \frac{N^2-1}{2}\sin(2\pi z) \right) \sin(2\pi x)\cos(2\pi y)\sin(\sigma t + 0.1),$$

$$\rho_0 v = \exp^{-\frac{1}{2}(N^2+1)z} \frac{2\pi}{8\pi^2 - \sigma^2} \left(-2\pi\cos(2\pi z) - \frac{N^2-1}{2}\sin(2\pi z) \right) \cos(2\pi x)\sin(2\pi y)\sin(\sigma t + 0.1),$$

$$\rho_0 w = \exp^{-\frac{1}{2}(N^2+1)z} \sin(2\pi z)\cos(2\pi x)\cos(2\pi y)\sin(\sigma t + 0.1),$$

$$\rho = \exp^{-\frac{1}{2}(N^2+1)z} \frac{\sigma}{8\pi^2 - \sigma^2} \left(\left(\frac{N^2+1}{2} - \frac{8\pi^2 N^2}{\sigma^2} \right) \sin(2\pi z) \right.$$
$$\left. - 2\pi\cos(2\pi z) \right) \cos(2\pi x)\cos(2\pi y)\cos(\sigma t + 0.1),$$

$$p = \exp^{-\frac{1}{2}(N^2+1)z} \frac{\sigma}{8\pi^2 - \sigma^2} \left(-\frac{N^2-1}{2}\sin(2\pi z) - 2\pi\cos(2\pi z) \right) \cos(2\pi x)\cos(2\pi y)\cos(\sigma t + 0.1)$$
$$\tag{6.8}$$

with dispersion relation

$$2\sigma^2 = 12\pi^2 + \frac{1}{4}\left(N^2+1\right)^2 + \sqrt{\left(12\pi^2 + \frac{1}{4}\left(N^2+1\right)^2\right)^2 - 32\pi^2 N^2}. \tag{6.9}$$

The boundary condition is no normal flow in the z–direction. The boundary conditions in the x–direction and the y–direction can be either no normal flow or periodic. The energy of the system is found from (2.13) as

$$\mathcal{H} = \int_0^1 \int_0^1 \int_0^1 \frac{1}{2}\frac{1}{\rho_0}\left((\rho_0 u)^2 + (\rho_0 v)^2 + (\rho_0 w)^2 \right) + \frac{1}{2}\frac{1}{\rho_0 N^2}(\rho - p)^2 + \frac{1}{2}\frac{p^2}{\rho_0}\, \mathrm{d}x\mathrm{d}y\mathrm{d}z$$
$$\approx 0.180519. \tag{6.10}$$

The numerical discretization is initialized at time $t = 0$ and compared to the exact solution. Table 6-3 presents the L^2–error and order of convergence of the numerical solution after three periods. The total energy is conserved up to machine precision. Figure 6-6 shows the error in the total energy, mass, and momentum in three directions for 100 periods for a polynomial order one. Figure 6-7 shows the numerical solution after five periods.

Table 6-3: L^2–error and order of convergence of the numerical solution after three periods for three-dimensional waves in a solid wall domain for a stratified compressible fluid. The polynomial is varied from zero to three. The number of time steps per period equals ten times the square of the number of elements in a direction. Due to symmetry the error in the horizontal velocities is equal.

$p = 0$	$\rho_0 u, \rho_0 v$		$\rho_0 w$		ρ		p	
h	L^2–error	Order	L^2–error	Order	L^2–error	Order	L^2–error	Order
4	7.790E-2	-	5.628E-2	-	4.968E-1	-	4.508E-1	-
8	2.136E-1	-1.46	2.003E-1	-1.46	5.441E-1	-0.13	5.424E-1	-0.27
16	1.011E-1	1.08	9.573E-2	1.08	7.277E-2	2.90	6.934E-2	2.97
32	2.604E-2	1.96	2.499E-2	1.96	1.166E-2	2.64	9.863E-3	2.81
64	6.386E-3	2.03	6.179E-3	2.03	3.775E-3	1.63	3.078E-3	1.68
$p = 1$	$\rho_0 u, \rho_0 v$		$\rho_0 w$		ρ		p	
h	L^2–error	Order	L^2–error	Order	L^2–error	Order	L^2–error	Order
4	8.479E-2	-	1.236E-1	-	2.683E-1	-	2.282E-1	-
8	3.889E-2	1.12	3.747E-2	1.12	4.315E-2	2.64	4.378E-2	2.38
16	1.493E-2	1.38	1.583E-2	1.38	6.332E-3	2.77	6.506E-3	2.75
32	4.359E-3	1.78	6.309E-3	1.78	1.042E-3	2.60	1.074E-3	2.60
$p = 2$	$\rho_0 u, \rho_0 v$		$\rho_0 w$		ρ		p	
h	L^2–error	Order	L^2–error	Order	L^2–error	Order	L^2–error	Order
4	9.573E-2	-	1.150E-1	-	9.010E-2	-	6.608E-2	-
8	8.632E-3	3.47	7.880E-3	3.47	1.574E-2	2.52	1.771E-2	1.90
16	4.639E-4	4.22	4.203E-4	4.22	5.922E-4	4.73	5.745E-4	4.95
32	2.467E-5	4.23	2.457E-5	4.23	6.352E-5	3.22	4.254E-5	3.76
$p = 3$	$\rho_0 u, \rho_0 v$		$\rho_0 w$		ρ		p	
h	L^2–error	Order	L^2–error	Order	L^2–error	Order	L^2–error	Order
4	2.154E-2	-	2.792E-2	-	6.965E-2	-	5.559E-2	-
8	1.860E-4	6.86	8.853E-4	6.86	3.312E-3	4.39	1.795E-3	4.95
16	7.827E-6	4.57	7.712E-5	4.57	2.537E-4	3.71	1.653E-4	3.44
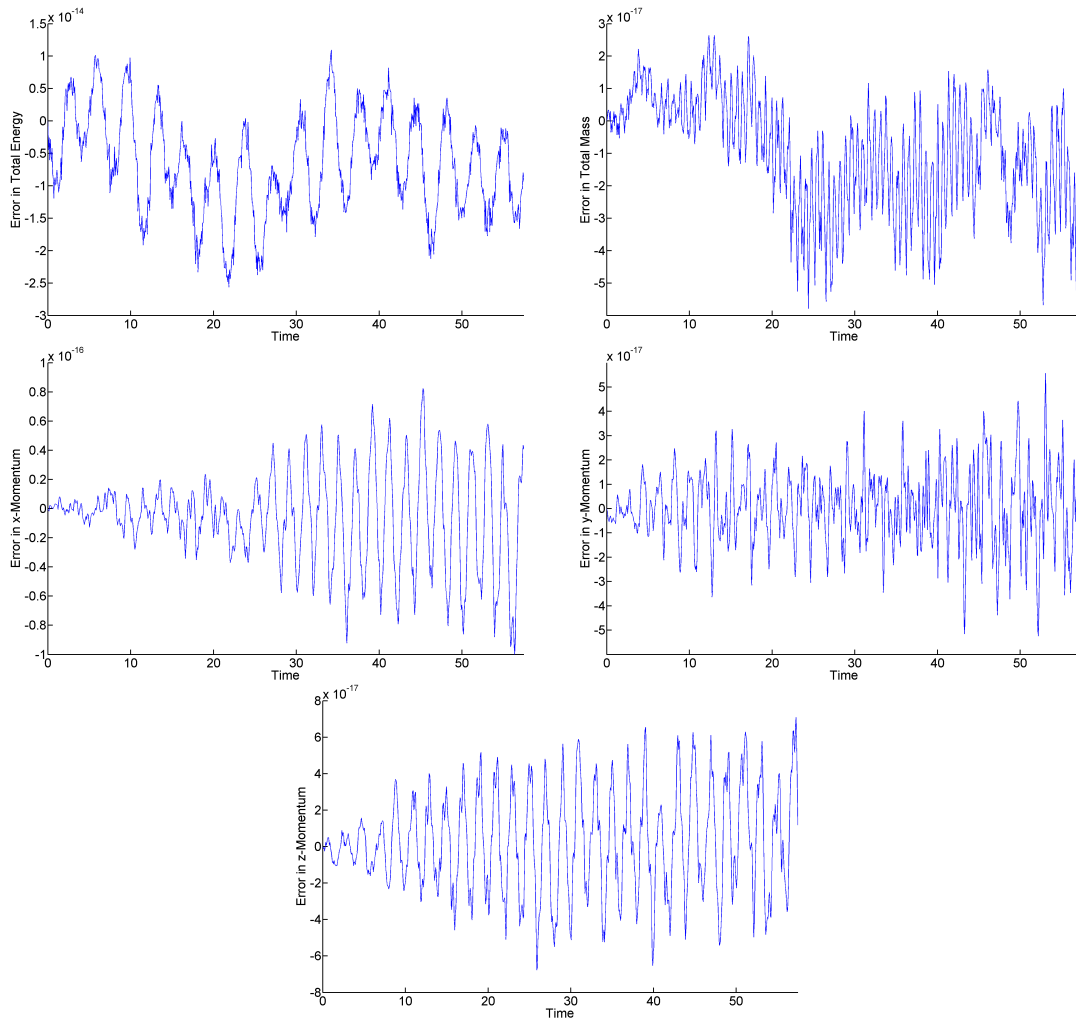
Figure 6-6: The conserved quantities for the numerical solution for three-dimensional waves in a solid wall domain for a stratified compressible fluid during 100 periods. The top left image shows the error in the total energy, the top right image the error in the total mass, the middle left image the error in the total momentum in the x–direction, and the middle right image the error in the total momentum in the y–direction and the bottom image the error in the total momentum in the z–direction. The spatial and temporal step size was $1/8$ and the polynomial order was one.
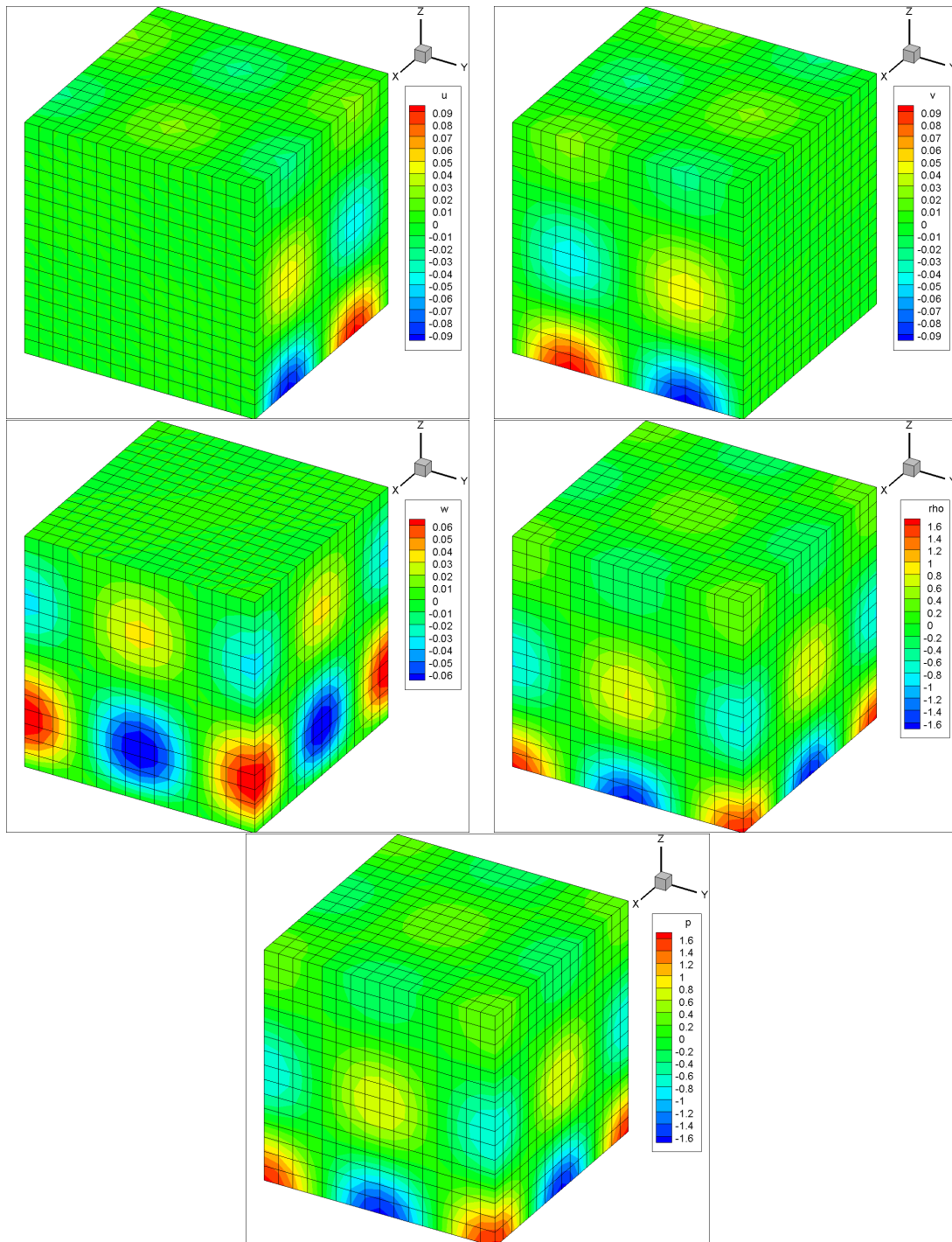
Figure 6-7: The numerical solution for three-dimensional waves in a stratified compressible fluid. The top left image shows the horizontal velocity in the x–direction, the top right image the horizontal image in the y–direction, the middle left image the vertical velocity in the z–direction, the middle right image the density and the bottom image the pressure. The spatial step size was $1/16$ and the polynomial order was three.

6-1-4   Two-dimensional Waves, Random Theta

In Subsection 6-1-2 a two-dimensional solution was verified for the stratified compressible equations. The θ^e–parameter in the numerical flux was chosen as 0.5 for each boundary. In this subsection the θ^e–parameter is chosen randomly for each boundary. For each boundary the value of θ^e is drawn from a uniform distribution between 0 and 1. Table 6-4 presents the L^2–error and order of convergence of the numerical solution after three periods. Again, the energy is conserved up to machine precision. For a polynomial order of zero the solution is not correct, for higher polynomial orders the solution is correct.

Table 6-4: L^2–error and order of convergence of the numerical solution after three periods for two-dimensional waves in a solid wall domain for a stratified compressible fluid. The polynomial is varied from zero to three. The number of time steps per period equals ten times the square of the number of elements in a direction. The parameter θ^e is drawn from a uniform distribution between $(0,1)$ for each boundary.

$p = 0$	$\rho_0 u$		$\rho_0 w$		ρ		p	
K	L^2–error	Order	L^2–error	Order	L^2–error	Order	L^2–error	Order
4	6.982E-2	-	1.151E-1	-	9.165E-1	-	9.726E-1	-
8	1.413E-1	-1.02	1.473E-1	-0.36	5.545E-1	0.72	5.741E-1	0.76
16	1.142E-1	0.31	1.314E-1	0.16	3.509E-1	0.66	3.650E-1	0.65
32	1.291E-1	-0.18	1.259E-1	0.06	1.603E-1	1.13	1.637E-1	1.16
64	1.863E-1	-0.53	1.767E-1	-0.49	1.603E-1	-0.00	1.656E-1	-0.02
128	1.960E-1	-0.07	1.853E-1	-0.07	1.704E-1	-0.09	1.764E-1	-0.09
256	1.962E-1	-0.00	1.865E-1	-0.01	1.726E-1	-0.02	1.795E-1	-0.02
$p = 1$	$\rho_0 u$		$\rho_0 w$		ρ		p	
K	L^2–error	Order	L^2–error	Order	L^2–error	Order	L^2–error	Order
4	1.911E-1	-	2.692E-1	-	3.022E-1	-	2.819E-1	-
8	8.684E-2	1.14	7.817E-2	1.78	5.619E-2	2.43	5.233E-2	2.43
16	2.436E-2	1.83	2.255E-2	1.79	1.648E-2	1.77	1.206E-2	2.12
32	6.670E-3	1.87	6.359E-3	1.83	5.664E-3	1.54	2.770E-3	2.12
64	1.740E-3	1.94	1.788E-3	1.83	2.330E-3	1.28	6.440E-4	2.10
128	4.249E-4	2.03	5.226E-4	1.77	1.001E-3	1.22	1.622E-4	1.99
$p = 2$	$\rho_0 u$		$\rho_0 w$		ρ		p	
K	L^2–error	Order	L^2–error	Order	L^2–error	Order	L^2–error	Order
4	8.847E-2	-	8.000E-2	-	8.492E-2	-	9.370E-2	-
8	6.784E-3	3.70	6.020E-3	3.73	7.845E-3	3.44	8.696E-3	3.43
16	6.050E-4	3.49	6.384E-4	3.24	1.988E-3	1.98	1.658E-3	2.39
32	5.952E-5	3.35	1.223E-4	2.38	2.905E-4	2.77	9.692E-5	4.10
64	7.200E-6	3.05	2.604E-5	2.23	6.366E-5	2.19	1.078E-5	3.17
$p = 3$	$\rho_0 u$		$\rho_0 w$		ρ		p	
K	L^2–error	Order	L^2–error	Order	L^2–error	Order	L^2–error	Order
4	7.826E-3	-	1.021E-2	-	3.949E-2	-	1.933E-2	-
8	2.330E-4	5.07	1.007E-3	3.34	2.752E-3	3.84	9.204E-4	4.39
16	1.802E-5	3.69	8.452E-5	3.57	2.345E-4	3.55	9.002E-5	3.35
32	1.375E-6	3.71	8.124E-6	3.38	2.147E-5	3.45	4.992E-6	4.17
64	1.161E-7	3.57	7.204E-7	3.50	1.929E-6	3.48	3.046E-7	4.03

6-2   Incompressible Stratified Euler Equations

Consider (2.14) and nondimensionalize as in Section 4-4. Scale such that $Fr = \delta = 1$. Then (2.14) reduces to

$$
\begin{aligned}
\frac{\partial(\rho_0 u)}{\partial t} &= -\frac{\partial P}{\partial x}, \\
\frac{\partial(\rho_0 v)}{\partial t} &= -\frac{\partial P}{\partial y}, \\
\frac{\partial(\rho_0 w)}{\partial t} &= -\rho - \frac{\partial P}{\partial z}, \\
\frac{\partial \rho}{\partial t} &= N^2(\rho_0 w), \\
0 &= \frac{\partial(\rho_0 u)}{\partial x} + \frac{\partial(\rho_0 v)}{\partial y} + \frac{\partial(\rho_0 w)}{\partial z} + N^2(\rho_0 w).
\end{aligned}
\tag{6.11}
$$

6-2-1   Two-dimensional Waves

A two-dimensional solution to (6.11), with constant N^2, is obtained from (2.16) and (2.17). Taking a background density field of $\rho_0 = \exp(-2z)$ yields a buoyancy frequency of $N^2 = 2$. For $H_x = H_z = 1$ and $n_x = n_z = 2$ in (2.10), a two-dimensional solution is

$$
\begin{aligned}
\rho_0 u &= \exp^{-\frac{1}{2}N^2 z}\left(-\frac{N^2}{4\pi}\sin(2\pi z) - \cos(2\pi z)\right)\sin(2\pi x)\sin(\sigma t + 0.1), \\
\rho_0 w &= \exp^{-\frac{1}{2}N^2 z}\sin(2\pi z)\cos(2\pi x)\sin(\sigma t + 0.1), \\
\rho &= -\frac{N^2}{\sigma}\exp^{-\frac{1}{2}N^2 z}\sin(2\pi z)\cos(2\pi x)\cos(\sigma t + 0.1), \\
P &= \exp^{-\frac{1}{2}N^2 z}\left(-\frac{N^2\sigma}{8\pi^2}\sin(2\pi z) - \frac{\sigma}{2\pi}\cos(2\pi z)\right)\cos(2\pi x)\cos(\sigma t + 0.1)
\end{aligned}
\tag{6.12}
$$

with dispersion relation

$$
\sigma^2 = \frac{16\pi^2 N^2}{N^4 + 32\pi^2}.
\tag{6.13}
$$

The boundary condition is no normal flow in the z–direction. The boundary condition in the x–direction can either be no normal flow or periodic. The energy of the system is

$$
\mathcal{H} = \int_0^1 \int_0^1 \frac{1}{2}\frac{1}{\rho_0}\left((\rho_0 u)^2 + (\rho_0 w)^2\right) + \frac{1}{2}\frac{1}{\rho_0 N^2}\rho^2 \, \mathrm{d}x\mathrm{d}z \approx 0.26123.
\tag{6.14}
$$

The numerical discretization is initialized at time $t = 0$ and compared to the exact solution. Table 6-5 presents the L^2–error and order of convergence of the numerical solution after three periods. The total energy is conserved up to machine precision. Figure 6-8 shows the error in the total energy, mass, momentum in two directions and divergence of the velocity for 100 periods for a polynomial order zero. The error in the total mass behaves for the incompressible case behaves differently than for the compressible case (For example, the top right image of Figure 6-3). Figure 6-9 shows the numerical solution after five periods.

As noted in Section 4-4 the combination of a divergence-free velocity field and a stratification in density means mass is not conserved by the continuous system (6.11). It was claimed that due to the oscillatory nature of waves this loss of mass conservation was not a severe problem. Since the continuous system does not posses mass conservation, the discrete system also does not posses mass conservation. The top right image of Figure 6-8 shows the total mass is not conserved up to machine precision, but has a small error. This shows the loss of mass conservation is indeed not a problem. So for all compressible test cases, the total mass is conserved up to machine precision, while for all incompressible test cases, the total mass is not conserved up to machine precision, but the error is small.

Table 6-5: L^2–error and order of convergence of the numerical solution after three periods for two-dimensional waves in a solid wall domain for a stratified incompressible fluid. The polynomial is varied from zero to three. The number of time steps per period equals ten times the square of the number of elements in a direction.

$p = 0$	$\rho_0 u$		$\rho_0 w$		ρ		P	
K	L^2–error	Order	L^2–error	Order	L^2–error	Order	L^2–error	Order
4	3.794E-1	-	3.337E-1	-	7.864E-1	-	5.540E-2	-
8	2.767E-2	3.78	4.471E-2	2.90	2.423E-1	1.70	1.941E-2	1.51
16	6.901E-3	2.00	1.653E-2	1.44	7.107E-2	1.77	3.991E-3	2.28
32	1.917E-3	1.85	6.310E-3	1.39	2.386E-2	1.57	9.947E-4	2.00
64	5.905E-4	1.70	2.221E-3	1.51	7.766E-3	1.62	2.999E-4	1.73
128	1.772E-4	1.74	7.870E-4	1.50	2.656E-3	1.55	9.456E-5	1.67
$p = 1$	$\rho_0 u$		$\rho_0 w$		ρ		P	
K	L^2–error	Order	L^2–error	Order	L^2–error	Order	L^2–error	Order
4	4.230E-2	-	7.594E-2	-	3.385E-1	-	8.160E-3	-
8	1.083E-2	1.97	1.307E-2	2.54	8.101E-2	2.06	1.679E-3	2.28
16	3.917E-3	1.47	3.389E-3	1.95	2.366E-2	1.78	6.059E-4	1.47
32	9.748E-4	2.01	8.595E-4	1.98	6.888E-3	1.78	1.535E-4	1.98
$p = 2$	$\rho_0 u$		$\rho_0 w$		ρ		P	
K	L^2–error	Order	L^2–error	Order	L^2–error	Order	L^2–error	Order
4	7.616E-2	-	4.599E-2	-	2.383E-1	-	5.651E-3	-
8	4.574E-3	4.06	1.246E-2	1.88	1.489E-2	4.00	5.675E-4	3.32
16	3.636E-4	3.65	1.381E-3	3.17	2.153E-3	2.79	3.424E-5	4.05
32	3.896E-5	3.22	1.700E-4	3.02	2.629E-4	3.03	3.502E-6	4.51
$p = 3$	$\rho_0 u$		$\rho_0 w$		ρ		P	
K	L^2–error	Order	L^2–error	Order	L^2–error	Order	L^2–error	Order
4	7.183E-2	-	8.053E-2	-	9.052E-2	-	2.468E-3	-
8	2.645E-3	4.76	7.990E-3	3.33	7.310E-3	3.63	2.299E-4	3.42
16	1.526E-4	4.11	6.893E-4	3.54	1.072E-3	2.77	3.548E-6	6.02
32	6.113E-6	4.64	5.466E-5	3.66	1.014E-4	3.40	1.247E-6	1.51
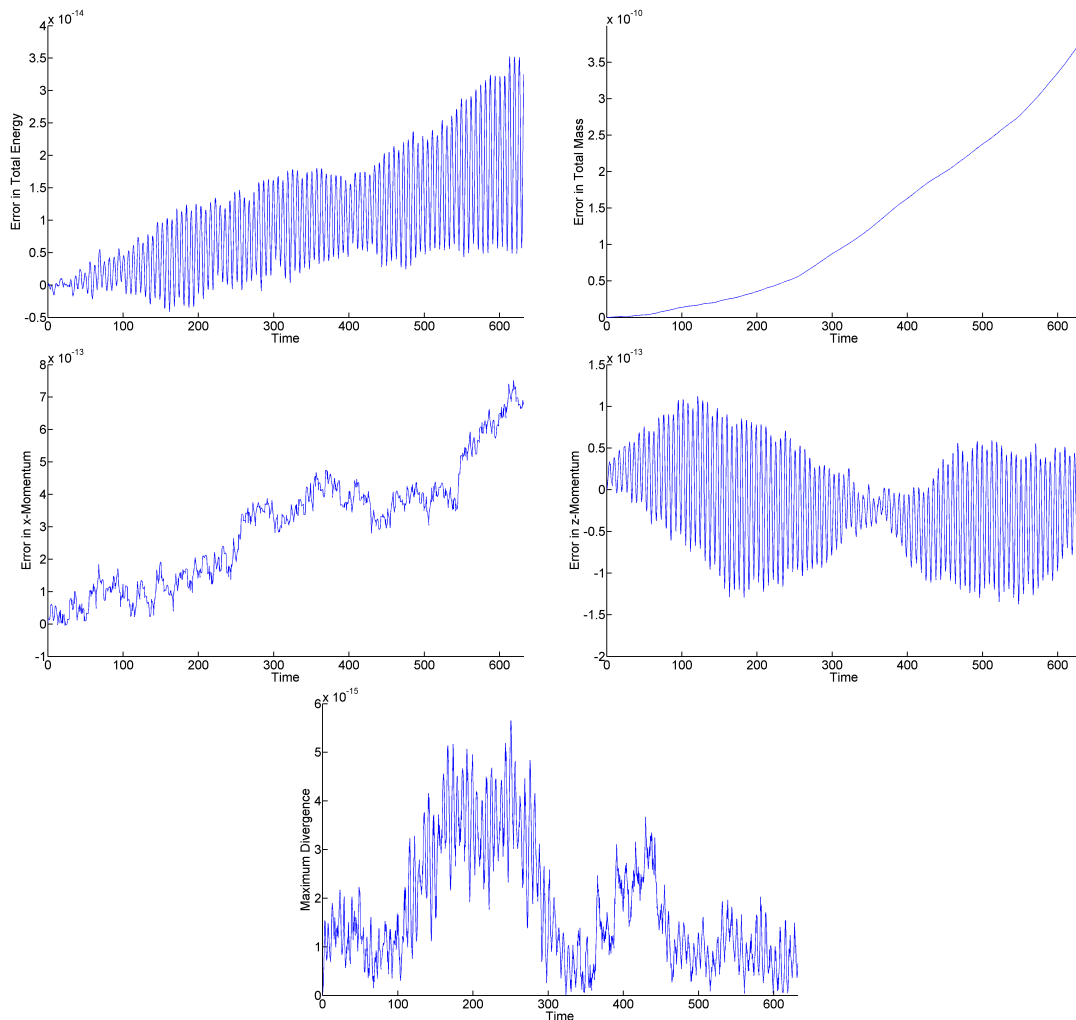
Figure 6-8: The conserved quantities for the numerical solution for two-dimensional waves in a solid wall domain for a stratified incompressible fluid during 100 periods. The top left image shows the error in the total energy, the top right image the error in the total mass, the middle left image the error in the total momentum in the x–direction, and the middle right image the error in the total momentum in the z–direction and the bottom image the error in the divergence of the velocity. The total mass is not conserved up to machine precision due to the combination of a divergence-free velocity field and a stratification in density. However, the error in total mass is small. The spatial and temporal step size was $1/16$ and the polynomial order was zero.

Figure 6-9: The numerical solution for two-dimensional waves in a solid wall domain for a stratified incompressible fluid after three periods. The top left image shows the horizontal velocity field, the top right image the vertical velocity field, the bottom left image the density field and the bottom right image the pressure field. The spatial step size was $1/128$ and the polynomial order was zero.

6-3 Euler-Boussinesq Equations

Consider (2.19) and nondimensionalize as in Section 4-4. Scale such that $Fr = \delta = \rho^* = 1$. Then (2.19) reduces to

$$
\begin{aligned}
\frac{\partial u}{\partial t} &= -\frac{\partial P}{\partial x}, \\
\frac{\partial v}{\partial t} &= -\frac{\partial P}{\partial y}, \\
\frac{\partial w}{\partial t} &= -\rho - \frac{\partial P}{\partial z}, \\
\frac{\partial \rho}{\partial t} &= N^2 w, \\
0 &= \frac{\partial u}{\partial x} + \frac{\partial v}{\partial y} + \frac{\partial w}{\partial z}.
\end{aligned}
\tag{6.15}
$$

6-3-1 Two-dimensional Waves

A two-dimensional solution to (6.15), with constant N^2, is obtained from (2.21) and (2.22). Taking a background density field of $\rho_0 = \exp(-2z)$ yields a buoyancy frequency of $N^2 = 2$. For $H_x = H_z = 1$ and $n_x = n_z = 2$ in (2.10), a two-dimensional solution is

$$
\begin{aligned}
u &= -\cos(2\pi z)\sin(2\pi x)\sin(\sigma t + 0.1), \\
w &= \sin(2\pi z)\cos(2\pi x)\sin(\sigma t + 0.1), \\
\rho &= -\frac{N^2}{\sigma}\sin(2\pi z)\cos(2\pi x)\cos(\sigma t + 0.1), \\
P &= -\frac{\sigma}{2\pi}\cos(2\pi z)\cos(2\pi x)\cos(\sigma t + 0.1),
\end{aligned}
\tag{6.16}
$$

with dispersion relation

$$
\sigma^2 = \frac{N^2}{2}.
\tag{6.17}
$$

The boundary condition is no normal flow in the z–direction. The boundary condition in the x–direction can either be no normal flow or periodic. The energy of the system is

$$
\mathcal{H} = \int_0^1 \int_0^1 \frac{1}{2}\left(u^2 + w^2\right) + \frac{1}{2}\frac{\rho^2}{N^2}\, \mathrm{d}x\mathrm{d}z \approx 0.35252.
\tag{6.18}
$$

The numerical discretization is initialized at time $t = 0$ and compared to the exact solution. Table 6-6 presents the L^2–error and order of convergence of the numerical solution after three periods. The total energy is conserved up to machine precision. Figure 6-10 shows the error in the total energy, mass, momentum in two directions and divergence of the velocity for 100 periods for a polynomial order zero. Figure 6-11 shows the numerical solution after five periods.

Table 6-6: L^2–error and order of convergence of the numerical solution after three periods for two-dimensional waves in a solid wall domain for the Euler-Boussinesq equations. The polynomial order is varied from zero to two. The number of time steps per period equals ten times the square of the number of elements in a direction.

$p = 0$	$\rho_0 u$		$\rho_0 w$		ρ		P	
K	L^2–error	Order	L^2–error	Order	L^2–error	Order	L^2–error	Order
4	4.324E-2	-	4.324E-2	-	8.617E-1	-	2.532E-2	-
8	1.619E-2	1.42	1.619E-2	1.42	3.223E-1	1.42	5.096E-3	2.31
16	5.453E-3	1.57	5.453E-3	1.57	1.087E-1	1.57	1.137E-3	2.16
32	1.842E-3	1.57	1.842E-3	1.57	3.672E-2	1.57	2.679E-4	2.09
64	6.330E-4	1.54	6.330E-4	1.54	1.262E-2	1.54	6.497E-5	2.04
128	2.203E-4	1.52	2.203E-4	1.52	4.391E-3	1.52	1.599E-5	2.02
$p = 1$	$\rho_0 u$		$\rho_0 w$		ρ		P	
K	L^2–error	Order	L^2–error	Order	L^2–error	Order	L^2–error	Order
4	5.564E-2	-	1.222E-1	-	4.406E-1	-	9.153E-3	-
8	1.399E-2	1.99	1.485E-2	3.04	1.252E-1	1.82	2.578E-3	1.83
16	4.244E-3	1.72	4.681E-3	1.67	4.092E-2	1.61	9.264E-4	1.48
32	1.222E-3	1.80	1.490E-3	1.65	1.382E-2	1.57	2.403E-4	1.95
64	3.683E-4	1.73	4.862E-4	1.62	4.752E-3	1.54	5.963E-5	2.01
$p = 2$	$\rho_0 u$		$\rho_0 w$		ρ		P	
K	L^2–error	Order	L^2–error	Order	L^2–error	Order	L^2–error	Order
4	1.707E-2	-	2.616E-2	-	1.808E-1	-	8.781E-3	-
8	1.270E-3	3.75	2.500E-3	3.39	1.766E-2	3.36	6.002E-4	3.87
16	7.956E-5	4.00	1.632E-4	3.94	1.805E-3	3.29	4.042E-5	3.89
32	6.947E-6	3.52	1.138E-5	3.84	1.540E-4	3.55	4.319E-6	3.23
$p = 3$	$\rho_0 u$		$\rho_0 w$		ρ		P	
K	L^2–error	Order	L^2–error	Order	L^2–error	Order	L^2–error	Order
4	6.162E-2	-	1.048E-1	-	1.775E-1	-	3.488E-3	-
8	1.885E-3	5.03	4.711E-3	4.48	5.366E-3	5.05	1.838E-4	4.25
16	1.743E-4	3.43	8.344E-4	2.50	1.053E-3	2.35	3.667E-6	5.65
32	4.577E-6	5.25	7.566E-5	3.46	1.149E-4	3.20	1.711E-6	1.10
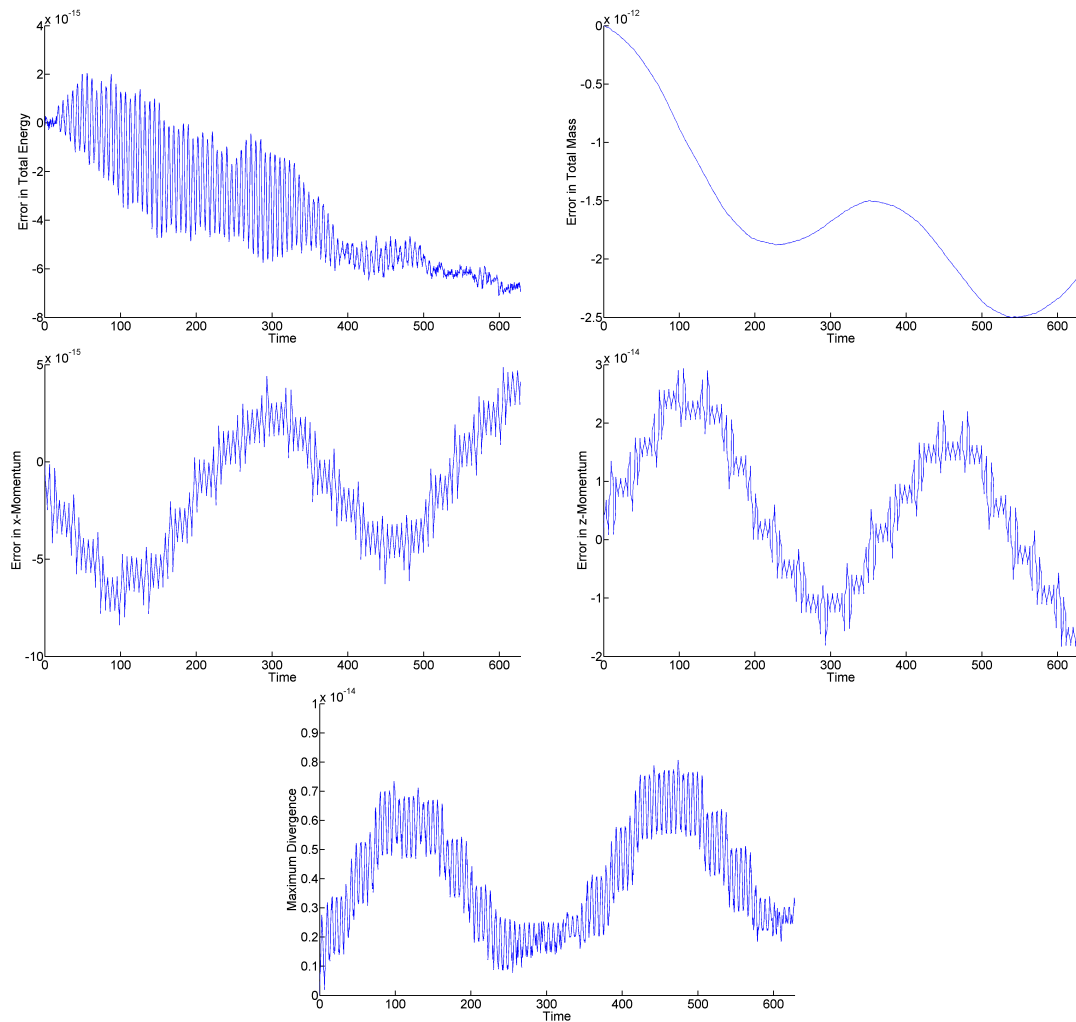
Figure 6-10: The conserved quantities for the numerical solution in a solid wall domain for the two-dimensional Euler-Boussinesq waves during 100 periods. The top left image shows the error in the total energy, the top right image the error in the total mass, the middle left image the error in the total momentum in the x–direction, and the middle right image the error in the total momentum in the z–direction and the bottom image the error in the divergence of the velocity. The total mass is not conserved up to machine precision due to the combination of a divergence-free velocity field and a stratification in density. However, the error in total mass is small. The spatial and temporal step size was $1/16$ and the polynomial order was zero.
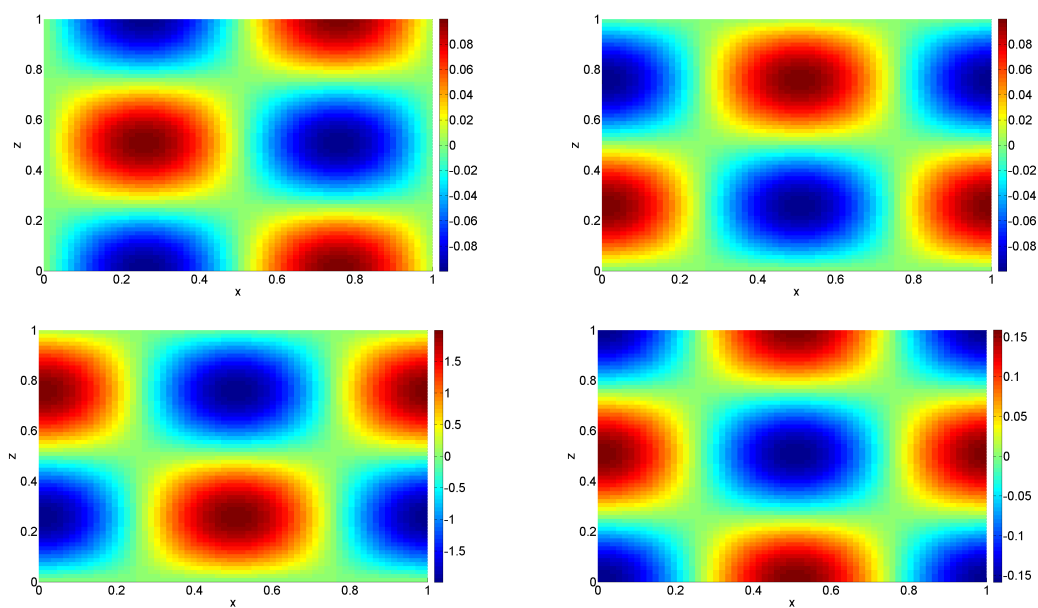
Figure 6-11: The numerical solution for two-dimensional waves in a solid wall domain for the Euler-Boussinesq equations. The top left image shows the horizontal velocity field, the top right image the vertical velocity field, the bottom left image the density field and the bottom right image the pressure field. The spatial step size was $1/64$ and the polynomial order was zero.

6-3-2   Internal Gravity Waves

A two-dimensional solution to (6.15) that describes internal gravity waves, with constant N^2, is obtained from (2.25) and (2.26). For $k = m = n\pi$, $k_n = n\pi$ and $H_z = a_n = 1$ the frequency is $\sigma = \frac{1}{2}\sqrt{2}N$. Using the first ten modes the solution becomes

$$
\begin{aligned}
u &= \sum_{n=1}^{10} \cos\left(n\pi z\right) \cos\left(n\pi x - \sigma t\right), \\
w &= \sum_{n=1}^{10} \sin\left(n\pi z\right) \sin\left(n\pi x - \sigma t\right), \\
\rho &= \sum_{n=1}^{10} \frac{N^2}{\sigma} \sin\left(n\pi z\right) \cos\left(n\pi x - \sigma t\right), \\
P &= \sum_{n=1}^{10} \frac{\sigma}{n\pi} \cos\left(n\pi z\right) \cos\left(n\pi x - \sigma t\right).
\end{aligned}
\tag{6.19}
$$

The domain is a rectangle $\Omega_h = [0, 2] \times [0, 1]$ and is periodic in the x–direction and is closed with walls in the z–direction. Taking a background density field of $\rho_0 = \exp(-2z)$ yields a buoyancy frequency of $N^2 = 2$. The energy of the system is

$$
\mathcal{H} = \int_0^1 \int_0^2 \frac{1}{2}\left(u^2 + w^2\right) + \frac{1}{2}\frac{\rho^2}{N^2}\, \mathrm{d}x\mathrm{d}z = 10.
\tag{6.20}
$$

The numerical discretization is initialized at time $t = 0$ and compared to the exact solution. Table 6-7 presents the L^2–error and order of convergence of the numerical solution after three periods. The energy and divergence of the velocity field are conserved up to machine precision.

Figure 6-12 shows the numerical solution after five periods. A internal gravity wave is seen propagating through the domain. The internal gravity wave beam reflects from the top and bottom boundaries. With time the beam moves to the right and the reflection locations also move to the right. Since the domain is symmetric with respect to the direction of gravity, no wave attractors can occur.

Table 6-7: L^2–error and order of convergence of the numerical solution after three periods for the two-dimensional internal gravity waves for the Euler-Boussinesq equations. The polynomial order is varied from zero to three. The number of elements in the x–direction is twice the number of elements in the z–direction. The number of time steps per period equals ten times the square of the number of elements in the z–direction.

$p = 0$	$\rho_0 u$		$\rho_0 w$		ρ		P	
K	L^2–error	Order	L^2–error	Order	L^2–error	Order	L^2–error	Order
8×4	2.849E+0	-	2.709E+0	-	1.453E+0	-	2.662E-1	-
16×8	2.796E+0	0.03	2.279E+0	0.25	1.764E+0	-0.28	1.203E-1	1.15
32×16	9.284E-1	1.59	1.038E+0	1.13	2.007E+0	-0.19	1.638E-2	2.88
64×32	2.671E-1	1.80	3.698E-1	1.49	6.921E-1	1.54	3.764E-3	2.12
128×64	6.834E-2	1.97	1.216E-1	1.60	2.175E-1	1.67	9.109E-4	2.05
$p = 1$	$\rho_0 u$		$\rho_0 w$		ρ		P	
K	L^2–error	Order	L^2–error	Order	L^2–error	Order	L^2–error	Order
8×4	4.515E+0	-	3.392E+0	-	1.955E+0	-	2.164E-1	-
16×8	2.726E+0	0.73	2.605E+0	0.38	1.956E+0	-0.00	1.010E-1	1.10
32×16	9.545E-2	4.84	5.485E-1	2.25	8.703E-1	1.17	9.363E-3	3.43
64×32	7.641E-2	0.32	1.611E-1	1.77	2.830E-1	1.62	2.228E-3	2.07
$p = 2$	$\rho_0 u$		$\rho_0 w$		ρ		P	
K	L^2–error	Order	L^2–error	Order	L^2–error	Order	L^2–error	Order
8×4	2.985E+0	-	2.454E+0	-	3.812E+0	-	1.037E-1	-
16×8	1.013E+0	1.56	9.826E-1	1.32	3.202E+0	0.25	4.079E-2	1.35
32×16	4.167E-1	1.28	2.569E-1	1.94	4.800E-1	2.74	6.754E-3	2.59
64×32	3.673E-2	3.50	3.199E-2	3.01	5.492E-2	3.13	4.509E-4	3.91
$p = 3$	$\rho_0 u$		$\rho_0 w$		ρ		P	
K	L^2–error	Order	L^2–error	Order	L^2–error	Order	L^2–error	Order
8×4	3.307E+0	-	4.122E+0	-	6.326E+0	-	1.646E-1	-
16×8	1.245E+0	1.41	2.278E+0	0.86	4.729E+0	0.42	5.593E-2	1.56
32×16	1.575E-1	2.98	3.907E-1	2.54	7.905E-1	2.58	6.713E-3	3.06
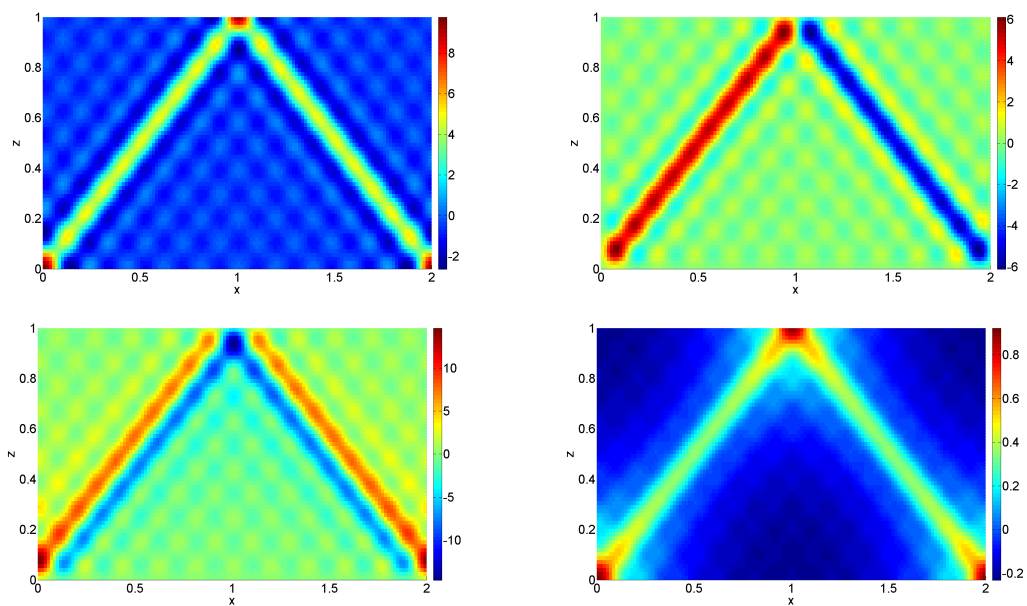
Figure 6-12: The numerical solution for the two-dimensional internal gravity waves for the Euler-Boussinesq equations, (6.19). The top left image shows the horizontal velocity field, the top right image the vertical velocity field, the bottom left image the density field and the bottom right image the pressure field. The spatial step size was $1/32$ and the polynomial order was one.

6-4 Wave Attractors

In the previous test cases, the walls are either parallel or perpendicular to the direction of gravity. Wave attractors appear when there is a geometric asymmetry with respect to the direction of gravity. A slight tilt in one of the walls results in symmetry breaking and hence in wave focussing and defocussing. Often focussing dominates and wave attractors appear. Here the symmetry is broken by rotating the direction of gravity with respect to the geometry.

Consider (6.15) in a two dimensional geometry. Instead of rotating the geometry, the direction of gravity is rotated. The changed direction of gravity also breaks the reflection symmetry. Rotate the direction of gravity by an angle γ,

$$
\begin{aligned}
\frac{\partial u}{\partial t} &= -\rho \sin(\gamma) - \frac{\partial P}{\partial x}, \\
\frac{\partial w}{\partial t} &= -\rho \cos(\gamma) - \frac{\partial P}{\partial z}, \\
\frac{\partial \rho}{\partial t} &= N^2 (u \sin(\gamma) + w \cos(\gamma)), \\
0 &= \frac{\partial u}{\partial x} + \frac{\partial w}{\partial z}.
\end{aligned}
\tag{6.21}
$$

The angle γ controls the appearance of wave attractors. For $\gamma = 0$ the direction of gravity is aligned with the geometry and the symmetry is not broken. No wave attractors can appear. For $\gamma \neq 0$ the direction of gravity is inclined with respect to the geometry and the symmetry is broken. Wave attractors can appear.

No analytical solutions exist for wave attractors in tilted squares. So no analytical solution is available to compare the numerical solution with. The qualitative behaviour of the numerical solution is checked. For no rotation, $\gamma = 0$, wave attractors are absent and for rotation, $\gamma \neq 0$, wave attractors appear. In Bajars et al. (2013) the free evolution of wave attractors for three different initial condition is discussed. For the same parameters ($N^2 = 1$ and $\gamma = \pi/20$) and the same initial conditions the resulting wave attractors are similar. As initial condition was used

$$
\begin{aligned}
u &= -m\pi sin(n\pi x)cos(m\pi z), &&(n,m) = (1,1),(1,2),(1,3) \\
w &= n\pi cos(n\pi x)sin(m\pi z), &&(n,m) = (1,1),(1,2),(1,3) \\
\rho &= 0, \\
P &= 0.
\end{aligned}
\tag{6.22}
$$

The $(n,m) = (1,1)$ initial condition evolved into a $(1,1)$ wave attractor and the $(n,m) = (1,3)$ initial condition evolved into a $(1,3)$ wave attractor. The $(n,m) = (1,2)$ initial condition did not lead to a wave attractor but to solution consisting of a strong periodic component with smaller fluctuations.

Figure 6-14 shows the solution of the $(n,m) = (1,1)$ initial condition at $t = 200$. The structure of the solution completely changed due to the asymmetry in the geometry. Since the system is unforced, no frequency is forced on the system. Waves propagate with a continuous frequency band, resulting in a whole family of $(1,1)$ wave attractors.

Figure 6-15 shows the solution of the $(n, m) = (1, 2)$ initial condition at $t = 200$. A strong periodic component dominated the solution. Figure 6-16 shows the solution the $(n, m) = (1, 3)$ initial condition at $t = 200$. A whole family of $(1, 3)$ wave attractors appeared (seen best in the pressure field). Appendix E shows the time evolution leading to Figures 6-14, 6-15 and 6-16.

For the same three initial conditions, (6.22), as in Bajars et al. (2013), the behaviour of the solution is qualitatively the same. The energy and the momentum and the divergence of the velocity field are conserved up to machine precision. So the numerical solution of the wave attractors in a tilted box is accurate.

Vertical Velocity   Density Perturbations   Energy
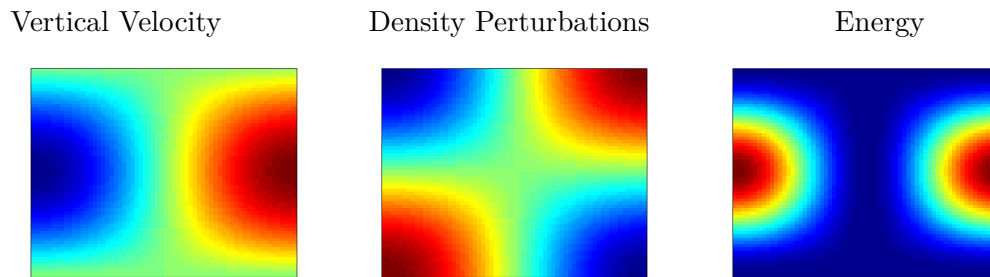
Figure 6-13: The numerical solution of the $(1, 1)$ initial condition at $t = 200$. The left image shows the vertical velocity, the middle image the pressure and the right image the energy. The number of elements in each direction was 64 and the polynomial order was zero.

Vertical Velocity   Density Perturbations   Energy
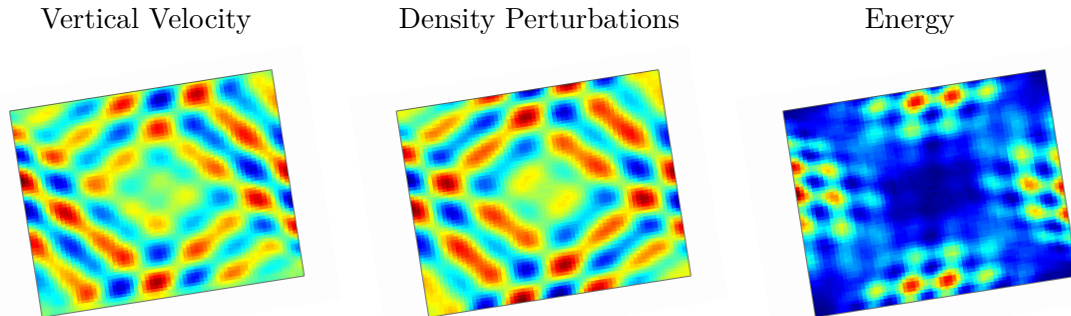
Figure 6-14: The numerical solution of the $(1, 1)$ initial condition at $t = 200$. The left image shows the vertical velocity, the middle image the pressure and the right image the energy. The number of elements in each direction was 64 and the polynomial order was zero.

Vertical Velocity   Density Perturbations   Energy
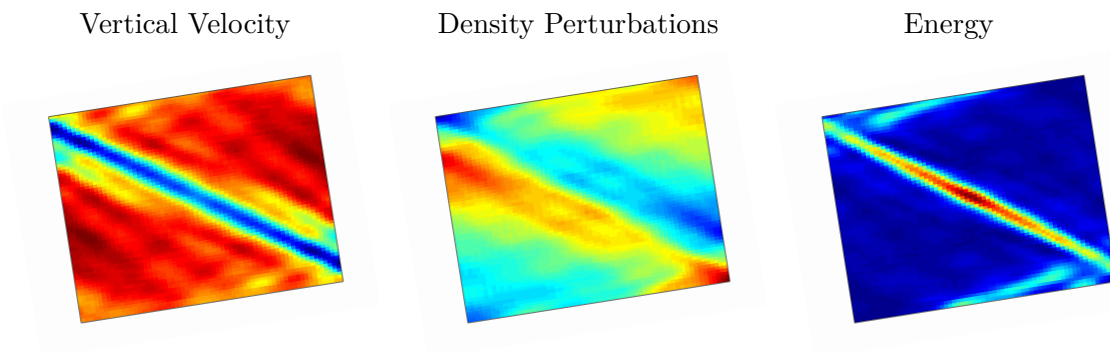
Figure 6-15: The numerical solution of the $(1,2)$ initial condition at $t = 200$. The left image shows the vertical velocity, the middle image the pressure and the right image the energy. The number of elements in each direction was 64 and the polynomial order was zero.

Vertical Velocity   Density Perturbations   Energy
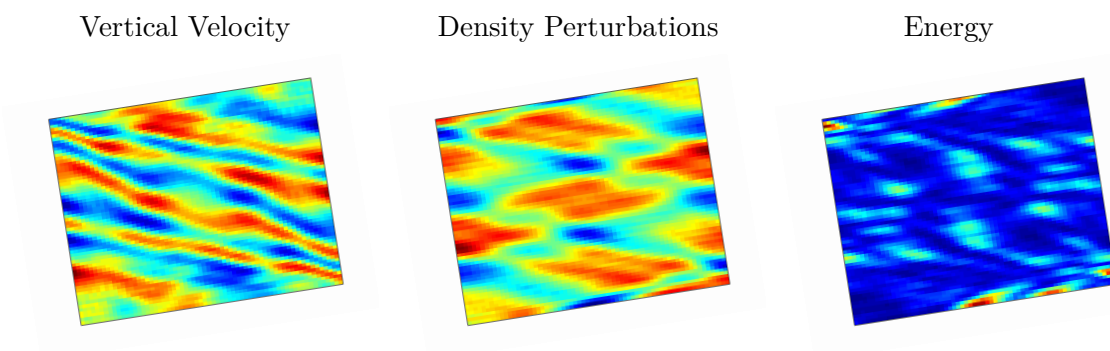
Figure 6-16: The numerical solution of the $(1,3)$ initial condition at $t = 200$. The left image shows the vertical velocity, the middle image the pressure and the right image the energy. The number of elements in each direction was 64 and the polynomial order was zero.

6-5   Concluding Remarks

This chapter verified the developed numerical method using several test problems. Starting with the compressible equations (6.1) in Section 6-1 the DGFEM discretization for compressible flows was tested. One-, two- and three-dimensional test problems were solved. The generalized flux function (5.12) was tested by randomly varying the θ^e–parameter. Appendix C shows the verification for simple one-dimensional problems. Appendix D shows the verification for Lamb and acoustic waves.

The DGFEM discretization for the incompressible equations (6.11) were tested in Section (6-2) for a two-dimensional test problem. A three-dimensional test problem also showed good behaviour, but a full convergence analysis was never completed. In Section 6-3 the DGFEM discretization for the Euler-Boussinesq equations (6.15) were tested. A two-dimensional modal solution was tested. A three-dimensional test problem also showed good behaviour, but a full convergence analysis was never completed. A more complex test problem were the internal gravity waves. Tests were also performed for slightly modified problems, in which one of the horizontal boundaries was periodic. For other values of θ^e, different from 0.5, similar results were obtained. Similar results were also obtained when using triangular elements instead of rectangular elements.

The convergence analysis showed, in general, an order of convergence of polynomial order plus one. The zeroth-order polynomials did well, often achieving an order of convergence approaching two. The third-order polynomials sometimes seemed to perform less than expected: the order of convergence was less than four. This was caused by two reasons. (1) Third-order polynomials were computationally most demanding, putting restrictions on the mesh size. Sometimes, convergence can be slow, and the expected order of convergence is only reached for larger mesh sizes. (2) The temporal step size was too large. The temporal step size in all test cases was chosen small, ten times the square of the spatial step size. Choosing a smaller temporal step size might improve convergence rates.

All test problems showed conservation of energy and momentum up to machine precision. The compressible tests showed conservation of mass up to machine precision. This was lost in the incompressible tests due to the continuous formulation. The incompressible test showed conservation of the divergence of the velocity field up to machine precision.

The combination of correct convergence rates and the conservation of invariants for compressible problems and incompressible problems show the numerical method is correct. The behaviour of wave attractors in the numerical model seems correct since: (1) qualitatively, they behave the same as in Bajars et al. (2013) and (2) the invariants were conserved.

Chapter 7

Conclusion

A DGFEM discretization has been developed for the Hamiltonian dynamics of stratified incompressible linear fluid flow. The developed discretization can handle the numerical challenges posed by wave attractors: the three dimensionality of the domain, the focusing of wave energy and the incompressibility of the flow. The discretization is unconditionally stable. The conservation of phase space and energy ensure that the numerical error is physically more correct since an unphysical numerical error that changes the total energy is not possible.

From the continuous Hamiltonian dynamics corresponding to the primitive Euler equations the Poisson bracket and Hamiltonian for linear compressible stratified flow were derived. By applying Dirac's method of constraints the incompressibility of the flow was ensured. The Boussinesq approximation conserved the Hamiltonian dynamics. The continuous Poisson bracket and continuous Hamiltonian corresponding to linear compressible stratified flow were discretized, yielding a discrete Poisson bracket and discrete Hamiltonian. These discrete objects yielded the discrete equations of motion for linear compressible stratified flow. By constructing these discrete equations from a Poisson bracket, the discrete equations possessed a Hamiltonian structure. Together with a symplectic time integration, the modified midpoint rule, this Hamiltonian structure ensured phase space preservation and an exact preservation of the discrete energy. Dirac's method of constraints was again applied, now to the discrete Poisson bracket, to enforce the incompressibility of the flow. This yielded the discrete Poisson bracket and Hamiltonian for linear incompressible stratified flow. These discrete objects yielded the discrete equations of motion for linear incompressible flow. The construction using a Poisson bracket and Dirac's method of constraints ensured the discrete energy was exactly preserved. Performing a discrete Boussinesq approximation conserved the discrete Hamiltonian dynamics and the discrete equations of motion for Euler-Boussinesq flow were derived.

This DGFEM discretization has been verified with analytical solutions. Simulations were performed for a range of elements and for a range of polynomial orders of discretization. The discretization was verified per approximation. First, the DGFEM discretization for stratified compressible flow was tested. A single mode solution was tested in one–, two– and three–dimensions. Then Dirac's method of constraints was applied to this space discrete compress-

ible flow system. The resulting DGFEM discretization for stratified incompressible flow was tested with a single mode solution in two–dimensions. Then the Boussinesq approximation was made. The DGFEM discretization for Euler-Boussinesq flow was tested with a single mode solution in two–dimensions and an internal gravity wave solution in two–dimensions. For all tests the order of convergence was as expected. For all tests the discrete energy was conserved up to machine precision.

By changing the direction of gravity in the model a geometric asymmetry was introduced. Starting from a Fourier mode as initial condition the asymmetry led to a focusing of wave energy and wave attractors. Despite the focusing of wave energy, the energy of the system was conserved up to machine precision by construction.

The use of Hamiltonian dynamics in the discretization did not only yield energy preservation up to machine precision, but also other quantities were preserved. The discrete divergence of the velocity was preserved up to machine precision by the dynamics. Ensuring the initial discrete divergence of the velocity was zero ensured the discrete divergence of the velocity was zero for all time. The discrete system also possessed mass conservation and momentum conservation in three directions. The design of the discretization was aimed at obtaining energy conservation. These extra conserved quantities were inherited from the Poisson bracket for free. All these quantities are conserved in a system with a varying the background density.

The developed numerical method is unconditionally stable. Usually, DGFEM discretizations have to satisfy the inf-sup condition to attain numerical stability. The numerical method was developed using Poisson brackets, which is different from most DGFEM discretizations. If and how the developed numerical method satisfies the inf-sup condition is not clear at this moment.

Future theoretical work will focus on the derivation of the Poisson bracket for nonlinear, stratified, rotating, incompressible flow. Rotation allows the propagation of inertial waves, which can also lead to wave attractors. Nonlinearity allows a saturation of the wave attractor, preventing the focusing of wave energy to smaller and smaller scales. Furthermore, the Hamiltonian dynamics will be extended to allow a nonzero Dirichlet boundary condition to be prescribed on the boundary: this allows energy to enter or leave the computational domain while conserving the energy in the domain up to the boundary. This allows modeling of a real world experiment: by forcing a state of rest, a wave attractor is generated.

Future practical work will focus on extending the geometric domain to allow wave attractors to form in complex geometries. For a trapezoidal domain exact analytical solutions for wave attractors have been obtained. Numerical wave attractor solutions will be verified using these analytical solutions. The implementation will be extended to allow a varying buoyancy frequency. This allows further verification of internal gravity wave solutions. The combination of more complex geometries and varying buoyancy frequencies allows simulating real-world internal gravity waves propagation in oceans. The DGFEM implementation will be extended to allow hp-refinement or r-refinement of the domain.

References

Andrews, D. G. (1981). A note on potential energy density in a stratified compressible fluid. *J. Fluid Mech.*, *107*(1), 227–236.

Bajars, J., Frank, J., & Maas, L. (2013). On the appearance of internal wave attractors due to an initial or parametrically excited disturbance. *J. Fluid Mech.*, *714*, 283–311.

Balay, S., Brown, J., Buschelman, K., Eijkhout, V., Gropp, W., Kaushik, D., et al. (2013). *PETSc users manual revision 3.4.*

Balay, S., Buschelman, K., Gropp, W. D., Kaushik, D., Knepley, M. G., McInnes, L. C., et al. (2004). *PETSc web page, 2001.*

Bokhove, O. (2002). Balanced models in geophysical fluid dynamics: Hamiltonian formulation, constraints and formal stability. *Large-Scale Atmosphere-Ocean Dynamics*, *2*, 1–63.

Dirac, P. A. (1958). Generalized Hamiltonian dynamics. *Proc. Phys. Soc. London, Sect. A.. Mathematical and Physical Sciences*, *246*(1246), 326–332.

Dirac, P. A. (2001). *Lectures on quantum mechanics* (No. 2). Courier Dover Publications.

Gerkema, T., & Zimmerman, J. (2008). *An introduction to internal waves.* Royal NIOZ.

Gill, A. E. (1982). *Atmosphere-Ocean Dynamics* (Vol. 30). Academic press.

Hairer, E., Lubich, C., & Wanner, G. (2006). *Geometric numerical integration: structure-preserving algorithms for ordinary differential equations* (Vol. 31). Springer.

Hazewinkel, J., Tsimitri, C., Maas, L., & Dalziel, S. B. (2010). Observations on the robustness of internal wave attractors to perturbations. *Physics of fluids*, *22*, 107102.

Landau, L., & Lifshitz, E. (1966). *Fluid Mechanics, Course of Theoretical Physics.* Pergamon Press Ltd.

Maas, L. (2005). Wave attractors: linear yet nonlinear. *INT. J. BIFURCAT. CHAOS*, *15*(09), 2757–2782.

Maas, L. (2009). Exact analytic self-similar solution of a wave attractor field. *Phys. D: Nonlinear Phenomena*, *238*(5), 502–505.

Maas, L. (2012). *Reader wave attractors.* Royal NIOZ.

Maas, L., & Lam, F. P. A. (1995). Geometric focusing of internal waves. *J. Fluid Mech.*, *300*, 1–42.

Manders, A. M., & Maas, L. (2004). On the three-dimensional structure of the inertial wave field in a rectangular basin with one sloping boundary. *Fluid dynamics research*, *35*(1), 1–21.

Morrison, P. J. (1982). Poisson brackets for fluids and plasmas. In *AIP Conference Proc.* (Vol. 88, p. 13).

Morrison, P. J. (1998). Hamiltonian description of the ideal fluid. *Rev. Mod. Phys.*, *70*(2), 467.

Morrison, P. J., & Greene, J. M. (1980). Noncanonical Hamiltonian density formulation of hydrodynamics and ideal magnetohydrodynamics. *Phys. Rev. Lett.*, *45*(10).

Nurijanyan, S., Van Der Vegt, J., & Bokhove, O. (2013). Hamiltonian discontinuous Galerkin FEM for linear, rotating incompressible Euler equations: Inertial waves. *J. Comp. Phys.*, *241*, 502–525.

Pesch, L., Bell, A., Sollie, H., Ambati, V. R., Bokhove, O., & Van Der Vegt, J. J. (2007). hpGEM—a software framework for discontinuous Galerkin finite element methods. *ACM Trans. Math. Software*, *33*(4), 23.

Salmon, R. (1988a). Hamiltonian fluid mechanics. *Ann. Rev Fluid Mech.*, *20*(1), 225–256.

Salmon, R. (1988b). Semigeostrophic theory as a Dirac-bracket projection. *J. Fluid Mech*, *196*, 345–358.

Shepherd, T. G. (1990). Symmetries, conservation laws, and Hamiltonian structure in geophysical fluid dynamics. *Adv. Geophys*, *32*(287-338), 2.

Shepherd, T. G. (1993). A unified theory of available potential energy 1. *Atmosphere-Ocean*, *31*(1), 1–26.

Sollie, W. (2001). *A 3D Finite Element Model of Internal Waves* (Tech. Rep.). University of Twente.

Staquet, C., & Sommeria, J. (2002). Internal gravity waves: From instabilities to turbulence. *Ann. Rev Fluid Mech.*, *34*(1), 559–593.

Sutherland, B. (2010). *Internal Gravity Waves.* Cambridge University Press.

Turner, J. S. (1979). *Buoyancy Effects in Fluids.* Cambridge University Press.

Vanneste, J., & Bokhove, O. (2002). Dirac-bracket approach to nearly geostrophic hamiltonian balanced models. *Phys. D: Nonlinear Phenomena*, *164*(3), 152–167.

Xu, Y., Vegt, J. J. van der, & Bokhove, O. (2008). Discontinuous Hamiltonian finite element method for linear hyperbolic systems. *J. Sci. Comput.*, *35*(2-3), 241–265.

Appendix A

Fluid Mechanics Fundamentals

In this appendix the fundamental equations of ideal fluid mechanics are derived from basic considerations. First conservations laws for inviscid flows are derived from basic physical arguments: the change of a quantity in a control volume is equal to the flow over the boundary of the control volume. No dissipative processes, as a result of internal friction in a moving fluid or heat exchange between different parts of the fluid, are considered. Such fluids are called ideal fluids. Most of material is based on Landau & Lifshitz (1966). Second, Reynolds' Transport Theorem is used to derive the Navier-Stokes equation for incompressible flow. The Reynolds Transport Theorem allows the rephrasing of conservation laws for systems (e.g., the mass of a system is conserved) into a conservation law for control volumes.

A-1 Equation of Continuity

Consider some volume V_0 with density ρ. The change in mass per unit time in this volume is

$$\frac{\partial}{\partial t} \int \rho \, \mathrm{d}V$$

and the mass of the fluid flowing into this volume per unit time is

$$-\oint \rho \underline{v} \cdot \mathrm{d}\underline{f},$$

where $\underline{v}$ is the velocity of the fluid and $\underline{f}$ is a vector at the boundary of V_0 and has a magnitude equal to the area and is directed along the outward pointing normal vector. Using the divergence theorem this surface integral can be transformed into a volume integral, yielding

$$-\oint \rho \underline{v} \cdot \mathrm{d}\underline{f} = -\int \nabla.(\rho \underline{v}) \, \mathrm{d}V.$$

Equating the change in mass to the mass flowing into the volume yields

$$\int \left(\frac{\partial \rho}{\partial t} + \nabla.(\rho \underline{v}) \right) \mathrm{d}V = 0.$$

Since this holds for any volume, the equation of continuity is obtained

$$\frac{\partial \rho}{\partial t} + \nabla.(\rho \underline{v}) = 0 \qquad (A.1)$$

A-2   Euler's Equation

Consider again a volume V_0 with density ρ. The total force acting on this volume is

$$- \oint p \, d\underline{f},$$

where p is the pressure. Again using the divergence theorem, the total force can be written as

$$- \oint p \, d\underline{f} = - \int \nabla p \, dV.$$

Force equals mass per unit volume times acceleration, so the total force acting on a volume element is

$$\int \rho \frac{d\underline{v}}{dt} \, dV = - \int \nabla p \, dV$$

and this holds for every volume, so

$$\rho \frac{d\underline{v}}{dt} = - \nabla p.$$

Writing out the material derivative yields Euler's equation. In a gravitational field an extra force $\rho \underline{g}$ acts on the volume, resulting in

$$\frac{\partial \underline{v}}{\partial t} + (\underline{v} \cdot \nabla) \underline{v} = - \frac{\nabla p}{\rho} + \underline{g} \qquad (A.2)$$

This result is proved in Subsection A-7 with the help of Reynolds' Transport Theorem.

A-3   Conservation of Entropy

In ideal fluids no heat exchange takes place between different parts of the fluid and thus any motion in fluid is adiabatic. In adiabatic motion the entropy per unit mass s of a particle is constant

$$\frac{ds}{dt} = \frac{\partial s}{\partial t} + \underline{v} \cdot \nabla s = 0. \qquad (A.3)$$

Adding ρ times (A.3) and s times (A.1), the equation of continuity, yields the equation of continuity for entropy

$$\frac{\partial (\rho s)}{\partial t} + \nabla.(\rho s \underline{v}) = 0. \qquad (A.4)$$

If the entropy is constant in a fluid at any instant, it will remain constant. Such a fluid is called isentropic and the conservation of entropy is simply represented by $s = constant$.

A-4   Conservation of Energy

Consider again a fixed volume V_0. The energy per unit volume is

$$\frac{1}{2}\rho v^2 + \rho U,$$

where U is the internal energy per unit mass. The first term is the kinetic energy and the second term is the internal energy. The change in time of this energy is

$$\frac{\partial}{\partial t}\left(\frac{1}{2}\rho v^2 + \rho U\right) = \frac{\partial(\frac{1}{2}\rho v^2)}{\partial t} + \frac{\partial(\rho U)}{\partial t}.$$

Substituting (A.1), the equation of continuity, and (A.2), Euler's equation, without the gravitational component into the first term yields

$$\frac{\partial(\frac{1}{2}\rho v^2)}{\partial t} = -\frac{1}{2}v^2\nabla.(\rho\underline{v}) - \underline{v}\cdot\nabla p - \frac{1}{2}\rho\underline{v}\cdot\nabla v^2.$$

Using the thermodynamic relation $\delta h = T\delta s + \frac{1}{\rho}\delta p$, where h is the heat function per unit mass of the fluid (enthalpy), gives $\nabla p = \rho\nabla h - \rho T\nabla s$. Substituting this expression yields

$$\frac{\partial(\frac{1}{2}\rho v^2)}{\partial t} = -\frac{1}{2}v^2\nabla.(\rho\underline{v}) - \rho\underline{v}\cdot\nabla(\frac{1}{2}v^2 + h) + \rho T\underline{v}\cdot\nabla s.$$

From the thermodynamic relation $\delta U = T\delta s - p\delta\nu = T\delta s + \frac{p}{\rho^2}\delta\rho$, where ν is the specific volume and $h = U + p\nu = U + \frac{p}{\rho}$ follows for the second term

$$\frac{\partial(\rho U)}{\partial t} = U\frac{\partial\rho}{\partial t} + \rho\frac{\partial U}{\partial t} = (U + \frac{p}{\rho})\frac{\partial\rho}{\partial t} + \rho T\frac{\partial s}{\partial t} = h\frac{\partial\rho}{\partial t} + \rho T\frac{\partial s}{\partial t}.$$

Substituting the (A.1), the equation of continuity, and (A.3), the conservation of entropy, yields

$$\frac{\partial(\rho U)}{\partial t} = -h\nabla.(\rho\underline{v}) - \rho T\underline{v}\cdot\nabla s.$$

Finally, the rate of change of the energy can be expressed as

$$\frac{\partial}{\partial t}\left(\frac{1}{2}\rho v^2 + \rho U\right) = -(\frac{1}{2}v^2 + h)\nabla.(\rho\underline{v}) - \rho\underline{v}\cdot\nabla(\frac{1}{2}v^2 + h)$$

The conservation of energy can be written as

$$\frac{\partial}{\partial t}\left(\frac{1}{2}\rho v^2 + \rho U\right) = -\nabla.(\rho\underline{v}(\frac{1}{2}v^2 + h)). \tag{A.5}$$

Integrating over a volume and applying the divergence theorem to the right hand side yields

$$\frac{\partial}{\partial t}\int\left(\frac{1}{2}\rho v^2 + \rho U\right)\,\mathrm{d}V = -\oint\rho\underline{v}(\frac{1}{2}v^2 + h)\,\mathrm{d}\underline{f}.$$

So the change in energy of a volume is equal to the energy flux across the boundary. Since $h = U + \frac{p}{\rho}$ the energy flux can be written as

$$-\underbrace{\oint\rho\underline{v}(\frac{1}{2}v^2 + U)\,\mathrm{d}\underline{f}}_{\text{kinetic and internal energy transport}} - \underbrace{\oint p\underline{v}\,\mathrm{d}\underline{f}}_{\text{work done by pressure forces}}$$

A-5   Incompressible Fluids

Incompressible fluids are fluids for which the material derivative of their density is zero. The equation of continuity, (A.1), simplifies to

$$\nabla.(\underline{v}) = 0. \tag{A.6}$$

When considering two-dimensional flow this simplification allows the introduction of a stream-function ψ such that

$$u = \frac{\partial \psi}{\partial z}, \qquad w = -\frac{\partial \psi}{\partial x}. \tag{A.7}$$

This streamfunction automatically satisfies the equation of continuity and is a powerful tool to solve the equations of motion of an incompressible two-dimensional fluid.

A-6   Mechanical Equilibrium

A fluid is in mechanical equilibrium when it is at rest. Euler's equation, (A.2), then reduces to

$$\nabla p = \rho \underline{g}. \tag{A.8}$$

Since the pressure can only be a function of altitude (direction of $\underline{g} = (0, 0, -g)$) in a fluid at rest, the density can only be a function of altitude.

A fluid can be in mechanical equilibrium without being in thermal equilibrium. If a large enough temperature difference exists in a fluid motion sets in to remove this temperature difference. This motion is called convection. The mechanical equilibrium is stable if no convection is present. If convection is present the mechanical equilibrium is not stable. Here the condition for the onset of convection is investigated.

Consider a fluid in mechanical equilibrium. In this fluid a particle at height z is present with specific volume $\nu(p, s)$, where p is the equilibrium pressure at that height and s is the equilibrium entropy at that height. Suppose this particle is adiabatically displaced upward by a small interval ζ. Its specific volume becomes $\nu(p', s)$, where p' is the pressure at height $h + \zeta$.

For the mechanical equilibrium to be stable the particle should return to its equilibrium position. This is a necessary but not sufficient condition for mechanical stability. The particle experiences a downward force if its mass is larger than the mass of the other particles at height $z + \zeta$. This leads to the heuristic stability criterion

$$\nu(p', s') - \nu(p', s) > 0,$$

where $\nu(p', s')$ is the specific volume of a particle originally at height $z + \zeta$. This difference approximates a derivative in s

$$\left(\frac{\partial \nu}{\partial s}\right)_p \frac{ds}{dz} > 0.$$

From thermodynamics follows $\left(\frac{\partial \nu}{\partial s}\right)_p = \frac{T}{c_p}\left(\frac{\partial \nu}{\partial T}\right)_p$, where c_p is the specific heat at constant pressure. Since most species expand on heating, $\left(\frac{\partial \nu}{\partial T}\right)_p > 0$ and since $c_p > 0$ and $T > 0$ the stability condition becomes

$$\frac{ds}{dz} > 0,$$

the entropy must increase with height. From the definition of entropy follows

$$\frac{ds}{dz} = \left(\frac{\partial s}{\partial T}\right)_p \frac{dT}{dz} + \left(\frac{\partial s}{\partial p}\right)_T \frac{dp}{dz} = \frac{c_p}{T}\frac{dT}{dz} - \left(\frac{d\nu}{dT}\right)_p \frac{dp}{dz} > 0$$

The mechanical equilibrium yields $\frac{dp}{dz} = -g\rho$, so

$$\frac{dT}{dz} > -\frac{gT\rho}{c_p}\left(\frac{d\nu}{dT}\right)_p. \tag{A.9}$$

So convection can occur if the temperature falls with increasing height and the magnitude of the temperature gradient exceeds the critical value. For a ideal gas holds $\left(\frac{T}{V}\right)\left(\frac{\partial V}{\partial T}\right)_p = 1$ and the criterion for convection simplifies to

$$\frac{dT}{dz} > -\frac{g}{c_p}. \tag{A.10}$$

A-7 Reynolds' Transport Theorem

In the previous subsections physical arguments were used to derive the fundamental equations of fluid mechanics. In deriving the conservation laws each time the same arguments were applied: the change in time of a quantity in a control volume is equal to the flow across the boundary of the control volume. Reynolds' Transport Theorem casts conservation principles for systems into conservation laws for control volumes, allowing an natural introduction of extra terms, like gravity in Euler's equations, as in (A.2).

Let $\underline{B}$ be any physical parameter of the fluid (mass, velocity, temperature, ..) and let $\underline{b}$ be the amount of that parameter per unit mass, so $\underline{B} = m\underline{b}$. $\underline{B}$ and $\underline{b}$ can be vectors or a scalars. Reynolds' Transport Theorem states

$$\left(\frac{d\underline{B}}{dt}\right)_{\text{System}} = \frac{\partial}{\partial t}\int_{\text{Control Volume}} \rho\underline{b}\,dV + \oint_{\text{Control Surface}} \rho b\underline{v}^{cs} \cdot \underline{n}\,dA, \tag{A.11}$$

where ρ is the density, $\underline{v}^{cs}$ is the velocity of the area element and $\underline{n}$ an outward pointing unit vector at the boundary. For an incompressible flow $\underline{v}^{cs} = \underline{v}$.

As an example, consider the conservation of mass of a system. The physical fluid parameter B is mass m, yielding $b = 1$. Substituting this into (A.11) yields

$$0 = \left(\frac{dm}{dt}\right)_{\text{System}} = \frac{\partial}{\partial t}\int \rho\,dV + \oint \rho\underline{v} \cdot \underline{n}\,dA.$$

Applying the divergence theorem on the boundary integral and interchanging integration and differentiation in the first term yields

$$\int \frac{\partial \rho}{\partial t} + \nabla.(\rho\underline{v})\,dV = 0.$$

This holds for all control volumes, yielding the equation of continuity (A.1).

Next, consider the conservation of linear momentum for a system. Then $B = m\underline{v}$ and $b = \underline{v}$, yielding

$$\int \underline{c}\,\mathrm{d}V = \left(\frac{dm\underline{v}}{dt}\right)_{\text{System}} = \frac{\partial}{\partial t}\int \rho\underline{v}\,\mathrm{d}V + \oint \rho\underline{v}\underline{v}\cdot\underline{n}\,\mathrm{d}A,$$

where $\underline{c}$ represents body forces which can act as sources or sinks for linear momentum. Interchanging integration and differentiation and applying the divergence theory yields

$$\int \frac{\partial \rho\underline{v}}{\partial t} + \nabla.(\rho\underline{v}\underline{v}) - \underline{c}\,\mathrm{d}V = 0.$$

Since this holds for every volume the integrand must be zero. Writing out divergence, using the product rule for differentiation and using (A.1) yields

$$\rho\frac{d\underline{v}}{dt} = \underline{c}.$$

The body force $\underline{c}$ can be decomposed into two terms: $\underline{c} = \nabla.\underline{\sigma} + \underline{f}$, where σ is a stress tensor and $\underline{f}$ accounts for other forces, e.g. gravity. Substituting the hydrostatic part of the stress tensor and substituting the force of gravity $\rho\underline{g}$ for $\underline{f}$ yields Euler's equations in a gravitational field, (A.2).

Method of Characteristics for Wave Attractors

In two-dimensions and for a constant buoyancy frequency the method of characteristics can be used to solve (2.19) (Maas & Lam, 1995). Dividing (2.19) by the mean background density, ρ^*, and defining $p = P/\rho^*$ and $b = -g\rho/\rho^*$ yields

$$
\begin{aligned}
\frac{\partial u}{\partial t} &= -\frac{\partial p}{\partial x}, \\
\frac{\partial w}{\partial t} &= -\frac{\partial p}{\partial z} + b, \\
\frac{\partial b}{\partial t} &= -wN^2, \\
\frac{\partial u}{\partial x} + \frac{\partial w}{\partial z} &= 0.
\end{aligned}
\tag{B.1}
$$

Due to the incompressibility of the flow a streamfunction ψ can be introduced such that

$$
u = -\frac{\partial \psi}{\partial z}, \quad w = \frac{\partial \psi}{\partial x}.
\tag{B.2}
$$

Substituting (B.2) into (B.1) yields

$$
\begin{aligned}
-\frac{\partial^2 \psi}{\partial t \partial z} &= -\frac{\partial p}{\partial x} \\
\frac{\partial^2 \psi}{\partial t \partial x} &= -\frac{\partial p}{\partial z} + b \\
\frac{\partial b}{\partial t} &= -\frac{\partial \psi}{\partial x} N^2
\end{aligned}
$$

Assume monochromatic waves of frequency ω of the form $\psi(x, z, t) = \Psi(x, z)e^{-i\omega t}$. Eliminating the buoyancy yields

$$
\begin{aligned}
\psi_{ttx} + p_{zt} &= -\psi_x N^2, \text{ or} \\
(-\omega^2 + N^2)\Psi_x &= i\omega p_z
\end{aligned}
\tag{B.3}
$$

The momentum equation in x-direction becomes

$$-i\omega\Psi_z = -p_x, \text{ or}$$
$$\omega^2\Psi_z = i\omega p_x \tag{B.4}$$

Cross-differentiation and subtraction of (B.3) and (B.4) yields

$$\left(N^2 - \omega^2\right)\Psi_{xx} - \omega^2\Psi_{zz} = 0 \tag{B.5}$$

This is a wave equation when $\omega^2 < N^2$. For plane waves $\Psi = \tilde{\Psi}e^{i(kx+mz)}$, where wave vector $\underline{k} = (k, m) = \kappa(\cos(\theta), \sin(\theta))$ and θ is the angle of the wave vector $\underline{k}$ with the horizontal, the dispersion relation

$$\omega^2 = N^2\frac{k^2}{k^2 + m^2} = N^2\cos^2(\theta) \tag{B.6}$$

is found; hence $\omega^2 \leq N^2$. The wave frequency ω is independent of the wavenumber magnitude and depends only the wavenumber direction. Equation (B.6) reveals a remarkable feature of the reflection of internal waves. The frequency ω is preserved by reflection on a fixed wall so the angle θ must be preserved as well. Reflections on walls inclined with the direction of gravity lead to (de)focusing (Maas & Lam, 1995; Maas, 2005; Staquet & Sommeria, 2002). Figure 2-2 showed the geometry of a reflection.

Consider a fluid contained in a container of rectangular shape with depth H and half-width L. The spatial wave equation, (B.5), is non-dimensionalized by $x' = x/L$ and $z' = z/D$, where D is a scale depth given by

$$D = \frac{L\omega}{\sqrt{N^2 - \omega^2}}. \tag{B.7}$$

The deepest point is expressed by

$$\tau = \frac{H}{D} = \frac{H}{L}\frac{\sqrt{N^2 - \omega^2}}{\omega}. \tag{B.8}$$

Here τ is a lumped parameter that contains the basin aspect ratio H/L as well as the frequency ratio N/ω (Maas, 2012). The shape of a basin is now contained in a square of size $-1 \leq x' \leq 1$ and $-\tau \leq z' \leq 0$ and the shape is described by some function $z'(x')$. Dropping the primes this leads to

$$\Psi_{xx} - \Psi_{zz} = 0. \tag{B.9}$$

For certain simple symmetric domains this wave equation can be solved by the method of separation of variables, as performed in Chapter 2.

The method of characteristics can solve the hyperbolic wave equation, (B.9). A general solution is

$$\Psi = f(x + z) - g(x - z). \tag{B.10}$$

Along the characteristics $x \pm z$ the function $f(x \pm z)$ is constant.

Defining a scaled (perturbation) pressure P as

$$P = \frac{i}{\sqrt{N^2 - \omega^2}}p, \tag{B.11}$$

Equations (B.3) and (B.4) become

$$\Psi_z = P_x,$$
$$\Psi_x = P_z.$$

Now the pressure can be expressed as (Maas, 2005)

$$P = f(x + z) + g(x - z). \tag{B.12}$$

So the value of the functions f or g can be seen as a partial pressure.

In the system of transformed coordinates the characteristics travel with an angle of 45°. This is a direct result of the applied scaling and can be seen in the arguments of the general solution of the wave equation, (B.10). This characteristic will hit a boundary, after which it will travel with an angle of 45° with respect to the direction of gravity. At the point where the characteristic hits the boundary holds $\psi = 0$, so the value of f is carried over onto the connected characteristic. The set of connected characteristics is called a web. Thus the partial pressure of a characteristic web is constant along a web (Maas, 2005).

The webs generally hit multiple points on the boundary and arbitrarily prescribing a partial pressure along the entire boundary leads to an overdetermined system: the value on a web is constant and prescribing two different pressures that are connected by one web leads to an inconsistency. The task is now to specify the partial pressure on the boundary such that the problem can be solved uniquely: All the webs should be specified by the boundary condition but each web not more than once. Since $\psi = 0$ at the boundary, the pressure is twice the partial pressure there.

The boundary segments where the partial pressure needs to be prescribed to make the problem well-posed are called the fundamental intervals (Maas & Lam, 1995). Once the partial pressure is prescribed on these fundamental intervals the problem can be uniquely solved.

B-1 Parabolic Basin: Analytical Construction

As an example a parabolic basin is discussed. Figure B-1 shows the geometry of the problem, where the coordinates x and z in the figure are the scaled coordinates x' and z' defined above. In the scaled coordinates the shape of the bottom of the parabolic basin is given by $H(x) = \tau(1 - x^2), x \in [-1, 1]$ (Maas & Lam, 1995). The parameter τ describes the depth of the basin.

The bottom slope $\frac{dH}{dx} = -2\tau x$ implies that when $\tau < \frac{1}{2}$ the characteristic slope (± 1) is everywhere larger than that of the bottom. The bottom is then subcritical (the bottom slope is less than one) everywhere and waves in parabolic bains with $\tau < \frac{1}{2}$ propagate to the top left or right corners (Maas, 2012). Figure B-1 shows an internal wave propagating into the top right corner.

When $\tau > \frac{1}{2}$ the bottom near the two corners is supercritical: the slope $\frac{dH}{dx}$ is larger than the characteristic slope (the bottom slope is large than one). When an internal wave hits a supercritical part of the bottom it reflects backwards to the middle of the domain.
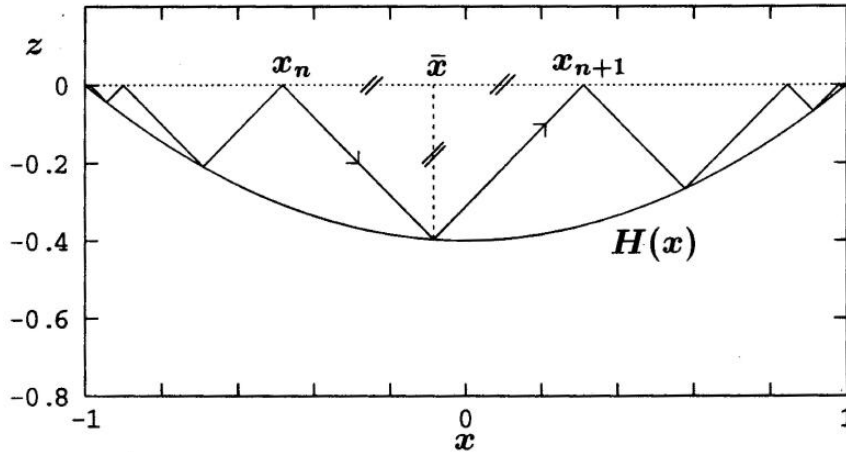
Figure B-1: A parabolic basin with characteristics. The slope is everywhere subcritical and the maximum depth is $\tau = 0.4$. Image taken from Maas (2012).

A single characteristic can now be followed through the basin: whenever it hits a subcritical part of the boundary it reflects 'forwards', i.e., it flips its vertical direction and keeps its horizontal direction. Whenever it hits a supercritical part of the boundary it reflects 'backwards', i.e., it flips its horizontal direction and keeps its vertical direction (Maas, 2012). Figure B-2 shows an example of this procedure. This figure shows that the characteristic approaches a limit orbit, a so-called wave attractor (Maas & Lam, 1995). The approach of a wave attractor happens in general and is not problem-specific.
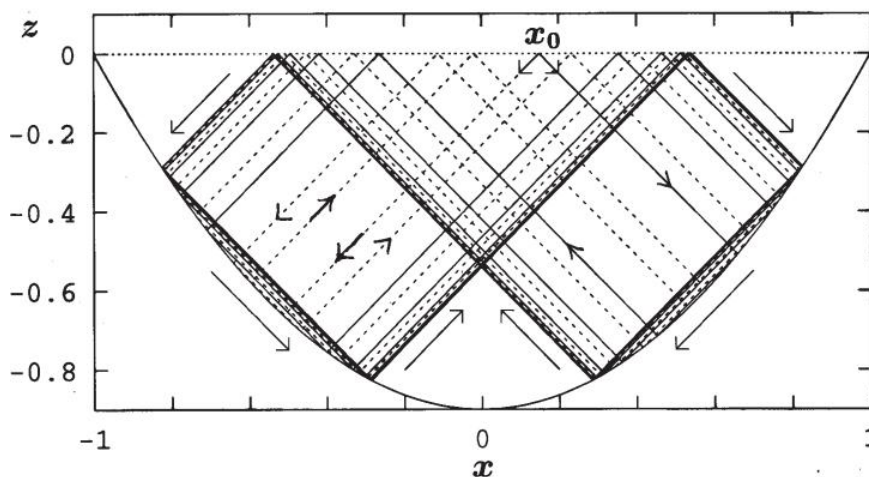
Figure B-2: A parabolic basin with characteristics launched from x_0. The slope is supercritical near the corners and subcritical near the deepest part. Maximum depth is $\tau = 0.9$. Image taken from Maas (2012).

To compute the web a relation between the current surface position, x_n, and the next surface position, x_{n+1}, is needed. Since the characteristics move at angles of $45°$ the distance between two reflections is given by $x_{n+1}-x_n = 2H\left(\frac{x_{n+1}-x_n}{2}\right)$, see Figure B-1. Substituting the relation for the bottom topography $H(x)$ yields (Maas & Lam, 1995)

$$x_{n+1} = -x_n - \frac{1}{\tau} + \sqrt{\frac{4x_n}{\tau} + 4 + \frac{1}{\tau^2}} \equiv X(x_n), \tag{B.13}$$

for rightward propagation and $x_{n+1} = -X(-x_n)$ for leftward propagation (Maas, 2012). For a partly supercritical bottom the mapping should be backwards, so changing from rightward to leftward or vice versa. This mapping is given by

$$Y(x_n) = \frac{2}{\tau} - x_n - 2X(x_n), \quad s \to -s, \tag{B.14}$$

where $s = +1$ indicates rightward movement and $s = -1$ indicates leftward movement. Combining this the mapping becomes

$$T(x,s) = \begin{cases} (X(x),s) \text{ if } s = +1, -1 \le x \le x_s, \\ (Y(x),-s) \text{ if } s = +1, x_s \le x \le 1, \\ (-X(-x),s) \text{ if } s = -1, -x_s \le x \le 1, \\ (-Y(-x),-s) \text{ if } s = -1, -1 \le x \le -x_s, \end{cases} \tag{B.15}$$

where $x_s = \frac{2}{\tau} - 3$ is the point which under a rightward map would be mapped onto the corner $x = 1$. This mapping allows the rapid computation of the characteristic web for different basin sizes. Many parabolic shapes result in a wave attractor (Maas & Lam, 1995). The position of the starting position is arbitrary and the same wave attractor is reached from different starting positions.

When $\tau > \frac{1}{2}$ there are locations at the bottom where the slope is exactly critical: $|\frac{dH}{dx}| = 1$. The characteristic starting at this critical points intersects the surface at $x_c = \frac{3}{4\tau} - \tau$ (Maas & Lam, 1995).
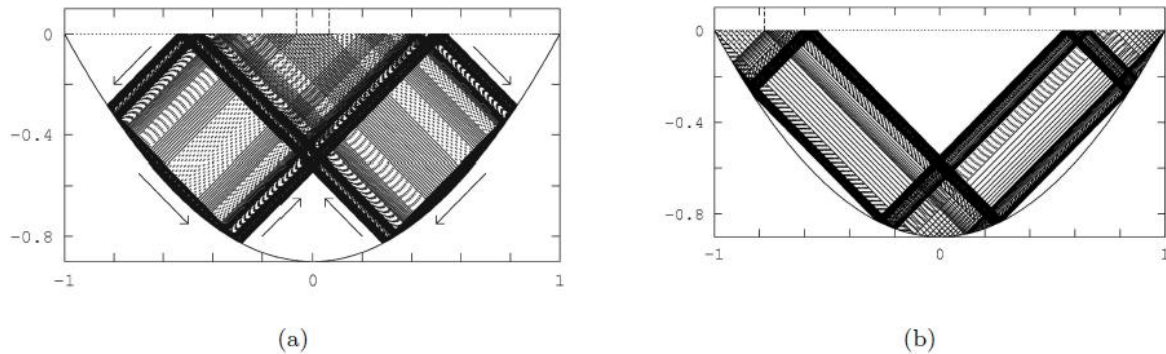
Figure B-3: Webs constructed using the map B.15 from two fundamental intervals. The first fundamental interval is located between the dashed lines in the left figure, the second fundamental interval is located to the left of the dashed line in the right figure. Maximum depth is $\tau = 0.9$. Image taken from Maas (2012).

From the critical characteristic the fundamental intervals are found. The region $x \in (-x_c, x_c)$, Figure B-3 a, is a first fundamental interval. The second fundamental interval is given by $x \in (-1, x_s)$, Figure B-3 b, (Maas & Lam, 1995). The characteristic webs from the two intervals fill the complete basin.

By prescribing the partial pressure at the fundamental intervals the problem, Equation B.9 in a parabolic basin, is solved uniquely. This is done numerically by creating a grid inside the fluid domain. From each grid point the characteristic is followed until it hits the surface at the fundamental intervals. At the fundamental interval the partial pressure is prescribed and since this is invariant on a characteristic the partial pressure of a characteristic at each point is known. This is done for both characteristics stemming from each grid point. Equation B.10 then gives the value of the streamfunction at each grid point.

The streamfunction is related to the velocities by Equations B.2. Unfortunately this requires taking a derivative of the streamfunction, for which only the values on the grid points is known. The derivative can be approximated numerically, but the behaviour of the velocity field cannot be described by some function. Only for one special case the problem was solved analytically, resulting in a expression for the velocity field (Maas, 2009). Finding other analytic solutions is an area of active research. The exact solution from Maas (2009) allows verification of numerical methods and is a starting point for three-dimensional or viscous problems.

The above procedure can be summarized into

1. Define the basin shape;

2. Find the surface reflection of the critical characteristic, x_c, and the surface reflection of the point that is mapped into the right corner, x_s;

3. Determine a mapping as Equation B.15;

4. Find the fundamental intervals;

5. Create a grid inside the fluid domain and follow the characteristics through each grid point until a fundamental interval is reached;

6. Prescribe a partial pressure on the fundamental intervals;

7. Compute the value of the streamfunction at each grid point.

With this recipe each 2D problem can be solved. The value of the partial pressure on the fundamental intervals only determines the amplitude of the solution and not the location of the wave attractors itself. The shape of the wave attractor is set by the shape of the domain, which depends on the assumed frequency of the solution. When the domain is not convex an extra complication arises due to the presence of more bottom locations where the slope is equal to the characteristic slope.

B-2   Trapezoidal Basin: Graphical Construction

When only the limit path of a wave attractor is desired construction of a map as (B.15) and the prescription of partial pressures on fundamental intervals is not needed. Due to the scaling, rays travel at angles of $45°$. Starting from a point in the domain, the ray can be traced as it reflects from the boundary. This can be done graphically or using a computer program. The starting point does not matter as the wave attractor ensures all rays approach the limit cycle.

By releasing rays and following them for many reflections the presence of wave attractors can be investigated. The presence and shape of wave attractors are governed by the dimensionless period τ. For the domain shown in Figure B-4 this ray tracing was performed.

Figure B-4: A sketch of the trapezoidal basin.

A Poincaré plot shows the location of the surface reflection of rays as a function of τ. The x-variable indicates the position in the horizontal direction at the surface where $x = 0.3$ corresponds to the rightmost position and $x = -1$ to the leftmost position. If the ray approaches a limit cycle (a wave attractor) the location of the surface reflections will be the same. If the ray does not approach a limit cycle (a wave attractor) the ray bounces through the domain and has many surface reflection locations. Figure B-5 contains the Poincaré plot as a function of τ. The Poincaré plot was asymmetric due to the asymmetric basin: no rays reached surface locations for $x > 0.3$ since that was on the other side of the tilted wall.

The mapping (B.15) can be used to create a plot of the Lyapunov exponent as a function of τ, similar to B-5. This Lyapunov exponent yields similar information as Figure B-5 (Maas & Lam, 1995).
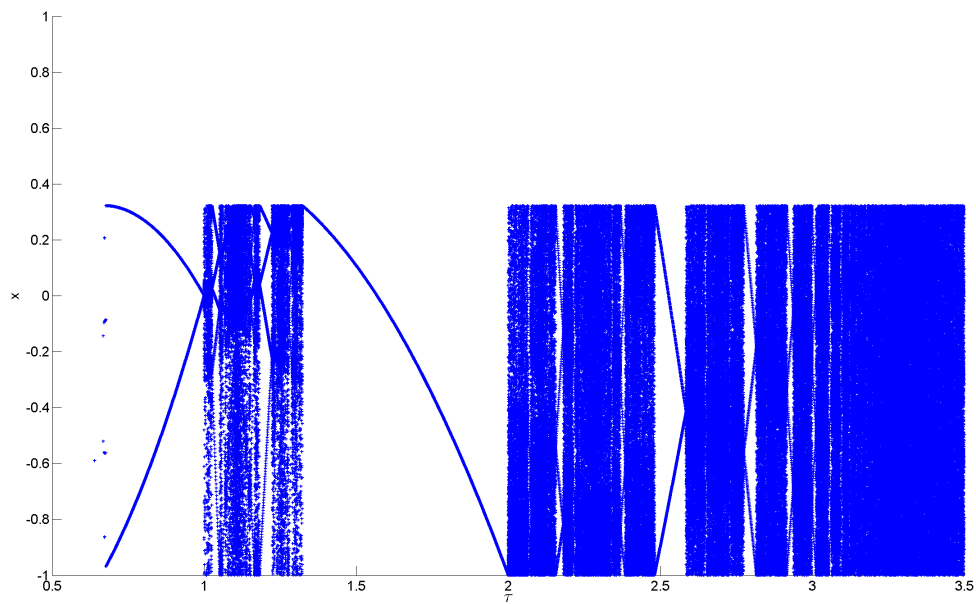
Figure B-5: The theoretical Poincaré plot as a function of τ. The x-variable indicates the position in the horizontal direction where $x = 1$ corresponds to the rightmost position and $x = -1$ to the leftmost position. If the ray approaches a limit cycle (a wave attractor) the location of the surface reflections will be the same. If the ray does not approach a limit cycle (a wave attractor) the ray bounces through the domain and has many surface reflection locations.

Appendix C

Verification: Reduced Equations

The discrete equations of motion for compressible stratified flow (5.34) form a complicated system: 28 Terms relate the 5 variables. The most simple verification problem in Chapter 6, the one dimensional solution in Subsection 6-1-1, still involves 14 terms. In this appendix simpler problems are verified. Taking $\rho_0 = exp(-\beta z)$ and $c_0^2 = 1$ simplifies the analysis.

These simpler problems appear by the following three observations:

- In the discrete Hamiltonian (5.32) any number of terms can be taken and the resulting equations of motion are still Hamiltonian and still preserve the discrete energy. Energy conservation is a property of the Poisson bracket and not of the Hamiltonian. The only requirement placed on the Hamiltonian in this appendix is that it follows the anti-symmetry of the Poisson bracket. Removing the velocity terms from the Hamiltonian destroys the anti-symmetry of the resulting equations. So the velocity terms are needed in the Hamiltonian. However, pressure and density terms can be removed from the Hamiltonian without destroying the the anti-symmetry of the resulting equations.

- In the discrete Poisson bracket (5.31) any number of operators ($\underline{DIV}_{kl}^1, \underline{DIV}_{kl}^2, N_{kl}$, and $\underline{N}_{kl}$) can be taken and the resulting equations of motion still preserve the discrete energy. The anti-symmetry of the terms between brackets ensures energy conservation, not the operators.

- A solution for stratified compressible flow can be simplified by considering homogeneous (constant background density) compressible flow. This only works when the pressure variable is included.

A.M. van Oers

C-1   One Dimensional Problems

C-1-1   Pressure Terms

In this section only the pressure terms in the Hamiltonian are considered. Removing the density terms from the Hamiltonian (5.32) yields

$$H = \frac{1}{2}\,^1M_{ij}W_iW_j + \frac{1}{2}\,^4M_{ij}P_iP_j + \frac{1}{2}\,^5M_{ij}P_iP_j. \tag{C.1}$$

Either $^4M_{ij}$ or $^5M_{ij}$ can be set to zero to simplify the problem.

Case 0

Removing the operators $\underline{DIV}^1_{kl}$, N_{kl}, and $\underline{N}_{kl}$ from the discrete Poisson bracket (5.31) yields

$$[F,G] = \left(\frac{\partial G}{\partial W_j}\frac{\partial F}{\partial P_i} - \frac{\partial F}{\partial W_j}\frac{\partial G}{\partial P_i} \right)\hat{\underline{z}}.\underline{DIV}^2_{kl}M_{ik}^{-1}M_{jl}^{-1}. \tag{C.2}$$

Substituting $^4M_{ij} = 0$ into (C.1) yields

$$H = \frac{1}{2}\,^1M_{ij}W_iW_j + \frac{1}{2}\,^5M_{ij}P_iP_j. \tag{C.3}$$

Substituting (C.3) into (C.2) yields the discrete equation of motion

$$\begin{aligned}
\frac{dW_j}{dt} &= -\,^5M_{il}\hat{\underline{z}}.\underline{DIV}^2_{kl}P_lM_{ik}^{-1}M_{jl}^{-1}, \\
\frac{dP_l}{dt} &= W_j\hat{\underline{z}}.\underline{DIV}^2_{jk}\,^1M_{ij}M_{ik}^{-1}M_{jl}^{-1}.
\end{aligned} \tag{C.4}$$

The continuous Hamiltonian (4.43) and continuous bracket (4.45) reduce to

$$\mathcal{H} = \int_\Omega \frac{1}{2}\frac{1}{\rho_0}\left(\rho_0 w\right)^2 + \frac{1}{2}\frac{1}{\rho_0}p^2\,\mathrm{d}z \tag{C.5}$$

and

$$\{\mathcal{F},\mathcal{G}\} = \int_\Omega \frac{\delta\mathcal{G}}{\delta p}\rho_0\nabla.\left(\frac{\delta\mathcal{F}}{\delta(\rho_0 w)}\right) - \frac{\delta\mathcal{F}}{\delta p}\rho_0\nabla.\left(\frac{\delta\mathcal{G}}{\delta(\rho_0 w)}\right)\,\mathrm{d}z. \tag{C.6}$$

The continuous equations of motion are

$$\begin{aligned}
\frac{\partial(\rho_0 w)}{\partial t} &= -\nabla p, \\
\frac{\partial p}{\partial t} &= -(N^2 + 1)(\rho_0 w) - \nabla(\rho_0 w).
\end{aligned} \tag{C.7}$$

The boundary condition is no normal flow in z-direction. Using separation of variables a solution can be constructed

$$\begin{aligned}
\rho_0 w &= e^{-\frac{1}{2}\left(N^2+1\right)z}\sin(mz)\sin(\sigma t + 0.1), \\
p &= e^{-\frac{1}{2}\left(N^2+1\right)z}\left[\frac{N^2+1}{2\sigma}\sin(mz) + \frac{m}{\sigma}\cos(mz)\right]\cos(\sigma t + 0.1),
\end{aligned} \tag{C.8}$$

with dispersion relation

$$4\sigma^2 = \left(N^2 + 1\right)^2 + 4m^2. \tag{C.9}$$

For a homogeneous fluid $N^2 = -1$. For a stratified fluid $N^2 > 0$. As test case a background density $\rho_0 = \exp -3z$ is taken, yielding $N^2 = 2$.

The numerical discretization is initialized at time $t = 0$ and compared to the exact solution. The phase difference ensures the numerical solution is nonzero at $t = 0$ and at every period. Table C-1 presents the L^2-error and order of convergence of the numerical solution after five periods. In both cases the order of convergence is polynomial order plus one. Only the convergence rate for the stratified case with first order polynomials is performing less than expected. The energy is conserved up to machine precision. Figure C-1 shows the error in total energy during 100 periods.

Table C-1: L^2-error and order of convergence of the numerical solution after five periods for the reduced equations, pressure terms, case 0.

|	Homogeneous Fluid				Stratified Fluid			
$p = 0$	$\rho_0 w$		p		$\rho_0 w$		p	
K	L^2-error	Order	L^2-error	Order	L^2-error	Order	L^2-error	Order
4	8.8136e-1	-	8.0379e-1	-	8.3269e-2	-	6.1661e-1	-
8	2.0553e-1	2.10	1.9507e+0	-1.28	2.7088e-1	-1.70	1.0736e+0	-0.80
16	7.4335e-1	-1.85	2.8734e-1	2.76	3.8319e-1	-0.50	1.6338e-1	2.72
32	2.0089e-1	1.89	9.7638e-2	1.56	1.0545e-1	1.86	6.2849e-2	1.38
64	5.0414e-2	1.99	4.9075e-2	0.99	2.8342e-2	1.90	3.3259e-2	0.92
128	1.2767e-2	1.98	2.4463e-2	1.00	8.7762e-3	1.69	1.6665e-2	1.00
256	3.3623e-3	1.92	1.2216e-2	1.00	3.4149e-3	1.36	8.3625e-3	0.99
$p = 1$	$\rho_0 w$		p		$\rho_0 w$		p	
K	L^2-error	Order	L^2-error	Order	L^2-error	Order	L^2-error	Order
4	1.0438e+0	-	1.1046e+0	-	5.1547e-1	-	4.2903e-1	-
8	3.8764e-1	1.43	7.1403e-2	3.95	2.0504e-1	1.33	1.4448e-1	1.57
16	1.1416e-1	1.76	5.1083e-2	0.48	6.5693e-2	1.64	1.0266e-1	0.49
32	2.7298e-2	2.06	2.7541e-3	4.21	2.0341e-2	1.69	5.2804e-2	0.96
64	6.4862e-3	2.07	2.3619e-4	3.54	8.0634e-3	1.33	2.6386e-2	1.00
128	1.5975e-3	2.02	4.4766e-5	2.40	3.7356e-3	1.11	1.3164e-2	1.00
256	3.9788e-4	2.01	1.0703e-5	2.06	1.8296e-3	1.03	6.5776e-3	1.00
$p = 2$	$\rho_0 w$		p		$\rho_0 w$		p	
K	L^2-error	Order	L^2-error	Order	L^2-error	Order	L^2-error	Order
4	3.1494e-2	-	2.9026e-2	-	2.7806e-2	-	7.1372e-2	-
8	7.4607e-4	5.40	4.3825e-3	2.73	1.7135e-3	4.02	5.3042e-3	3.75
16	6.7482e-5	3.47	5.1567e-4	3.09	1.8223e-4	3.23	3.9506e-4	3.75
32	9.4935e-6	2.83	6.4066e-5	3.01	5.1466e-5	1.82	5.3732e-5	2.88
64	5.7249e-7	4.05	7.8587e-6	3.03	6.7931e-6	2.92	7.4102e-6	2.86
128	1.2184e-7	2.23	9.7987e-7	3.00	8.0504e-7	3.08	1.0410e-6	2.83
256	6.1373e-8	1.03	1.2265e-7	3.00	1.0381e-7	2.96	1.2645e-7	3.04
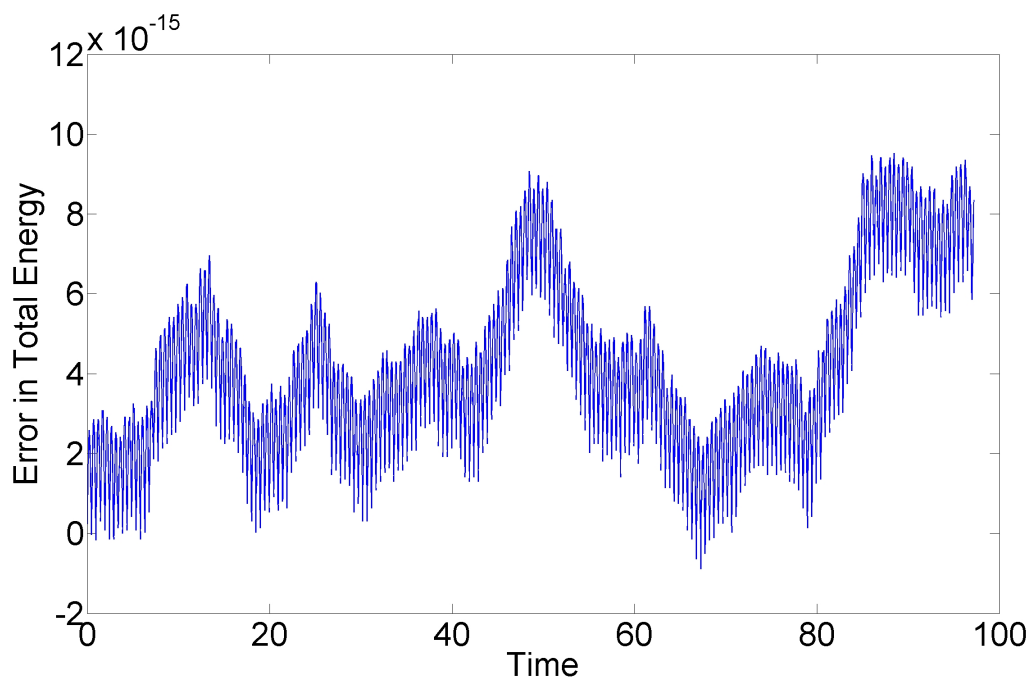
Figure C-1: The error in total energy during 100 periods for a stratified fluid. The spatial and temporal step size was $1/32$ and the polynomial order was one. The tolerance of the iterative solver was 10^{-14}.

Case 1

Using (C.1) as Hamiltonian

$$H = \frac{1}{2}{}^1 M_{ij} W_i W_j + \frac{1}{2}{}^4 M_{ij} P_i P_j + \frac{1}{2}{}^5 M_{ij} P_i P_j \qquad (\text{C.10})$$

and substituting into (C.2) yields the discrete equation of motion

$$\frac{dW_j}{dt} = \left(-{}^4 M_{il} \hat{\underline{z}}.\underline{DIV}_{kl}^2 - {}^5 M_{il} \hat{\underline{z}}.\underline{DIV}_{kl}^2 \right) P_l M_{ik}^{-1} M_{jl}^{-1},$$
$$\frac{dP_l}{dt} = W_j \hat{\underline{z}}.\underline{DIV}_{jk}^2 {}^1 M_{ij} M_{ik}^{-1} M_{jl}^{-1}. \qquad (\text{C.11})$$

The exact solutions is still (C.8). The dispersion relation changes to

$$4\sigma^2 = \frac{N^2 + 1}{N^2} \left(\left(N^2 + 1 \right)^2 + 4m^2 \right). \qquad (\text{C.12})$$

For a homogeneous fluid $N^2 = -1$ and the solution is no longer a wave. For this test case only stratified fluids are considered. As test case a background density $\rho_0 = \exp -3z$ is taken, yielding $N^2 = 2$.

The numerical discretization is initialized at time $t = 0$ and compared to the exact solution. The phase difference ensures the numerical solution is nonzero at $t = 0$ and at every period. Table C-2 presents the L^2-error and order of convergence of the numerical solution after five periods. The order of convergence is polynomial order plus one. Only the convergence rate for the stratified case with first order polynomials is performing less than expected. The energy is conserved up to machine precision. Figure C-2 shows the error in total energy during 100 periods.

Table C-2: L^2-error and order of convergence of the numerical solution after five periods for the reduced equations, pressure terms, case 1.

Stratified Fluid				
$p = 0$	$\rho_0 w$		p	
K	L^2-error	Order	L^2-error	Order
4	8.3269e-2	-	5.0346e-001	-
8	2.7088e-1	-1.70	8.7660e-001	-0.80
16	3.8319e-1	-0.50	1.3340e-001	2.72
32	1.0545e-1	1.86	5.1316e-002	1.38
64	2.8342e-2	1.90	2.7156e-002	0.92
128	8.7762e-3	1.69	1.3607e-002	1.00
256	3.4149e-3	1.36	6.8279e-003	0.99
$p = 1$	$\rho_0 w$		p	
K	L^2-error	Order	L^2-error	Order
4	5.1547e-1	-	3.5030e-1	-
8	2.0504e-1	1.33	1.1797e-1	1.57
16	6.5693e-2	1.64	8.3818e-2	0.49
32	2.0341e-2	1.69	4.3115e-2	0.96
64	8.0634e-3	1.33	2.1544e-2	1.00
128	3.7356e-3	1.11	1.0748e-2	1.00
256	1.8296e-3	1.03	5.3706e-3	1.00
$p = 2$	$\rho_0 w$		p	
K	L^2-error	Order	L^2-error	Order
4	2.7806e-2	-	5.8275e-2	-
8	1.7135e-3	4.02	4.3309e-3	3.75
16	1.8223e-4	3.23	3.2256e-4	3.75
32	5.1466e-5	1.82	4.3872e-5	2.88
64	6.7931e-6	2.92	6.0503e-6	2.86
128	8.0519e-7	3.08	8.4996e-7	2.83
256	1.0381e-7	2.96	1.0325e-7	3.04
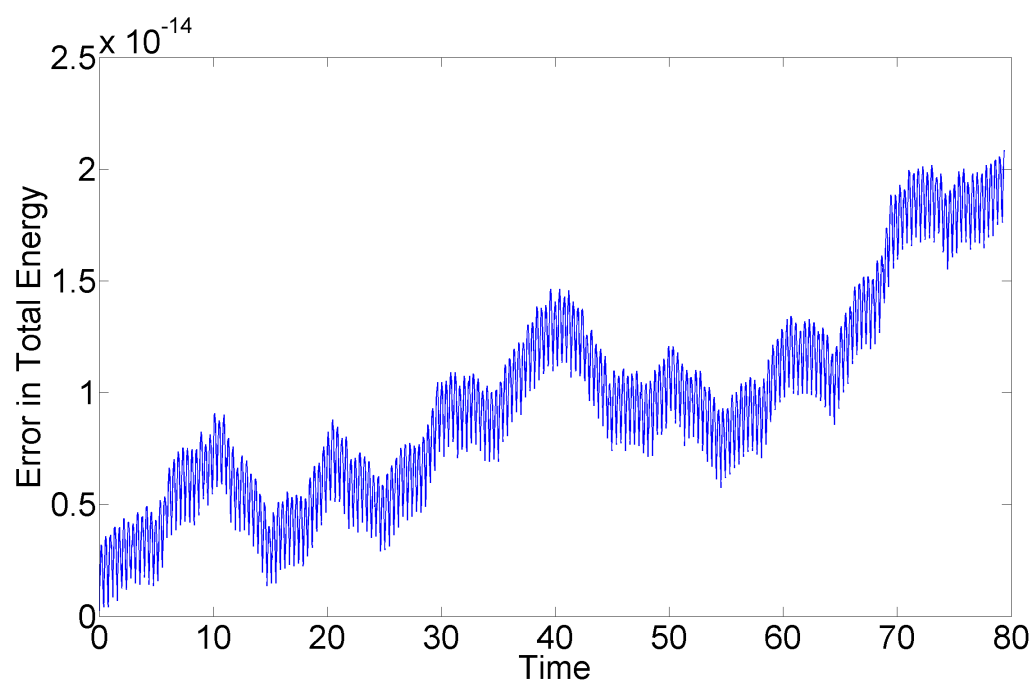
Figure C-2: The error in total energy during 100 periods for a stratified fluid. The spatial and temporal step size was $1/32$ and the polynomial order was one. The tolerance of the iterative solver was 10^{-14}.

Case 2

Using (C.1) as Hamiltonian

$$H = \frac{1}{2}\,^1M_{ij}W_iW_j + \frac{1}{2}\,^4M_{ij}P_iP_j + \frac{1}{2}\,^5M_{ij}P_iP_j \tag{C.13}$$

and removing the operators $\underline{DIV}^1_{kl}$ and $\underline{N}_{kl}$ from the discrete Poisson bracket (5.31)

$$
\begin{aligned}
[F,G] = & \left(\frac{\partial G}{\partial \underline{U}_j}\frac{\partial F}{\partial P_i} - \frac{\partial F}{\partial \underline{U}_j}\frac{\partial G}{\partial P_i} \right).\underline{DIV}^2_{kl}M_{ik}^{-1}M_{jl}^{-1} \\
& + \left(\frac{\partial G}{\partial W_j}\frac{\partial F}{\partial P_i} - \frac{\partial F}{\partial W_j}\frac{\partial G}{\partial P_i} \right) N_{kl}M_{ik}^{-1}M_{jl}^{-1}
\end{aligned}
\tag{C.14}
$$

yields the discrete equation of motion

$$
\begin{aligned}
\frac{dW_j}{dt} &= \left(-\,^4M_{il}\underline{\hat{z}}.\underline{DIV}^2_{kl} - \,^5M_{il}\underline{\hat{z}}.\underline{DIV}^2_{kl} - \,^4M_{il}N_{kl} - \,^5M_{il}N_{kl} \right)P_lM_{ik}^{-1}M_{jl}^{-1}, \\
\frac{dP_l}{dt} &= W_j\,^1M_{ij}N_{jk}M_{lj}^{-1}M_{ik}^{-1} + W_j\underline{\hat{z}}.\underline{DIV}^2_{jk}\,^1M_{ij}M_{ik}^{-1}M_{jl}^{-1}.
\end{aligned}
\tag{C.15}
$$

Note that the pressure equation has the same complexity as the pressure equation of the full one dimensional system. An exact solutions is

$$
\begin{aligned}
\rho_0 w &= e^{-\frac{1}{2}\left(N^2+1\right)z}\sin(mz)\sin(\sigma t + 0.1), \\
p &= e^{-\frac{1}{2}\left(N^2+1\right)z}\left[\frac{N^2-1}{2\sigma}\sin(mz) + \frac{m}{\sigma}\cos(mz) \right]\cos(\sigma t + 0.1),
\end{aligned}
\tag{C.16}
$$

with dispersion relation

$$\sigma^2 = \frac{N^2+1}{N^2}\left[\frac{1}{4}\left(N^2-1\right)^2 + m^2 \right]. \tag{C.17}$$

For a homogeneous fluid $N^2 = -1$ and the solution is no longer a wave. For this test case only stratified fluids are considered. As test case a background density $\rho_0 = \exp{-3z}$ is taken, yielding $N^2 = 2$.

The numerical discretization is initialized at time $t = 0$ and compared to the exact solution. The phase difference ensures the numerical solution is nonzero at $t = 0$ and at every period. Table C-3 presents the L^2-error and order of convergence of the numerical solution after five periods. The order of convergence is polynomial order plus one. Only the convergence rate for the stratified case with first order polynomials is performing less than expected. The energy is conserved up to machine precision. Figure C-3 shows the error in total energy during 100 periods.

Table C-3: L^2-error and order of convergence of the numerical solution after five periods for the reduced equations, pressure terms, case 2.

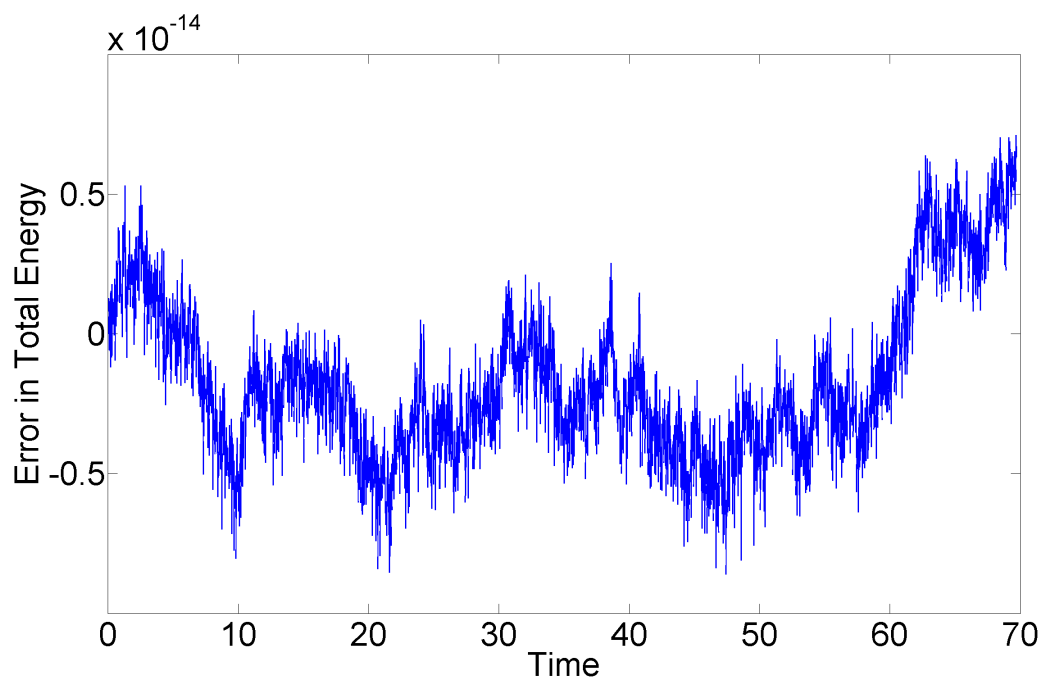|	Stratified Fluid			
$p = 0$	$\rho_0 w$		p	
K	L^2-error	Order	L^2-error	Order
4	4.8548e-1	-	8.7632e-1	-
8	1.5576e-1	1.64	8.8452e-1	-0.01
16	3.9974e-1	-1.36	1.3876e-1	2.67
32	1.0879e-1	1.88	5.1828e-2	1.42
64	2.7691e-2	1.97	2.6570e-2	0.96
128	7.1778e-3	1.95	1.3460e-2	0.98
256	2.0236e-3	1.83	6.7677e-3	0.99
$p = 1$	$\rho_0 w$		p	
K	L^2-error	Order	L^2-error	Order
4	5.6029e-1	-	4.6318e-1	-
8	2.1363e-1	1.39	1.2345e-1	1.91
16	5.9597e-2	1.84	7.3180e-2	0.75
32	1.6497e-2	1.85	3.1289e-2	1.23
64	4.5137e-3	1.87	1.5209e-2	1.04
128	1.4731e-3	1.62	7.5685e-3	1.01
256	6.0162e-4	1.29	3.7804e-3	1.00
$p = 2$	$\rho_0 w$		p	
K	L^2-error	Order	L^2-error	Order
4	3.7715e-002	-	2.5295e-002	-
8	2.0683e-003	4.19	4.4603e-003	2.50
16	3.0729e-004	2.75	4.2927e-004	3.38
32	2.1196e-005	3.86	6.8470e-005	2.65
64	1.7802e-006	3.57	8.7579e-006	2.97
128	2.5985e-007	2.78	1.1398e-006	2.94
256	4.4992e-008	2.53	1.4500e-007	2.97
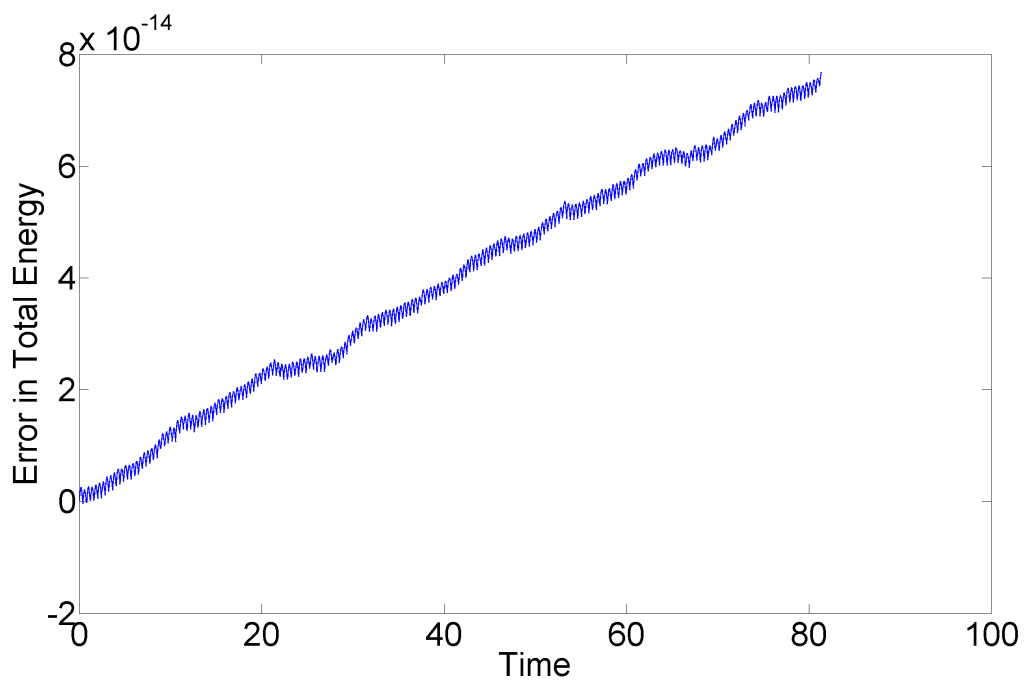
Figure C-3: The error in total energy during 100 periods for a stratified fluid. The spatial and temporal step size was $1/32$ and the polynomial order was 1. The tolerance of the iterative solver was 10^{-14}.

C-1-2   Density Terms

In this section only the density terms in the Hamiltonian are considered. Removing the pressure terms from the Hamiltonian (5.32) yields

$$H = \frac{1}{2}{}^1 M_{ij} W_i W_j + \frac{1}{2}{}^2 M_{ij} R_i R_j. \tag{C.18}$$

The case with only the operator $\underline{DIV}^1_{kl}$ in the Poisson bracket is nearly identical to including only the pressure terms, Case 0. Removing the operators $\underline{DIV}^2_{kl}$ and N_{kl} from the discrete Poisson bracket (5.31) yields

$$
\begin{aligned}
[F,G] = &\left(\frac{\partial G}{\partial W_j} \frac{\partial F}{\partial R_i} - \frac{\partial F}{\partial W_j} \frac{\partial G}{\partial R_i} \right) \hat{\underline{z}}.\underline{DIV}^1_{kl} M^{-1}_{ik} M^{-1}_{jl} \\
&- \left(\frac{\partial G}{\partial W_j} \frac{\partial F}{\partial R_i} - \frac{\partial F}{\partial W_j} \frac{\partial G}{\partial R_i} \right) \hat{\underline{z}}.\underline{N}_{kl} M^{-1}_{ik} M^{-1}_{jl}.
\end{aligned}
\tag{C.19}
$$

Substituting (C.18) into (C.19) yields the discrete equation of motion

$$
\begin{aligned}
\frac{dW_j}{dt} &= \left(-{}^2 M_{il} \hat{\underline{z}}.\underline{DIV}^1_{kl} + {}^2 M_{il} \hat{\underline{z}}.\underline{N}_{kl} \right) R_l M^{-1}_{ik} M^{-1}_{jl}, \\
\frac{dR_l}{dt} &= W_j \hat{\underline{z}}.\underline{DIV}^1_{jk}{}^1 M_{ij} M^{-1}_{ik} M^{-1}_{jl} - W_j \hat{\underline{z}}.\underline{N}_{jk}{}^1 M_{ij} M^{-1}_{ik} M^{-1}_{jl}.
\end{aligned}
\tag{C.20}
$$

Note that the density equation has the same complexity as the density equation of the full one dimensional system. An exact solutions is

$$
\begin{aligned}
\rho_0 w &= e^{-\frac{1}{2}(N^2+1)z} \sin(mz) \sin(\sigma t + 0.1), \\
\rho &= e^{-\frac{1}{2}(N^2+1)z} \left[-\frac{N^2+1}{2\sigma} \sin(mz) + \frac{m}{\sigma} \cos(mz) \right] \cos(\sigma t + 0.1),
\end{aligned}
\tag{C.21}
$$

with dispersion relation

$$4N^2 \sigma^2 = \left(N^2 + 1 \right)^2 + 4m^2. \tag{C.22}$$

For a homogeneous fluid $\underline{N}_{jk} = 0$ and this test case is nearly identical to including only the pressure terms, Case 0. As test case a background density $\rho_0 = \exp[-3z]$ is taken, yielding $N^2 = 2$.

The numerical discretization is initialized at time $t = 0$ and compared to the exact solution. The phase difference ensures the numerical solution is nonzero at $t = 0$ and at every period. Table C-4 presents the L^2-error and order of convergence of the numerical solution after five periods. The order of convergence is polynomial order plus one. The energy is conserved up to machine precision. Figure C-4 shows the error in total energy during 100 periods.

Table C-4: L^2-error and order of convergence of the numerical solution after five periods for the reduced equations, pressure terms, case 2.

		Stratified Fluid		
$p = 0$	$\rho_0 w$		ρ	
K	L^2-error	Order	L^2-error	Order
4	4.1343×10^{-1}	–	1.1198×10^{0}	–
8	2.0975×10^{-1}	0.98	1.4815×10^{0}	−0.40
16	3.8567×10^{-1}	−0.88	2.2246×10^{-1}	2.74
32	1.0343×10^{-1}	1.90	8.5719×10^{-2}	1.38
64	2.5989×10^{-2}	1.99	4.2998×10^{-2}	1.00
128	6.6009×10^{-3}	1.98	2.1455×10^{-2}	1.00
$p = 1$	$\rho_0 w$		ρ	
K	L^2-error	Order	L^2-error	Order
4	5.5251×10^{-1}	–	1.0210×10^{0}	–
8	2.3509×10^{-1}	1.23	1.3380×10^{-1}	2.93
16	6.1975×10^{-2}	1.92	9.6313×10^{-2}	0.47
32	1.5459×10^{-2}	2.00	4.9208×10^{-2}	0.97
64	4.8770×10^{-3}	1.66	2.3755×10^{-2}	1.05
128	1.9549×10^{-3}	1.32	1.1728×10^{-2}	1.02
$p = 2$	$\rho_0 w$		ρ	
K	L^2-error	Order	L^2-error	Order
4	2.6153×10^{-2}	–	6.8036×10^{-2}	–
8	1.1812×10^{-3}	4.47	4.8457×10^{-3}	3.81
16	1.0825×10^{-4}	3.45	5.3298×10^{-4}	3.18
32	2.7505×10^{-5}	1.98	6.5948×10^{-5}	3.01
64	3.6276×10^{-6}	2.92	8.5899×10^{-6}	2.94
128	4.2769×10^{-7}	3.08	1.1374×10^{-6}	2.92
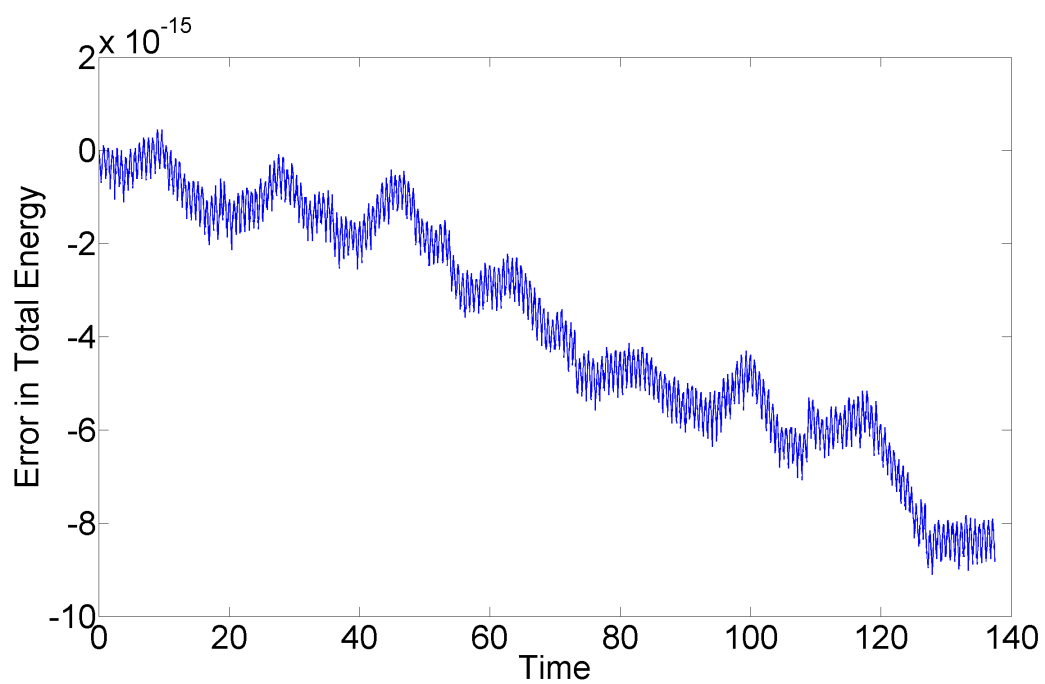
Figure C-4: The error in total energy during 100 periods for a stratified fluid. The spatial and temporal step size was $1/32$ and the polynomial order was one. The tolerance of the iterative solver was 10^{-14}.

C-2   Two Dimensional Problems

C-2-1   Pressure Terms

In this section only the pressure terms in the Hamiltonian are considered. Removing the density terms from the Hamiltonian (5.32) yields

$$H = \frac{1}{2}\,{}^1M_{ij}\underline{U}_i.\underline{U}_j + \frac{1}{2}\,{}^4M_{ij}P_iP_j + \frac{1}{2}\,{}^5M_{ij}P_iP_j. \tag{C.23}$$

Either ${}^4M_{ij}$ or ${}^5M_{ij}$ can be set to zero to simplify the problem.

Case 0

Removing the operators $\underline{DIV}^1_{kl}$, N_{kl}, and $\underline{N}_{kl}$ from the discrete Poisson bracket (5.31) yields

$$[F,G] = \left(\frac{\partial G}{\partial \underline{U}_j} \frac{\partial F}{\partial P_i} - \frac{\partial F}{\partial \underline{U}_j} \frac{\partial G}{\partial P_i} \right).\underline{DIV}^2_{kl} M^{-1}_{ik} M^{-1}_{jl}. \tag{C.24}$$

Substituting ${}^4M_{ij} = 0$ into (C.23) yields

$$H = \frac{1}{2}\,{}^1M_{ij}\underline{U}_i.\underline{U}_j + \frac{1}{2}\,{}^5M_{ij}P_iP_j. \tag{C.25}$$

Substituting (C.25) into (C.24) yields the discrete equation of motion

$$\begin{aligned} \frac{d\underline{U}_j}{dt} &= -{}^5M_{il}\underline{DIV}^2_{kl}P_l M^{-1}_{ik} M^{-1}_{jl}, \\ \frac{dP_l}{dt} &= \underline{U}_j\underline{DIV}^2_{jk}\,{}^1M_{ij} M^{-1}_{ik} M^{-1}_{jl}. \end{aligned} \tag{C.26}$$

The continuous Hamiltonian (4.43) and continuous bracket (4.45) reduce to

$$\mathcal{H} = \int_\Omega \frac{1}{2}\frac{1}{\rho_0}\left|\rho_0\underline{v}\right|^2 + \frac{1}{2}\frac{1}{\rho_0}p^2 \, \mathrm{d}z \tag{C.27}$$

and

$$\{\mathcal{F},\mathcal{G}\} = \int_\Omega \frac{\delta\mathcal{G}}{\delta p}\rho_0\nabla.\left(\frac{\delta\mathcal{F}}{\delta(\rho_0\underline{v})}\right) - \frac{\delta\mathcal{F}}{\delta p}\rho_0\nabla.\left(\frac{\delta\mathcal{G}}{\delta(\rho_0\underline{v})}\right) \, \mathrm{d}\underline{x}. \tag{C.28}$$

The continuous equations of motion are

$$\begin{aligned} \frac{\partial(\rho_0\underline{v})}{\partial t} &= -\nabla p, \\ \frac{\partial p}{\partial t} &= -(N^2+1)(\rho_0 w) - \nabla.(\rho_0\underline{v}). \end{aligned} \tag{C.29}$$

The boundary condition is no normal flow in all directions. Using separation of variables a solution can be constructed

$$\begin{aligned} \rho_0 u &= e^{-\frac{1}{2}\left(N^2+1\right)z}\frac{k}{\sigma^2-k^2}\left[\frac{N^2+1}{2}\sin(mz) + m\cos(mz)\right]\sin(kx)\cos(\sigma t + 0.1), \\ \rho_0 w &= e^{-\frac{1}{2}\left(N^2+1\right)z}\sin(mz)\cos(kx)\sin(\sigma t + 0.1), \\ p &= e^{-\frac{1}{2}\left(N^2+1\right)z}\frac{\sigma}{\sigma^2-k^2}\left[\frac{N^2+1}{2}\sin(mz) + m\cos(mz)\right]\cos(kx)\cos(\sigma t + 0.1), \end{aligned} \tag{C.30}$$

with dispersion relation

$$\sigma^2 = \frac{1}{4}\left(N^2 + 1\right)^2 + m^2 + k^2. \tag{C.31}$$

For a homogeneous fluid $N^2 = -1$. For a stratified fluid $N^2 > 0$. As test case a background density $\rho_0 = \exp -3z$ is taken, yielding $N^2 = 2$.

The numerical discretization is initialized at time $t = 0$ and compared to the exact solution. The phase difference ensures the numerical solution is nonzero at $t = 0$ and at every period. Table C-5 presents the L^2-error and order of convergence of the numerical solution after five periods. In both cases the order of convergence is polynomial order plus one. Only the convergence rate for the stratified case with first order polynomials is performing less than expected. The energy is conserved up to machine precision. Figure C-5 shows the error in total energy during 100 periods.

Table C-5: L^2-error and order of convergence of the numerical solution after five periods for the reduced equations in two dimensions, pressure terms, case 0. The time step was chosen small enough to ensure that timestep errors can be neglected.

$p = 0$	$\rho_0 u$		$\rho_0 w$		p	
K	L^2-error	Order	L^2-error	Order	L^2-error	Order
4	3.484E-1	-	4.378E-1	-	1.428E+0	-
8	1.619E-1	1.11	1.843E-1	1.25	1.504E+0	-0.08
16	4.143E-1	-1.36	3.900E-1	-1.08	2.754E-1	2.45
32	1.135E-1	1.87	1.078E-1	1.86	1.174E-1	1.23
64	2.921E-2	1.96	2.887E-2	1.90	6.290E-2	0.90
$p = 1$	$\rho_0 u$		$\rho_0 w$		p	
K	L^2-error	Order	L^2-error	Order	L^2-error	Order
4	1.864E-1	-	1.659E-1	-	8.541E-1	-
8	1.607E-1	0.21	1.612E-1	0.04	2.052E-1	2.06
16	6.393E-2	1.33	7.342E-2	1.13	8.892E-2	1.21
32	2.020E-2	1.66	3.123E-2	1.23	4.924E-2	0.85
64	8.380E-3	1.27	1.446E-2	1.11	2.535E-2	0.96
$p = 2$	$\rho_0 u$		$\rho_0 w$		p	
K	L^2-error	Order	L^2-error	Order	L^2-error	Order
4	1.179E-1	-	1.386E-1	-	2.255E-1	-
8	1.638E-2	2.85	1.918E-2	2.85	3.763E-2	2.58
16	1.891E-3	3.11	2.446E-3	2.97	1.553E-2	1.28
$p = 3$	$\rho_0 u$		$\rho_0 w$		p	
K	L^2-error	Order	L^2-error	Order	L^2-error	Order
4	2.282E-1	-	2.090E-1	-	5.975E-2	-
8	1.453E-2	3.97	1.372E-2	3.93	3.656E-3	4.03
16	9.206E-4	3.98	8.779E-4	3.97	2.829E-4	3.69

Figure C-5: The error in total energy during 100 periods for a stratified fluid. The spatial and temporal step size was $1/32$ and the polynomial order was one. The tolerance of the iterative solver was 10^{-14}.

Appendix D

Acoustic and Lamb Waves

This chapter extends the description of Chapter 2 to acoustic and Lamb waves. The compressible stratified Euler equations describe more than internal gravity waves. Two additional types of waves exist, acoustic waves and Lamb waves. Unlike internal gravity waves, acoustic and Lamb waves can also exist in homogeneous fluids. The compressible stratified Euler equations can be simplified to the compressible homogeneous Euler equations by using a homogeneous background density ($\rho_0 \to 1$). When applying this homogeneity approximation and the incompressibility approximation the equations reduce to trivial equations with only trivial solutions. Figure D-1 shows an extension to the systems of equations introduced in Chapter 2. This chapter presents solutions for acoustic and Lamb waves for the compressible stratified Euler equations and the compressible homogeneous Euler equations. These analytical solutions are used to verify the numerical simulations for these types of waves. The verification of Chapter 6 is extended to acoustic and Lamb waves.

D-1 Mathematical Model

In this section the mathematical model describing the behaviour of acoustic and Lamb waves is set up. Two sets of governing equations can be used to described these types of waves: the compressible stratified Euler equations and the compressible homogeneous Euler equations. The compressible stratified Euler equations are copied from Section 2-1 and the acoustic and Lamb wave solutions are derived. The compressible stratified Euler equations are homogenized to yield the compressible homogeneous Euler equations. These are solved for acoustic and Lamb waves.
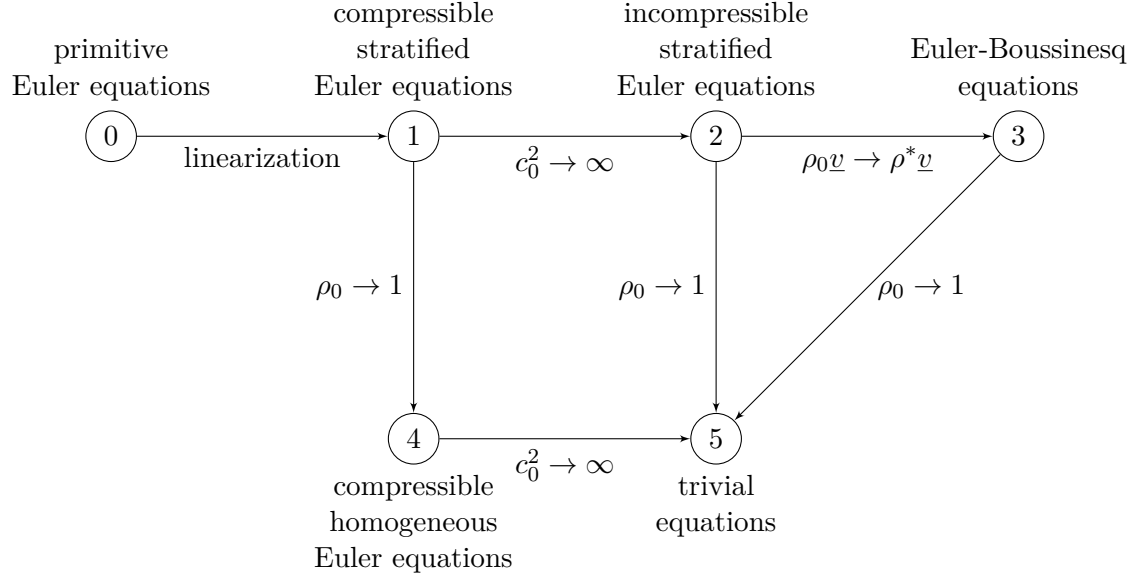
Figure D-1: The systems of equations discussed in this thesis and their connections. The circled numbers indicate the different systems and the arrows indicate approximations: linearization, incompressibility ($c_0^2 \to \infty$), homogeneity ($\rho_0 \to 1$) and Boussinesq ($\rho_0 \underline{v} \to \rho^* \underline{v}$). The primitive Euler equations are used as a starting point for the derivations. Systems (1) to (4) are analytically and numerically solved.

D-1-1 Compressible Stratified Euler Equations

Two additional solutions to (2.3) can be found. Performing substitution (2.5) dispersion relation (2.9) is found. Solving for the square of the frequency yields

$$
\begin{aligned}
\sigma^2 = \frac{1}{2} c_0^2 & \left[\left(k^2 + l^2 + m^2 \right) + \frac{1}{4} \left(\frac{N^2}{g} + \frac{g}{c_0^2} \right)^2 \right] \\
& \pm \frac{1}{2} c_0^2 \sqrt{ \left[-\left(k^2 + l^2 + m^2 \right) - \frac{1}{4} \left(\frac{N^2}{g} + \frac{g}{c_0^2} \right)^2 \right]^2 - \frac{4 N^2 (k^2 + l^2)}{c_0^2} }.
\end{aligned}
\tag{D.1}
$$

The frequencies belonging to the minus in (D.1) correspond to internal gravity waves and the frequencies belonging to the plus in (D.1) correspond to acoustic waves.

The other type of solutions are Lamb waves. A feature of this solution is that the velocity is everywhere parallel to the horizontal plane, i.e., $w = 0$. Performing substitution (2.5) and solving for $P(z)$ yields two equations,

$$
\begin{aligned}
\frac{\partial P}{\partial z} + \frac{g}{c_0^2} P &= 0, \\
\sigma^2 &= c_0^2 \left(k^2 + l^2 \right).
\end{aligned}
\tag{D.2}
$$

Together they represent the Lamb wave solution.

D-1-2 Compressible Homogeneous Euler Equations

A final simplification can be made to the equations describing waves in compressible stratified fluids. For a homogeneous fluid the background density is constant. Then system ④ in Figure D-1, is obtained

$$\frac{\partial \rho^* \underline{v}}{\partial t} = -\nabla p - \rho g \hat{\underline{z}},$$

$$\frac{\partial \rho}{\partial t} = -\nabla.(\rho^* \underline{v}),$$

$$\frac{\partial p}{\partial t} = \rho^* g w - c_0^2 \rho^* \nabla.\underline{v}.$$

$$(D.3)$$

When the incompressibility assumption is made, system ⑤ in Figure D-1 is obtained and only trivial solutions exist. For system ④ the buoyancy frequency reduces to

$$N^2 = -\frac{g^2}{c_0^2}. \tag{D.4}$$

The total energy for system ④ is

$$\mathcal{A}_4 = \int_\Omega \frac{1}{2} \rho^* |\underline{v}|^2 - \frac{c_0^2 \rho^2}{2\rho^*} + \frac{\rho p}{\rho^*} \, d\underline{x}. \tag{D.5}$$

To obtain acoustic solutions to the compressible homogeneous Euler equations, use separation of variables or substitute $\rho_0 = \rho^*$ and (D.4) into (2.9) and (2.11) to obtain

$$\frac{\sigma^4}{c_0^2} - \left(k^2 + l^2 + m^2\right) \sigma^2 - \frac{g^2}{c_0^2} \left(k^2 + l^2\right) = 0 \tag{D.6}$$

and

$$\rho^* u = \frac{k c_0^2}{c_0^2 \left(k^2 + l^2\right) - \sigma^2} \left[-\frac{g}{c_0^2} \sin(mz) + m \cos(mz)\right] \cos\left(kx + ly - \sigma t\right),$$

$$\rho^* v = \frac{l c_0^2}{c_0^2 \left(k^2 + l^2\right) - \sigma^2} \left[-\frac{g}{c_0^2} \sin(mz) + m \cos(mz)\right] \cos\left(kx + ly - \sigma t\right),$$

$$\rho^* w = \sin(mz) \sin\left(kx + ly - \sigma t\right),$$

$$p = \frac{\sigma c_0^2}{c_0^2 \left(k^2 + l^2\right) - \sigma^2} \left[-\frac{g}{c_0^2} \sin(mz) + m \cos(mz)\right] \cos\left(kx + ly - \sigma t\right),$$

$$\rho = \frac{\sigma}{c_0^2 \left(k^2 + l^2\right) - \sigma^2} \left[-\frac{g \left(k^2 + l^2\right)}{\sigma^2} \sin(mz) + m \cos(mz)\right] \cos\left(kx + ly - \sigma t\right).$$

$$(D.7)$$

Here the solid wall boundary condition is used. However, since the system is no longer stratified in density a periodic boundary condition in z-direction can also be prescribed. This extends the range of possible solutions.

Lamb wave solutions are obtained by substituting (2.5) into (D.3). This yields (D.2) and completing the derivation yields solutions

$$
\rho^* u = -\frac{k}{\sigma} e^{-\frac{g}{c_0^2} z} \cos\left(kx + ly - \sigma t\right),
$$
$$
\rho^* v = -\frac{l}{\sigma} e^{-\frac{g}{c_0^2} z} \cos\left(kx + ly - \sigma t\right),
$$
$$
\rho^* w = 0, \tag{D.8}
$$
$$
\rho = c_0^2 e^{-\frac{g}{c_0^2} z} \cos\left(kx + ly - \sigma t\right),
$$
$$
p = e^{-\frac{g}{c_0^2} z} \cos\left(kx + ly - \sigma t\right),
$$

with dispersion relation

$$
\sigma^2 = c_0^2 \left(k^2 + l^2\right). \tag{D.9}
$$

The Lamb wave solutions are similar in stratified and homogeneous fluids.

D-2 Verification: Compressible Homogeneous Euler Equations

In this section the numerical model for the compressible homogeneous Euler equations, system ④ in Figure D-1, is verified.

Consider (D.7) and nondimensionalize as in Section 4-4. Scale such that $Ma = Fr = \delta = \rho^* = 1$. Assume c_0^2 is uniform and scale such that $c_0^2 = 1$. Then the equations reduce to

$$
\frac{\partial u}{\partial t} = -\frac{\partial p}{\partial x},
$$
$$
\frac{\partial v}{\partial t} = -\frac{\partial p}{\partial y},
$$
$$
\frac{\partial w}{\partial t} = -\rho - \frac{\partial p}{\partial z}, \tag{D.10}
$$
$$
\frac{\partial \rho}{\partial t} = -\left(\frac{\partial u}{\partial x} + \frac{\partial v}{\partial y} + \frac{\partial w}{\partial z}\right),
$$
$$
\frac{\partial p}{\partial t} = w - \left(\frac{\partial u}{\partial x} + \frac{\partial v}{\partial y} + \frac{\partial w}{\partial z}\right).
$$

D-2-1 One Dimensional Acoustic Equations

A one-dimensional solution to (D.10), with constant N^2, is obtained from (D.6) and (D.7). For $H_z = 1$ and $n_z = 2$ a one-dimensional solution is

$$
u = 0,
$$
$$
v = 0,
$$
$$
w = \cos\left(2\pi\left(t - z\right)\right), \tag{D.11}
$$
$$
\rho = \cos\left(2\pi\left(t - z\right)\right),
$$
$$
p = \frac{1}{2\pi} \sin\left(2\pi\left(t - z\right)\right) + \cos\left(2\pi\left(t - z\right)\right).
$$

The boundary conditions in z-direction is periodic. The buoyancy frequency is negative, i.e. $N^2 = -1$. The energy of the system is

$$H = \int_0^1 \frac{1}{2}\left(u^2 + v^2 + w^2\right) - \frac{1}{2}\rho^2 + \rho p \, \mathrm{d}z = \frac{1}{2}. \tag{D.12}$$

The numerical discretization is initialized at time $t = 0$ and compared to the exact solution. Table D-1 presents the L^2-error and order of convergence of the numerical solution after one period. The order of convergence is 2, corresponding to the expected convergence rate of polynomial order plus one. The energy is conserved up to machine precision. Figure D-2 shows the error in energy for 1000 periods.

Table D-1: L^2-error and order of convergence of the numerical solution after one period for the one dimensional acoustic wave in a periodic domain for a compressible homogeneous fluid. The polynomial order is one. The temporal step size equals the spatial step size.

| | w | | ρ | | p | |
h	L^2-error	Order	L^2-error	Order	L^2-error	Order
1/4	1.4038e+0	-	1.3970e+0	-	1.4642e+0	-
1/8	4.1836e-1	1.75	4.1797e-1	1.74	4.2728e-1	1.78
1/16	1.1163e-1	1.91	1.1161e-1	1.90	1.1330e-1	1.92
1/32	2.8386e-2	1.98	2.8384e-2	1.98	2.8768e-2	1.98
1/64	7.1266e-3	1.99	7.1265e-3	1.99	7.2191e-3	1.99
1/128	1.7836e-3	2.00	1.7836e-3	2.00	1.8064e-3	2.00
1/256	4.4602e-4	2.00	4.4602e-4	2.00	4.5168e-4	2.00
1/512	1.1151e-4	2.00	1.1151e-4	2.00	1.1292e-4	2.00
1/1024	2.7879e-5	2.00	2.7879e-5	2.00	2.8230e-5	2.00
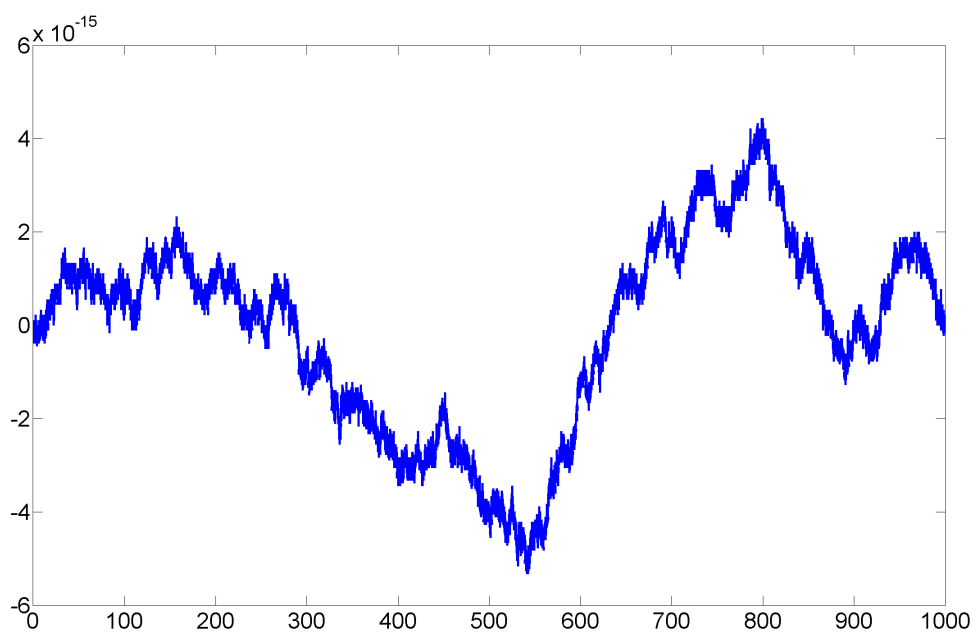
Figure D-2: The error in total energy during 1000 periods. The spatial and temporal step size was $1/16$ and the polynomial order was 1.

D-2-2   Lamb Waves, Mixed Boundary Conditions

A solution to (D.10) is obtained from (D.8) and (D.9)

$$
\begin{aligned}
u &= -\frac{1}{\sqrt{2}} e^{-z} \cos\left(2\pi x + 2\pi y + 2\sqrt{2}\pi t\right), \\
v &= -\frac{1}{\sqrt{2}} e^{-z} \cos\left(2\pi x + 2\pi y + 2\sqrt{2}\pi t\right), \\
w &= 0, \\
\rho &= e^{-z} \cos\left(2\pi x + 2\pi y + 2\sqrt{2}\pi t\right), \\
p &= e^{-z} \cos\left(2\pi x + 2\pi y + 2\sqrt{2}\pi t\right).
\end{aligned}
\tag{D.13}
$$

The boundary conditions in x- and y-direction are periodic and in z-direction is no-normal flow. The buoyancy frequency is negative, i.e. $N^2 = -1$. The energy of the system is

$$
H = \int_0^1 \int_0^1 \int_0^1 \frac{1}{2}\left(u^2 + v^2 + w^2\right) - \frac{1}{2}\rho^2 + \rho p \, \mathrm{d}x\mathrm{d}y\mathrm{d}z = \frac{1}{4}\left(1 - \frac{1}{e^2}\right).
\tag{D.14}
$$

The numerical discretization is initialized at time $t = 0$ and compared to the exact solution. Table D-2 presents the L^2-error and order of convergence of the numerical solution at $t = 1$. The order of convergence is around 2, corresponding to the expected convergence rate of polynomial order plus one. The energy is again conserved up to machine precision. Figure D-3 shows the numerical solution at $t = 1$.

Table D-2: L^2-error and order of convergence of the numerical solution at $t = 1$ for the three dimensional Lamb wave in a domain with periodic boundary conditions in x- and y-direction and a solid wall boundary condition in z-direction for a compressible homogeneous fluid. The polynomial order is one. The temporal step size equals the spatial step size.

	u, v		w		ρ		p	
h	L^2-error	Order	L^2-error	Order	L^2-error	Order	L^2-error	Order
1/4	9.5830e-1	-	1.7510e-2	-	1.1652e+0	-	1.1642e+0	-
1/8	2.9014e-1	1.72	4.3251e-3	2.02	3.9419e-1	1.56	3.9360e-1	1.56
1/16	7.6085e-2	1.93	1.4861e-3	1.54	1.0388e-1	1.92	1.0373e-1	1.92
1/32	1.8546e-2	2.04	5.1996e-4	1.52	2.6131e-2	1.99	2.6094e-2	1.99
1/64	4.7719e-3	1.96	1.8178e-4	1.52	6.4880e-3	2.01	6.4786e-3	2.01
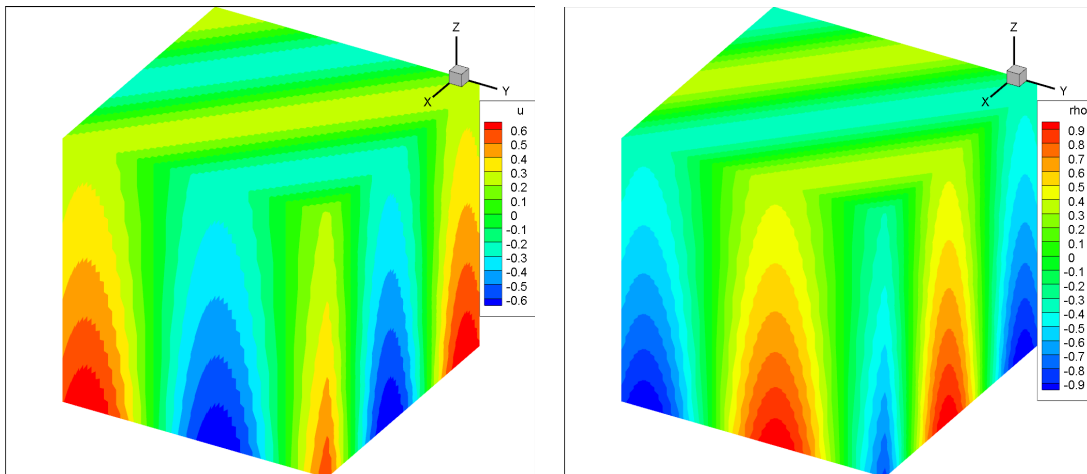
Figure D-3: The numerical solution for the three dimensional Lamb waves in a homogeneous compressible fluid. The left image shows the horizontal velocity and the right image the density. The spatial step size was $1/64$ and the polynomial order was one.

D-2-3   Lamb Waves, Solid Wall Boundary Conditions

A solution to (D.10) is obtained from (D.8) and (D.9)

$$
\begin{aligned}
u &= -\frac{1}{\sqrt{2}} e^{-z} \sin\left(2\pi x\right) \cos\left(2\pi y\right) \cos(2\sqrt{2}\pi t + 0.1),\\
v &= -\frac{1}{\sqrt{2}} e^{-z} \cos\left(2\pi x\right) \sin\left(2\pi y\right) \cos(2\sqrt{2}\pi t + 0.1),\\
w &= 0,\\
\rho &= e^{-z} \cos\left(2\pi x\right) \cos\left(2\pi y\right) \sin(2\sqrt{2}\pi t + 0.1),\\
p &= e^{-z} \cos\left(2\pi x\right) \cos\left(2\pi y\right) \sin(2\sqrt{2}\pi t + 0.1).
\end{aligned}
\tag{D.15}
$$

The boundary conditions are no-normal flow in all directions. Physically this type of solution corresponds to Lamb waves. The phase difference is introduced to ensure the solution is nonzero at time $t = 0$. The buoyancy frequency is negative, i.e. $N^2 = -1$. The energy of the system is

$$
H = \int_0^1 \int_0^1 \int_0^1 \frac{1}{2}\left(u^2 + v^2 + w^2\right) - \frac{1}{2}\rho^2 + \rho p \,\mathrm{d}x\mathrm{d}y\mathrm{d}z = \frac{1}{16}\left(1 - \frac{1}{e^2}\right). \tag{D.16}
$$

The numerical discretization is initialized at time $t = 0$ and compared to the exact solution. Table D-3 presents the L^2-error and order of convergence of the numerical solution at $t = 1$. The order of convergence is around 2, corresponding to the expected convergence rate of polynomial order plus one. The energy is again conserved up to machine precision. Figure D-4 shows the numerical solution at $t = 1$.

Table D-3: L^2-error and order of convergence of the numerical solution at $t = 1$ for the three dimensional Lamb wave in a domain with solid wall boundary conditions for a compressible homogeneous fluid. The polynomial order is one. The temporal step size equals the spatial step size.

| | u, v | | w | | ρ | | p | |
h	L^2-error	Order	L^2-error	Order	L^2-error	Order	L^2-error	Order
1/4	6.4273e-1	-	1.3775e-2	-	1.6526e-1	-	1.5978e-1	-
1/8	1.4407e-1	2.16	3.0551e-3	2.17	2.2164e-1	-0.42	2.2101e-1	-0.47
1/16	2.6965e-2	2.42	1.0849e-3	1.49	6.8547e-2	1.69	6.8422e-2	1.69
1/32	6.9637e-3	1.95	3.7211e-4	1.54	1.6173e-2	2.08	1.6142e-2	2.08
1/64	1.8757e-3	1.89	1.2851e-4	1.53	3.8776e-3	2.06	3.8700e-3	2.06
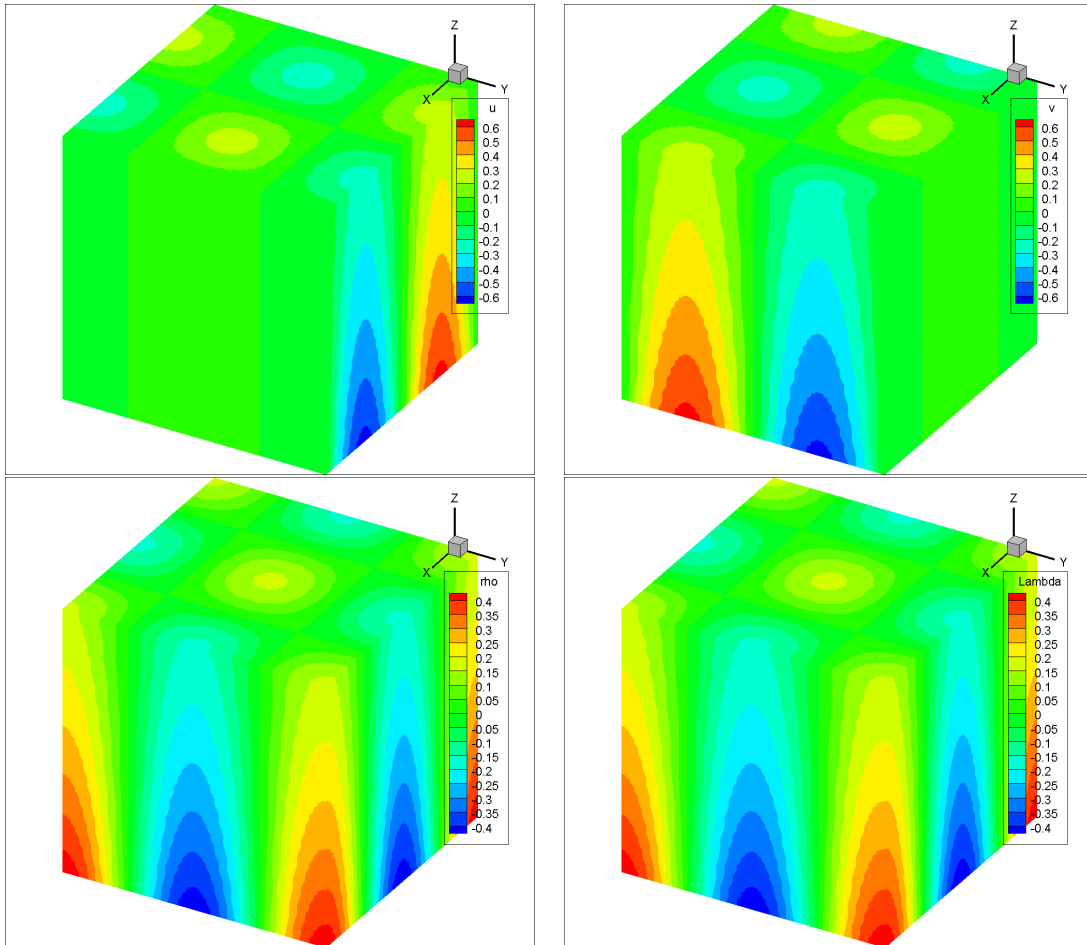
Figure D-4: The numerical solution for the three dimensional Lamb wave in a homogeneous compressible fluid with solid wall boundary conditions. The top images show the horizontal velocites and the bottom images show the density and pressure. The spatial step size was $1/64$ and the polynomial order was one.

Appendix E

Time Evolution Wave Attractors

The time evolution of the wave attractors of Section 6-4 is shown here.

Figure E-3 shows the evolution of the $(1, 1)$ initial condition into a $(1, 1)$ wave attractor. Each row shows the vertical velocity, pressure and energy of the numerical solution. The first row shows the solution at $t = 0$ and the time increases by 20 for each row. So the time at the last row is 200. The geometric asymmetry completely changed the solution. Smaller and smaller scales appear in the numerical solution. Wave are focused by reflections on the tilted walls. In the linear, inviscid case, this process continues forever. In the numerical solution, the scales get smaller and smaller until the scale of the size of the elements is reached. So, eventually, the numerical solution depends on the scale of the elements. The solution in the last row of Figure E-3 has not yet reached this limit.

Vertical Velocity   Pressure   Energy
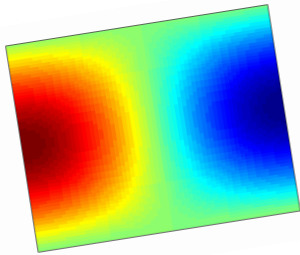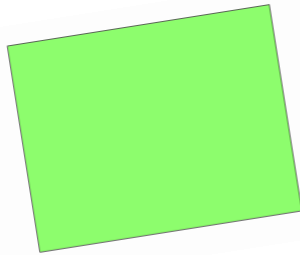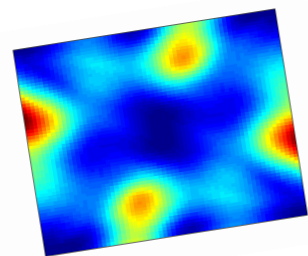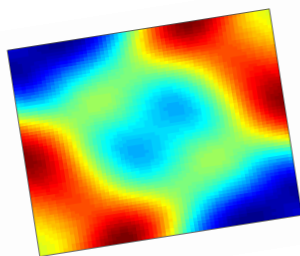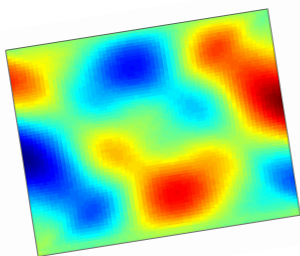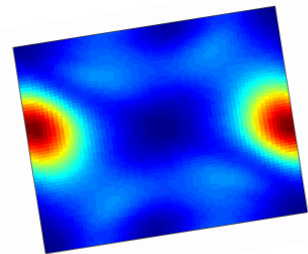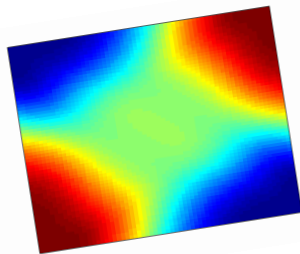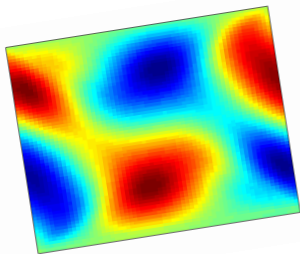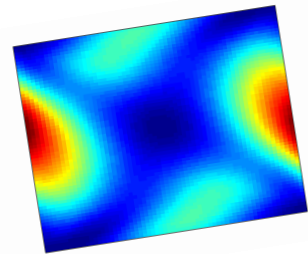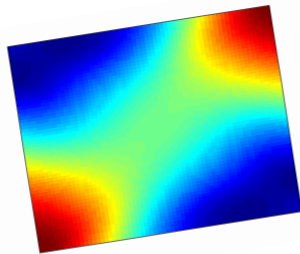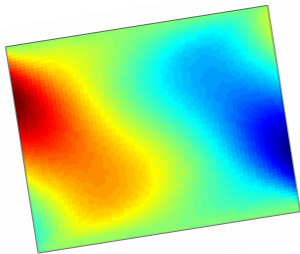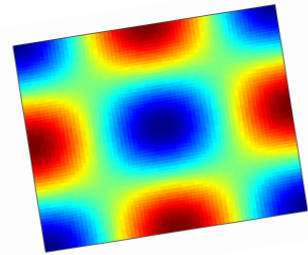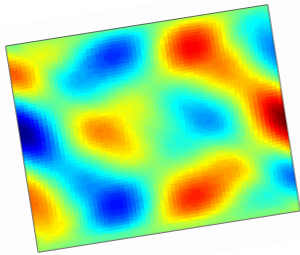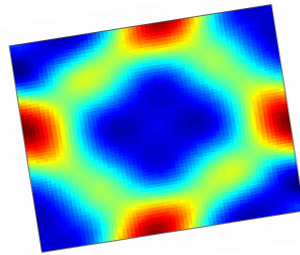
Vertical Velocity   Pressure   Energy
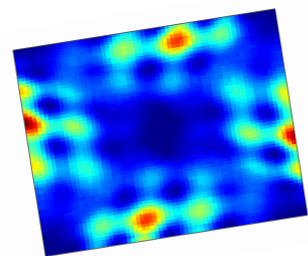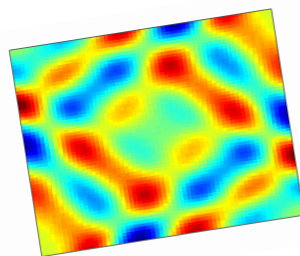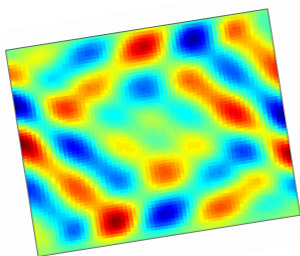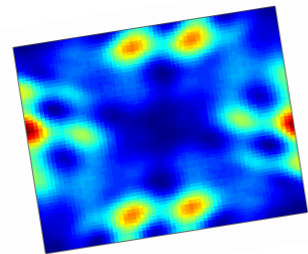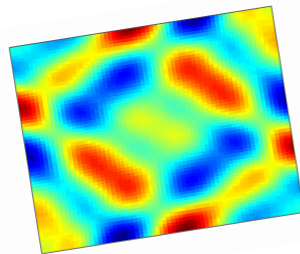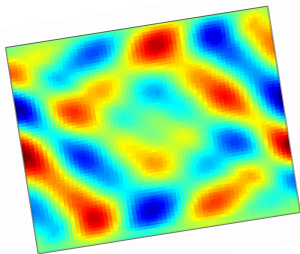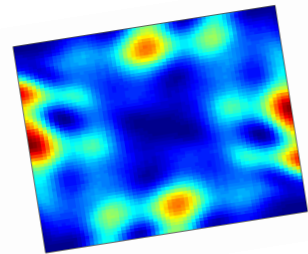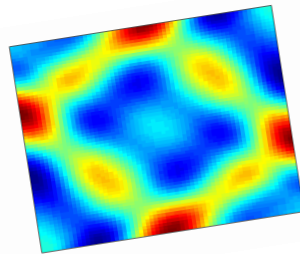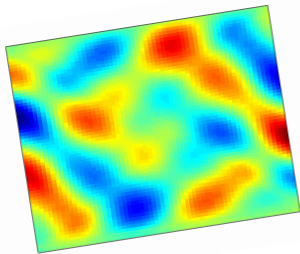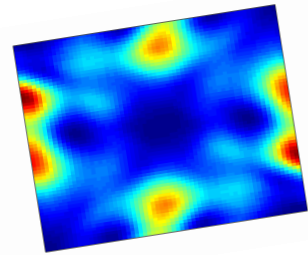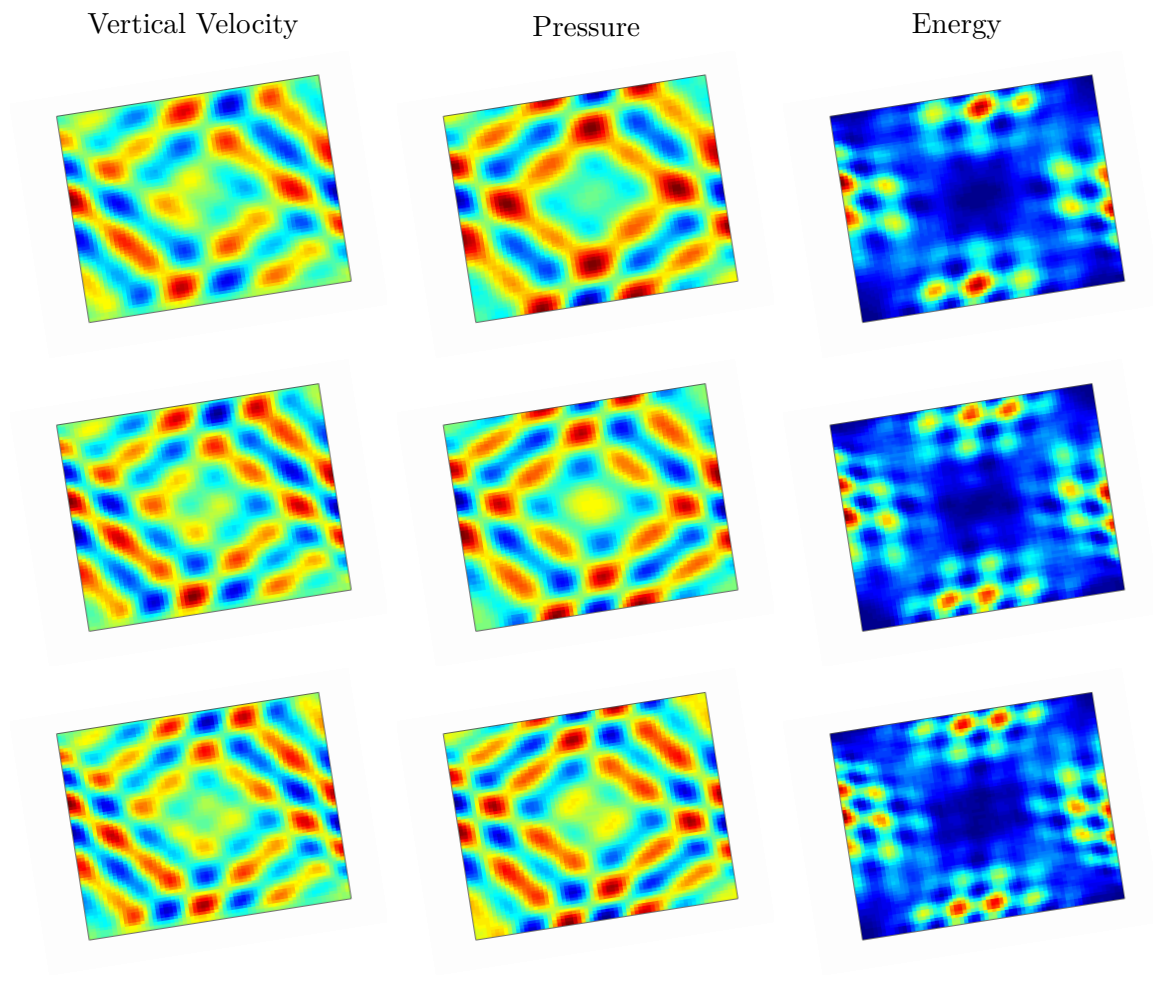
Figure E-3: The time evolution of the numerical solution of the $(1,1)$ initial condition. The left image shows the vertical velocity, the middle image the pressure and the right image the energy. With each row the (dimensionless) time increases by twenty. The number of elements in each direction was 64 and the polynomial order was zero.
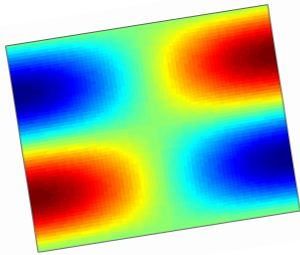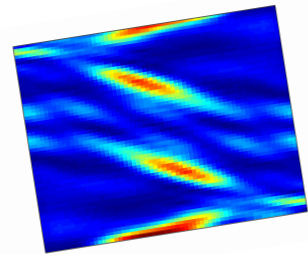
Vertical Velocity   Pressure   Energy
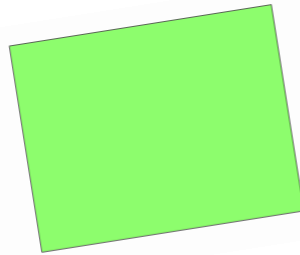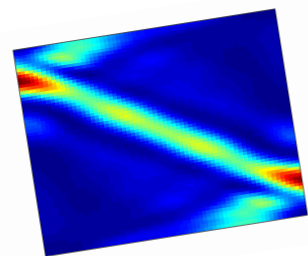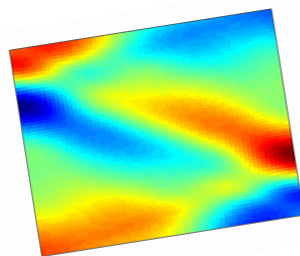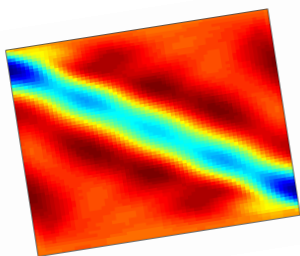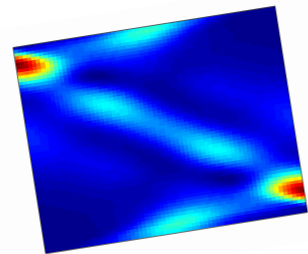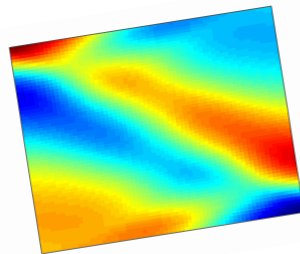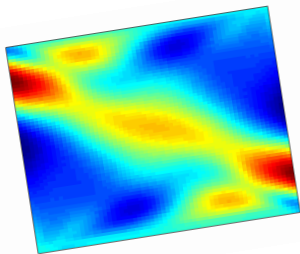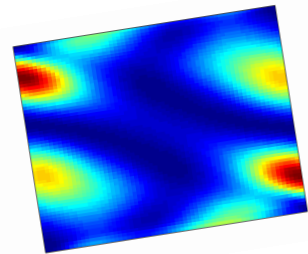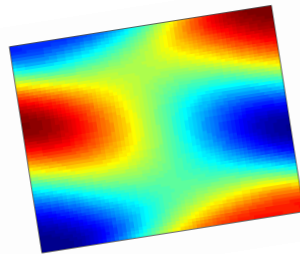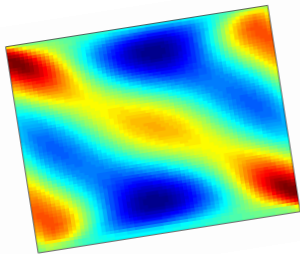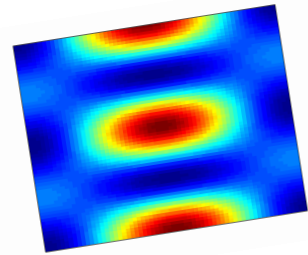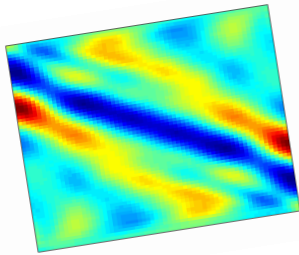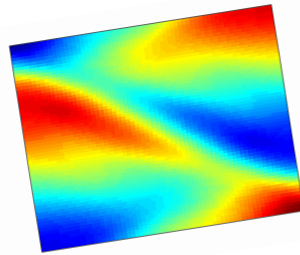
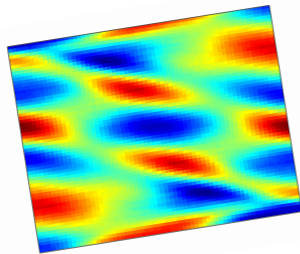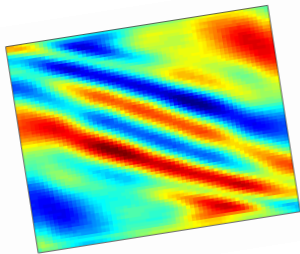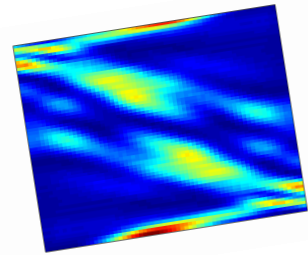Vertical Velocity   Pressure   Energy
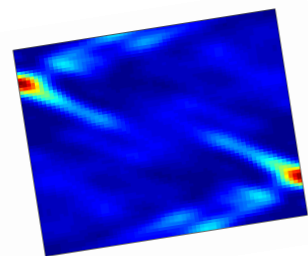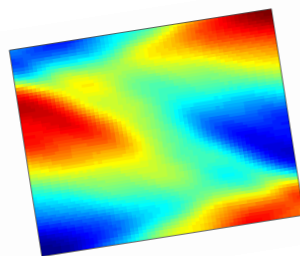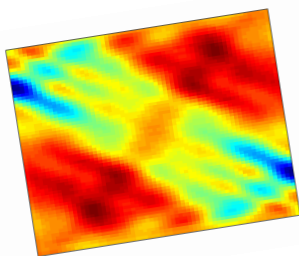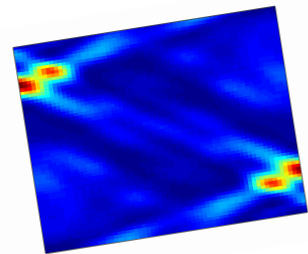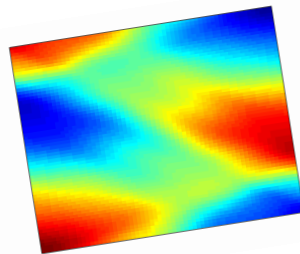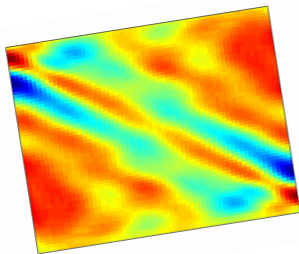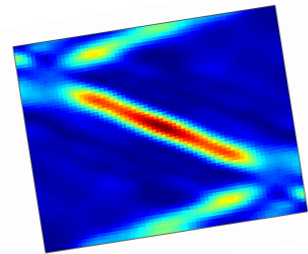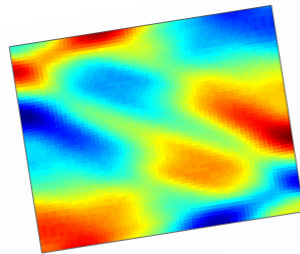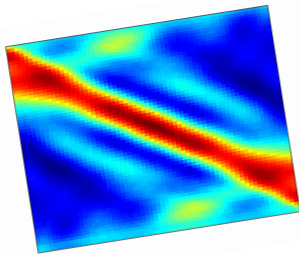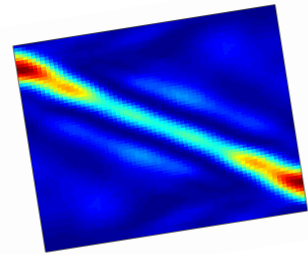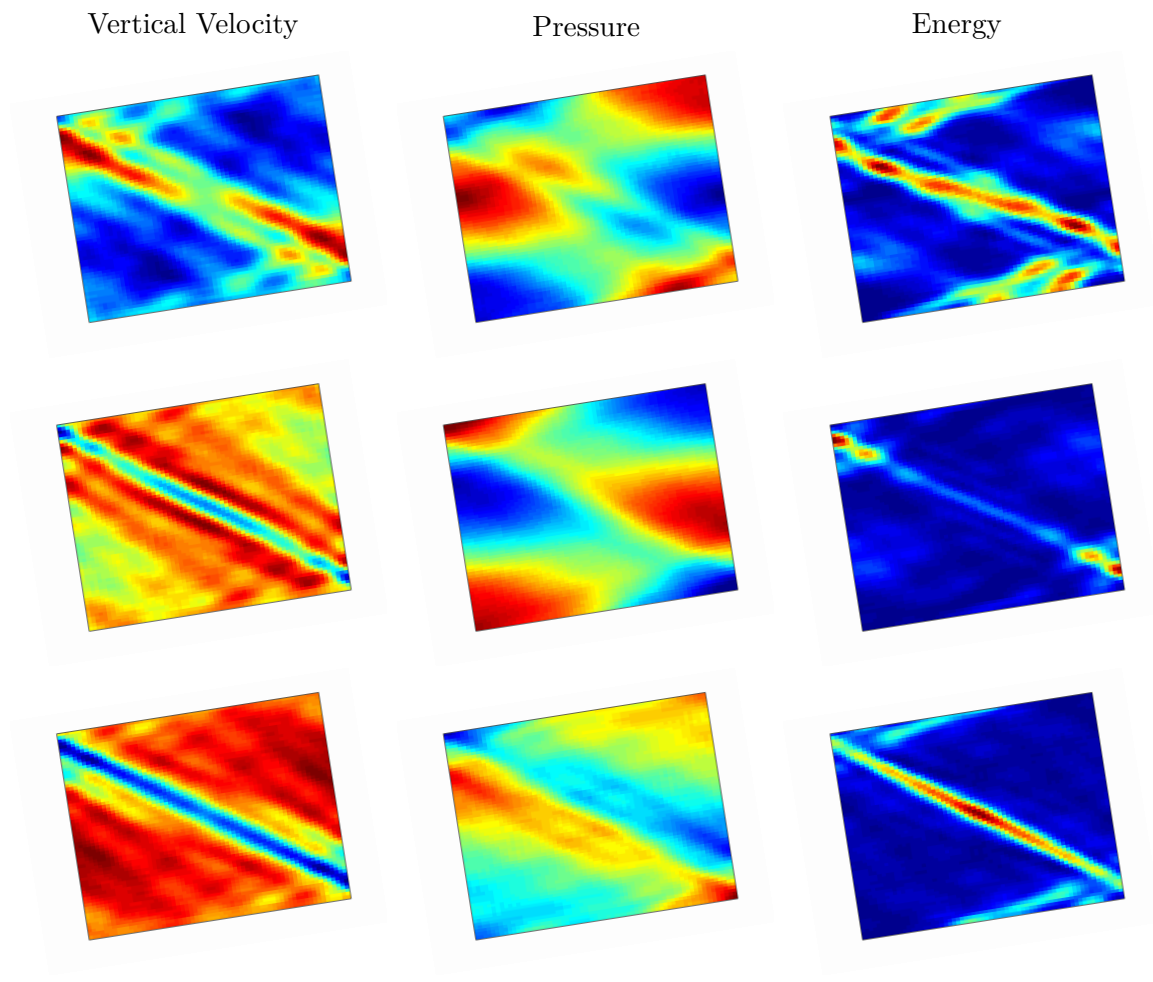
Figure E-6: The time evolution of the numerical solution of the $(1,2)$ initial condition. The left image shows the vertical velocity, the middle image the pressure and the right image the energy. With each row the (dimensionless) time increases by twenty. The number of elements in each direction was 64 and the polynomial order was zero.
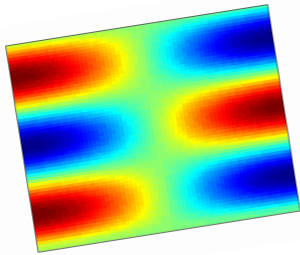
Vertical Velocity   Pressure   Energy
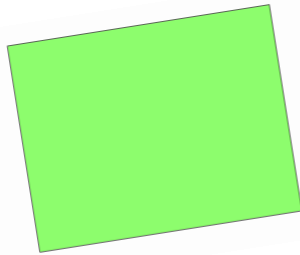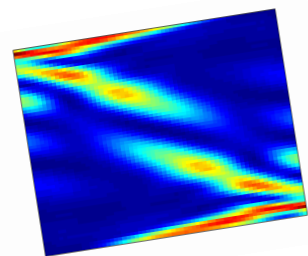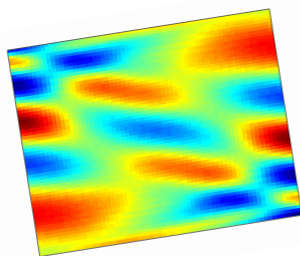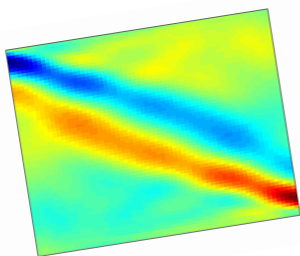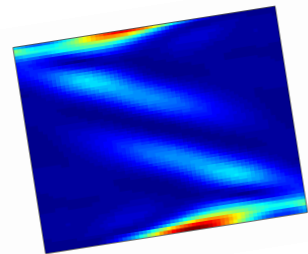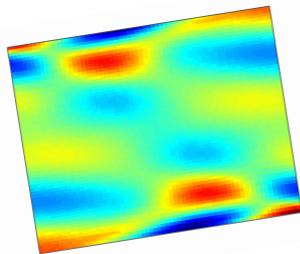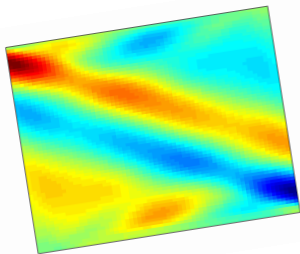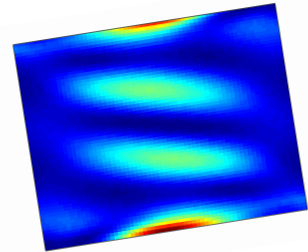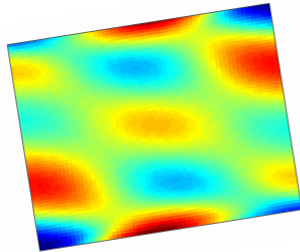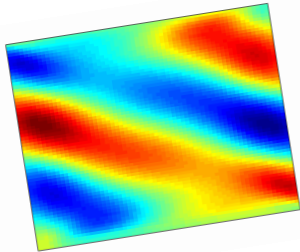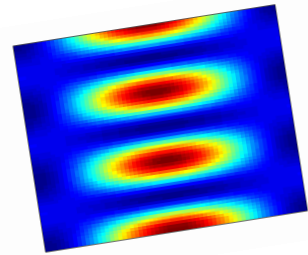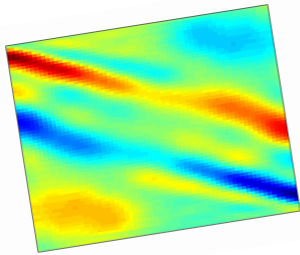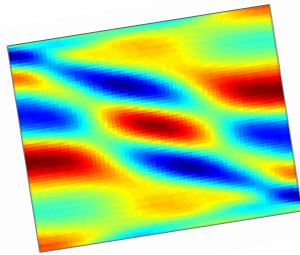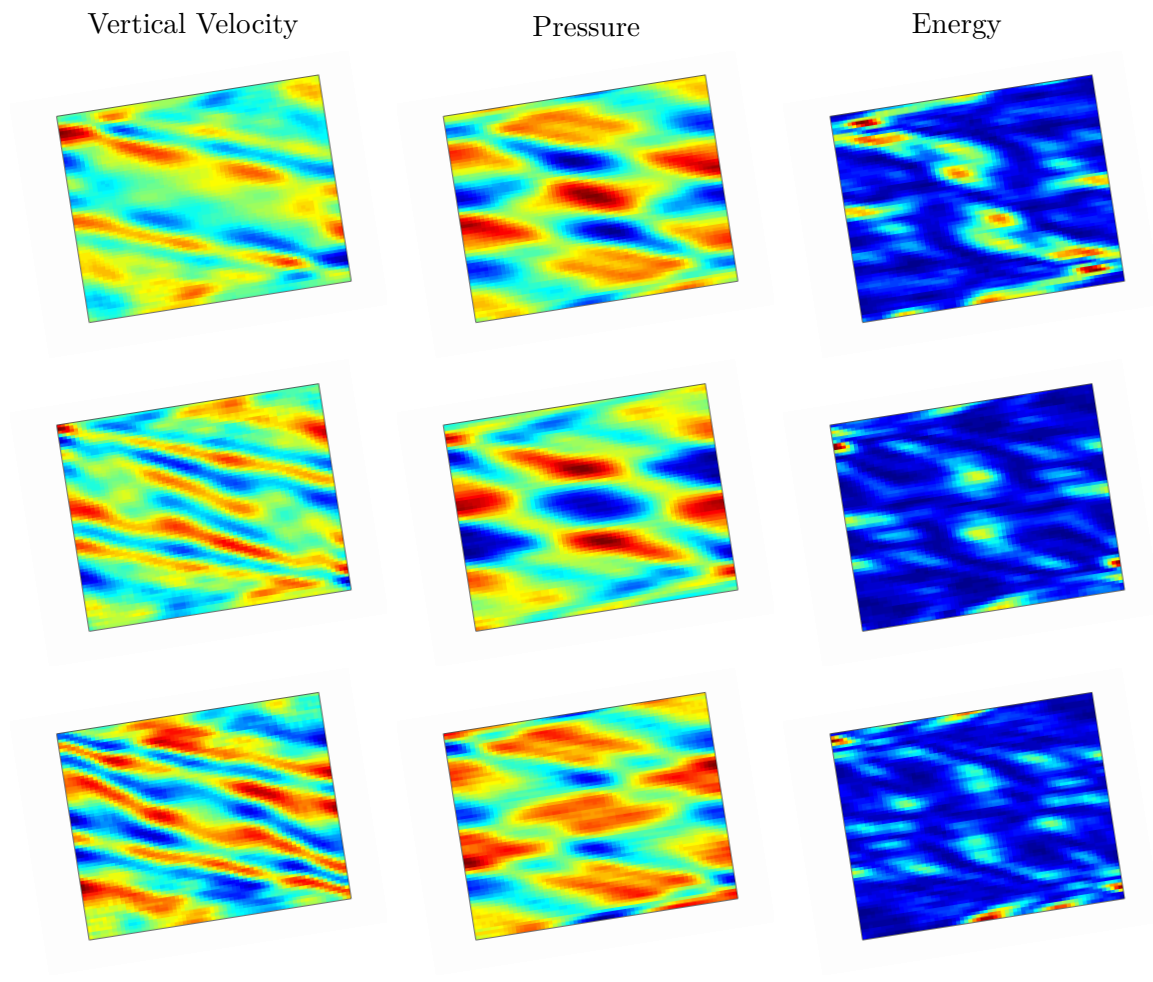
Vertical Velocity Pressure Energy
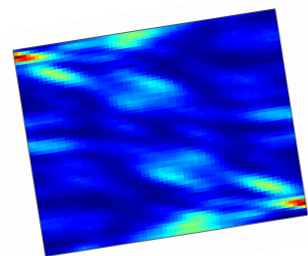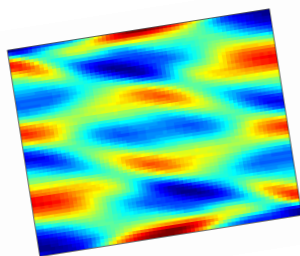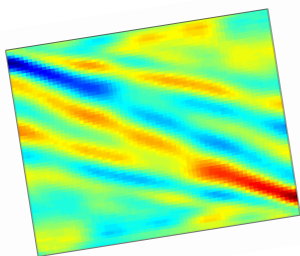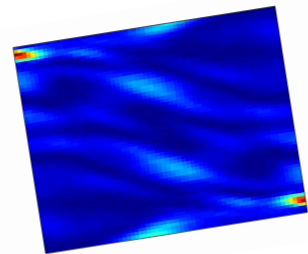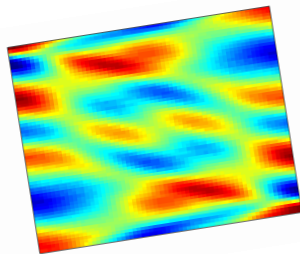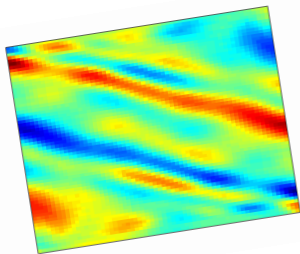
Figure E-9: The time evolution of the numerical solution of the $(1,3)$ initial condition. The left image shows the vertical velocity, the middle image the pressure and the right image the energy. With each row the (dimensionless) time increases by twenty. The number of elements in each direction was 64 and the polynomial order was zero.